Macro- and microvascular complications of diabetes:

Studies on NFAT (Nuclear Factor of Activated T-cells) as a novel target for the treatment of atherosclerosis and vascular dysfunction in diabetes.

Fabiana Blanco Cámera

LUND UNIVERSITY

UNIVERSIDAD DE LA REPÚBLICA URUGUAY

DOCTORAL DISSERTATION
by due permission of the Faculty of Medicine, Lund University, Sweden & the Faculty of Sciences, Universidad de la República, Uruguay.
To be defended at Videoconference room, Faculty of Medicine, Av. General Flores 2125.

Thursday 6th of December, 2018 at 9.30

Faculty opponent
Professor María Teresa Perez-García, Universidad de Valladolid, Spain

Faculty examination committee

Associate Professor Silvia Chifflet, Associate Professor Verónica Abudara; Universidad de la República, Associate Professor Juan Claudio Benech; Instituto de Investigaciones Biológicas Clemente Estable, Uruguay.

Organization LUND UNIVERSITY	Document name DOCTORAL DISSERTATION
Department of Clinical Sciences, Malmö	Date of issue December 6th, 2018
Author(s) Fabiana Blanco Cámera	Sponsoring organization

Macro- and microvascular complications of diabetes: Studies on NFAT (Nuclear Factor of Activated T-cells) as a novel target for the treatment of atherosclerosis and vascular dysfunction in diabetes.

Abstract

Diabetes is associated with devastating chronic complications including coronary heart disease and stroke (macrovascular complications) as well as microvascular disorders leading to damage of the small vessels and the development of retinopathy, nephropathy and neuropathy. The underlying pathogenesis is not clear, but hyperglycemia has been identified as an important risk factor. Previous work from our group demonstrated that hyperglycemia effectively activates the Ca^{2+}/calcineurin transcription factor NFAT in macro and microvessels, both *ex vivo* and *in vivo*. Once activated, NFAT enhances vascular smooth muscle cell (VSMC) excitability and vasoconstriction and promotes the expression of inflammatory markers in the arterial wall. This thesis focuses on elucidating the role of NFAT in the context of diabetes-induced atherosclerosis and retinopathy. In **paper I**, we showed that *in vivo* inhibition of NFAT signalling with the NFAT blocker A-285222 for 4 weeks completely suppressed the accelerated atherosclerosis in the aortic arch of type 1 diabetic $ApoE^{-/-}$ mice, having no effect in non-diabetic mice. This effect was independent of changes in plasma glucose or lipid levels and was not due to systemic immunosuppression. Inhibition of NFAT resulted in reduced lipid contents in the plaques of diabetic mice, reduced expression of interleukin 6 (IL-6), osteopontin (OPN), monocyte chemotactic protein-1 (MCP-1), intracellular adhesion molecule 1 (ICAM-1), CD68 (macrophage marker) and tissue factor (TF) in the arterial wall, as well as in lowered plasma IL-6. Further, in **paper II**, we showed that *in vivo* treatment with A-285222 reduced atherosclerotic plaque area and degree of stenosis in the brachiocephalic artery of IGF-II/$LDLR^{-/-}$$ApoB^{100/100}$ mice. This is a mouse model characterized by mild hyperglycaemia and hyperinsulinaemia, a human-like hypercholesterolaemic lipid profile, and advanced and complex atherosclerotic lesions, hence replicating features of human type 2 diabetes disease. The effects of NFAT inhibition on atherosclerosis in this model were not only due to limited plaque progression but also to plaque regression, as assessed by comparing plaque size non-invasively using ultrasound biomicroscopy prior and after treatment with A-285222. Treatment had no impact on plaque composition and the effects on plaque size could not be explained by effects of A-285222 on plasma glucose, insulin or lipids. Interestingly, NFAT inhibition resulted in increased expression of the atherosprotective NADPH oxidase 4 (NOX4) and of the anti-oxidant enzyme catalase in aortic VSMCs. In **paper III**, we demonstrated that NFAT is expressed in the endothelium of retinal microvessels and is readily activated by both acute and chronic hyperglycemia. Activation seemed mediated by a mechanism involving the release of extracelllar nucleotides. In both Akita (*Ins2*$^{+/-}$) and streptozotocin- (STZ-) induced diabetic mice, NFAT transcriptional activity was elevated in retinal vessels. *In vivo* inhibition of NFAT with A-285222 decreased the expression of OPN and ICAM-1 mRNA in retinal vessels, prevented a diabetes driven down-regulation of anti-inflammatory IL-10 in retina, and limited the increased vascular permeability observed in diabetic mice. Finally, in **paper IV**, we performed a systematic mapping of the pattern of NFAT isoform expression in 13 different regions of the mouse vascular tree using absolute qPCR quantification. We found that NFATc3 is the most predominant isoform in all vessels examined and that NFATc2 expresion was increased in the aortic wall of diabetic mice, suggesting that this isoform can be induced or enhanced in pathological situations or under certain stimulatory conditions. We also found that genetic deletion of NFATc2 or NFATc3 differentially affected the expression of Kruppel-like factor 4 (Klf4), Kruppel-like factor 5 (Klf5) and Gata4, genes that have been implicated in the regulation of VSMC phenotypic modulation. Moreover, deletion of NFATc3 resulted in increased expression of angiotensin I converting enzyme (peptidyl-dipeptidase A) 1 (Ace) and of smooth muscle marker genes calponin 1 (Cnn1) and transgelin (Tagln), as well as in higher VSMC proliferation. In summary, NFAT seems to play a role in the development of diabetic-driven atherosclerosis and retinopathy, and targeting the NFAT signalling pathway may be an attractive approach for the treatment of diabetic complications. The differential isoform expression and effects observed upon NFATc2 and NFATc3 deletion support the idea of functional non-redundancy of NFAT isoforms in the vasculature.

Key words: NFAT, VSMCs, diabetes, hyperglycemia, aterosclerosis, diabetic retinopathy, oxidative stress

Classification system and/or index terms (if any)

Supplementary bibliographical information		Language English
ISSN 1652-8220		ISBN 978-91-7619-729-5
Recipient's notes	Number of pages 214	Price
	Security classification	

Macro- and microvascular complications of diabetes:

Studies on NFAT (Nuclear Factor of Activated T-cells) as a novel target for the treatment of atherosclerosis and vascular dysfunction in diabetes.

Fabiana Blanco Cámera

UNIVERSIDAD
DE LA REPÚBLICA
URUGUAY

Supervisor: Professor Maria F. Gomez, Lund University, Sweden

Deputy supervisors: Professor Gustavo Brum, Universidad de la República, Uruguay

Lisa M. Berglund, PhD, Lund University, Sweden

Front cover by Fabiana Blanco

(design by www.bar.com.uy)

Back cover by Fabiana Blanco

Faculty of Medicine
Department of Clinical Sciences, Malmö, LU
Department of Biophysics, Montevideo, UDELAR

ISBN 978-91-7619-729-5
ISSN 16528-220

Printed in Sweden by Media-Tryck, Lund University
Lund 2018

To my family

"The most beautiful thing we can experience is the mysterious. It is the source of all true art and science"

Albert Einstein

El camino es la recompensa ("the way is the reward")

Maestro Óscar W.Tabárez

Table of contents

Papers included in this thesis

This thesis is based on the following papers, which are referred in the text by their roman numerals:

I. Anna V. Zetterqvist, Lisa M. Berglund, **Fabiana Blanco**, Eliana Garcia-Vaz, Maria Wigren, Pontus Dunér, Anna-Maria Dutius Andersson, Fong To, Peter Spegel, Jan Nilsson, Eva Bengtsson, Maria F. Gomez. Inhibition of Nuclear Factor of Activated T-cells (NFAT) Suppresses Accelerated Atherosclerosis in Diabetic Mice. *PLOS ONE, 8(6), 1-14, 2013*. DOI:10.1371/journal.pone.0065020

II. **Fabiana Blanco**, Suvi E. Heinonen, Erika Gurzeler, Lisa M Berglund, Anna-Maria Dutius Andersson, Olga Kotova, Ann-Cathrine Jönsson-Rylander, Seppo Ylä-Herttuala and Maria F. Gomez. *In vivo* inhibition of Nuclear Factor of Activated T-cells (NFAT) leads to atherosclerotic plaque regression in IGF-II/LDLR$^{-/-}$ApoB$^{100/100}$ mice. *Diabetes & Vascular Disease Research 15(4), 302-313; 2018*. DOI:10.1177/1479164118759220

III. Anna V. Zetterqvist, **Fabiana Blanco**, Jenny Öhman, Olga Kotova, Lisa M. Berglund, Sergio de Frutos García, Raed Al-Naemi, Maria Wigren, Paul G. McGuire, Laura V. Gonzalez Bosc, and Maria F. Gomez. Nuclear factor of activated T cells is activated in the endothelium of retinal microvessels in diabetic mice. *Journal of Diabetes Research 15(428473), 1-14; 2015.* DOI:10.1155/2015/428473

IV. **Fabiana Blanco,** Lisa M. Berglund, Olga Kotova, Anna-Maria Dutius Andersson, Petr Volkov, Maria F. Gomez. Differential effects of NFATc2 and NFATc3 deletion on vascular smooth muscle gene expression and proliferation. *Manuscript, 2018.*

Reprints were made with permission from the respective publisher.

Paper not included in this thesis

I. Maria A. Gómez, Ignacio Migues, Maria Caggiani, Ximena Arias, Mariajose Laprovitera, **Fabiana Blanco**, Maria V. Cesio, Eduardo R. Migliaro, Horacio Heinzen. Vasorelaxant effect of a Baccharis trimera infusion on precontracted rat aortic rings. *Natural Product Communications*, 11(3):283-286; 2016.

II. Luis E. Gómez, Jorge Rodríguez, Adriana Carlomagno, María Eugenia Cruces, Martín Gabay, **Fabiana Blanco**, María Lamas, Nuria Campillo, Juan A. Páez, Kaleigh Giles, Jeffrey Atkinson, Paola Contreras, Carlos Escande, María Laura Lavaggi, Hugo Cerecetto, Mercedes González, Homero Rubbo, Carlos Batthyány, Ana M. Ferreira, Gloria V. López. Synthesis, biological evaluation and early pre-clinical studies of nitrooxy-tocopherol analogues designed as antiatherogenic agents. *Submitted, 2018.*

Abbreviations

Ace	Angiotensin I converting enzyme
ADP	Adenosine diphosphate
AGE	Advanced glycation end product
AP-1	Activator protein 1
$ApoB^{100/100}$	Apolipoprotein $B^{100/100}$
ApoE	Apolipoprotein E
ATP	Adenosine triphosphate
BRB	Blood-retinal barrier
CaN	Calcineurin
$[Ca^{2+}]_i$	Intracellular calcium concentration
Ccna2	Cyclin A2
Ccnd1	Cyclin D1
Cdks	Cyclin-dependent protein kinases
Cnn1	Calponin1
CRAC	Calcium Release Activated Channels
CsA	Cyclosporin
C_t	Cycle threshold
CVD	Cardiovascular disease
DR	Diabetic retinopathy
EC	Endotheial cell
EGFP	Enhanced green florescence protein
ECM	Extracellular matrix
FK506	Tacrolimus
GLO1	Glyoxalase I
GLUT	Glucose transporter
H_2O_2	Hydrogen peroxide

HDL	High-density lipoprotein
HFD	High fat diet
HKG	Housekeeping gene
HMEC	Human microvascular endothelial cell
HRMVEC	Human retinal microvascular endothelial cell
HUVEC	Human umbilical vein endothelial cell
ICAM-1	Intracellular adhesion molecule 1
IGF-II	Insulin-like growth factor II
IL	Interleukin
ILDL	Intermediate-low density lipoprotein
IP3	Inositol triphosphate
IP3R	IP3 receptor
IP-GTT	Intraperitoneal glucose tolerance test
JNK	c-Jun terminal kinase
KLF	Krüppel-like factor
LDL	Low-density lipoprotein
LDLR	LDL receptor
MCP-1	Monocyte chemoattractant protein 1
MMP	Matrix metalloproteinase
NES	Nuclear export signal
NFAT	Nuclear factor of activated T cells
NF-KB	Nuclear factor kappa-B
NLS	Nuclear localization signal
•NO	Nitric oxide
NOX	NADPH oxidase
$O_2^{\bullet-}$	Superoxide
$ONOO^-$	Peroxynitrite
OPN	Osteopontin
PKA	Protein kinase A

PKC	Protein kinase C
RAGE	Receptor of AGE
RNS	Radical nitrogen species
ROS	Radical oxygen species
RT-PCR	Real-time polymerase chain reaction
SMα-actin	Smooth muscle alpha actin (also known as Acta2)
SMC	Smooth muscle cell
SM22	Smooth muscle protein 22-alpha or actin-associated protein p27 or transgelin (Tagln)
SR	Sarcoplasmic reticulum
SRF	Serum response factor
STZ	Streptozotocin
Tagln	Transgelin
T1D	Type 1 diabetes
T2D	Type 2 diabetes
TF	Tissue factor
TNFα	Tumor necrosis factor α
UDP	Urudine diphosphate
USB	Ultrasound biomicroscopy
UTP	Uridine triphosphate
VCAM-1	Vascular cell adhesion molecule 1
VDCC	Voltage-dependent Ca^{2+} channels
VEGF	Vascular endothelial growth factor
VLDL	Very low-density lipoprotein
VSMC	Vascular smooth muscle cell

Introduction

Diabetes Mellitus

Diabetes mellitus (diabetes) is a worldwide disease characterized by high glucose level in plasma. According to the World Health Organization diagnostic criteria, diabetes is defined by fasting plasma glucose ≥7.0 mmol/L (126 mg/dL) or by 2-h plasma glucose ≥11.1 mmol/l (200mg/dL) during an oral glucose tolerance test [1]. More recently, the American Diabetes Association widened the criteria to also allow diagnosis based on hemoglobin A1c (HbA1c) ≥6.5% (48 mmol/mol) or in a patient with classic symptoms of hyperglycemia or hyperglycemic crisis, by a random plasma glucose ≥11.1 mmol/L (200 mg/dL) [2]. This chronic disease is one of the global health emergencies of this century, with an estimated prevalence of 415 million adults (20-79 years old) in 2015 and predicted to rise to 700 million people in 2025 [3].

The most common types of diabetes are type 1 (T1D) and type 2 (T2D). T1D is an autoimmune disease that typically appears in childhood or adolescence. Antibodies destroy the insulin producing β cells of the pancreas, causing deficiency of insulin secretion which leads to increased circulating glucose level in the blood. Therefore, exogenous insulin therapy is the main form of treatment for individuals with T1D. T2D instead appears mainly in adult life and the elevated plasma glucose is caused at least initially by insulin resistance, which is the reduced ability of insulin to mediate the glucose-lowering effects. In the early stages of the disease, more insulin is secreted as a compensatory effect, but in later stages, β cells can become exhausted and insulin levels may decline [2]. On top of that, most individuals with T2D are overweight and dyslipidemic. The abnormalities in the lipid profile are mainly characterized by reduced HDL/LDL ratio and increased plasma triglycerides, while in T1D patients, lipids abnormalities are less observed [4]. Guidelines for treatment of patients with T2D recommend lifestyle changes, either alone or in combination with pharmacologic treatment to reach an appropriate metabolic control. The most often prescribed antidiabetic drug as first line of therapy is the biguanide metformin, but combinations of metformin with other glucose-lowering drugs are considered if HbA1c is 1% or 2% above target. Preferred combinations may include metformin plus sulfonylureas, dipeptidiyl peptidase-4 inhibitor or sodium/glucose

cotransporter 2 inhibitor [5]. Thus, hyperglycemia is a common denominator in T1D and T2D, and results as a consequence of either inadequate insulin secretion and/or diminished tissue responses to insulin.

Recent work from the Lund University Diabetes Centre proposed a more refined patient stratification than simply dividing patients into T1D and T2D [6]. By means of a data-driven cluster analysis of six variables (glutamate decarboxylase antibodies, age at diagnosis, body mass index, HbA1c, and homoeostatic model assessment 2 estimates of β-cell function and insulin resistance), in combination with prospective data from patient records on development of complications and prescription of medication, 5 replicable clusters of patients were identified. These 5 subgroups or clusters have different disease progression and risk of diabetes complications; and may help individualize the treatment or earlier identify those patients at higher risk of developing complications. With the available therapies, diabetic patients still suffer from long-term severe vascular complications, affecting both large and small vessels. Macrovascular diabetic complications are driven by an exacerbated risk and more aggressive presentation of atherosclerosis, leading to stroke, coronary heart disease and peripheral artery disease. Microvascular complications affecting small vessels can lead to blindness (retinopathy), renal failure (nephropathy) and nerve damage (neuropathy) [7, 8].

There is no doubt about the deleterious role of hyperglycemia in the development of microvascular complications. This has been well established by large-scale prospective studies for both T1D and T2D, such as the Diabetes Control and Complications Trial (DCCT/EDIC) [9, 10], the UK Prospective Diabetes Study (UKPDS) [11] and the Steno-2 study [12]. For example, in the DCCT/EDIC trial in T1D patients, intensive insulin treatment to maintain at near-normal levels of glucose reduced the risk of developing retinopathy by 76% [10].

The link between hyperglycemia and macrovascular complications has been more difficult to demonstrate in large scale studies. Data from the Action to Control Cardiovascular Risk in Diabetes (ACCORD) study [13], the Action in Diabetes and Vascular Disease (ADVANCE) study [14], and the Veterans Affairs Diabetes Trial (VADT) [15] failed to demonstrate beneficial effects of intensive glucose control on primary cardiovascular endpoints in T2D. However, further subgroup analyses suggested potential beneficial effects depending on patients' characteristics, again highlighting the heterogeneity of diabetes and the need for stratification to better understand disease pathogenesis. The very recent results from trials assessing the effects of sodium/glucose cotransporter 2 inhibitors [16] and glucagon-like peptide-1 receptor agonists [17, 18], which very effectively reduce HbA1c, substantiate the importance of glucose control for reduction of cardiovascular disease (CVD) morbidity and mortality and clearly suggest a role for hyperglycemia in the pathogenesis of macrovascular disease.

The vascular wall

The vascular wall of arteries and veins is composed of three concentric layers, tunica intima, tunica media and tunica adventitia (Figure 1). The inner layer, tunica intima, is a monolayer of endothelial cells (ECs) orientated in the direction of the blood flow and attached to the basal lamina, which consists of extracellular matrix (ECM) proteins, collagen and proteoglycans. The intima is the main barrier towards the blood, and capillaries are constituted solely by this layer. The media layer, delimitated by the hydrophobic internal and external elastic laminas, is the main structural component of the arterial wall, mostly composed by several layers of circumferentially orientated vascular smooth muscle cells (VSMCs) but also by ECM components, such as collagen and elastin. Together, VSMCs, collagen and elastin, provide mechanical strength and contractile power to the vessel. The most external layer is the adventitia, which consists of a network of connective tissue, nerve endings, fibroblasts and vascular vessels (vasa vasorum).

The abundance of all these components may be slightly different, depending on the vessel type. Large conduit elastic arteries, such as the aorta and iliac artery, are rich in elastin, allowing them to expand. The aorta receives large volumes of blood from the heart transforming the pulsatile blood flow into continuous blood flow by modulating the lumen diameter of the vessel (distensibility property). However, the smaller resistance arteries, in which the tunica media is thicker in relation to the lumen because of a larger number of VSMCs, experience steady blood flow and regulate the vasomotion at the organ level to maintain blood pressure homeostasis [19]. The very small vessels, located for instance in the brain and retina, contain pericytes instead of VSMCs, which support the endothelium and regulate endothelial proliferation and angiogenesis [20].

VSMCs are responsible for important properties of the vessels, such as contraction, compliance, regulation of blood vessel tone-diameter and blood distribution. Within the vascular system, the embryonic origin of the VSMCs is heterogeneous. There are at least seven unique and non-overlapping sources of VSMCs progenitors, each with its own lineage. VSMCs from different embryonic origin respond differently to common stimuli, in a lineage-dependent way [21].

Moreover, the VSMCs origin seems to be an important determinant for the development of vascular disease, as evidenced by clear differences in susceptibility to develop atherosclerosis depending on the origin of the vascular segments studied and less depending on position-dependent hemodynamic effects [21].

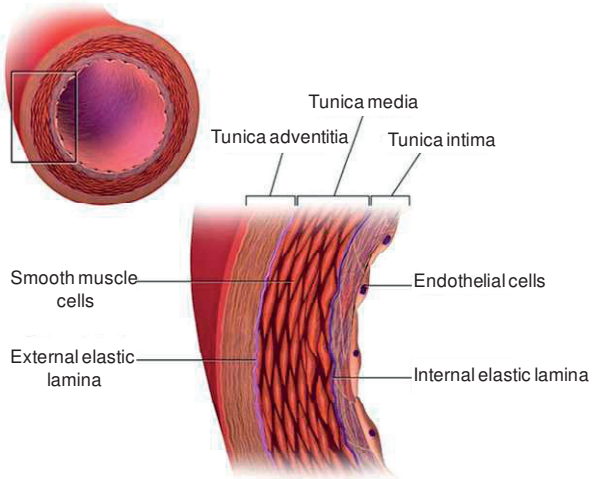

Figure 1. Structure of the wall from a normal large artery. Three different layers compose the wall of a normal artery. The tunica intima faces the lumen, has a single endothelial cell layer and an extracellular matrix basal membrane. The tunica media contains smooth muscle cells and the outermost tunica, adventitia, contains principally connective tissue. Adapted from [22]

Phenotypes of vascular smooth muscle cells

Even though the VSMCs come from diverse lineages, all the cells express the same genes which characterize the VSMC. For instance, smooth muscle α-actin (SMα-actin) is by far the most widely used SMC marker [23]. Classically, two phenotypes of VSMCs are described: contractile or differentiated and synthetic or de-differentiated. In a healthy vessel and under normal conditions, VSMCs are in a differentiated state, with an elongated spindle-shaped morphology, characterized by the expression of quite specific/selective contractile markers, including SMα-actin, smooth muscle myosin heavy chain (SM-MHC), transgelin (Tagln; also known as SM22 or SM22 alpha), calponin (Cnn), caldesmon, desmin and metavinculin [23, 24]. The expression of these contractile genes is regulated directly by the serum response factor (SRF) transcription factor which binds into CArG-box elements placed in the vicinity of transcription start sites [25]. In addition to all the repertory of contractile proteins, they also have contractile regulatory proteins, increased content of collagen I and IV in the ECM, as well as

reduced enzyme matrix modifier (matrix metalloproteinases, MMPs) [19]. Differentiated VSMCs are not prone to migrate, have a low rate of proliferation, low synthesis of ECM components and their primary function is to contract and relax [23, 24].

However, synthetic phenotype of VSMCs with a flattened appearance when in culture, express fewer genes related to contractile proteins and instead, they increase the capacity to synthesize and degrade the ECM components, such as collagen, elastin and proteoglycans [24]. In addition, de-differentiated VSMCs have higher rate of proliferation and easily migrates [19].

In contrast to skeletal or cardiac muscle cells, which are terminally differentiated, VSMCs have the ability to switch their phenotypes reversibly in response to both physiological and pathophysiological changes in the local environment. This phenomenon is defined as phenotypic modulation or phenotypic switching and is associated with changes in a) proliferation rate, b) expression of smooth-muscle characteristic proteins, c) contractility (i.e. calcium signalling, ion channels, pumps) [26-29] and d) VSMCs ultrastructure. Multiple stimuli are capable of inducing the switch, including growth factors, mechanical influences, inflammatory mediators, cell-cell and cell-matrix interactions, reactive oxygen species (ROS), among others [23, 30]. VSMCs phenotypic modulation not only contributes to physiological vascular adaptations associated for example with pregnancy and exercise training, but it plays a major role in numerous pathological processes such as atherosclerosis, restenosis, vascular repair, aneurysms and angiogenesis [23, 31, 32].

Recently, a third phenotype of VSMCs has been described: a synthetic inflammatory phenotype, in which VSMCs besides the synthetic-mentioned characteristics, secrete cytokines (IL-8, IL-6), express cell adhesion molecules (VCAM-1, ICAM-1) and chemokines (MCP-1). This phenotype typically appears in atherosclerosis and contributes to plaque growth and fibrotic cap formation [31].

Although the induction of phenotype modulation is likely to be ascribed to the combined and often synergistic effects of multiple stimuli, it has been demonstrated that high glucose leads to phenotypic modulation, promoting the inflammatory phenotype of the vascular cells by increasing the expression of osteopontin (OPN), vascular endothelial growth factor (VEGF), cytokines and adhesion molecules [33-36]. Hyperglycemia has also been associated with increased contractility and elevated expression of contractile markers in smooth muscle cells (SMCs). One underlying mechanism proposed involves the Rho-protein kinase C (PKC) pathway. Glucose induces Rho-PKC activation in SMCs, in part by elevation of intracellular Ca^{2+} ($[Ca^{2+}]_i$). Rho-PKC activation results in increased phosphorylation of the myosin light chain via inhibition of the light

chain phosphatase, leading to increased SMCs contractility and also results in contractile smooth muscle markers expression by promoting actin polymerization and activation of myocardin/SRF-dependent transcription [37, 38].

Macro- and microvascular complications of diabetes

Macrovascular disease: Atherosclerosis

Atherosclerosis is a chronic inflammatory disease of the arterial wall, which involves a complex response of each cell in the vascular wall to an external stimulus and culminates with the atheromatous plaque formation in the inner layer and narrowing the lumen of the arteries.

From the cellular perspective, the endothelium is the site where atherosclerotic process is initiated, followed by leukocytes (mainly monocytes, macrophages and lymphocytes) and VSMCs.

The endothelium synthesizes and releases bioactive molecules, including vasodilator mediators such as the free radical nitric oxide (•NO), prostacycline (PGI2) and endothelial-derived hyperpolarizing factor (EDHF), but also vasoconstrictor substances, for instance endothelin-1 (ET-1), angiotensin-II (Ang-II), tromboxane 2 (TXA_2). In healthy vessels, the endothelium plays an important role in maintaining vascular homeostasis. For that, the endothelial production of •NO prevails over other substances, avoiding platelet and immune cells adhesion through the production of antithrombotic protein tissue plasminogen activator (tPA) and contributing to maintenance of VSMCs contractile phenotype [39]. Endothelial dysfunction is observed under certain conditions such as hemodynamic perturbations due to changes in shear stress or induction of turbulent flow, and in response to pro-atherogenic stimuli such as hyperglycemia, dyslipidemia and hypertension. Endothelial dysfunction is a pathological condition, characterized by a reduction of •NO bioavailability, and an impairment of anti-inflammatory, anti-coagulant and vascular regulatory properties of the endothelium [40].

The initiating event in the formation of atherosclerotic plaques is a chronic inflammatory reaction caused by endothelial dysfunction (response to injury hypothesis) [41], coupled to subendothelial retention and accumulation of LDL (oxidation hypothesis) [42].

Plaque formation and progression

The atherosclerotic lesion formation is a sequential dynamic process. As it was mentioned before, the first and key event is endothelial dysfunction. Next, as a result, changes in endothelial permeability occur, attributable to the loss of tight junctions, and changes in ECM composition, allowing the entrance of LDL particles into the sub-endothelial space [43]. Next, the LDL gets oxidized (oxLDL) either by metal ions (Fe^{2+}, Cu^{2+}), by specific enzymes such as lipoxygenases and myeloperoxidases, or by generated ROS [44]. OxLDL lead to ECs activation, characterized by the expression of adhesion molecules in the cell surface, such as intercellular adhesive molecule-1 (ICAM-1), vascular-cell adhesion molecule-1 (VCAM-1) and P- and L-selectin, increasing the adhesive properties of endothelium. Consequently, monocytes are captured from the circulation and together with resident monocytes, they mature and differentiate into macrophages, which in the presence of high concentrations of oxLDL, can take up these lipoproteins through scavenger receptors to become foam cells [43, 45]. These macrophages (predominantly M1 subtype) do not constitute a passive oxLDL storage. Indeed, they actively promote inflammation and T lymphocyte activation, through the secretion of pro-inflammatory cytokines such as interleukin-1β (IL-1β), interleukine-6 (IL-6) and chemoattractant mediators, like monocyte chemoattractant protein-1 (MCP-1). After that, a vicious circle results, since these cytokines act on the endothelial cells promoting the expression of more adhesion molecules and facilitating the transmigration of monocytes to the subendothelial space. In addition, T cells produce interferon-ɣ (IFN-ɣ) and tumor necrosis factor alpha (TNF-α), which in turn activate macrophages promoting the inflammatory response [40]. Recruitment of VSMCs from the tunica media is also involved in the atheroma formation. VSMCs migrate into the intima and proliferate in response to growth factors secreted by foam cells, ECs and macrophages [44]. In the intima, the VSMCs produce ECM molecules, including collagen and elastin, which build up a fibrous cap that surrounds a collection of foam cells. Accumulation of foam cells leads to the formation of a fatty streak, the hallmark of early atherosclerotic lesions [4]. In more advanced plaques, some of these foam cells and VSMCs die (for example, by apoptosis) and as result of the inefficient clearance of dead cells, accumulation of extracellular lipids and cellular debris arises, forming a necrotic core. MMPs released from activated macrophages digest collagen and cause thinning of the fibrous cap making the plaque more vulnerable to rupture and thrombus formation in the vessel. This could have fatal consequences, if the thrombus occludes coronary arteries or arteries in the brain, causing ischemia in the heart or brain, respectively [43].

Atherosclerotic process exacerbated by diabetes

Epidemiological studies have associated both T1D and T2D diabetes with premature formation and diffuse distribution of atherosclerotic plaques. Diabetic patients have 2 to 4-fold increase in the risk of cardiovascular events. In fact, diabetes abolishes the benefit of women compared with men related to gender protection from CVD, at the age when it should exist. Moreover, the incidence of myocardial infarction in diabetic patients is as high as in non-diabetic patients with previous myocardial infarction events. Besides, the risk of stroke rises more than 150% for diabetic patients, which also exhibit reduced survival after a stroke [4, 46].

The metabolic changes in diabetes (hyperglycemia, insulin resistance and elevated free fatty acids) lead to severe atherosclerotic lesions, in which the initiation and progression processes are accelerated and plaques are more vulnerable to rupture.

Post-mortem studies have revealed that diabetic plaques are associated with a higher content of inflammatory infiltrated cells, a greater apoptosis of VSMCs and macrophages, as well as a larger necrotic core size. Furthermore, increased plaque calcification was pointed out as a characteristic of atherosclerotic lesion from T2D diabetes rather than T1D [47].

The molecular mechanisms leading to exacerbated atherosclerosis in diabetic patients are not fully delineated, however, hyperglycemia has been suggested as a possible driver. High glucose seems to exacerbates the inflammatory response in all vascular cells, promote endothelial dysfunction, VSMCs phenotypic modulation and more complex lesion formation.

Hyperglycemia has been associated with endothelial dysfunction. As it was mentioned before, the endothelial dysfunction is the consequence of impaired endothelial •NO production. It has been shown that insulin resistance and hyperglycemia markedly reduced the activity of endothelial •NO synthase (eNOS), either by reducing the availability of the substrate, L-arginine or by uncoupling of eNOS due to degradation of its cofactor by $ONOO^-$ (formed from the reaction of •NO and $O_2^{\bullet-}$) [48].

In diabetes, endothelial dysfunction leads to an augmented production of vasoagonist mediators such as ET-1 and Ang-II, an increased expression of inflammatory molecules (i.e. IL-6, IL-8) and an increased expression of adhesion molecules (VCAM-1, MCP-1, ICAM-1, TF) in the ECs [46, 48]. These adhesion molecules in the activated ECs, potentially explain the effect of diabetes on macrophage accumulation in the lesion region. Moreover, macrophages responded to high glucose, activating NFκB, increasing the expression of pro-inflammatory molecules including IL-6, IL-1β, CD36 (scavenger receptor for modified LDL) and MCP-1 [46, 49]. Furthermore, studies done in diabetic rats and patients,

demonstrated that macrophages present in the aorta lesion increased the expression and activity of MMP-9, which could weaken the ECM of the plaque, turning it more unstable [49].

On top of that, VSMCs experience a phenotype switching in response to hyperglycemia, which is crucial for lesion development, plaque composition and stability. The change from contractile into inflammatory phenotype brings about loss of differentiated markers (SM-MHC, Tagln or SM22, SMα-actin, among others) and therefore increases the capacity of proliferation and migration [49, 50]. This is also accompanied by increased expression of cytokines, adhesion molecules, chemokines in response to high glucose, but also expression of the matrix cytokine OPN and secreted growth factors like VEGF and platelet-derived growth factor (PDGF) [31, 32, 50, 51].

All these inflammatory mediators, released by macrophages or by VSMCs, induce migration of the latest into the intimal space. At the early stage of the plaque, the VSMCs secrete collagen that contribute to create and stabilized the fibrous cap. Nonetheless, in mature plaques, VSMCs as well as macrophages within the lesion release MMPs that degrade the collagen thus making the plaque prone to rupture. Identification of molecular determinants, circulating and imaging biomarkers of plaque instability is an intensive area of research, to determine individuals at risk for plaque rupture [52-55]. Additionally, plaque calcification might occur in the advanced stage of the atherosclerosis process. This is a consequence of calcium mineral deposition in necrotic areas of the lesion and the presence of VSMCs differentiated into osteoblast-like cells induced by pro-inflammatory cytokines such as oncostatin M (OSM) [56].

Microvascular disease: Diabetic Retinopathy

Diabetic retinopathy (DR) is a long-term microvascular diabetic complication and the most frequent cause of blindness in the adult population. Epidemiological studies have shown that around 35% of the diabetic population develop DR, and its prevalence is much higher in T1D than in T2D. The major risk factors for DR are hyperglycemia, hypertension and dyslipidemia, but also the non-modifiable factors such as the ethnic origin, duration of diabetes, pregnancy and puberty [57-59]. Even though the full picture of molecular and cellular mechanisms underlying DR is missing, both clinical and experimental studies, have emphasised the role of glucose as a key factor [60, 61]. The same pathways involved in glucose-induced cellular toxicity in vascular cells in arteries, are triggered by diabetes in the retinal ECs, in combination with impaired cellular antioxidant systems [62].

The retina is a vascularised neural tissue, composed by a network of neurons (photoreceptors, bipolar, horizontal, amacrine and ganglional cells), glia

(astrocytes, Müller cells and microglial cells), and blood vessels, which represent around 95% and 5% of the whole retina, respectively. The neuroglial cells generate vision whereas the blood vessels provide nutritional support for this function [60, 63].

The retinal vessels are capillaries composed of non-fenestrated ECs surrounded by pericytes and glial end feet. The complex and tight cell-cell interactions between ECs are essential to maintain the retinal homeostasis under normal situations, since they conform the inner blood-retinal barrier (BRB). These interactions include tight junctions, adherent junctions and gap junctions, formed for instance by occludins, vascular endothelial-cadherin (VE-cadherin) and connexons (or connexin hemichannels), respectively [64, 65]. The outer BRB is composed of tight junctions between retinal pigmented epithelial cells, which together with the inner BRB they shape the BRB. Pericytes, are also involved in the preservation of vascular homeostasis, including regulation of angiogenesis by controlling endothelial proliferation, of blood flow through contractile mechanisms and structural stabilization of the vasculature and of vascular permeability [66]. It has been described, that pericytes are a heterogeneous population, which acquire specific roles and vary morphologically depending on their location. Along the arterious-venous axis, there are transitional pericytes (pre and post-capillaries) and mid-capillary pericytes [67, 68]. They have in common the expression of platelet-derived growth factor receptor β (PDGFRβ) [68]. Transitional pericytes (and some mid-capillary pericytes) shared contractile SMC characteristics and express SMα-actin [68]. Non-contractile pericytes deprived of SMα-actin act as regulators of ECs and as mediators between the vascular and neural parts of the retina [20].

Although dysfunctional neurovascular crosstalk play a key role in DR [69], robust evidence have associated this complication with structural and functional changes in the vasculature. These changes occur in two stages, an early non-proliferative and late proliferative stage. The early stage is characterized by vaso-regression, increased vascular permeability and formation of microaneurysms. Prolonged exposure to diabetes leads to an inflammatory response in the ECs, which become activated and start expressing leukocytes adhesion molecules (i.e. ICAM-1, VCAM-1, E-selectin) [70]. This leukocyte-endothelium interaction results in physical occlusion of capillaries, generating localized ischemic regions. Another functional consequence of diabetes at this early stage of DR is the thickening of the basement membrane, the loss of pericytes (apoptosis) and subsequently the loss of ECs, producing acellular capillaries, which also are non-perfusable. Interestingly, hypoxia is one of the most potent stimulus for increasing the expression of VEGF in various cells [71, 72]. VEGF disrupts the tight junctions between ECs resulting in breakdown of the BRB, vascular leakage and increased vascular permeability, and the development of retinal edema, which is the earliest clinical feature of non-proliferative DR [65, 71, 73]. Finally, the late proliferative

stage is characterized by neovascularization, as a compensatory response to ischemia and metabolic deficiency from vasoregression. This stage is driven by pro-angiogenic growth factors, such as VEGF, which stimulate the defective formation of new and fragile capillaries that can result in blurred vision and even blindness when retinal haemorrhages occur [69, 71].

High glucose levels induce cellular damage

Under normal extracellular glucose levels, cells metabolize glucose through the glycolytic pathway to obtain energy in ATP form. Glucose uptake is mediated by glucose transporters (GLUTs) in the plasma membrane. There are several GLUT isoforms, the conventional GLUT1-5 and the novel GLUT6-14. Glucose transporters have different kinetic properties, cellular localization and functional regulation[74]. The predominant transporter expressed in VSMCs and ECs is GLUT1, but depending on the VSMCs phenotype, the relative abundance of the other GLUT isoforms can vary. While GLUT1 is the predominant transporter in synthetic VSMCs, GLUT10 is also expressed at almost the same proportion than GLUT1 in differentiated human aortic VSMCs [74].

Since the 40s, it has been known that high extracellular glucose exerts deleterious effects on many cells [75]. It was proposed that these effects were predominant in cells in which the influx of glucose was not dependent on insulin, such as vascular cells, and that this was because these cells were unable to efficiently down-regulate the entrance of glucose into the cell under hyperglycemic conditions [76]. However, cultured VSMCs and ECs have been shown to exhibit an auto-regulatory mechanism that can lead to down-regulation of GLUT1 expression when cells are exposed to a glucose overload. The down-regulation of GLUT1 was faster in VSMCs than in ECs (4 hours vs. 36 hours) [77] and it was shown to be at the transcriptional and post-transcriptional levels [78, 79]. However, this has not yet been demonstrated *in vivo*.

Oxidative stress plays a critical role in the progression of diabetes-induced cellular injury. Elevated intracellular glucose can results in an increased production of ROS, engaging five major pathways implicated in the development of diabetic complications [80]. Increased ROS leads to over activity of: a) the polyol pathway, b) the hexosamine pathway and c) PKC isoforms and to [79] d) increased intracellular formation of advanced glycation end products (AGEs) and e) increased expression of the receptor for AGEs (RAGEs) and activating ligands [8, 81].

Interestingly, ROS has been shown to prevent the down-regulation of GLUT1 in cultured ECs under hyperglycemic conditions. Instead, an up-regulation of GLUT1 expression was observed in the ECs exposed to high glucose levels, accelerating endothelial dysfunction, which is one characteristic feature in the development of diabetic vascular disease [82].

ROS are a variety of molecules and free radicals (chemical species with at least one unpaired electron) derived from molecular oxygen. ROS include radical superoxide anion ($O_2^{\bullet-}$), hydroxyl radical ($^{\bullet}OH$) and hydrogen peroxide (H_2O_2) [81]. The primary source of *in vivo* $O_2^{\bullet-}$ generation is the mitochondria, through one-electron reduction of oxygen in the respiratory chain, but this $O_2^{\bullet-}$ can amplify its damaging effects, activating other superoxide production pathways. For instance, amplification includes activation of various NADPH oxidases (NOXs) in vascular cells and uncoupling of endothelial nitric oxide synthase (eNOS) dimmers to monomers in ECs [62].

Under physiological conditions, ROS species function as signalling molecules required for cellular homeostasis for example for intracellular communication and cell differentiation [83]. However, under hyperglycemic conditions, ROS overproduction occurs for too long, at inappropriate sub cellular locations and therefore the intrinsic antioxidant capacity is overwhelmed, leading to cellular damage.

$O_2^{\bullet-}$ is the precursor of most of the ROS, due to the fact that it is dismutated to H_2O_2, either spontaneously or through a reaction catalysed by superoxide dismutases (SOD). H_2O_2 has low reactivity but it can penetrate cellular membranes and generate one of the strongest oxidants, the radical $^{\bullet}OH$ via Fenton's reaction ($H_2O_2 + Fe^{2+} \rightarrow Fe^{3+} + OH^- + {}^{\bullet}OH$) [84]. This radical cleaves bonds in macromolecules, inducing DNA strand breaks and thereby a DNA repair mechanism is activated, including the poly(ADP-ribose) polymerase (PARP). Normally, PARP resides in the nucleus in an inactive form, until DNA damage occurs. Once activated, PARP divides the NAD^+ molecule into its two components: nicotinic acid and ADP-ribose. Then, the glycolytic enzyme glyceraldehyde 3-phosphate dehydrogenase (GAPDH) is modified because the polymers of ADP-ribose made by PARP accumulate on GAPDH, leading to a decrease in its activity. Since, GAPDH is essential for oxidation of glyceraldehyde-3 phosphate into 1,3-diphosphoglycerate, a reduced GAPDH activity results in accumulation of upstream metabolites from glycolysis. These metabolites are redirected into the four pathways of glucose over utilization(Figure 2) [85-87].

Polyol Pathway

In an hyperglycemic environment, an increased enzymatic reduction of glucose to the sugar alcohol sorbitol takes place and then sorbitol is converted to fructose. The first reaction is catalyzed by the aldose reductase enzyme that uses NADPH as a cofactor[62]. Interestingly, NADPH is also required for regenerating reduced glutathione (GSH), an intracellular antioxidant. Therefore, an increased depletion of this cofactor by the aldose reductase could exacerbate intracellular oxidative stress. Diabetic apolipoprotein E (ApoE) deficient mice that overexpress human aldose reductase develop accelerated atherosclerosis, providing evidence of a role for the polyol pathway in the development of diabetic cardiovascular complications [88, 89].

Hexosamine pathway

Excesses of intracellular glucose provide increased fructose-6 phosphate, which is finally converted to UDP-*N*-acetylglucosamine-6-phosphate (UDP-GlcNAc) by the enzyme *O*-GlcNAc. This substrate can increase the formation of *O*-linked glycoproteins, causing modifications in proteins and therefore resulting in a variety of changes in gene expression that contribute to the pathogenesis of diabetes complications [62, 81].

PKC activation

Under hyperglycemic conditions, the *de novo* synthesis of diacylglycerol (DAG) from glyceraldehyde-3-phosphate is elevated and leads to activate PKC. PKC activation in ECs affects the expression of several molecules through the transcription factor NF-$_{K}$B, activates NADP(H) oxidases and ET-1, increases the expression of IL-18 and VCAM-1, inhibits the expression of endothelial NOS (eNOS). In VSMCs, PKC activation increases the expression of VEGF and increases plaque formation [62, 90, 91].

AGEs formation

Advanced glycation end-products (AGEs) arise from non-enzymatic reactions between proteins and glucose. Three potential pathways lead to intracellular AGEs formation: auto-oxidation of glucose to glyoxal, decomposition of the Amadori products to 3-deoxyglucosone and the fragmentation of glyceraldehyde-3 phosphate to methylglyoxal (MG). The latest has been postulated to be the major source of intracellular and plasma AGEs. These AGEs precursors react with amino groups (lysine and arginine) of proteins, generating structural modifications and

causing cellular damage basically through three mechanisms: changes in protein function, impaired interaction between ECM components and increased expression of RAGEs on the cell surface [62].

The binding of AGEs to RAGEs promote and perpetuate cell injury by raising intracellular oxidative stress [92] and triggering inflammatory pathways which contribute to the atherosclerosis process [93].

Even though high glucose is not the exclusive source of AGEs, which can be generated endogenously by aging, lipid oxidation and exogenously by processed food intake and tobacco smoke, elevated levels of MG have been found in diabetic renal pathology [94] and have also been associated with rupture-prone atherosclerotic human plaques [95]. Moreover, intracellular AGEs formation increased a 5.4 fold in cultured bovine ECs exposed to 30mM of glucose [96].

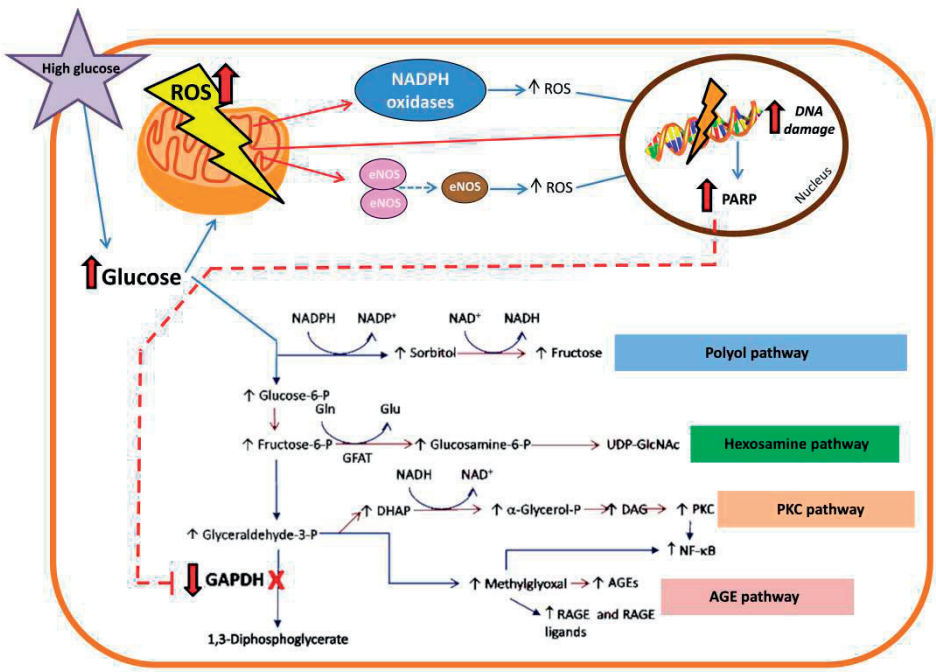

Figure 2. Four pathways suggested for hyperglycemia-induced damage through overproduction of reactive oxygen species (ROS). Excess of intracellular glucose causes mithochondrial overproduction of ROS, which in turn can be amplified by activation of NADPH oxidases and uncoupling of endothelial nitric oxide synthase (eNOS). ROS difusse into the nucleus, damage the DNA and activate poly(ADP-ribose) polymerase (PARP). This reduces glyceraldheyde-3-phosphate dehydrogenase (GAPDH) activity, causing up-stream accumulation of metabolites from glycolysis, which then diverted into the four pathogenic signalling pathways. DAG, diacylglycerol; DHAP, dihydroxyacetone phosphate; GFAT, glutamate fructose-6-phosphate amidotransferase; Gln, glucosamine. Modified from [62].

However, in all mammalian cells, MG is metabolized to unreactive D-lactate by the glyoxalase system. Glyoxalase I (GLO1) is a cytosolic enzyme and the first member of glyoxalase system, responsible for reducing reactive MG, playing a detoxifier role. Experimental studies have shown that overexpression of GLO1 in both cultured rat and human aortic ECs, was able to prevent the up-regulation of RAGE expression in cells exposed to high glucose level [97], as well as decreased the level of plasma AGEs and oxidative stress markers in the urine and tissues of diabetic rats [98]. However, studies performed in diabetic $ApoE^{-/-}$ mice which overexpressed GLO1 (transgenic mice), showed that increased GLO1 activity in ECs, VSMCs and macrophages was insufficient to protect against the initiation and progression of accelerated atherosclerosis in the aortic arch or thoracic aorta [99]. Indeed, the number of complex lesions in the aortic root was not different from the diabetic non transgenic $ApoE^{-/-}$ mice [100]. Other studies however, provided evidence of reduced GLO1 expression and activity and increased formation of AGEs in ruptured human carotids plaques [95, 101]. Also, GLO1 overexpression has been shown to reduce the expression of endothelial dysfunction markers in mesenteric arteries and attenuate early markers of renal dysfunction in diabetic rats [102].

Oxidative stress and NOXs in the vasculature

A large body of evidence have demonstrated elevated oxidative stress in diabetes, causing a complex dysregulation of cell metabolism and cell-cell homeostasis. The oxidative stress results from an imbalance between oxidants species and antioxidants, either by overproduction of oxidants, impaired antioxidant system, or by a combination of these factors [103]. Oxidants include the above described ROS and reactive nitrogen species (RNS). The latest refers to all species derived from the radical •NO, for instance, the very powerful oxidant peroxynitrite ($OONO^-$), which is the product of reaction between •NO and $O_2^{\bullet-}$ [84, 104]. Both, ROS and RNS, can react with multiple cellular components, such as proteins, lipids and DNA, to generate reversible or irreversible oxidative modifications, which contribute to the development of atherosclerosis and other vascular pathologies [45, 104]. A critical event that precedes the development of atherosclerosis is endothelial dysfunction. Increased formation of $O_2^{\bullet-}$ by NOXs, reduces the availability of •NO, given that $O_2^{\bullet-}$ quickly react with •NO to produce oxidative species, which in turn can promote the endothelial dysfunction.

Cells have antioxidant enzymatic and non-enzymatic systems to protect against the toxic effect of oxidants. The enzymatic mechanism, which provides endogenous antioxidant capacity to the cell, includes SOD, catalase (the major H_2O_2 detoxifying enzyme, which dismutes it to O_2 and H_2O) and glutathione peroxidase. The non-enzymatic mechanism involves exogenous substances such as ascorbate,

α-tocopherol, carotenoids, flavonoids [84, 104]. Under normal conditions, both mechanisms work together to maintain a balance between ROS generation and clearance, but in pathophysiological conditions, ROS production exceeds the scavenger capacity of the antioxidant systems, resulting in increased oxidative stress and subsequently, cellular damage [45].

Apart from the non-enzymatic *in vivo* $O_2^{\bullet-}$ generation by the mitochondria, the membrane-bound NADPH (nicotinamide adenine dinucleotide phosphate) oxidase or NOX, is the major enzymatic source of $O_2^{\bullet-}$ in vascular cells [84]. In mammals, NOX is a family of enzymes composed by seven isoforms, but only four, NOX1, NOX2, NOX4 and NOX5 are normally expressed in the vasculature, with NOX5 not being expressed in rodents. All enzymes except NOX4 catalyze the $O_2^{\bullet-}$ production from O_2 and NADPH, while NOX4 instead produces large amounts of H_2O_2 [105, 106]. NOXs are differentially expressed in ECs, VSMCs, fibroblast and in the context of atherosclerosis, the expression profiles have been show to vary depending on the disease stage [107]. Although under physiological conditions the rates of ROS production by NOXs in the vasculature is low compared with the high production in neutrophils and macrophages, NOXs activities can be increased both acutely and chronically in response to several stimuli, including hyperglycemia.

It has been reported that NOX1 is involved in signal transcription and cell proliferation, and increased expression of NOX1 and NOX2 in vascular cells and macrophages has contributed to atherosclerosis development and vascular disease [106, 108]. However, the role of NOX4 in vascular disease remains controversial. Recently, an atheroprotective role of NOX4 was described both in human and mouse [107, 109]. It was shown that NOX4-derived H_2O_2 could activate eNOS and eNOS expression was found to be low in $LDL^{-/-}NOX4^{-/-}$ mice [108]. Moreover, NOX4 was implicated in the regulation of VSMC differentiation, suggesting an homeostatic function [106]. In mouse kidney fibroblast instead, hyperglycemia resulted in increased NOX2 and NOX4 mRNA and protein expression and ROS generation. Interestingly, this seemed to require the activation of the calcineurin-NFAT pathway [110].

Nuclear factor of activated T cells (NFAT)

NFAT is a family of transcription factors that arose with the origin of vertebrates (approximately 500 million years ago) after the recombination of an ancient precursor with a Rel domain, so they are evolutionarily related to Rel/nuclear factor kappa B (NF-κB) [111]. Although NFAT proteins were first described in T-lymphocytes as inducers of cytokine gene expression [112], it is well known that

they play important roles outside the immune system, including the cardiovascular system. NFAT is essential for normal cardiac valve and septum formation [113], proper anatomical organization of the vasculature [114], myocardial hypertrophy [115] and for establishing fast or slow skeletal muscle-phenotype [116].

The NFAT family consists of five members. Four of them (NFATc1-NFATc4) are well characterized and dependent on Ca^{2+}/calcineurin for activation. However, the fifth member, NFAT5, which shares only partial structural and functional characteristics with the other family members, lacks the sensitivity to calcineurin (CaN) activity[117]. NFAT5 is activated by changes in osmolarity [117] and biomechanical stretch [118], and has been shown to be involved in the regulation of osmoprotective genes [117].

Structurally, NFATc1-c4 proteins consist of four domains schematically visualized in Figure 3, the NFAT homology region (NHR) that serves regulatory functions, the Rel homology domain (RHD) that mediates DNA binding, an amino (NH_2)-terminal transactivation domains (TAD) rich in prolines and acidic residues, and a variable carboxyl (COOH)-terminal region. The regulatory region contains a CaN binding motif (PxIxIT), a serine-rich region (SRR-1), serine-proline (SP) motif repeats (SPxx repeats, SRR-2 and KTS) and one or multiple nuclear localization signals (NLS) [119]. The RHD domain, contains highly conserved sequences with a 3D structure very similar to that of the Rel transcription factors. This domain is not only responsible for DNA-binding, but also for interaction with nuclear partners that stabilize the otherwise weak NFATc-DNA interaction [112].

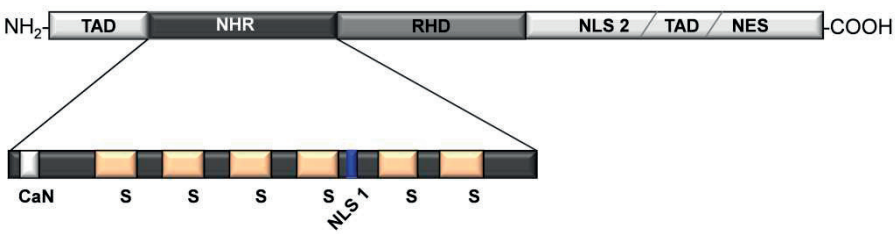

Figure 3. A schematic diagram of NFAT structure. It has two transactivation domain (TAD), a Rel homology domain (RHD), which carries the DNA-binding part of the proteins and an NFAT homology region (NHR). The regulatory domain contains several phosphorylation sites (noted as S) and a docking site for calcineurin (CaN). The proteins also have two nuclear localization signals (NLS1/2) and a nuclear export signal (NES). Modified from [120].

The TADs make possible the NFAT interaction with proteins of the transcription machinery. In addition, these domains experience important post-translational

modifications, which could confer functional specificity to each NFAT isoform [112, 120].

Although structurally NFAT proteins share conserved regions, they differ significantly in their (NH_2)- and (COOH)-terminal portions, potentially giving rise to 6-24 alternative transcripts for each NFAT isoform [121]. Differences have been found in NFAT isoforms expression, in the activation and inactivation requirements (i.e. the identity of the export kinases that phosphorylate the serine rich regions, the number of dephosphorylation sites required for activation), as well as in biological functions [120].

NFAT activation and its regulation

NFAT activation is determined by its subcellular localization (Figure 4). Under non-stimulated conditions, NFAT is in the cytosol and the serine-rich regions in the regulatory domain are highly phosphorylated [120].

An increase in $[Ca^{2+}]_i$, induced by a variety of stimuli, leads to activation of the Ca^{2+}-calmodulin-dependent phosphatase CaN [122]. Activated CaN dephosphorylates NFAT, inducing a conformational change that exposes the NLSs while masking the NES [120]. Under this alternative conformation, the NLSs bind to importins which rapidly transport NFAT into the nucleus through the nuclear pore complex [123]. Subsequently, NFAT binds to DNA and regulates gene expression.

Upon Ca^{2+} signalling termination, NFAT can be rephosphorylated by constitutive and/or inducible kinases, leading to unmasking of the NES and export of NFAT back to the cytosol with the aid of the export protein Crm-1 [120, 124].

NFAT nuclear accumulation and hence, NFAT activation is thus determined by the balance between the phosphatase activity of CaN and that of NFAT export kinases[120]. In vascular smooth muscle, unless constitutively elevated nuclear export activity is inhibited, NFAT does not accumulate in the nucleus even in the presence of high $[Ca^{2+}]_i$ [125].

Several protein kinases have been shown to phosphorylate NFAT. These include protein kinase A (PKA), glycogen-synthase kinase 3β (GSK3β) [126], JUN N-terminal kinases (JNK) [127], p38 mitogen-activated protein kinase (p38 MAPK) [128, 129], extracellular signal regulated kinases (ERK), casein kinase (CK1 and CK2) [130], dual-specificity tyrosine-phosphorylation regulated kinase (DYRK) [131] and mammalian target of rapamycin (mTOR) [132]. NFAT family members are differentially regulated according to the isoform, stimuli and the cell types, which means that distinct motifs and serine sites (for instance, Ser-Pro repeats, Ser^{172}, Ser^{187}, etc.) of NFAT regulatory domain can be phosphorylated by some of

these kinases, counteracting NFAT activation. For example, in VSMCs, JNK2 and GSK3β are involved in NFATc3 nuclear export [125, 133], whereas in ECs, NFATc3 is moved more rapidly back to the cytosol than NFATc1 after ATP stimulation, regulated by p38 MAPK in addition to JNK2 and GSK3β [134].

In the nucleus, NFAT proteins bind to DNA in the consensus sequence GGAAA (either in forward or reverse orientation) present in the target promoter elements. NFAT can bind to DNA as monomer, but the most common way is to bind together with partner proteins [112]. The weak individual binding of NFAT to DNA is due to the low affinity between them, but after forming a cooperative complex with partner proteins, DNA-binding becomes considerably more stable.

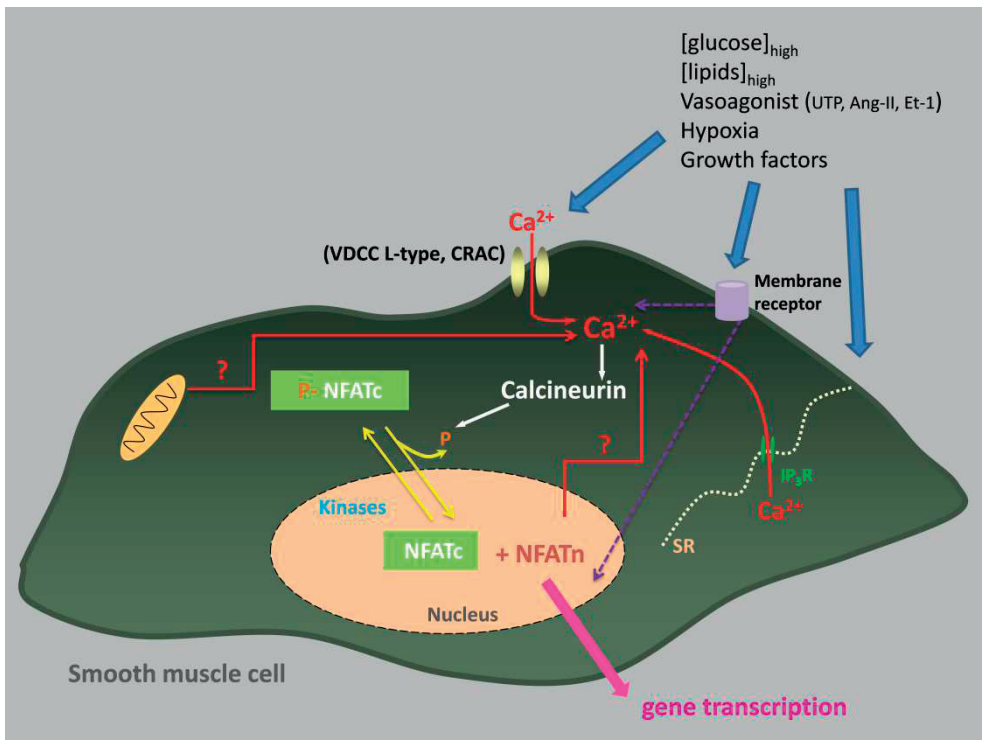

Figure 4. Schematic representation of basic elements involved in the regulation of NFATc3 activity in smooth muscle. Intracellular Ca^{2+} increases in response to different stimuli and activates CaN, which dephosphorylates cytoplasmic NFAT, leading to rapid import of the protein to the nucleus. Ca^{2+} release via IP_3R is necessary for an efficient NFAT nuclear accumulation. Although mitochondria control the spatial and temporal shape of Ca^{2+}, it is not fully known how much this modulation influences NFAT activation [135].It is also possible that NFATc3 activation additionally requires nuclear Ca^{2+} [136].Once in the nucleus, NFAT combines with partner proteins (NFATn) and binds to DNA in order to induce gene transcription. Opposing the action of CaN are kinases, which promote NFAT export from the nucleus by rephosphorylating the protein. SR: sarcoplasmic reticulum; VDCC: voltage dependent-calcium channels; CRAC: calcium-release-activated channels; UTP: uridine triphosphate; Ang-II: angiotensin II; Et-1: endothelin-1.

The partner proteins that have been reported include the activator protein-1 (AP-1) with its bZIP elements Fos and Jun, myocyte enhancer factor 2 (MEF2), members of the Gata family, FoxP3, RUNX1 and cAMP response element-binding protein 1 (CREB1) [112, 137-139]. After binding to DNA, NFAT not only promotes target gene expression, but it has also been shown to repress gene expression. One such example is the complex formation between NFAT and FoxP3, which leads to repression of IL-2 expression in T cells [139].

Requirements for NFAT activation

NFAT activation provides a direct link between intracellular Ca^{2+} signalling and gene expression. The molecular mechanisms that lead to increase $[Ca^{2+}]_i$ vary with the cell type and tissue. Consequently, NFAT activation is sensitive not only to the way of Ca^{2+} entry, but also to the amplitude, duration and localization of calcium signal (calcium spatial-temporal organization). The ability of Ca^{2+}-dependent transcription factors to dissect the spatio-temporal information in the Ca^{2+} signalling is key, given that Ca^{2+} is not only a second messenger involved in excitation-transcription coupling (E-T coupling) but also plays a central role in other cellular functions, such as in excitation-contraction coupling (E-C coupling) in contractile cells and excitation-secretion coupling (E-S coupling) in secretory cells.

In non-excitable cells, such as lymphocytes and ECs, Ca^{2+} influx occurs mainly through opening of plasma membrane calcium-release-activated channels (CRAC), also known as SOCE (store-operated calcium entry). Ligand stimulation of a G-protein coupled receptor (GPCR) results in activation of phospholipase C (PLC), which hydrolyses a membrane component phosphatidylinositol-4,5-biphosphate, leading to the burst of inositol-1,4,5-triphosphate (IP3) and diacylglycerol (DAG). This augmentation of IP3 induces a transient release of Ca^{2+} via IP3 receptors (IP3R) from internal stores, such as the endoplasmic reticulum. The store depletion of Ca^{2+} is sensed by STIM (stromal interaction molecules) proteins, which activate CRAC channels and generate a sustained low-amplitude increment of $[Ca^{2+}]_i$ that activates NFAT in these cells [140, 141]. NFAT isoforms were recently found to be differentially activated by distinct sub-cellular Ca^{2+} signals. In rat basophilic leukemia cells (RBL-1) and in human embryonic kidney 293 cells (HEK293), NFATc2 was activated by cytoplasmic Ca^{2+} microdomains from CRAC channels, whereas NFATc3 required both Ca^{2+} from CRAC channels and additional IP3-dependent nuclear Ca^{2+} mobilization from the inner envelop [136].

On the other hand, in excitable cells, such as neurons and striated muscle cells, the dominant Ca^{2+} source for NFAT activation is through voltage dependent calcium

channels (VDCC) [141]. In hippocampal neurons, NFATc4 was activated by depolarizations induced either by electrical activity or by elevated extracellular potassium, via transient increases of Ca^{2+} through L-type voltage-gated calcium channels [142] or NMDA (*N*-methyl-D-aspartate) receptor [143]. In skeletal muscle, depolarization also triggers the activation of NFAT, through extracellular Ca^{2+} entry and Ca^{2+} release by ryanodine receptors (RyR) [144]. Experiments using electrical field stimulation revealed that the frequency and number of pulses applied gave rise to different patterns of $[Ca^{2+}]_i$ engaging either RyR, IP_3 receptors (IP_3Rs) or both. The authors also showed that while NFAT activation required Ca^{2+} release from RyRs, activation of ERK or cAMP response element-binding protein required Ca^{2+} release from IP_3Rs and NF-κB required Ca^{2+} release from both channels. Increasing firing rates were directly correlated with the degree of NFAT nuclear accumulation.

Unlike immune and skeletal muscle cells or neurons, cardiac myocytes have continuously high levels of global $[Ca^{2+}]_i$, and cyclically regulated calcium-induced calcium release (CICR) transients critical for contraction. The exact mechanisms by which E-T and E-C coupling are separated are still not 100% clear. In cardiac myocytes, NFAT has been shown to mediate pathological (not physiological) cardiac hypertrophy leading to progressive heart failure [145]. In this context, T-type voltage-dependent Ca^{2+} channels [146] and transient receptor potential channels [147] seem to contribute to activation of NFAT. Angiotensin II, aldosterone, and norepinephrine, all known to increase the frequency of the $[Ca^{2+}]_i$ oscillations in cardiomyocytes, were shown to effectively activate NFAT-dependent transcriptional activity [148].

In SMCs, depolarization-induced global Ca^{2+} increases are not sufficient for activating the calcineurin/NFAT pathway [149]. Instead, activation of NFAT requires IP_3 release of Ca^{2+} from intracellular stores [150]. NFAT is effectively activated by GPCR stimulation with vasoagonists or growth factors capable to stimulate both the influx of extracellular Ca^{2+} through L-type VDCC and Ca^{2+} release from the sarcoplasmic reticulum through IP3R channels. Ca^{2+} release from RyRs in the form of Ca^{2+} sparks, exerted instead an inhibitory effect on NFAT nuclear accumulation, that was independent of their hyperpolarizing effects mediated by the activation of Ca^{2+}-activated K^+ channels [150]. Moreover, it has been described that intracellular Ca^{2+} signalling differs depending on VSMCs phenotype. For instance, cells with a contractile phenotype express more L-type VDCC, maintaining the resting cytosolic Ca^{2+} low and allowing dynamic changes of Ca^{2+} in the spatial-temporal domain for NFAT activation. Meanwhile synthetic VSMCs have reduced voltage dependent Ca^{2+} entry and their intracellular Ca^{2+} signalling mechanisms are more similar to non-excitable cells[27]. Along with a down-regulation of L-type VDCCs, an increased expression of SOCE characterizes VSMC phenotypic modulation towards a more proliferative state

[151, 152]. A global portrait of the changes in ion channel expression involved in the proliferative response of VSMCs also demonstrated significant alterations in voltage-dependent potassium channels also [28].

For NFAT nuclear accumulation and efficient transcriptional activation in VSMCs, the stimulus needs to provide the appropriate Ca^{2+} signalling modality and also suppress the constitutively elevated activity of NFAT nuclear export kinases JNK, GSK3β and PKA [125, 135].

Several studies have now demonstrated that potent stimuli for NFAT activation in VSMCs are high extracellular glucose, high oxLDL and VLDL, GPCR vasoagonists (i.e. UTP, Et-1, prostaglandin F2α, Ang-II and thrombin) and growth factors, such as PDGF and epidermal growth factor (EGF), with variable efficiencies depending on the arteries or cell-types (Figure 4) [133, 153-157].

NFAT in the vasculature

NFAT genes are expressed in a large number of tissues and the expression levels and patterns for each NFAT isoform are rather different. All NFAT isoforms are strongly expressed in the immune system, the thymus, the spleen as well as in peripheral blood lymphocytes. In addition to the immune system, NFAT proteins have been detected in the cardiovascular and digestive systems, in pancreas, brain, skeletal and smooth muscles, kidneys, lungs and adipose tissue [121].

Several studies which used NFAT knockout mice, have shown that these proteins have a fundamental role in the development of the cardiovascular system. Particularly, NFATc1 deficient mice die at 14.5-17.5 days of gestation due to abnormalities in their heart valves (aortic and pulmonary) and septum formation [113, 158], whereas double mutant mice lacking NFATc3 and NFATc4 die at around 11 days of gestation as a result of defective vessel assembly and angiogenesis [114].

In the adult vasculature, NFAT isoforms have also been identified in both, ECs and VSMCs. In ECs, it has been reported that NFAT mediates specific functions such as proliferation, migration, angiogenesis and inflammation, through the regulation of target genes such as: cyclooxygenase-2 (COX-2), vascular adhesion molecule (VCAM-1), intercellular adhesion molecule (ICAM-1), interleukin-8 (IL-8), tissue factor (TF), E-selectin and DSCR-1 (Down syndrome critical region) a negative feedback regulator of Ca^{2+}/calcineurin-NFAT signalling activated by both, VEGF and thrombin [159-162].

In adult VSMCs, several studies suggested that NFAT apart from regulating proliferation, migration [156, 157, 163, 164] and vascular inflammation [31, 51, 165, 166], it is also involved in: a) VSMCs phenotypic modulation [167, 168], b)

neointima formation after balloon angioplasty [169, 170], c) hypertension [171-173], d) pulmonary arterial hypertension and remodelling [174-177].

Therefore, NFAT is implicated in mediating physiological and pathophysiological vascular processes, regulating the expression of several genes. Some of these genes are pro-inflammatory genes like: interleukin-6 (IL-6) [156, 165], IL-8, VCAM-1 [31], ICAM-1 [165], OPN [51, 165], COX-2 and the allograft inflammatory factor-1 (AIF-1) which are also implicated in the process of neointima formation [169, 178]. Other genes that have been shown to be regulated by NFAT and that affect the progression in the cell cycle, proliferation and therefore neointima formation are cyclin D1 (Ccnd1), cyclin A and cyclin-dependent kinase 2 [170, 176, 179]. NFAT also regulates the expression of the β1 subunit of the Ca^{2+}-activated K^+ channels (BK channels, voltage-gated-K^+ channels (Kv2.1), Kv1.5 channel and SM-α actin, which all can potentially impact in VSMC depolarization, development of myogenic tone and consequently in the development of systemic hypertension [171, 172, 180] and pulmonary arterial hypertension [174, 176].

As mentioned before, an up-stream activator of NFAT in the vasculature is elevated extracellular glucose. Previously, our group has demonstrated that high levels of extracellular glucose activate NFAT in intact cerebral arteries *ex vivo* [133], as well as *in vivo*, both in large conduit arteries and medium sized resistance arteries (aorta and cerebral) [51]. The effect of glucose on NFAT activation involves at least two mechanisms: a) the local release of extracellular nucleotides, like uridine triphosphate (UTP) and its degradation product uridine diphosphate (UDP), acting on purinergic 2Y (P2Y) receptors, leading to increased $[Ca^{2+}]_i$ and subsequent activation of CaN and, b) inhibition of GSK3β, JNK1 and JNK2 yielding reduced nuclear export of NFATc3.

NFAT regulates cell proliferation and VSMCs phenotypic modulation

In the adult organisms, at homeostasis, the VSMCs in vessels are mostly in a contractile state and their proliferation rate is remarkably low. However, these cells can experience a phenotype switching and re-enter in the cell cycle in response to physiological or pathological stimuli. The cell cycle in mammalian cells consists of five phases, three of them are gap-phases (G0, G1 and G2), and the other two are synthesis- and mitotic-phases (S-phase and M-phase). G0, G1, G2 and S are collectively referred as interphase. In G0 the cell remains in a resting or quiescent state, whereas during G1 and G2, RNA and protein syntheses occur. In the course of the S-phase, DNA is replicated, while during the M-phase cells undergo mitosis and cell division [181]. Progression in the cell cycle is tightly controlled and driven by several cyclin-dependent protein kinases (Cdks), cyclins,

and Cdk inhibitors at the checkpoints, positioned mainly at the transition between phases. Activation of Cdks requires their association with their partners cyclins, whose individual levels fluctuate during the different phases of the cell cycle as a consequence of changes in transcription and ubiquitin-mediated degradation [181, 182]. For instance, initiate progression in G1-phase needs the cyclin D/Cdk4 and cyclin D/Cdk6 complexes, while the cyclin E/Cdk2 is important in the G1/S transition. Functional cyclin A/Cdk2 complex is necessary for DNA synthesis in the S-phase, whereas cyclin A/Cdk1 and cyclin B/Cdk1 pairs are required for the G2-phase and mitosis, respectively [182].

The fact that DNA synthesis stimulated by growth factors is Ca^{2+}-dependent and it is inhibited by drugs that block CaN activity, suggests that the NFAT signalling pathway may be involved in the cell cycle control. Indeed, NFAT can determine cell survival, proliferation or cell death, depending on the expression levels of isoforms and splicing variants and on the cell type in which they are being expressed [164].

In vitro and *in vivo* studies have shown that NFATc2 directly down-regulates cyclins A2 and E expression by suppressing cyclin A2 (Ccna2) and E promoters in pulmonary arterial smooth muscle [179] and in lymphocytes [183], respectively. Additionally, lymphocytes from NFATc2 deficient mice hyperproliferate, showing a shorter cell division period upon activation [163]. However, NFATc1 seems to be involved in cell cycle progression in VSMCs, via up-regulation of Ccna2, Ccnd1 and D3 expression, thereby leading to increases in Cdk2 and Cdk4 activities [164, 184, 185]. Another target of NFAT regulation is the tumour suppressor gene p21 (the main Cdk inhibitor), whose expression is induced by both NFATc1 and c2 isoforms in mice keratinocytes [164] (Figure5).

Besides this, NFATc3 and c4 have been implicated in apoptosis regulation. NFATc3 seems to have a protective effect under hypoxia condition in pulmonary vascular smooth muscle cells, whereas NFATc3 deficient mice displayed increased apoptosis in T-lymphocytes. However, NFATc4 promotes the survival of neurons and T-cells [164].

On the other hand, it is well known that Klf4 and Klf5, members of Krüppel-like factor (Klf) transcription factors family, influence proliferation of VSMCs and their phenotypic modulation. Both, Klf4 and Klf5 are important in cardiovascular remodelling and they have differential cellular effects, often opposing ones. Normally, Klf4 is associated with an anti-proliferative effect (growth arrest), whereas Klf5 with cell proliferation induction [186]. The mechanism through which Klf4 reduces the cell cycle progression, involves the up-regulation of p21 expression (which acts in a p53-dependent manner) and the down-regulation of cyclins D and E. However, Klf5 increased the expression of Ccnd1, B1 and Cdk2, resulting in accelerated cellular proliferation [187].

Regarding phenotypic modulation, it is established that Klf4 plays a key role in the VSMC phenotype switching from contractile towards a synthetic and/or inflammatory phenotype [187, 188]. In spite of the fact that Klf4 is usually not expressed in differentiated SMCs, it is up-regulated by PDGF and by blockers of CaN in VSMCs from rat carotid arteries, both *in vitro* and *in vivo*. The induction of Klf4 results in a down-regulation of the expression of contractile gene markers, including SM-α-actin (Acta2), Tagln, Smothelin (Smtn), Cnn1 and the transcription factor myocardin (Myocd)[186, 188, 189], but also in an up-regulation of cyclin-dependent kinase inhibitor-1A (CdkN1A or p21) and cytoskeleton related genes as the MMP3, MMP-9 and collagen-VIII (COL8) [188].

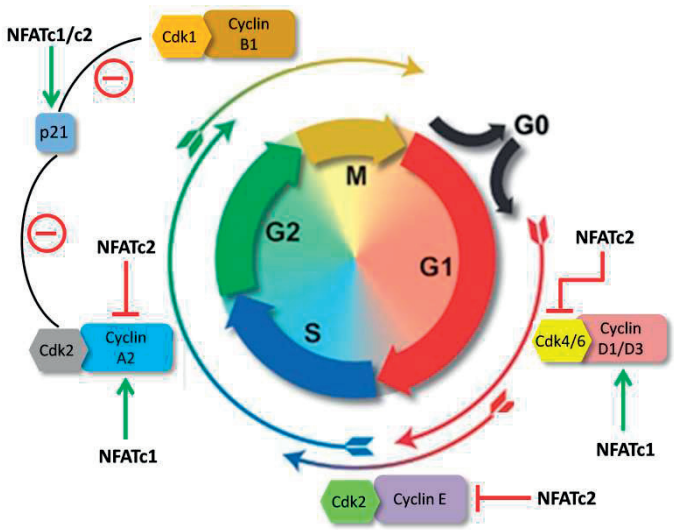

Figure 5. Simplified sketch depicting cell cycle regulation by NFAT proteins. Progression through the cell cycle requieres the sequential activation of specific cyclin/cyclin-dependent kinases (Cdk) complexes. Several negative cell cycle regulators exist, but the main Cdk inhibitor is p21. NFATc2 isoform negatively regulates the cell cycle by down-regulation of cyclins and up-regulation of p21. In contrast, NFATc1 regulates the cell cycle positively by up-regulation of cyclins expression but negatively by induction of p21 expression. Non-dividing cells are in G0, whereas the interphase includes G1, S and G2. Mitosis and cell division occur in M-phase. Adapted from [164].

Therefore, Klf4 works as negative regulator of contractile genes by mechanisms that include suppressing Myocd expression (a co-activator of SRF), direct interaction with SRF, or altering the surrounding sequence motif CArG box, a common denominator for those contractile genes [189, 190]. In contrast, Klf5 is

abundantly expressed in embryonic VSMCs, and is down-regulated during vascular development, but re-induced in proliferating neointimal VSMCs in response to vascular injury [186].

Even though the mechanism by which CaN blockers induce VSMC phenotypic modulation does not exclusively involve inhibition of NFAT activation, it has been demonstrated that *in vivo* treatment of rat carotid arteries with specific NFAT inhibitors leads to rise of KLF4 levels together with a down-regulation of VSMCs differentiation marker genes. Furthermore, it was shown that NFATc1 and c3 proteins positively regulate smooth muscle myosin heavy chain (Myh11) and SMα-actin, respectively. This evidence suggested that the NFAT signalling pathway participates in the phenotype switching of VSMCs [188].

All in all, phenotypic modulation of VSMCs is orchestrated by a coordinated molecular network in response to several physiological cues, which involve different signalling pathways, transcription factors, ROS, NOXs, microRNAs, among others [191]. For instance, it has been shown that hyperglycemic and diabetic conditions lead to down-regulation of KLF4 in VSMCs and arteries form diabetic mice or patients, and subsequently elevated expression of VSMCs differentiated marker genes by up-regulation of micro-RNAs as well as activation of different kinases [37, 192]. An important aspect is that proliferation and phenotypic modulation of VSMCs are critical components in the development of many vascular diseases, such as atherosclerosis.

Aims

- To investigate the pattern of NFAT isoform expression in various vascular beds.

- To investigate whether there is functional non-redundancy of NFAT isoforms in the vasculature.

- To investigate whether NFAT activation may be a link between diabetes and atherogenesis.

- To investigate whether *in vivo* pharmacological inhibition of NFAT has any impact on plaque size and/or composition in STZ-induced diabetic ApoE deficient mice (an atherosclerosis-prone T1D mouse model).

- To investigate whether *in vivo* pharmacological inhibition of NFAT had any impact on plaque size and/or composition in IGF-II/LDLR$^{-/-}$ ApoB$^{100/100}$ mice (an atherosclerosis-prone T2D mouse model).

- To explore the potential link between the NFAT signalling pathway and oxidative stress in the context of the IGF-II/LDLR$^{-/-}$ApoB$^{100/100}$ mouse model.

- To investigate whether NFAT is expressed in mouse retinal microvessels and human retinal microvascular endothelial cells.

- To determine whether NFAT activation is sensitive to changes in extracellular glucose in retinal microvessels, both *in vitro* and *in vivo*, and if so, to elucidate the activation properties in this tissue.

- To study the potential involvement of NFAT in the early changes leading to diabetic retinopathy.

Methods

In this section, some of the methods and techniques used in this thesis are explained and discussed. Further information about materials and methods can be found in each paper.

Animal models in biomedical research

Animals are used in a variety of scientific disciplines. Species such as mice, rats, rabbits, pigs, guinea pigs have significantly contributed to the better understanding of many human diseases and are routinely used because they share important aspects of our physiology and pathophysiology. Rodents, and particularly inbred mice are the dominant model organism in biomedical research due to their genetic homogeneity which reduces the number of confounding factors [193]. Moreover, the large number of available genetically modified mouse strains offers the possibility of studying the effect of single genes. Additional advantages include their small size, short generation time, and relatively low costs.

All research which involves animals must be approved by ethical committees, who critically review all aspects of animal handling and testing. Animal work should follow “The Three Rs", which are guiding principles for more ethical use of animals, defined in the early 1960s by Russel and Burch [194]. These 3 principles are Replacement, Reduction and Refinement. *Replacement* implies avoiding the use of animal models whenever this is possible or substituting them by alternative methods, such as cell culture models. *Reduction* refers to the use of a minimum number of animals; to either obtain information from fewer animals or obtain more information from the same number of animals. This should be accomplished without compromising the statistical power. *Refinement* refers to improving the conditions of breeding, housing and transportation, as well as improving the experimental procedures to minimize pain, suffering and distress in the animals, also by selecting non-invasive measurement techniques whenever possible. In addition, *refinement* takes into account the care of animals throughout the whole experiment as well as the methods chosen for euthanasia. Nowadays, a 4th R was added by Ronald Bank and it is being introduced in most legislations. This R

refers to *Responsibility*, which means to actively use scientific knowledge and to work to promote animal welfare [195].

Mice as a model for studying vascular complications in diabetes

Although a big effort has been made by researchers to find or generate appropriate animal models representative of human diabetes and its complications, it has been difficult to recreate the disease as it is seen in humans and most often, animals only replicate the very early stages of diabetic complications.

Every model used to explain biological phenomena have limitations and the mouse is not an exception. In the study of diabetes induced-atherosclerosis, we can point out the following limitations. First, most mouse strains are resistant to develop atherosclerosis. This has been attributed to a natural lack of the cholesteryl esters transfer protein (CETP) activity in mice. CETP plays a central role in lipoprotein metabolism, and its deficient activity in humans has been associated with an antiatherogenic state, whereas in rodents it has the consequence of low levels of plasma cholesterol (<2.5 mmol/L) on a normal diet [196]. Moreover, mice have a larger portion of HDL particles in which circulating cholesterol is transported, while in humans cholesterol is transported mainly in LDL particles [197]. However, through diet and genetic manipulation, it is possible to alter the lipid homeostasis and generate severe hyperlipidemia in mice, which leads to atherosclerotic lesion formation similar to that found in humans [198, 199]. Second, the site preferences for lesion development are different between humans and mice. The aortic sinus and aortic arch are the places where the majority of rodents develop atherosclerosis, whereas in humans, carotid, coronary and femoral arteries are the most prone regions to develop atherosclerotic plaques [200]. Third, diabetic rodent models do not develop very complex plaques that lead to plaque rupture in the late stage of atherosclerosis. Furthermore, most of the mechanistic information about atherosclerosis in mice is limited to the earliest stages of the disease (i.e. foam cell accumulation and fatty streaks), whereas the dominant mechanisms in the pathogenesis of fibrous plaque are less well understood [62].

Mouse models used in *in vivo* studies

In spite of the points listed above, mouse models are still valuable for understanding the molecular basis and pathogenesis of diabetic vascular complications, as long as one is aware of their limitations.

In vivo chronic Hyperglycemia

Epidemiological studies as well as *in vitro* and *in vivo* studies have shown that in addition to lipids, glucose has an important role in inducing vascular damage and in the development of atherosclerosis [46]. With the aim of studying the role of NFAT in development of vascular complications, we therefore used mouse models of chronic hyperglycemia. In mice, chronic hyperglycemia can be either induced chemically or genetically.

The use of the antibiotic streptozotocin (STZ) is widely established for chemical induction of diabetes in different strains. STZ is a toxic glucose analogue, which causes insulinopenic diabetes because it considerably reduces insulin secretion from pancreatic β-cells. STZ is taken up by GLUT2 glucose transporters on the pancreatic β-cells and selectively destroy them through mechanisms that involve the formation of free radicals, ROS and alkylation of the DNA [201]. In spite of the fact that STZ causes effects resembling T1D, it does not totally replicate it, because it does not necessarily generate ketosis and insulin therapy is not always required for STZ treated mice [202]. Usually, STZ is administrated i.p. in mice, in multiple low-doses (20-60 mg/kg body weight per day) or alternatively as a single high dose (100-200 mg/kg body weight). The latest has more toxic effects due to the fact that STZ causes complete β-cell necrosis and rapidly causes diabetes [202]. Moreover, it has been observed that the genetic background of the mice is critical for the development of hyperglycemia, with C57BL/6 being one of the most vulnerable when compared to other inbred strains (DBA/2>C57BL/6>MRL/Mp>129/SvEv>BALB/c) [203, 204]. In line with these comparisons, previous work from our group had previously also reported different susceptibility to STZ, with FVBN being even more susceptible than C57BL/6 (FVBN>C57BL/6>BALB/c) [205]. Gender also has an effect on the response to STZ, with males being more susceptible than females [203]. One disadvantage of using STZ is the nonspecific toxic effects on other organs apart from the pancreas. Kidney tubular cells and hepatocytes are particularly vulnerable since they also express GLUT2 transporters, while endothelial and vascular cells are less likely to be affected given that they express GLUT1. As a consequence, STZ presents hepatotoxic and nephrotoxic effects [201].

In vivo acute hyperglycemia

In order to investigate whether *in vivo* acute hyperglycemia could induce nuclear accumulation and activation of NFAT in whole retina and retinal vessels, we used in paper III a traditional intraperitoneal glucose tolerance test (IP-GTT) to raise blood glucose levels in mice.

IP-GTT is used to identify normal or impaired glucose metabolism. It measures the capacity of glucose clearance from the blood after a glucose load injected intraperitoneally (i.p; 2 g per kg of mice body weight), following a 16 hour fasting period. A normal healthy response is characterized by a blood glucose peak 30 minutes after the i.p. injection after which levels return to basal within 2 hours. In order to measure potential changes in NFATc3 nuclear accumulation in response to acute hyperglycemia, mice were euthanized 30 minutes after i.p. glucose administration, whole retinas and retinal vessels were isolated and NFATc3 nuclear accumulation was measured using confocal microscopy. Saline was used as vehicle control. To explore if a single peak of hyperglycemia is enough to induce NFAT-dependent transcriptional activity, the same experiments were performed in NFAT-luc reporter mice which were sacrificed instead 6 hours after the i.p. injection, sufficient time for the luciferase gene to be transcribed and translated.

NFAT-luciferase mouse

This is a transgenic mouse originally generated on a FVBN background. It is created with 9 tandem copies of the NFAT binding site (5'-TGGAAAATT-3') from the IL-4 promoter positioned 5' to a minimal promoter from the α-myosin heavy chain gene (-164 to +12) and inserted upstream of a luciferase reporter gene [145]. The fact that it carries 9 copies of the NFAT-binding site considerably increases the probability that NFAT binds to it, leading to reporter gene transcription. Thus, this model is a tool to measure NFAT-dependent transcriptional activity. NFAT-luc mice are phenotypically normal.

NFAT-luciferase (NFAT-luc) mice were used in papers I and III to determine the effects of acute hyperglycemia as explained in the previous paragraph, as well as to study the impact of diabetes (chronic hyperglycemia) and high fat diet (HFD) on NFAT transcriptional activity in various organs and vessels.

Akita mouse

The Akita mouse is characterized by a spontaneous dominant point-mutation in the insulin 2 gene (*Ins2*, mouse homologue of human proinsulin gene), that leads to pancreatic β-cell apoptosis and severe hyperglycemia (>400 mg/dl or > 20 mM throughout life, more prominent in the male mice), hypoinsulinemia and polydipsia at 3-4 weeks of age. This mutation involves a replacement of the cysteine residue by tyrosine at the seventh amino acid of the A chain, causing proinsulin misfolding with subsequent endoplasmic reticulum stress, and ultimately pancreatic β-cells apoptosis [206, 207].

Interestingly, Akita mice, similar to STZ-treated mice, do not require exogenous insulin for survival since some β-cells remain functional in the pancreas.

Since heterozygous Akita mice have previously been established as a good model of diabetic retinopathy [208], in paper III, we used 8-week-old male Akita (*Ins2*$^{+/-}$) and wild type littermates (WT, *Ins2*$^{+/+}$) on C57BL/6J background to determine whether inhibition of NFAT could prevent or ameliorate the changes in retinal vascular permeability observed in the diabetic mice. For this, animals were treated with the NFAT blocker (0.29 mg/kg) or saline during 2 weeks. Additionally, in paper III, we generated Akita/NFAT-luc mice to monitor changes in NFAT-dependent transcriptional activity in retinal vessels.

NFATc2 mouse

NFATc2 knockout (NFATc2$^{-/-}$) mice were generated on a C57BL/6 background by genetically altering exon 3 of the NFATc2 gene, located on chromosome 2. A sequence of amino acids (390-438) in exon 3, that has been shown to be critical for DNA binding activity, was deleted and replaced by a cassette containing the neomycin drug resistance (neo) gene. In the homozygous mutant mice, this predicted mutant fragment is either not made or is rapidly degraded. NFATc2 deficient mice were reported to grow up to normal size and they did not present any gross anatomical abnormalities, except that at 11-12 weeks of age the spleens were roughly 18% larger by weight than spleens from WT mice, but did not have differences in the histological architecture nor in the ratio of white to red pulp [209].

NFATc3 mouse

NFATc3 knockout (NFATc3$^{-/-}$) mice were generated on a BALB/c background by deletion of a region of the NFATc3 gene that encodes the DNA-binding domain (amino acids 535-592, exon 5) and replaced with a neomycin cassette (neo) gene. Although the NFATc3 deficient embryos tend to be smaller, they do not present any pathologic or histological abnormalities and they are healthy until at least 14 months old. Curiously, NFATc3$^{-/-}$ mice were not born at expected Mendelian ratio, with heterozygous mating yielding only 12% rather than the expected 25%. However, their lifespan was normal [210].

In paper II, to explore whether NFAT inhibition affected the expression of oxidative stress related genes under controlled oxidative stress environment, we used VSMCs explants from competent NFATc3 mice. In addition, to measure if NFAT inhibition had impact on the oxidative stress status (H_2O_2 and ROS/RNS levels) generated by high glucose, VSMCs explants from both NFATc3$^{+/+}$ and

NFATc3$^{-/-}$ mice were used. In paper IV, were used VSMCs explants from NFATc3$^{+/+}$, NFATc3$^{-/-}$,NFATc2$^{+/+}$ and NFATc2$^{-/-}$ to study the role of these two NFAT isoforms in the regulation of vascular smooth muscle gene expression.

In vivo chronic hyperglycemia in dyslipidemic backgrounds

ApoE deficient mouse (ApoE$^{-/-}$)

The ApoE protein is a structural component of almost all lipoproteins (except LDL), that is synthesized by the liver, the brain, the adipose tissue and macrophages. ApoE plays an important role in lipoprotein removal from the plasma to the liver, contributing to maintained normal plasma lipids levels [211]. Consequently, ApoE$^{-/-}$ mice have a delayed clearance of lipoproteins, causing 5-fold increment in plasma cholesterol levels, even with a normal chow diet (in average 400 mg/dL vs. 85 mg/dL in ApoE competent mice), regardless the age or sex of the animals [212]. The lack of ApoE results in accumulation of chylomicrons and VLDL remnants, which leads to the development of extensive atherosclerotic lesions in the aortic arch and its branches, as well as in the thoracic aorta, albeit to a lesser extent [196]. The ApoE deficient mouse presents the entire sequential events involved in lesion formation during atherogenesis, except for the plaque rupture, which is a fairly common event in humans [213]. The severity of the atherosclerotic lesions increase with the age of ApoE$^{-/-}$ mice. As early as 6-8 weeks of age, adhesion of monocytes to the endothelium has been reported. At the age of 9-10 weeks, lipid deposits and fatty acid streaks appear, followed by progression to mature fibrous plaques between 15-20 weeks of age [213-215].

STZ-treated ApoE deficient mice have been used for studies of diabetic macroangiopathy, since mice exhibit increased lesion area and accelerated atherosclerosis lesion formation characteristics of human macroangiopathy [199]. Even though there are robust studies supporting the fact that glucose is an independent risk factor for the generation and progression of atherosclerosis [49, 216], the effect of high glucose in lesion initiation is overshadowed under severe dyslipidemia conditions (cholesterol > 600 mg/dL or 16 mM), in which atherosclerosis is primarily driven by lipids [49]. Therefore, a mouse model with moderate basal plasma cholesterol levels would be preferable to study the impact of hyperglycemia on atherosclerosis. Therefore, to avoid the confounding effects of hyperlipidemia, in paper I we used 22 week old ApoE$^{-/-}$ mice (with C57BL/6 background) fed with normal diet to keep the cholesterol levels within acceptable ranges (400-600 mg/dL; 10.7-16 mM). In order to study whether the NFAT-signalling pathway is involved in diabetes-driven atherosclerosis, control and diabetic ApoE$^{-/-}$ mice were treated either with the NFAT blocker A-285222 (0.29

mg/kg) or saline during 1 or 4 weeks. We also used this model in paper III, where OPN expression levels were measured in retinal vessels from control and diabetic $ApoE^{-/-}$ mice.

IGF-II/$LDLR^{-/-}ApoB^{100/100}$ mouse

This is a novel mouse model obtained by crossbreeding LDL receptor deficient mice ($LDLR^{-/-}$) that only expresses apolipoprotein B100 ($ApoB^{100/100}$; genetic background 75% C57BL/6 and 25% 129/SvJae) with C57BL6/SJL mice overexpressing insulin-like growth factor II (IGF-II) in pancreatic β-cells for at least 10 generations, maintaining the mice in a C57BL/6 background [217]. The LDLR is important for lipoprotein homeostasis, because it is involved in clearing LDL and lipoprotein remnants containing ApoE as well as regulating hepatic lipoprotein production. As a consequence, the absence of LDLR mainly affects lipoprotein uptake and clearance, resulting in a preponderance of LDL as the cholesterol carrying plasma lipoprotein. LDLR deficient mice require HFD supplementation to accumulate larger very low density lipoprotein (VLDL)/remnant lipoproteins, to get higher cholesterol levels (much higher than even the chow fed $ApoE^{-/-}$ mice) and therefore develop significant atherosclerotic lesions. In this way, lesions are not only limited to old $LDLR^{-/-}$ animals, but also develop in young animals [197, 200]. To best recreate the human-like lipoprotein profile defined by increased LDL and decreased HDL serum levels, $LDLR^{-/-}$ mice that exclusively synthesize ApoB100 ($LDLR^{-/-}ApoB^{100/100}$) can be generated by either inhibition of the synthesis of apolipoprotein B48 (apoB48) or by preventing enzymatic editing of ApoB mRNA [196]. The $LDLR^{-/-}ApoB^{100/100}$ mouse used to generate the IGF-II/$LDLR^{-/-}ApoB^{100/100}$ mice were purchased from Jackson and have a CTA to TTA mutation in codon 2153 in sequences corresponding to the apoB48 editing codon, yielding mice lacking apoB48 [218]. ApoB100 is the apolipoprotein of chylomicrons, VLDL, ILDL (intermediate-low density lipoprotein) and LDL, responsible for carrying lipids, including cholesterol, to the cells through linking with LDL receptors present on the cells surface. In consequence, $LDLR^{-/-}ApoB^{100/100}$ mice have a background prone to develop atherosclerosis.

IGF-II is a growth-promoting polypeptide, which shares a high degree of structural homology with insulin. IGF-II is expressed during the embryonic development but the level decreases considerably after birth and is very low in adult rodents. In transgenic mice overexpressing IGF-II in pancreatic β cells, autocrine or paracrine interaction of IGF-II with either IGF-I receptor or insulin receptor in islets may lead to increased β cell proliferation and development of early hyperplasia, which leads to hyperinsulinemia [219].

All in all, IGF-II/LDLR$^{-/-}$ApoB$^{100/100}$ mice have insulin resistance, mild hyperglycemia and hypercholesterolemia, with a human-like hypercholesterolemic lipid profile. Moreover, they develop calcified and complex advanced atherosclerotic lesions with less organized structure, larger necrotic core and thinner fibromuscular cap. Another important feature is the fact that plasma lipids levels remain identical to those in non-diabetic control LDLR$^{-/-}$ApoB$^{100/100}$ mice [196, 217]. Furthermore, it has been shown that IGF-II/LDLR$^{-/-}$ApoB$^{100/100}$ animals receiving a Western diet for three months develop thicker atherosclerotic plaques, allowing for additionally exacerbating the diabetic phenotype by means of simply altering the diet [217].

With the aim to investigate whether NFAT inhibition has an effect on atherosclerosis in T2D, in paper II, we used IGF-II/LDLR$^{-/-}$ApoB$^{100/100}$ mice. Two separate studies were carried out with young (10 to 16 weeks old) and old (46 to 74 weeks old) mice, fed with high fat Western diet (TD 88137, Harlan Tekland: 42% of calories from fat; 0.15% from cholesterol) during 8 weeks. After 4 weeks on diet, mice were treated either with the NFAT blocker A-285222 (0.29 mg/kg) or with saline as control, for 4 additional weeks.

Determination of metabolic parameters

Total plasma cholesterol and triglycerides levels in mice undergoing the different experimental protocols in papers I and II, were determined in blood samples by colorimetric assays (Infinity^{TM}Cholesterol and Infinity^{TM}-Triglyceride) either before (paper II) or after treatments with the NFAT blocker (papers I and II). Plasma insulin and OPN levels were measured after overnight fasting at the end of treatments using Mercodia mouse insulin ELISA kit and Quantikine mouse OPN ELISA kit, respectively. All assays were performed according to the manufacturers' instructions and the lower limits of detection were 0.2 µg/L for insulin and 5.7 pg/mL for OPN.

NFAT inhibitors

Commonly, the way to study the involvement of one signalling pathway in physiology and pathophysiology, is through pharmacologically blocking or genetically eliminating intermediary elements in that pathway. In the studies carried out in the four papers included in this thesis, we have used both strategies. As mentioned before, knockout mice for NFATc2 and c3 isoforms were used and

in addition, *in vivo* and *in vitro* pharmacological inhibition of NFAT was employed.

Traditionally, potent immunosuppressant drugs such as cyclosporine A (CsA) and tacrolimus (FK506), have been used to study the NFAT signalling pathway. These drugs have been widely used in the clinic for organ transplant and for treatment of autoimmune diseases [220, 221]. Both are fungal metabolites, and in spite of having very different molecular structure, their mechanism of action, biological- and side-effects are very similar. CsA and FK506 bind to the cytosolic immunophilin proteins cyclophilin A and FK506-binding proteins, respectively. The resultant drug-protein complex binds tightly to CaN between the catalytic and regulatory subunits and blocks its phosphatase activity by preventing substrate access [220]. Thus, CsA and FK506 inhibit all down-stream targets of CaN, including NFAT, which may contribute to the broad and serious side-effects observed (i.e. neurotoxicity and nephropathy) [222, 223]. By blocking the phosphatase activity of CaN, CsA and FK506 prevent the subsequent dephosphorylation of NFAT and its translocation to the nucleus [220, 222].

Since these drugs are not only affecting NFAT activation, the peptide VIVIT was developed as a more specific NFAT blocker. VIVIT selectively blocks the calcineurin-NFAT interaction through binding to one of the two docking sites on CaN with high affinity via the consensus sequence PxIxIxT [224]. As a result, VIVIT prevents NFAT activation without compromising the phosphatase activity of CaN and without affecting other down-stream targets of CaN [222]. However, the *in vivo* use of VIVIT is limited due to its hydrophilic characteristic that hinders its passage across cell membranes.

Another more recently reported inhibitor of this signalling pathway is tributylhexadecylphosphoniumbromide (THPB), which has been shown to inhibit NFAT-dependent reporter activity as well as the expression of IL-2 in Jurkat cells [225] and inflammatory genes in the kidney of diabetic rats [226]. Even though the molecular mechanism underlying this inhibition are still unclear, THBP seems to indirectly prevent NFAT nuclear accumulation by suppressing the phosphorylation of p70S6K a protein kinase that induces protein synthesis in the ribosome and that has been suggested to interact with NFAT [225].

While searching for novel and safer immunosuppressant drugs, a small, 416 Daltons organic cell-permeable molecule A-285222 (Figure 5) was identified as a potent NFAT inhibitor. A-285222, also called BTP-19 belongs to a series of 3,5-bis-trifluoromethyl pyrazoles (BTP) and was found to have superior pharmacokinetics properties when compared to all other 20 BTP compounds synthesized. For instance, it has long half-life between 6-8 hours and relatively low plasma protein binding [227]. A-285222 maintains NFAT in a phosphorylated state, blocking its nuclear import and subsequent transcriptional activity [228]. As

opposed to other commonly used immunosuppressant drugs, A-285222 inhibits NFAT activity without affecting CaN phosphatase activity, as demonstrated by the inability of A-285222 to block the *in vitro* dephosphorylation of other CaN substrates including the type II regulatory subunit of PKA and the transcription factor, Elk-1 [227, 228].

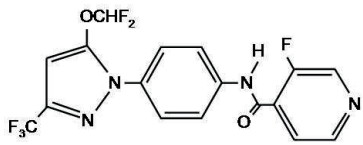

Figure 5- Chemical structure of A-285222. Adapted from [229].

Even though the exact mechanism of action of A-285222 is not clear, it does not affect NF-κB or AP-1 activation or the activity of nuclear export kinases such as GSK-3, JNK2 and p38 [228]. Unpublished EMSA (electrophoretic mobility shift assay) data from our lab showed that A-285222 has no effect on the activation of NF-κB, AP-1 or Oct in mouse aortic VSMCs. Previous studies in cynomolgus monkeys had shown that A-285222 is well tolerated and did not cause neurological effects when the plasma concentration is maintained below 4 mg/mL (9.6 μM), a level which was achieved by oral administration of the drug twice daily at 5–7.5 mg/kg body weight [230]. In paper I we demonstrate that plasma levels of A-285222 sufficient to reduced atherosclerosis were much lower and only reached 100–200 nmol/L 2 hours after administration (0.15–0.29 mg/kg body). As in previous studies from our lab, this dose was well-tolerated [205], [165, 231, 232].

Histological evaluations of atherosclerotic plaques and their composition

In order to evaluate the atherosclerotic lesion status in several vessels from different mice models and to monitor the *in vivo* effects of the NFAT blocker on atherosclerosis, the aorta, the aortic root and brachiocephalic arteries were isolated, fixed and stained for quantification of several parameters.

Atherosclerotic lesion was assessed in paper I by *en face* preparation of the aortic arch and the descending aorta from diabetic and non-diabetic ApoE$^{-/-}$ mice treated for 4 weeks with A-285222 or saline. Briefly, descending aortas were fixed and stained with the fat-soluble dye Oil-red-O (ORO). Lipids were stained red, which makes the plaques bordeaux-colored. Stained plaque area and total aortic area were quantified under blinded conditions using a computer-aided morphometry software (Image-Pro Plus, Media Cybernetics, Bethesda, MD) [233]. Plaque size was expressed as ORO stained area as percentage of total aortic arch area or total descending aorta area. This technique allows an overview of lesion severity and location in the aorta.

An alternative method for measuring lesion size is the determination of cross-sectional plaque area in aortic roots and in arteries. To fully understand the pathogenic process of atherosclerosis it is important not only to quantify the lesion area, but also the plaque composition changes. This method allows quantifying changes for instance in collagen and elastin content within the lesion as well as in the media layer of the artery. Content of those components, among others, are related to plaque stability. A stable plaque phenotype is associated with high collagen content in the lesion, whereas unstable and plaques prone to rupture have lower collagen content.

In paper I, sections from the aortic root were stained with Harris hematoxylin to easily determine lesion borders, media and lumen areas, whereas in paper II they were determined based on the Mayer's hematoxylin & eosin staining in sections from the aortic root and the brachiocephalic artery. In paper II, plaque and media contents of smooth muscle, collagen and elastin were assessed through Elastin van Gieson (EvG) staining. In paper I collagen was determined by modified Masson's trichrome staining [233], whereas immunohistochemistry technique was used for determining SMα-actin and macrophage content (MOMA-2; monocyte/macrophage2) in the aortic root sections (paper I and paper II) and brachiocephalic artery sections (paper II). No staining was observed when the primary antibody was omitted from the protocol. Collagen, elastin, SMα-actin, media thickness (paper II) and MOMA-2, were quantified under blind conditions using BioPix iQ2.3.1 software. Sections were counterstained with Harris or Mayer's haematoxylin in paper I and II, respectively, to determine the lesion area and data were expressed either as percentage of plaque area or as percentage of media area.

In paper I, expression of OPN and TF was evaluated also in aortic root sections through confocal immunofluorescence microscopy as it was described in [205]. The examination of sections was done under blinded conditions at 20X in a ZeissLMS 5 Pascal laser scanning confocal microscope and the mean of

fluorescence intensities of OPN and TF in the aortic root was calculated using the Zeiss LSM 5 Analysis software and ImageJ (version 1.47 m), respectively.

Ultrasound evaluation of atherosclerosis

Ultrasound biomicroscopy (USB) is a non-invasive technique that has recently been validated for following lesion progression in atherosclerotic mice. Due to the very high heart rate and small size, few imaging techniques are adequate to study cardiovascular function in mice [234]. The imaging device consists of a high resolution scan head, which has a high probe frequency (between 30-70 MHz), limited maximum penetration depth (around 1.2-1.8 cm) and a resolution nearly reaching that of light microscopy [234, 235]. This allows the measurement of atherosclerotic lesion progress through accurate real time images in individual animals. The USB protocol has been used and validated for monitoring the initiation, growth and regression of plaque lesion in the aortic root, carotid and brachiocephalic arteries from several atherosclerotic mouse models [234-237]. All these previous studies have revealed good correlation between cross-sectional plaque areas determined by USB and by histology.

In paper II, brachiocephalic plaque size and lesion progression were assessed non-invasively by USB in young and old IGF-II/LDLR$^{-/-}$ApoB$^{100/100}$ mice before and after treatment with the NFAT blocker A-285222. For that, we used a Vevo2100 ultrasound system (Visualsonic, Toronto, Canada) with a transducer frequency of 40 MHz, which provided a theoretical high resolution of 40 μm at a frame rate of 32 Hz. Before scanning, animals were anesthetized with isoflurane and were then maintained under light anaesthesia during the procedure (4.5% isoflurane 450 mL air for induction and 2% isoflurane 200 mL air for maintenance). The hair from the anterior chest wall was removed using chemical hair remover and ultrasound transmission gel was applied to guarantee optimal image resolution. The brachiocephalic artery was visualized in a cross-section short-axis and the lesion measured within the proximal 200 μm of the vessel from its bifurcation from the aortic arch. Loops of at least 100 frames were stored and the frame with the largest plaque was chosen for off-line analysis.

USB is a very useful tool for longitudinal studies due to the fact that arteries can be monitored all along the experimental protocol. Consequently, it is not necessary to sacrifice animals at various time points and therefore it requires fewer animals than those needed for histological plaque assessments. However, the main limitations of the technique are the intra- and inter-observer variabilities. For this reason, it is recommendable that measurements are done at least on two different occasions by the same operator to minimize user dependency. Ideally,

measurements should be done by a second observer to evaluate the inter-observer variability [235]. In our case, plaque size measurements were performed twice by an expert operator blinded to the animal identity and treatment. The intra-observer coefficient of variance (calculated by dividing the standard deviation by the mean and multiplying by 100 [234], for the brachiocephalic plaque size was 2.7%.

It has been reported that USB can yield slightly larger plaque values than those measured by the histology, due to the *ex vivo* shrinkage of the histological preparation during fixation [234].

Cell based procedures

As a complementary approach to the *in vivo* experiments, we used cultured splenocytes (in paper I), VSMCs from the thoracic aorta (in paper II and IV), human microvascular endothelial cells (HMEC) (in paper II), human retinal microvascular endothelial cells (HRMVEC) and human umbilical vein endothelial cells (HUVEC) (both in paper III). As mentioned above, even though the cell culture cannot substitute the *in vivo* experiments, it is a useful alternative technique in several situations.

Cell cultures present several advantages, among others, the culture environment can be strictly controlled (pH, temperature, ppO_2 and $ppCO_2$) and cells can be cryopreserved and used when needed. The cell culture is a reductionistic model that enables studies with molecular and mechanistic approaches. In addition and most importantly, cell culture implies a reduction in the number of animals used (being in line with the 3Rs principle). The most difficult part of the cell culture technique is to recreate the fully characteristics that they have *in situ*, in the animal and to preserve sterile aseptic conditions to avoid chemical and microbial contamination. Furthermore, cells can naturally change their phenotypic characteristics from the original tissue (dedifferentiation) when removed from their physiological context as well as after several passages. Although pros and cons, the outcomes obtained from cell cultures must be assessed in the whole animal where all the cell types and mediators interact to control physiological mechanisms [238].

Single cell suspensions of splenocytes were prepared from the spleen of diabetic and control $ApoE^{-/-}$ mice treated with A-285222 or vehicle for one week (in paper I). The spleen was pressed through a 70 µm cell strainer and the suspension was cultured in medium containing 10% heat-inactivated FCS, 1 mM sodium pyruvate, 10 mM Hepes, 50 U of penicillin, 50 µg/mL streptomycin, 0.05 mM β-mercaptoethanol and 2 mM L-glutamine. The same procedure was applied for

splenocytes from C57BL/6 control mice treated with A-285222 or vehicle for four weeks (in paper I).

Primary cultures of VSMCs were obtained from thoracic aorta explants from NFAT competent and NFATc2 or NFATc3 deficient mice (in papers II and IV). VSMCs were cultured in DMEM/HAM´s F-12 (1:1) medium supplemented with 15% fetal bovine serum (FBS), 2 mM L-glutamine, 50 U/mL penicillin and 50 µg/mL streptomycin and were kept in a water-jacketed incubator at 37°C and 5% CO_2.

Oxidative stress environment induction and ROS/RNS levels

In order to determine whether NFAT inhibition could modulate gene expression pattern in VSMCs under oxidative stress conditions, we stimulated cells with strong oxidative stress inducers. For this, in paper II VSMCs from NFATc3$^{+/+}$ and NFATc3$^{-/-}$ mice (between passages 10-15) were seeded in 24-well plates (7.5 x 10^4 cells/well) and cultured for 24 hours in DMEM containing 5 mmol/L D-glucose and supplemented with 10% FBS before stimulations. As oxidative stress inducers, hydrogen peroxide (H_2O_2, 500 µmol/L) or 3-Morpholinosydnonimine hydrochloride (SIN-1, 100 µmol/L) were used. H_2O_2 induced production $O_2^{\bullet-}$ in VSMCs by activating NOX, whereas, SIN-1 induced peroxynitrite ($ONOO^-$) formation upon decomposition into $O_2^{\bullet-}$ and •NO in aqueous solution. After stimulating VSMCs with oxidative stress inducers during 48 hours in the presence or absence of NFAT blocker (A-285222, 1µM), cells were harvested for gene expression analyses.

In addition, H_2O_2 levels were measured in the culture media 24 hours after incubation of VSMCs or HMEC, in high glucose conditions (25 mM) either in the presence or absence of A-285222 (1µM). Cells were cultured in 96-well plates (1x104 cells/well). H_2O_2 levels released from the cells were measured by Amplex® Red Hydrogen Peroxide/Peroxidase Assay Kit. The Amplex® Red reacts with H_2O_2 in presence of peroxidase (horseradish peroxidase, HRP) in a 1:1 stoichiometry, producing resorufin, a red fluorescent-oxidation product, which fluorescence intensity is proportional to the level of H_2O_2 generated by cells. ROS/RNS levels produced by VSMCs from NFATc3$^{+/+}$ and NFATc3$^{-/-}$ mice cultured in high glucose conditions (25 mM) were measured in the cell culture media after 48 hours incubation. Total ROS/RNS free radical activity was assessed by an indirect method using OxiSelect™ In Vitro ROS/RNS Assay Kit. This assay employs a specific ROS/RNS probe (DCFH-DiOxyQ), which in its reactive state (DCFH) can interact with ROS and RNS species from the sample. This interaction leads to rapid oxidation of DCFH into DCF and fluorescence emission, whose

intensity is proportional to the total free radical activity, translated in ROS/RNS levels.

NFATc2 and NFATc3 transfection

In paper IV, one objective was to study the impact of NFATc2 and NFATc3 deletion or their overexpression on vascular smooth muscle gene expression and proliferation rate. Therefore, thoracic VSMCs (between passages 4 to 11) from NFAT competent, NFATc2 and NFATc3 deficient mice were cultured ($5x10^4$ cells/well, seeded in 24-well plates) in antibiotic free DMEM/HAM´s F-12 (1:1) medium supplemented with 15% FBS and 2 mM L-glutamine during 24 hours. The following day, thoracic VSMCs were transfected either with pNFATc2-EGFP or pNFATc3-EGFP plasmids (0.8 µg or 1 µg of plasmid DNA), complexed with Lipofectamine® 2000 (1.6 µL or 2 µL) in antibiotic and serum free culture medium. Transfection complexes were removed after 4 hours, and cells were incubated for another 20 hours in fresh antibiotic and serum free culture medium. At 24 hours after the transfection start, cells were cultured for 7 days in medium supplemented with serum, L-glutamine and antibiotics (50 U/mL penicillin and 50 µg/mL streptomycin). Transfection efficiency was determined by measuring EGFP fluorescence using a Zeiss LSM 5 laser scanning confocal microscope.

Proliferation of splenocytes and VSMCs

With the aim to study whether NFAT inhibition affects the capacity of immune cells to proliferate, in paper I, we used thymidine incorporation technique to measure proliferation. Hence, splenocytes were cultured ($2x10^5$ cell/well, seeded in 96-well plates) with T cells activators, such as concavalin A (ConA, 2.5µg/mL; Sigma-Aldrich) or CD3/CD28 beads (beads to cell ratio 1:1; Invitrogen, Life Technologies, Carlsbad, CA) for 88 hours. Splenocytes incubated without mitogens were used as controls.

To determine the differential role of isoforms NFATc2 and NFATc3 in a basic cellular function as is proliferation, in paper IV, we used thymidine incorporation technique to measure proliferation in control and transfected thoracic VSMCs ($5x10^3$ cells/well, seeded in 96-well plates).

In this technique radioactive thymidine (^{3}H-Thymidine) is incorporated into the new strands of DNA upon cell division. As a consequence, the amount of incorporated thymidine increases with increased proliferation rates. Radioactive thymidine (methyl-^{3}H, PerkinElmer; 1µCi) was added to splenocytes during the last 16 hours and to the VSMCs during the last 24 hours of culture. Splenocytes and VSMCs were cultured for 88 and 48 hours, respectively. Thymidine

incorporation into the cells was ended by freezing the cell culture before harvesting them on a glassfiber filter (Printed Filtermat A; Wallac Oy, Turku, Finland). Later, the amount of thymidine incorporated into the cells was assessed with a liquid scintillation counter (Wallac, TRILUX 6DET1450021), which measures the energy emitted by the radioactive substance, and it was expressed as counts per minute (cpm).

NFAT transcriptional activity

The increment in NFAT nuclear accumulation does not always translate directly into increased NFAT-dependent transcriptional activity. This is because the availability of co-factors and the inadequate exposure of DNA can limit the possibility of NFAT to induce transcription. Here, we have used a luciferase reporter assay to study the basal level of NFAT-dependent transcriptional activity in diverse organs and to explore how high glucose or other stimuli affect the NFAT-dependent transcriptional activity in different vessels.

Luciferase is an enzyme that catalyses the reaction of luciferin and ATP to produce light. Luciferase reporter assay reflects transcriptional activity of all NFAT isoforms (NFATc1-c4) since all of them have the ability to bind to the NFAT binding site from the IL-4 promoter inserted upstream of luciferase reporter gene.

In paper I, we used control and diabetic NFAT-luc mice treated with A-285222 (0.15 mg/kg) or saline for 16 days to measure luciferase activity in the aortic arch, spleen, thymus, brain, heart, liver and kidney. In paper III, we determined the luciferase activity in intact retinas and in isolated retinal vessels from NFAT-luc mice and Akita/NFAT-luc mice subjected to acute (6 hours after IP-GTT) and chronic hyperglycemia.

An aliquot of the homogenized tissue in lysis buffer was added to luciferase substrate reagent containing ATP and luciferin. Optical density was measured using a Tecan Infinite M200 instrument (Tecan Nordic AB, Mölndal, Sweden) and data were normalized to protein concentration and results were expressed as relative luciferase units (RLU/µg protein).

Quantitative and absolute PCR

Real-time polymerase chain reaction (RT-PCR) is a powerful and often used technique in the research field of molecular medicine and biotechnology for

measuring gene expression. It combines amplification and detection of target genes in a single step. Detection is achieved using either gene-specific fluorescent probes (in TaqMan technique) or a generic fluorescent dye that intercalates non-specifically into double stranded-DNA (SYBR Green technique). PCR product concentration correlates with fluorescence intensity. Target amplification is first detected and is referenced as cycle threshold (C_t), which is the point at which fluorescence intensity exceeds the background fluorescence. Hence, this is an important value used for quantifying levels of gene expression. The greater the quantity of target DNA in the biological sample, the earlier an increase in fluorescence signal will appear, generating a lower C_t [239-241].

RT-PCR is a simple, sensitive and specific technique. It does not need a post-amplification manipulation and it allows comparison between RNAs that could differ in abundance into 7 to 8 orders of magnitude. However, it requires expensive equipment and reagents [239, 240].

Basically, there are four general steps performed for measurement of gene expression using RT-PCR: RNA extraction from biological sample, cDNA synthesis, real-time PCR data acquisition and data analysis.

In our research, in the first step, total RNA from different tissues was isolated through organic extraction using TRI Reagent BD or RNeasy® Plus Mini Kit with spin columns for cultured VSMCs. Then, isolated RNA quantity and integrity were measured, since high quality, DNA-free and non-degraded RNA are needed for successful and accurate measurements. To avoid introduce more variability to the inherent variation in RNA yield from biological samples [239] special care has been taken during the purification process and RNA storage since the RNA is rather unstable and easily degraded.

In the second step, a single-stranded complementary DNA copy (cDNA) of the RNA is performed through the reverse transcription reaction. This reaction entails a source of variability due to the fact that the efficiency of the reverse transcription can be affected by different factors, such as the RNA quality. Small presence of any contaminates, for instance alcohol, phenol, etc, carried over the RNA isolation process can introduce variability in the reverse transcription reaction efficiency. Another source of variability is the priming method chosen for the synthesis of cDNA, which can be either target specific-gene or non-specific (random hexamer primers, oligo-dT or a combination of both). Most importantly, RT-PCR results are comparable only when the same priming strategy and reaction conditions are used [239, 241].

For target specific primers, one reaction per each interesting gene must be done. In all papers where quantitative PCR was used for lots of different target genes, RNA isolation from different tissues was followed by reverse transcription using

random hexamer primer. In paper III, cDNA synthesis for NFAT family members was done with oligo-dT primers to lower the risk of detecting genomic DNA. The oligo-dT primer starts the reverse transcription on the poly-A tail which is present only in mRNA templates. Consequently, it is a particularly good primer for studying gene expression from mRNA. However, the reverse transcription from RNA to cDNA might not be successfully completed for the whole mRNA template [239, 241]. Particularly, the cDNA yield could be significantly lower for long genes, where the interesting sequences are far away from the poly-A tail. In those cases, the use of random hexamer primers might be advantageous as they can initiate the conversion in random locations. Moreover, random hexamer primers must be used for synthesizing cDNA from ribosomal RNA, as in the case of 18S.

The third step is characterized by the quantitative detection of amplicons. For target sequence amplification, synthesized cDNA was used as a PCR template and sequence-specific fluorescent probes from TaqMan Gene Expression assays. Probes are labelled with a fluorophore on the 5' and a quencher dye on the 3', which reduces fluorescence when the probe is intact. During the extension step of the PCR, which in our case consisted of 40 cycles, the *Taq* polymerase included in the assay hydrolyzes the probes bound to target sequences, resulting in increased fluorescence emission [240].

In the four papers, cDNA was amplified on a 7900HT TaqMan System or Quant Studio 7 Flex System instrument (Applied Biosystems, Carlsbad, CA) using different TaqMan Gene Expression assays to measure expression changes in inflammatory response targets in the aortic arch (paper I), the aorta (paper II) and retinal vessels (paper III); in adhesion molecules targets in the aortic arch (paper I) and retinal vessels (paper III); in oxidative stress targets in the aorta and VSMCs (paper II); in the whole retinal structural markers genes (paper III); in all NFAT isoforms in the arterial vascular beds of mouse and in transfected VSMCs (paper IV).

To have a reliable internal control of RNA and cDNA synthesis, PCR amplification of housekeeping genes (HKG) were also performed. Even though HKG are preserved reference genes, it has been shown that their expression can be affected by the experimental treatments, biological process and even different tissues[240]. For that reason, in all papers we have selected different HKGs, such as HPRT (Mm0046968_m1), β-actin (Mm00607939_s1), Cyclophilin B (Mm00478295_m1), 18S (Hs999999021_s1) and GAPDH (4352339E), which have previously been tested in our lab and deemed stable under experimental conditions used in our studies .

Another essential control which must be included in the experimental design, is the non-template control (containing only water) in order to confirm the absence of any contamination with nucleic acid in the reagents.

Generally, the fluorescence curve from RT-PCR reaction has a sigmoid shape with four phases: linear ground phase, early exponential phase, log-linear (also called exponential) phase, and plateau phase [240, 241]. In the first phase, the fluorescence emission is below the background level, whereas in the early exponential phase, the amount of fluorescence emitted is detected, when it has reached the threshold and it exceeds the background. The cycle at which this occurs is known as C_t and this value is used to calculate the gene expression results [240]. C_t value is representative of the starting copy number in the original template. Lower C_t values are associated with a higher number of amplicons, which means fewer cycles of amplification are required for the fluorescence to reach the threshold level of detection. During the log-linear phase there exists an optimal amplification period in which the PCR products are duplicated after each cycle. In the plateau phase, there is an attenuation in the rate of product amplification, which is reached when some of the reagents become limited [240].

Regarding the analysis of data, we used relative quantification in all papers and absolute quantification in paper IV to determine NFAT isoform expression in VSMCs and in different vascular beds from C57BL/6 mice. For that, thymus cDNA was amplified using specific assay of TaqMan gene expression for each NFAT isoform. The thymus was chosen to create standard curves because all NFAT isoforms are expressed at good level in it. Then, PCR products were isolated using NucleoSpin Gel and PCR Clean-up kit and concentrations were determined spectrophotometrically (NanoDrop ND-1000). A standard curve was generated with ten-fold serial dilutions with known copy number input per well for each of the NFAT isoforms. The standard curves produce a linear relationship between C_t value and copy number, allowing the calculation of input copy number for each unknown sample. Equal amplification efficiencies were assumed in all standards and samples.

For relative quantification changes in sample gene expression are expressed in relation to a reference gene (HKG). The relative quantification strategy does not require a standard curve and we used the comparative C_t method as a mathematical model ($R= 2^{-[\Delta Ct\ samlpe\ -\ \Delta CtHKG]}$ or $R= 2^{-[\Delta\Delta Ct]}$) [241] to calculate changes in gene expression.

In addition, we also used a custom RT^2 Profiler PCR Array in paper IV to analyse expression changes in a panel of 42 genes related to the modulation of phenotype and function of VSMCs. RT^2 Profiler PCR Arrays is a reliable system which take the advantage of the combination of real-time PCR performance and the ability of microarrays to detect the expression of abundant and rare genes simultaneously. In

this opportunity, total RNA from cultured thoracic transfected VSMCs was extracted using RNeasy® Plus Mini Kit and cDNA was synthesized with RT^2 First Strand Kit, in which a combination of oligo-dT and random hexamer primers was used. The cDNA was amplified during 40 cycles in a StepOnePlus qPCR cycler using RT^2 SYBR Green ROX qPCR Master mix. As control and to normalized data, three HKG were used, Gapdh (NM_008084), Rn18s (NR_003278) and Hsp90ab1 (NM_008302). Moreover, we used GDC (genomic DNA control) for detecting non-transcribed genomic DNA contamination, RTC (reverse-transcription control) for testing the efficiency of the reverse-transcription reaction performed with the kit and PPC (positive PCR control) for testing the efficiency of the polymerase chain reaction itself. Primer sequences were proprietary of Qiagen. The fold-change expression for each target gene was normalized to the geometric mean of the three HKG, employing the comparative threshold method ($\Delta\Delta C_t$; same mathematical model mentioned above) of the GeneGlobe Data Analysis Center provided by Qiagen. The fold-changes <0.5 were considered as down-regulation, whereas fold-changes >2 as up-regulation. Nine out of the 42 genes in the PCR array were further validated by regular quantitative PCR. These 9 target genes were: Cnn1 (Mm00487032_m1); Klf4 (Mm00516104_m1); Klf5 (Mm00456521_m1); Tagln (Mm00441661_g1); Ace (Mm00802048_m1); Gata4 (Mm00484689_m1); Ccna2 (Mm00438063_m1); Ccnd1 (Mm00432359_m1) and Cdk4 (Mm00726334_s1).

Statistics

Results are expressed as mean±SEM unless otherwise specified. Analyses of distributions were performed before statistical tests were carried out using GraphPad software (Prism 7.0). For parametric data, significance was determined using Student's t-test, or one- or two-way ANOVA followed by Bonferroni's multiple comparison post-test. Non-parametric data was analyzed using Mann-Whitney or Kruskal-Wallis test followed by Dunn's post-test. *$p<0.05$, **$p<0.01$ and ***$p<0.001$.

Results and Discussion

In this section, key results from papers included in this thesis are outlined and discussed. For a more detailed presentation, please refer to Papers I-IV.

Patterns of NFAT isoform expression in various regions of the mouse vasculature (Papers III, IV)

NFAT isoforms are expressed in a large number of tissues, but the expression levels of the individual isoforms seems to vary considerably depending on the tissue and experimental conditions.

With the purpose of measuring the pattern and absolute levels of NFAT isoform expression along the mouse vascular tree and under basal conditions, vessels from 13 different vascular regions were isolated from control C57Bl/6 mice for absolute qPCR NFAT isoform quantification (paper IV, figure 1). These regions included retinal vessels, cerebral and carotid arteries, aorta, hepatic artery, portal vein, renal, mesenteric, femoral and tail arteries.

Based on the results from paper IV (figure1), all NFAT family members were present, but NFATc3 was by far the most abundant isoform expressed in all vessels examined, with expression levels ranging between 815 and 3667 million copies per µg of total RNA for the hepatic and tail arteries, respectively. NFATc3 was followed in abundance by NFATc1, which had an intermediate expression level, with around 150 million copies per µg of total RNA. NFATc2 and NFATc4 were expressed at lower levels, with approximately 10 million copies per µg of total RNA in the majority of the vessels examined.

Interestingly, we found in retinal vessels the highest NFATc2 expression, with 34 million copies per µg of total RNA and the lowest NFATc1 transcript number, with 19 million copies per µg of total RNA, among all vessels studies. This seems in line with the results obtained in paper III (figure1), in which not only NFATc3 but also NFATc2 were detected in isolated retinal vessels using conventional RT-PCR. We found an enrichment of NFATc2 in the retinal vessels when compared to the levels found in whole retina. In paper III (figure 1) however, we were unable to

detect NFATc1 or NFATc4 in retinal vessels, although all 4 isoforms were detected in intact whole retina. It is possible that the extremely low copy numbers of NFATc1 and NFATc4 (<20 and 5 million copies per µg total mRNA, respectively),calculated using the more sensitive absolute quantification method, translated in insufficient amounts of products to be detected in agarose gels after conventional RT-PCR. Another potential explanation for this discrepancy could be the different background of the strains used in papers III and IV (FVBN vs. C57BL/6). Although this cannot be ruled out unless a more systematic comparison is done, we have not noticed differences in detection frequencies of NFAT transcripts or intensity of the immunostainings when examining the same preparation from mice of different backgrounds in the past (i.e. cerebral arteries from CD1, NMRI, FVBN, BALB/c) [51, 133, 149]. Another interesting observation in paper IV (supplemental figure 1) was that cultured aortic VSMCs had lower levels of NFATc1 and NFATc2 expression, and higher levels of NFATc3 than the levels measured in intact native aorta.

Is there functional non-redundancy of NFAT isoforms in the vasculature? (Paper IV)

Vascular NFATc3 has been extensively studied in our lab and by others, while much less is known about NFATc2, may be because of its low abundance. Very little is known about the expression patterns of NFATc2, what regulates or induced expression of NFATc2, its activation requirements and whether it has a functional role in the vasculature. Previously, we demonstrated that the same stimuli can differentially activate NFAT isoforms that are simultaneously co-expressed in the same cell[232]. Here in paper III (figure 2 and supplemental figure 3) of this thesis, we found that acute hyperglycemia induced an robust NFATc3 activation response in the endothelium of retinal microvessels, whereas NFATc2 was not activated by the same stimulus in the same cells. These observations suggest at least differential activation requirements for these 2 isoforms.

Plasticity of NFATc2 isoform expression in the aorta

Previous works from our group and others have shown that vascular NFATc2 expression could be induced in pathological situations or under certain stimulatory circumstances [156, 174]. In native non-stimulated human myometrial arteries, NFATc2 expression was absent or undetectable, whereas it was increased or easily detected after arteries had been cultured for 4 days in organ culture, conditions

promoting a proliferating and less differentiated phenotype of VSMCs [156]. Furthermore, an increased NFATc2 expression and activation was found in pulmonary arterial smooth muscle cells (PASMCs) from patients with pulmonary arterial hypertension when compared to healthy patients and in normal PASMCs exposed to chronic hypoxia [174]. To further explore this plasticity of expression under other pathological conditions, in paper IV (figure 2) we explored if the expression of NFATc2 could be altered in arteries from diabetic mice. The expression levels of all NFAT isoforms were assessed in the aorta of STZ-induced diabetic and control non-diabetic mice. After 2 weeks of the first STZ injection, mice had significantly higher blood glucose levels compared to control vehicle-injected mice (8.9±0.6 mM vs. 23.2±1.9 mM for control and diabetic mice, respectively). At this experimental time point, the expression of NFATc2 was significantly increased in the aorta of diabetic mice compared to non-diabetic mice, while the levels of all other isoforms remained unchanged. This supports the idea that NFATc2 has some degree of plasticity and that expression can be induced or enhanced in response to experimental and/or pathological stimuli, including by the metabolic changes associated with diabetes.

Compensatory effects in NFAT isoform expression evoked by deficiency of NFATc2 and NFATc3 in VSMCs

The absence of copies of NFATc3 transcripts, measured by absolute qPCR, confirmed the genotype of the VSMCs explanted from NFATc3$^{-/-}$ mice. However, VSMCs explanted from NFATc2$^{-/-}$ mice, still expressed a very low level of NFATc2 transcript (0.018 vs. 0.16 million copies per µg total RNA in NFATc2 competent cells). This is in line with data describing the NFATc2 deficient mice showing the expression of an aberrant fragment that is either not produced or rapidly degraded [209].

Deficiency of either NFATc3 or NFATc2 in VSMCs resulted in compensatory changes in the expression of the other NFAT isoforms. Lack of NFATc3 was accompanied by decreased expression of NFATc1, no impact on NFATc2 and increased expression of NFATc4. Lack of NFATc2 had no impact on NFATc1 or NFATc3 and only resulted in decreased expression of NFATc4. Thus, NFATc3 and NFATc2 deficiency seem to have opposing effects on the expression of NFATc4 (paper IV, figure 4).

In order to study the potential effect of modified NFATc2 and NFATc3 expression on smooth muscle gene expression, competent and deficient VSMCs were transfected with plasmids encoding NFATc2 or NFATc3 (paper IV, figure 4). Transfection with plasmid encoding NFATc2 resulted in a significant overexpression of NFATc2 in both competent and deficient cells, whereas

transfection with plasmid encoding NFATc3 resulted in a significant overexpression of NFATc3 in competent cells but a lower efficiency in NFATc3 deficient VSMCs. Neither NFATc2 overexpression nor NFATc3 induced any changes on the expression level of the other NFAT isoforms.

NFAT as a regulator of gene expression and proliferation in VSMCs

Differential effects of NFATc2 and NFATc3 deletion on gene expression in VSMCs (Paper IV)

We explored the expression of genes related to the regulation of VSMCs phenotypic modulation (for example: transcriptional activators and co-activators of specific smooth muscle gene expression, regulators of actin polymerization, miR143/145 target genes) and smooth muscle marker genes (for instance: Tagln, Myocd, Myh11, Smtn, Cnn1) in cultured VSMCs from NFAT WT mice and from either NFATc2 or NFATc3 deficient mice. For that, 41 genes were analyzed in a custom-designed PCR Profiler Array. The fold change differences in gene expression between NFATc deficient and competent cells were calculated and plotted in a two-dimensional matrix (paper IV, figure 3). Deletion of NFATc3 generated an up-regulation of the expression of 10 genes, whereas 9 genes were down-regulated, in at least > or <2-fold, respectively, compared to competent cells. The lack of NFATc2 resulted in the up-regulated expression of 2 genes and down-regulation of 7 genes. Among all those genes, we focused on 6 genes, including Gata4, Klf4, Klf5, Angiotensin I converting enzyme (Ace), Cnn1 and Tagln, which were validated in a larger number of samples.

The most affected gene was Ace, with 31-fold higher expression in NFATc3 deficient cells compared to competent cells, but the lack of NFATc2 did not affect its expression. Interestingly, several genes were differentially altered in cells that lacked NFATc2 or NFATc3 proteins, including Gata4, Klf4 and Klf5. Gata4 was down-regulated in NFATc2 deficient cells, but up-regulated in NFATc3 deficient cells. Other gene target that was regulated in a similar way than Gata4, was Klf5, whereas Klf4 was regulated in exactly the opposite way. In brief, high expression levels of Gata4 and Klf5 as well as low expression of Klf4 were observed in NFATc3 deficient cells, while in NFATc2 deficient cells the opposite pattern was found (paper IV, figure 5). Overexpression of NFATc2 and NFATc3 failed to affect Gata4 or Klf5, but a modest increment of Klf4 expression was observed in NFATc2 competent cells upon NFATc2 overexpression.

Gata4 belongs to the Gata family of transcription factors, predominantly expressed in the cardiac system and originally described as a regulator of cardiac hypertrophy, which interacts with NFAT in the nucleus [164, 242]. It has also been shown that Gata4 controls the proliferation of PASMCs through direct binding and activation of cyclin D2 and cyclin-dependent kinase 4 (Cdk4) in mice and bovines [243, 244], and activation of cyclin D1 in *Xenopus laevis* [245]. Depletion of Gata4 has been associated with marked cardiac myocyte apoptosis and hypoplasia [242, 246]. We were surprised to observed such a dramatic increment of Gata4 expression in deficient NFATc3 cells, given that low or undetected levels of Gata4 have been described in the vascular tree outside of the pulmonary system and aortic root. In VSMCs, Gata6 has been the focus of attention and not much data is available about Gata4 [247].

It is well known that Klf4 is an inhibitor of proliferation, via the regulation of the cyclin-dependent kinase inhibitor-1A (CdkN1A or p21), a cell cycle regulator [248], whereas Klf5 has exactly the opposite effects, which means that it induces cell proliferation[186]. Klf4 acts a repressor of contractile gene markers [189, 190, 192].

Overall, lack of NFATc2 or NFATc3 proteins in VSMCs had differential impact on the expression of Gata4, Klf4 and Klf5. The significantly higher expression of Gata4 and Klf5 in NFATc3 deficient VSMCs can potentially drive the increase in cell proliferation observed in these cells.

NFATc3 deletion influences on the expression of differentiated cell markers and proliferation in VSMCs (Paper IV)

Several studies have reported a direct influence of NFAT on the regulation of cell cycle progression markers [156, 157, 164, 184, 249]. For instance, it has been shown that NFAT regulates the expression of Ccna2, cyclin E, Cdk4 and the cdk inhibitor p21 in VSMCs, lymphocytes and thymocytes from humans and mice [164, 184, 250, 251].

In paper IV (figure 7), we provide evidence that deletion of NFATc3 yields VSMCs with significantly higher proliferation rates and this was associated to higher expression of Ccna2. The higher expression of Ccna2, together with the higher expression of Gata4 and Klf5 in NFATc3 deficient VSMCs could potentially underlie the increased proliferative capacity of these cells. On the other hand, lack of NFATc2 had no measurable impact on VSMC proliferation, despite the fact that the expression of Ccnd1 was significantly increased when compared to control cells. Lack of NFATc2 in VSMCs also resulted in higher expression of Klf4, which could potentially engage other signalling pathways counteracting the effects of increased Ccnd1 mRNA (or maybe the increased mRNA levels of

Ccnd1 were simply not sufficient to translate on changes in thymidine incorporation rates). Interestingly, overexpression of NFATc2 resulted in inhibition of cell proliferation, which can be partially explained by the observed increased Klf4 expression, but not by increased Ccnd1 expression, considering the role of these genes. Overexpression of NFATc3 had no impact on proliferation or the expression of cell cycle markers. Cdk4 is an important G0/G1 restriction point which controls the entrance of the cells into the cell cycle when they leave the resting state. No differences in Cdk4 expression were observed between NFAT competent or deficient cells.

The contractile phenotype of SMC is characterized by high expression of SMC differentiation marker genes, such as SMα-actin, SM myosin heavy chain (SM-MHC), Tagln, calponin (Cnn1), Smtn, and Myocd. Particularly, SMCs undergo changes in their phenotype during specific situations like neointimal formation in response to vessel injury, within atherosclerotic plaques and under conditions mirroring the metabolic changes that occur in diabetes or in arteries from diabetic patients [185, 192, 252]. In *in vitro* conventional culture systems, VSMCs spontaneously acquire features of de-differentiated cells with characteristics found in vascular lesions, such as in atherosclerotic plaques and restenosis after angioplasty. Primary cultures of VSMCs rapidly lose their contractile capacity and gain proliferative capacity. In addition, loss of actin filament organization is progressively observed in VSMCs isolated from rat aortas when cultured for various passages. A random actin filament distribution was observed in VSMCs at passage 10 compared to cells at passage 4 [253]. During this structural transition, a decreased expression of contractile markers, including Myh11, Myocd, Tagln, SMα-actin, N-cadherin, Smtn has been observed in VSMCs in a passage-dependent manner [253, 254].

In paper IV (figure 6), it was shown that deletion of NFATc3 up-regulated the expression of the contractile markers Cnn1, Tagln and also of Ace when compared with NFATc3 competent VSMCs. However, lack of NFATc2 had no effect on the expression of those genes. Interestingly, overexpression of NFATc2 significantly reduced Ace expression levels in both competent and deficient NFATc2 VSMCs, whereas NFATc3 overexpression only decreased Tagln expression in NFATc3 deficient cells with respect to competent mock transfected VSMCs.

Cnn1 and Tagln are accessory proteins that play an important role in the phenotypic modulation and contractility of VSMCs. Tagln is required to generate polymeric (F)-actin and thus enhance cell contractility [255]. On the other hand, Cnn1, a protein that is structurally similar to SM22, directly regulates smooth muscle contractility, since both PKC and Ca^{2+}-calmodulin kinase II phosphorylate Cnn1, resulting in the loss of its capacity to bind actin and thus to inhibit the (AM)ATPase [256]. Moreover, the expression of contractile markers is modulated

by SRF and co-activators (myocardin-related transcription factors, MRTF), which bind to CArG box DNA sequences within the promoter of these genes [252]. Interestingly, it has been reported that NFAT and SRF interact cooperatively regulating the α-actin expression in SMCs by overlapping CArG box/NFAT site. In addition, inhibition of NFAT signalling with CsA or FK506 resulted in reduced α-actin expression in VSMCs [257]. Monomeric actin sequesters MRTF and prevents its interaction with SRF. Actin polymerization is a crucial event for the expression of SMCs contractile markers genes, due to the fact that after actin polymerization, MRTF is released and it can associate with SRF in the nucleus. Then, SRF binds to CArG box sequences in the promoter.

Recently, microRNAs (miRNAs) (short noncoding RNAs with 18-25 nucleotides long) have gained attention as important regulators in the development, differentiation and function of VSMCs. Specifically, the cluster miR143/145 is highly expressed in VSMCs during development and is important for the transition to a VSMCs contractile phenotype[37, 258]. In addition, it has been reported that the expression of Ace in VSMCs is up-regulated by miR143/145 [258, 259]. Apparently, Ace in VSMCs is associated with a less contractile phenotype, which might explain the reduced contractile response in vessels from miR143/145 knockout mice [260].

The original dogma used to describe VSMCs proliferation and differentiation as opposite processes. However, it was demonstrated that cessation of proliferation alone was not sufficient to induce VSMCs differentiation. Beside this, it has also been shown that contractile and synthetic VSMCs phenotypes are regulated by separated intracellular mechanisms and the two phenotypes can co-exist. Both phenotypes are not mutually exclusive and it is possible to find differentiated VSMCs that do proliferate and vice-versa [37, 261]. Our findings seem to reflect this new paradigm as well; NFATc3 deficient VSMCs exhibited higher proliferation rates, increased expression of cell cycle progression related genes, but at the same time, increased expression of smooth muscle marker gene characteristic of a more contractile phenotype.

All together, despite the huge differences in the abundance (~400-fold lower) of NFATc2 with respect to NFATc3 transcripts in both the vascular wall and in VSMCs, lack of the lower abundant NFATc2 in VSMCs had a clear impact on the expression of transcription factors and co-activator of smooth muscle specific gene expression. So how can the very low abundant NFATc2 still have such an impact on gene expression? In an interesting study conducted in HEK293, RBL-1 and HBE cells, NFATc2 and NFATc3 were shown to have different activation requirements and deactivation kinetics [136]. While NFATc2 only required release of Ca^{2+} from store-operated CRAC channels in the plasma membrane, NFATc3 required not only the engagement of CRAC channels but also nuclear Ca^{2+} and

engagement of IP_3R in the inner nuclear membrane. Moreover, these isoforms also differ in the kinetics of rephosphorylation, with a slower inactivation of NFATc2 acting as a kind of short-term memory to gene expression [136].

A-285222, a novel NFAT blocker

With the ambition of evaluating the contribution of NFAT activation to diabetes-induced macro- and microvascular complications, the NFAT signalling pathway was inhibited with A-285222 in *in vivo* experimental models of diabetic atherosclerosis and diabetic retinopathy, and in *in vitro* studies (Papers I-III).

Bioavailability and pharmacokinetics of A-285222 (Paper I)

A-285222 is a low molecular weight (416 Dalton) and cell-permeable molecule [228] with a reduced capacity to bind plasma proteins in the bloodstream [227]. In previous works, A-285222 has been orally administrated to rats and cynomolgus monkeys for 2 weeks and it was well tolerated when plasma levels were below 4 μg/mL (9.6 μM) [227, 230]. In our studies, oral administration was not the preferred route for delivery of A-285222 due to the fact that diabetic mice drink more water than non-diabetic control mice, imposing challenges in achieving and monitoring comparable target doses in all animals treated. Therefore, an i.p. route of administration was chosen, which also has the advantage of being a faster absorption route than orally. To know how well A-285222 was absorbed after i.p. administration, the plasma concentration of this compound 5 minutes after an i.p. injection was compared to levels obtained after intra-cardiac delivery (i.c.) at two different doses (0.15 and 1.5 mg/Kg). Gas chromatography-mass spectroscopy (GC/MS) was employed to identify and quantify A-285222 in plasma samples, using an analogous inactive compound A-216491 as internal control. Both compounds were extracted with ethyl acetate and the evaporated organic phase redissolved in chlorophorme. Plasma levels of A-285222 were at the same range regardless the route of administration (3.4 μM vs. 3.2 μM for the low doses; 4.6 vs. 5.1 μM for the high doses; i.p. vs. i.c. respectively), suggesting that the drug was sufficiently absorbed and it had high bioavailability after i.p. injections.

We also studied the pharmacokinetics of A-285222 after i.p. administration. Previous studies in rats and cynomolgus monkeys, had reported that the half-life of A-285222 was between 6 to 8 hours in plasma after oral administration [227]. To measure the plasma concentration of A-285222 after i.p. administration (0.29 mg/Kg), blood samples from $ApoE^{-/-}$ mice were collected through cardiac puncture at different time points (30 minutes, 1, 2, 4, 6, 12 and 24 hours). During the first

six hours, the level of A-285222 in plasma was between 100-200 nM with a peak at 2 hours and it was no longer detected at 12 and 24 hours. Moreover, the drug was not detected in the plasma of mice that had been treated for either one or four weeks with daily injections of A-285222 (0.29 mg/Kg/day) using blood samples obtained 24h after the last injection, ruling out a potential accumulation of the drug in the circulation.

Treatment with A-285222 was well-tolerated and no changes were observed in body weight or the behaviour of the mice. Plasma triglycerides were not affected by A-285222, regardless the mouse strain or background studied ($ApoE^{-/-}$, IGF-II/$LDLR^{-/-}ApoB^{100/100}$, FVBN, C57BL/6) , the duration of treatment (1, 2 or 4 weeks), or the diabetes status. Treatment with A-285222 did not result in hepatosteatosis, which could occur if the drug accumulated in the liver (paper I, supplemental figure 3). Visual inspection and histological examination of the spleen showed no abnormalities in any of the study groups and spleen weight was not affected by A-285222.

The mechanism of action of A-285222 is not known. As other BTP compounds, A-285222 maintains NFAT in the cytosol in a phosphorylated state, preventing NFAT nuclear translocation and subsequently, NFAT-transcriptional activity. Inhibition of NFAT does not affect NF-κB or AP-1 activation, or dephosphorylation of other CaN substrates such as the type II regulatory subunit of PKA and the transcription factor Elk-1 [228]. Unpublished data from our laboratory also showed that A-285222 has no effect on the activation of NF-κB, AP-1 or Oct in VSMCs. In addition, acute doses of A-285222 (0.1, 1 and 10 μM) had no effects on basal force, high-potassium- and ET-1 induced contractile responses in human resistance arteries , suggesting it less likely that the blocker could have acute effects on EC-coupling [156].

In paper I (figure 4) we also found that A-285222 was able to reduced NFAT-transcriptional activity only in those tissues in which NFAT had been previously activated. This is puzzling, considering the very large variation in basal NFAT-transcriptional activity observed in the different tissues examined. For example the brain had the highest level of NFAT basal activity and yet A-285222 treatment had no effect on NFAT-luciferase activity, despite the fact that A-285222 is expected to cross the blood-brain barrier [230]. More studies will be required to determine the exact mechanism of action of A-285222. A systematic testing of the effects of A-285222 on the nuclear export machinery and the activity of constitutive or inducible kinases and identification of potential binding targets of A-285222 will be needed to answer this question. It may be possible that there is yet an unidentified phosphatase or kinase able to alter the very dynamic import-export balance of NFAT to and from the nucleus.

NFAT is activated in vessels by hyperglycemia (Papers I and III)

Previous work from our laboratory had demonstrated that a modest elevation of extracellular glucose *ex vivo* was enough to activate NFAT in the smooth muscle layer of mice cerebral arteries and in aorta [133]. The effect of glucose on NFAT activation was dose- and time-dependent, with a 3.5 mM increment of high glucose for 8 minutes was sufficient to increase NFATc3 nuclear accumulation. This NFATc3 activation was inhibited by pre-incubation with the CaN blocker CsA and by A-285222. Neither mannitol, nor L-glucose were able to increase NFATc3 nuclear accumulation, ruling out a potential osmotic effect of glucose and showing that glucose needed to be metabolized for the effects to occur. In paper III (figure 2) of this thesis, we showed that NFATc3 is readily activated by high extracellular glucose also in the endothelium of retinal microvessels *ex vivo*. Since one of the aims of this thesis was to investigate whether NFAT signalling contributes to the development of vascular complications of diabetes, we conducted a series of experiments to test whether hyperglycemia could activate NFAT *in vivo*. Considering also that in diabetes both acute glucose fluctuations and sustained hyperglycemia occur (*i.e* postprandial and interprandial periods) [262], NFAT activation was evaluated in the vascular wall under both situations.

In vivo NFAT activation by acute hyperglycemia (Paper III)

In paper III (figure 3), we tested if a single peak of glucose (IP-GTT) was enough to activate NFATc3 in mouse retinal microvessels. Nuclear accumulation of NFATc3 was significantly increased in retinal vessels 30 minutes after the start of the IP-GTT. Thirty minutes was determined in pilot experiments to be the optimal time at which the plasma glucose levels reach a maximum after a single IP-GTT. This is in line with what others have reported in mice [263]. NFATc3 nuclear accumulation was positively correlated to the blood glucose concentration ($r = 0.600$; $P = 0.017$). In addition, the increase in NFATc3 nuclear accumulation translated into increased NFAT-dependent transcriptional activity in retinal microvessels. This increase in NFAT-luciferase activity is likely originated mainly from ECs and VSMCs, but also potentially from pericytes that also seemed preserved using the protocol for isolation of retinal vessels. However, since non-vascular cell markers were not detected in the isolated retinal vessel preparation, we could rule out that the luciferase signal could be originated from neurons or glia cells. NFAT-dependent transcriptional activity did not changes in response to acute hyperglycemia when it was measured in the whole retina, suggesting a selective glucose-dependent activation of NFAT in the vascular retina.

Based on these results, a reasonable question would be whether a glucose peak after a meal is sufficient to activate NFAT in the vascular wall in humans. Under normal physiological conditions, blood glucose levels rise approximately 2 mM (from 4.5 to 6.5 mM) after a meal [264]. Hence it would probably not be sufficient to activate NFATc3. This plasma glucose peak after a meal is accompanied by an insulin peak. In previous work from our laboratory, we showed that insulin alone (0.6 and 6 ng/mL) could not affect NFAT nuclear accumulation in cerebral arteries *ex vivo*[51]. In diabetic patients who have an elevated basal blood glucose level as well as larger blood glucose peaks after meals [265], it is possible that these glucose fluctuations may be sufficient for NFAT activation in the vascular wall.

In vivo NFAT activation by chronic hyperglycemia (papers I, III)

In papers I and III, we studied whether sustained hyperglycemia could activates NFAT in macro- and microvessels. Using a protocol involving multiple low-doses of STZ to induce diabetes, our group had shown in the past a significant activation of NFAT transcriptional activity as evidenced by increase luciferase activity in the aorta of the diabetic mice 2 weeks after the onset of diabetes [51]. This increased NFAT-luciferase activity was driven by NFATc3, as demonstrated by no changes in transcriptional activity in NFATc3$^{-/-}$ mice undergoing the exact same protocol [51]. In papers I (figure 4) and III (figure4) of this thesis, STZ treatment rendered the transgenic NFAT-luc mice diabetic. The STZ treatment of NFAT-luciferase mice on the FVBN background was found to be a good model to study the glucose-dependent effects, because neither plasma lipids levels (paper I, supplemental figure 4) nor expression of inflammatory plasma cytokines (paper III, table 1) were affected by the chemical.

In retinal vessels (paper III, figure 4), we used two diabetic mice models to study whether NFAT was activated by chronic hyperglycemia; the chemically induced model using STZ and a genetically induced model (Akita/NFAT-luc mice). NFAT-dependent transcriptional activity was measured in retinal vessels in both models, either 12 days after the first injection of STZ or at 6 weeks of age in the Akita/NFAT-luc mice; being the diabetes duration equivalent in both models. NFAT-dependent transcriptional activity was increased in both models (68% and 148% increases for the STZ and Akita models, respectively). In agreement with the results after an IP-GTT, we could not detect changes in NFAT transcriptional activity when the whole retina (as opposed to isolated vessels) was examined, regardless of the time-point studied (7, 12 or 16 days after the first STZ injection). This observation supports the idea that NFAT activation selectively occurs in retinal vessels, and maybe also highlights that non-vascular cells may have other NFAT activation requirements.

Reinforcing the idea that NFAT activation is not a generalized phenomenon, NFAT-dependent transcriptional activity was only increased in the aortic arch after 16 days of the first STZ-injection, but was unchanged in spleen, thymus, brain, heart, liver and kidney, organs which were also exposed to high blood glucose levels during that period (paper I, figure 4). Interestingly, all these organs displayed variable basal and clearly detectable NFAT-dependent transcriptional activity, which was higher in those organs with considerable CaN protein expression [145].

To sum up, our results demonstrated that NFAT is sensitive to changes in blood glucose levels and that hyperglycemia is a potent stimulus for NFAT activation *in vivo* in the aortic arch and in retinal vessels, sites prone to develop vascular complications of diabetes.

Mechanism proposed for glucose-induced NFAT activation (paper III)

In previous work from our lab the mechanism of action through which high glucose activates NFAT in cerebral arteries was delineated [133]. In paper III (figure 2 and supplemental figure 2), we tested whether the same mechanism could explain the increased NFATc3 nuclear accumulation observed in retinal vessels stimulated *ex vivo* with high glucose.

We found that the high glucose-induced increase in NFATc3 nuclear accumulation in retinal was prevented by incubation with the exonucleotidase apyrase, strongly indicating the involvement of extracellular nucleotides in the activation of NFATc3. Exonucleotidases are present in the circulation and hydrolyze extracellular nucleotides such as ATP, ADP, UTP and UDP [266].

It has been reported that hyperglycemia increased ATP in retinal cell culture [267] and a more recent study showed that diabetic patients have increased intravitreal concentrations of ATP, ADP and AMP [268]. Several cells release nucleotides in response to mechanical or pharmacological stimuli, for instance, ECs, SMCs, lymphocytes, among others. These nucleotides can exert both auto-and paracrine effects by binding to purinergic P2 receptors in the plasma membrane [269] and increasing global $[Ca^{2+}]_i$ [270]. In smooth muscle from cerebral arteries, UTP was found to be an effective stimulus for NFATc3 nuclear accumulation, by virtue of both engaging Ca^{2+} release through IP3R and extracellular Ca^{2+} influx through L-type, VDCC, as well as by inhibiting Ca^{2+} sparks [150]. It was later shown also in mouse cerebral arteries, that the hyperglycemia-induced activation of NFATc3 was dependent on the local release of extracellular nucleotides, which acted locally on $P2Y_{2/4}$ and $P2Y_6$ receptors, based on experiments using the stable analogs UDPβs and UTPγs and the $P2Y_6$ receptor antagonist MRS2578 [133].

Taken together, NFATc3 activation in response to high glucose in the endothelium of retinal vessels is not due to an osmotic effect and seems to be dependent on 1) the metabolization of glucose intracellularly, 2) the production of extracellular nucleotides acting locally and 3) activation of CaN. Further studies are needed to determine the identity of the involved nucleotide (ATP, ADP, UTP or UTP) and purinergic receptor in this tissue.

Role of NFAT in diabetes-induced atherosclerosis (Paper I and II)

It is well-established that atherosclerosis development increases in the context of diabetes. In addition, it is also known that NFAT is activated by high glucose both *in vitro* and *in vivo* in the arterial wall. Once activated, NFAT can regulate the expression of pro-inflammatory molecules such as IL-6, OPN, AIF-1,VCAM-1, TF and MCP-1 [51, 156, 178, 271, 272]. Against this background, we asked whether the NFAT-signalling pathway was involved in the exacerbated atherosclerosis development observed in diabetes. For this, we used animal models that recreate both T1D (paper I) and T2D (paper II).

To address this question, in paper I (figure 1, figure 2 and supplemental figure 1), 22-week-old $ApoE^{-/-}$ mice were made diabetic with STZ injections. Eight weeks after the first STZ-injection, a 2.2 fold increase in atherosclerotic plaque area in the aortic arch was observed when compared to aged-matched non-diabetic control mice. In the descending aorta and in the aortic root, a similar effect of diabetes was observed (2.1 and 1.6 fold increases, respectively), but the overall plaque area was smaller than in the aortic arch. This reinforces the fact that the aortic arch is a privileged region for developing atherosclerosis in this mouse model. These findings were in line with previous studies showing differential effects of STZ-induced diabetes on specific regions of the aorta of $ApoE^{-/-}$mice [273, 274]. Our mice were treated with the NFAT blocker (A-285222; 0.29 mg/kg body weight) during the last 4 weeks of the experiment. Interestingly, NFAT inhibition completely suppressed the accelerated diabetes-induced atherosclerosis in the aortic arch. This effect was less pronounced in the descending aorta and negligible in the aortic root. An interesting secondary finding in this study was the total cross sectional area at the level of the aortic root was larger in diabetic than in non-diabetic mice. This larger total area was the combined result of increased plaque size (the 1.6 fold increase mentioned above), increased lumen area and thinning of the media layer, in line with previous reports describing erosion and focal dilation of the aortic wall in this mouse model. If the plaque area was expressed as percentage of total cross sectional area, which is often the preferred way to express

changes in plaque area in the field, only a modest size difference was found between diabetic and control mice (16.5%). This highlights the importance of expressing plaque size results both as percentage of cross-sectional area and as actual size values.

Another important observation was that treatment with A-285222 only affected the diabetes-driven aggravation of atherosclerosis, but had no impact on the non-diabetic control mice, suggesting that different mechanisms may underlie plaque formation under diabetic and non-diabetic conditions.

In paper II (figure 1 and figure 5), the same question was addressed but in a novel mouse model of T2D. For this, longitudinal studies were carried out in young (10-16 weeks-old) and old (46-74 weeks-old) IGF-II/LDLR$^{-/-}$ApoB$^{100/100}$ mice, fed with high fat Western diet (HFD Western; 0.15% cholesterol; 42% fat) during 8 weeks. In Heinonen, S. *et al.*, it was shown that atherosclerotic lesion progression was accelerated in the aortas of IGF-II/LDLR$^{-/-}$ApoB$^{100/100}$ mice when compared to LDLR$^{-/-}$ApoB$^{100/100}$ control mice [217]. In our study, mice were treated with A-285222 (0.29 mg/kg body weight) during the last 4 weeks of the experiment. Inhibition of NFAT significantly decreased atherosclerosis in the brachiocephalic artery, another vascular region prone to developing this disease. Particularly, the plaque size and the degree of stenosis in this artery were reduced by 64.3 and 49.3%, respectively after treatment in young males, whereas the plaque size was reduced by 30% in old female mice.

Could the concomitant hyperlipidemia induced by STZ be driving the accelerated atherosclerosis via NFAT activation? (Paper I)

Congruent with previous studies [49, 199, 271], elevation of total plasma cholesterol levels occurred in association with the hyperglycemia induced by STZ in ApoE$^{-/-}$ mice, a typical mouse model of T1D. Hyperlipidemia, alone or together with hyperglycemia, is a recognized driver of the accelerated atherosclerosis in diabetes [49, 275], but it has been difficult to dissect the molecular mechanisms engaged by each stimulus and whether there are common mechanisms engaged by both hyperlipidemia and hyperglycemia. In an attempt to better understand this issue, we investigated if NFAT could, at all be activated by hyperlipidemia *in vivo*. For this, NFAT-luc mice were fed with HFD (0.15% cholesterol, 21% fat) or chow diet for 4 or 8 weeks. Almost 2 fold increases in plasma total cholesterol level were observed in HFD-fed mice, but no changes were detected on NFAT-dependent transcriptional activity in the aorta. Even though some studies have shown that lipids can activate NFAT in ECs and in VSMCs *in vitro*, no studies have explored whether the same takes place in intact arteries *ex vivo* or *in vivo* [153, 155, 276, 277]. In our study, we cannot exclude a potential effect of high

triglycerides or high oxidized lipids on NFAT activation, given that plasma triglycerides levels were not affected by the HFD protocol. Interestingly, 8 weeks of HFD resulted in a small but significant increase of blood glucose in mice (from 9.7 to 12.7 mM), which was not translated to NFAT activation (paper I, figure 1, table 1, supplemental figure 4). This is in line with our previous results, in which it was shown that increments of blood glucose lower than 3.5 mM were not sufficient to activates NFAT in cerebral arteries [133]. The small increase of blood glucose could be a consequence of insulin resistance in peripheral tissues, with HFD causing an increase in the number and size of adipocytes, but these being refractive to insulin-induced glucose metabolism [278]. There are only a handful of models where diabetes induction does not provoke major lipid changes [196]; one such model is the one we used in paper II.

Gender issues in atherosclerosis (Paper II)

There are significant gender differences in the prevalence and burden of CVD between men and women [279]. Women have lower CVD mortality rates than age-matched men until 75 years of age, but because women have longer life expectancy than men, they represent a larger fraction of the elderly population living with CVD [280]. Even though the prevalence of T2D is similar in men and women, women with diabetes have greater risk of coronary heart disease than men with diabetes [279, 281].

In paper II (figure 1, supplemental figure 1, table 1 and figure 5), at the end of the experimental protocol, we observed in both animal cohorts sex-dependent differences in plaque size in the young IGF-II/LDLR$^{-/-}$ApoB$^{100/100}$ mice (10-16 weeks old), but not in the old mice (46-74 weeks old). Young male mice in the control untreated groups had larger atherosclerotic plaques and stenosis in the brachiocephalic artery than corresponding female mice (in average ~50% larger, both plaque and stenosis). Male mice had larger body weight and higher plasma triglycerides than female mice, potentially contributing to the observed differences in plaque size. However, sex-dependent differences in atherosclerotic plaque size, atherosclerotic vascular bed distribution and plaque composition have been reported in various experimental models [196].

In line with our findings in paper II, ApoE$^{-/-}$ female mice were found exhibited smaller atherosclerotic lesion area in the aorta and lower lipid- and macrophage plaque content than age-matched male mice (32-34 week-old of age) [282]. Differences in humans have been attributed to the atheroprotective role of estrogen, which promotes nitric oxide production and decreases the oxidative stress level in VSMCs, either acting as a free radical scavenger or down-regulating the expression of enzymes responsible for the generation of free radical species

such as NOXs [280, 282]. In experimental models, the underlying mechanisms leading to these sex differences are less well-mapped.

Interestingly, we found sex-dependent differences in the expression of oxidative stress hallmarks in paper II (supplemental figure 3). As detailed in previous sections of this thesis, oxidative stress is a key driver in the development of atherosclerosis, in particular in the context of diabetes [109]. NOX1 and NOX2 have been described as pro-atherogenic isoforms, whereas NOX4 has been recently shown to have an anti-atherogenic role [109]. In our hands, levels of NOX2 were relatively higher in males than in females, while levels of atheroprotective NOX4, catalase and GLO1 were relatively higher in arteries from female mice. These differences could potentially underlie the differences in overall plaque burden found between sexes.

Does inhibition of NFAT lead to limited plaque progression or plaque regression (or both)?

The histologically assessed smaller plaque sizes observed after treatment with the NFAT blocker A-285222 in papers I and II could be due to either limited plaque progression, plaque regression or a combination of both processes.

In paper I (figure 2, figure 3, supplemental figure 5), atherosclerosis in the aortic arch of diabetic ApoE$^{-/-}$ mice, was completely suppressed to levels of non-diabetic mice, after 4 weeks of A-285222 treatment. Moreover, inhibition of NFAT reduced the lipid contents in the plaques of diabetic mice at the level of the aortic root but had no effect on other plaque components such as collagen, SMCs and macrophages. In a separated group of 22-week-old ApoE$^{-/-}$ mice, 4 weeks of diabetes led to a significant up-regulation of pro-inflammatory and endothelial activation markers at the mRNA level in the aortic arch, including TF, MCP-1, VCAM-1, IL-1β, and COX2 compared with non-diabetic mice. This up-regulation of pro-inflammatory and endothelial activation markers at the mRNA level were measured at a time-point when no changes in plaque size had yet occurred. Treatment with A-285222 started at this time point (4 weeks), at a time when diabetes has not yet had an impact on atherosclerotic plaque size. Even though there is no doubt that NFAT inhibition in this setting limited plaque progression, the experimental design did not allow testing whether NFAT could cause plaque regression in this model. It is though clear that NFAT inhibition reverted some of the gene expression changes observed at 4 weeks of diabetes, as evidenced by the significantly lowered levels of TF and MCP-1.

In paper II (figure 1 and supplemental figure 1), the atherosclerosis in the brachiocephalic artery of IGF-II/LDLR$^{-/-}$ApoB$^{100/100}$ young mice was significantly reduced after 4 weeks of A-285222 treatment. This was assessed by non-invasive

ultrasound and histological measurements at the end of the experimental protocol. A good correlation between both techniques was observed in arteries from young mice, but not from the old mice. In addition, the use of non-invasive ultrasound allowed us to evidence a smaller plaque size in the artery at the end of the treatment compared with the plaque size from the same animals before treatment. As for $ApoE^{-/-}$ mice in paper I, the reduced plaque size observed after treatment with A-285222 was not due blood glucose-, insulin-, cholesterol- or triglyceride-lowering effects of A-285222. In fact, a modest elevation of fasted blood glucose was even observed in A-285222-treated young male mice (paper II, table 1), an effect that would in any case counteract any beneficial effect of the NFAT blocker. This effect on blood glucose could be due to direct effects of A-285222 on pancreatic β-cells, in which the involvement of NFAT-signalling in the regulation of insulin transcription is well established [283]. In addition, the NFAT blocker had no impact on neither plaque nor media composition in the $IGF\text{-}II/LDLR^{-/-}ApoB^{100/100}$ mice; muscle, collagen, macrophage and elastin contents were not affected at the end of the experiment (paper II, figure 2 and supplemental figure 2). However, after 4 weeks of treatment with A-285222, the expression of the macrophage marker CD68 was significantly reduced in the aorta of young female mice and tendencies for reduced IL-6 and OPN were observed although results did not reach statistical significance (paper II, figure 3). This finding was in line with the results obtain in paper I (figure 7), in which STZ-induced diabetic female $ApoE^{-/-}$ mice were treated with A-285222 for 4 weeks. The effect of the NFAT blocker on the expression of CD68 in the aorta of young $IGF\text{-}II/LDLR^{-/-}ApoB^{100/100}$ female mice was not translated into reduced macrophage infiltration at least when examined at the level of the aortic root. As it was expected, lower macrophage infiltration was observed in the aortic root of old compared to young $IGF\text{-}II/LDLR^{-/-}ApoB^{100/100}$ mice (paper II, figure 5), reflecting a more active plaque in younger mice. Recently, macrophage polarization has been linked to changes in atherosclerotic plaque states. While M1 macrophages contribute to inflammatory states and are predominant in plaques undergoing progression, M2 macrophages appears to participate in inflammation resolution and plaque remodelling and are enriched in plaques that experience regression [56].

All in all, our results suggest that NFAT inhibition in $IGF\text{-}II/LDLR^{-/-}ApoB^{100/100}$ young mice lead to plaque regression in addition to limiting plaque progression.

Potential mechanisms underlying the effects of A-285222 on atherosclerosis

Considering that treatment with A-285222 during 4 weeks did not change the levels of plasma glucose, cholesterol or triglycerides in diabetic $ApoE^{-/-}$ nor in

IGF-II/LDLR$^{-/-}$ApoB$^{100/100}$ mice, we ruled out the possibility that A-285222 acts on these metabolic parameters to reduce the atherosclerosis in these models. With the perspective that inflammation is an important regulator of atherosclerotic plaque formation and progression, in paper I and II we explored whether A-285222 reduced diabetic atherosclerosis via systemic immunosuppression.

Diabetes per se increased the inflammatory burden in ApoE$^{-/-}$ mice, as evidenced by the increased levels of circulating plasma cytokines IL-6, INF-γ, IL-12p70, IL-1β, IL-10, TNF-α, OPN and soluble VCAM-1. Treatment for 4 weeks with A-285222 resulted in a significant reduction in IL-6 levels in plasma and IL-6 mRNA in the aortic arch of diabetic mice (paper I, figure 5). All other circulating cytokines remained unaffected by A-285222, while we did see significant effects on gene expression apart from IL-6 in the aortic arch, including reduction of OPN, MCP-1, ICAM-1, CD68 and TF, the last 2 both at the mRNA and protein level (paper I, figure 7). This data would support a more local effect of the blocker on the arterial wall rather than a generalized systemic effect. Additional data that supports this concept is the NFAT-luciferase data showing that A-285222 had no impact on NFAT-dependent transcription activity in the spleen and thymus. A-285222 had no effect either on the capacity of immune cells to proliferate or on the cytokines secretion capacity of splenocytes, both under non-stimulated and stimulated conditions (paper I, supplemental figure 6). The reduced expression of IL-6 and OPN seems in line with previous work from our group showing NFAT-dependent regulation of these genes in VSMCs and in intact arteries [51, 156]. The reduced expression of OPN and ICAM-1 seems in line with results in paper III showing significantly lowered levels of expression of these genes in retinal vessels after 4 weeks of treatment with A-285222([231], paper III, figure 6). IL-6 and OPN are relevant pro-inflammatory cytokines in the course of atherogenesis. IL-6 can be generated and released by several cells, like macrophages, ECs and adipocytes, inducing endothelial dysfunction, VSMCs proliferation and migration, oxidized lipid accumulation in macrophage (resulting in foam cell formation) as well as recruitment and activation of T cells [284, 285]. Thus, the reduction of IL-6 levels in diabetic mice after treatment with A-285222, could explain the decreased lipid content within the plaque. OPN also enhances inflammation in the atherosclerotic plaque. Extracellular OPN acts as a chemotactic and adhesive molecule and promotes VSMCs proliferation and migration, whereas in its intracellular form regulates cytokine production [286-288].

In summary, the reduced plaque size observed after treatment with A-285222 in ApoE$^{-/-}$ mice does not seem to be due to systemic immunosuppression but rather to local effects of the blocker on the vascular cells

In paper II (figure 3), treatment with A-285222 for 4 weeks in a T2D mice model, reduced the expression of the inflammatory marker CD68 in the aorta of young

female IGF-II/LDLR$^{-/-}$ApoB$^{100/100}$ mice. As in paper I (figure 5), plasma levels of OPN were not affected by the treatment (paper II, table 1), supporting the idea that the effects of NFAT blocker are less likely systemic. OPN plasma levels were higher in old mice compared to young mice, regardless the treatment, reflecting that aging is accompanied with higher inflammation status (paper II, supplemental table 1). In paper II (figure 3) we also study whether NFAT inhibition affected genes related to oxidative stress. We found that 4 weeks of A-285222 treatment increased the expression of the vascular athero-protective NOX4 at mRNA level, but had no effect on NOX2, nor on the expression level of detoxifier enzymes, such GLO1 and catalase, in the aorta of young male mice. The up-regulation of NOX4 and catalase observed after A-285222 were replicated in *in vitro* experiments under strong oxidative stress conditions, in VSMCs incubated with H_2O_2 (100 μM) and the peroxynitrite donor SIN-1 (500 μM). Also, we found lower ROS/RNS level in the culture medium of NFATc3 deficient VSMCs was observed compared with competent cells cultured under high glucose conditions (25 mM) (paper II, figure 4).

All these findings suggested that reduced atherosclerosis in the brachiocephalic artery of IGF-II/LDLR$^{-/-}$ApoB$^{100/100}$ young male mice treated with the NFAT blocker could be explained, at least in part, by the production of an anti-oxidative environment through elevated expression of the athero-protective NOX4.

Role of NFAT in the early stages of diabetic retinopathy (Paper III)

We have determined using confocal imaging that NFATc3 is expressed in mouse retinal ECs and we have demonstrated, that hyperglycemia activates NFATc3 in retinal vessels, both *ex vivo* and *in vivo*. One important aim in paper III was to investigate whether NFAT was implicated in the development of diabetic retinopathy (DR), focusing on the changes that take place during the early disease stages. At the cellular level, the first changes observed in the pathogenesis of DR are the activation of ECs, the inflammatory response, the loss of pericytes, the breakdown of the integrity of the BRB and consequently increased vascular permeability.

Expression of pro-inflammatory molecules and endothelial activation markers has been shown to be increased in retinas of diabetic rodents. For instance, NF-κB, COX-2, VEGF, ICAM-1, VCAM-1 and tumor necrosis factor α (TNFα) were found to be up-regulated in the early stages of the pathology [70, 271]. In humans, DR is associated with elevated serum concentration of soluble IL-2, IL-8 and TNFα, which also correlate with the severity of the disease [289]. Furthermore, in

the vitreous from diabetic patients in the proliferative stages of the disease, elevated concentration of several cytokines and adhesion molecules has been reported, for example, IL-6, soluble IL-6 receptor, IL-8, MCP-1, soluble ICAM-1, soluble VCAM-1, TNFα and OPN [290-295].

Previous work in VSMCs has shown that NFAT can regulate the expression of the endothelial-activation marker VCAM-1 in response to changes in the ECM composition that mirror those that take place in vascular disease [31]. Also E-selectin was found to be regulated by NFAT in ECs [296]. Other identified target of NFAT in the context of hyperglycemia and diabetes is the ECM protein and inflammatory cytokine OPN, which was shown to be a direct target of NFAT in aortic VSMCs [51]. In paper I (figure 7), we found that inhibition of NFAT reduces mRNA expression of ICAM-1 in the aorta of diabetic ApoE deficient mice [165]. Therefore we specifically interrogated whether OPN and ICAM-1 could potentially be modulated by NFAT inhibition in the retinal vessels of diabetic mice.

Effect of NFAT inhibition on retinal endothelial activation and inflammatory cytokines

OPN and ICAM-1 mRNA expression levels were measured in isolated retinal vessels from STZ-induced diabetic and control BALB/c mice, which were treated either with A-285222 (0.15 and 0.29mg/Kg/day) or saline for 4 weeks. OPN contributes to the development of DR by promoting inflammation, cell adhesion, migration and angiogenesis [287, 297]. Surprisingly, OPN or ICAM-1 mRNA levels were not higher in retinal vessels from the diabetic animals when compared to level in control non-diabetic mice; regardless the animal model examined (6 weeks-old Akita mice and NFAT-luc mice after 2 weeks of diabetes) (paper III, figure 6 and supplemental figure 4). Contrary to these findings, in a previous work, our group had reported that 8 weeks of diabetes induced an up-regulation of OPN and ICAM-1 levels in retinal vessels of 22 weeks old $ApoE^{-/-}$ mice [271]. This discrepancy could be due to differences in the genetic background of the mice, in diabetes duration and/or blood lipid levels. Despite the lack of diabetes effects on the expression of OPN and ICAM-1, inhibition of the NFAT pathway with A-285222 for 4 weeks lowered the expression of both genes in retinal microvessels, denoting an NFAT-dependent regulation of their basal expression levels (paper III, figure 6).

We also measured the concentration of IL-10, TNF-α, INF-γ, IL-12p70, IL-1β, IL-6 and keratinocyte-derived chemokine (KC) using a multiplex assay, in whole retina homogenates from diabetic and control mice which were treated either with A-285222 (0.15mg/kg) or saline for 2 weeks. As mentioned before, all of these

cytokines have been implicated in the pathogenesis of DR, except for KC [298, 299]. KC is a murine homologue of the human chemokine IL-8, which is an inflammatory and angiogenic mediator produced by ECs and glia cells in retinas [291]. We found a significantly reduced level of IL-10 in diabetic mice when compared to controls, and 2-weeks treatment with A-285222 completely restored values to control levels (paper III, figure 5). We were not able to detect any additional changes in the levels of all the other cytokines after 2 weeks of diabetes. Maybe this was a too short diabetes duration to cause measurable changes, as suggested by previous work showing increased mRNA levels of TNFα, IL-6 and IL-1β after 8 weeks of diabetes in C57BL/6 mice [271]. This could be also be due to differences in genetic background between the mice.

Levels of the same set of cytokines measured in the intact retina were determined in plasma, but neither diabetes nor treatment with the NFAT blocker, generated changes in plasmatic cytokine levels (paper III, supplemental table 1). This suggests that the effect of A-285222 on IL-10 in retina is local rather than a systemic effect. In brief, inhibition of NFAT decreased the expression of OPN and ICAM-1 mRNA in retinal vessels of diabetic mice and prevented the down-regulation of anti-inflammatory IL-10. It is well-known that IL-10 limits the magnitude and duration of the inflammatory response [300]. Many immune cells produce IL-10, such as T helper cells, regulatory T cells, B cells, monocytes, macrophages, dendritic cells [301] and even vascular cells [302].

Effect of NFAT inhibition on retinal vascular permeability

The disruption of the BRB is an early feature of DR, which leads to vascular leakage and retinal edema, being the latter, the most common cause of visual loss [66]. Vascular permeability was determined by measurement of fluorescence of retinal extracts and a 1:1000 dilution of plasma, after injecting FITC-labelled albumin to 8-weeks-old Akita mice and non-diabetic control littermates that had been treated with A-285222 or saline for 2 weeks. Vascular permeability was increased 2.1-fold in diabetic compared to control mice. In line with what others have described [303], the change in retinal permeability is an early phenomenon in Akita mice. Inhibition of NFAT with A-285222 for 2 weeks completely prevented the diabetes-induced changes in retinal permeability, suggesting that NFAT signalling pathway may be involved in the BRB regulation (paper III, figure 7). The BRB breakdown in diabetes is associated with attenuated expression of tight junctions and adherens proteins in ECs [64]. Curiously, 26 NFAT consensus binding sequences were found in the promoter region of the gene encoding claudin-5, a tight junction protein. This observation will need to be tested experimentally.

Summary & Conclusions

- Absolute qPCR quantification of the NFATc isoforms in 13 different areas of the vasculature revealed that NFATc3 is by far the most abundantly expressed isoform, while NFATc2 and NFATc4 are expressed at substantially lower levels and NFATc1 was expressed at an intermediate level.
- Retinal vessels deviated from the more generalized pattern of expression, having the lowest NFATc1 expression and the highest NFATc2 expression of all 13 vessels examined.
- Cultured VSMCs had lower NFATc1 and NFATc2, and higher NFATc3 expression than the levels observed in native intact aorta.
- NFATc2 expression was increased in the aortic wall of diabetic mice, suggesting that this isoform can be induced or enhanced in pathological situations or under certain stimulatory conditions.
- Genetic deletion of NFATc2 or NFATc3 differentially affected the expression of Klf4, Klf5 and Gata4, genes that have been implicated in the regulation of VSMC phenotype.
- Genetic deletion of NFATc3 yielded increased expression of Ace1 and of smooth muscle markers Cnn1 and Tagln, as well as in higher VSMC proliferation.

Conclusion 1: The reported differential isoform expression and effects observed upon NFATc2 and NFATc3 deletion support the idea of functional non-redundancy of NFAT isoforms in the vasculature.

- NFAT-dependent transcriptional activity was examined in aorta, spleen, thymus, brain, heart, liver and kidney, but was found to be augmented only in the arteries of T1D mice.
- *In vivo* treatment with the NFAT blocker A-285222 completely inhibited diabetes-induced aggravation of atherosclerosis in a T1D mouse model, having no effect in non-diabetic mice. This was not due systemic immunosuppression or to glucose- or lipid lowering effects of the

treatment; instead NFAT inhibition resulted in reduced expression of pro-inflammatory and endothelial activation markers IL-6, OPN, MCP-1, ICAM-1, CD-68 and TF in the arterial wall as well as lowered IL-6 levels in plasma of those mice.

- *In vivo* inhibition of NFAT reduced atherosclerosis plaque area and degree of stenosis in the brachiocephalic artery of IGF-II/LDLR$^{-/-}$ApoB$^{100/100}$ mice, a T2D mouse model characterized by mild hyperglycemia, hyperinsulinemia and complex atherosclerotic lesions. The reduced plaque area could not be explained by effects on blood glucose, insulin or lipids, but NFAT inhibition was associated with increased expression of atheroprotective NOX4 and anti-oxidant enzyme catalase in aortic VSMCs.
- NFAT is expressed in the endothelium of retinal microvessels and readily activated by high glucose both *in vitro* and *in vivo* in 2 different animal models of T1D.
- *In vivo* inhibition of NFAT decreased the expression of OPN and ICAM-1 in retinal microvessels, prevented the down-regulation of anti-inflammatory IL-10 in retina and abrogated the increased vascular permeability observed in diabetic mice.

Conclusion 2: Targeting NFAT signalling may be a novel and attractive approach for the treatment of diabetic macro- and microvascular complications.

Science for everyone 

I am sure everyone knows someone who has been diagnosed with diabetes mellitus. The popular interpretation of this illness refers to having "high blood sugar". In general terms, this definition is right but not only is the sugar level high in blood but it is also in urine. It is because of this that it was given the name of diabetes mellitus. Diabetes is a word of Greek origin meaning siphon, i.e. to pass through, and it relates to the polyuria found in these patients (i.e. high urine production and elimination). The Latin word mellitus meaning honey was added due to the colour and sweetness of this urine.

In biomedical terms, diabetes is diagnosed if fasting blood glucose levels are equal or higher than 7 mmol/L (126 mg/dL) according to the World Health Organization. Glucose is known as sugar and comes from the food we eat and the liquids we drink. Diabetes is a chronic and irreversible disease with an estimated world prevalence of 415 million adults affected in 2015 and predicted to rise to 700 million people in 2025.

The most common types of diabetes are diabetes type 1 (T1D) and type 2 (T2D). T1D is an autoimmune disease that in general appears in childhood or adolescence, when the pancreas does not produce enough insulin. T2D generally appears in adult life when the body is not able to use the insulin the pancreas produces and it is often associated to overweight and blood lipids imbalance. Insulin is a hormone that helps glucose to enter the cells of our bodies and in this way supplies them with energy. Without enough insulin or without its efficient action, glucose remains in the blood at high levels (hyperglycemia).

Diabetes causes important complications in blood vessels, both in the small (capillaries) and in the big ones (arteries and veins). Damage to big arteries, known as macrovascular complications, lead to stroke, coronary heart disease and peripheral arterial disease, whereas damage to small vessels (microvascular complications) lead to generate ocular lesions (retinopathy) that lead to blindness, kidney lesions (nephropathy) that culminate with renal insufficiency and nerve lesions (neuropathy) that lead, for example, to loss of sensitivity in the limbs.

Although it is not clear which is the origin of these vascular complications, hyperglycemia has been identified as an important risk factor. Previous work from our group demonstrated that hyperglycemia effectively activates NFAT, which is

present in the blood vessel cells. The acronym NFAT stands for *Nuclear Factor of Activated T-cells*, since the presence and activity of this protein was found for the first time in T cells of the immune system; a type of cell whose function is to protect us from strange particles and agents. Therefore, it was known that this protein was present in other cells, like endothelial and smooth muscle cells present on the vascular wall. NFAT proteins are a family of nuclear transcription factors, which when are activated bind to specific portions of DNA and induce gene expression. Let's remember that DNA is a molecule present in the cell nucleus and it contains all the genetic information. The NFAT family is constituted by five different versions of proteins, called isoforms: NFATc1, NFATc2, NFATc3, NFATc4 and NFAT5. All of them (except NFAT5, which was not studied by us) have little structural differences among each other but share the same function and are present in all the blood vessel cells and in the rest of the tissues and organs of our body. In normal and non-stimulated conditions, NFAT stays inactive in the cell cytoplasm (outside the nucleus), but when it is activated in response to a stimulus (like hyperglycemia), NFAT enters the nucleus and promotes the expression of genes related to adhesion molecules and pro-inflammatory molecules on vascular wall cells, and also increases the smooth muscle cell contractility.

The fact that these adhesions and pro-inflammatory molecules are expressed on the vascular wall, makes, for example, that arteries accumulate and retain not only lipids, especially LDL particles (known as “bad cholesterol”), but also cells in the interior of the vessel wall. The gradual accumulation of these lipids and cells inside the vascular wall generates the atherosclerotic plaque bringing about atherosclerosis and narrowing the lumen of the vessels where blood circulates. Once the atherosclerotic plaque is formed, it keeps growing and the risk of its rupture increases, unless medication and lifestyle changes are initiated by the individual to regulate his lipids. If the atherosclerotic plaque breaks, a blood clot is formed, which can occlude the blood flow by the vessels. If this clot is formed in the heart vessels (coronary arteries), the individual experiences an heart attack, but when the same thing happens in plaques in the cerebral arteries, then a stroke event takes places. In diabetic patients atherosclerosis development is accelerated and it is present in most aggressive form. Besides, diabetic patients can have a blurred view that with time can lead to blindness. The expression of adhesion and pro-inflammatory molecules in retinal vessels, weaken the structure of these small vessels, allowing liquid filtration from the blood towards the eye interior, causing the loss of view. Retina is the eye tissue sensitive to the light and responsible for the sight sense.

The aim of this thesis was to study the role of NFAT proteins in diabetes-induced atherosclerosis and retinopathy, as well as to study the pattern of NFAT isoform expression in different vascular beds and the effects of the absence of NFATc2 or

NFATc3 in vascular cells. These studies generated 4 scientific articles, 3 of them (articles I, II and III) were published in peer-reviewed scientific journals and the fourth one (article IV) has not been published yet.

In article I, we wondered whether NFAT was involved in the development of diabetes-induced atherosclerosis. In order to answer this question, we used an experimental mouse model that presents high cholesterol blood level being a good model to generate atherosclerosis. Diabetes was induced in a group of these mice by injecting a substance (streptozotocin) that destroys the pancreas cells responsible of producing insulin. Since these mice could not generate insulin, glucose was not able to enter the cells and so remained circulating in the blood at high levels, simulating a T1D mouse model. Another group of mice was used as control and diabetes was not generated. Four weeks after starting the experiment, half of the mice from each group (control and diabetic groups) received another substance (called A-285222) whose function is to avoid NFAT entrance to the nucleus, and therefore this substance functions as an NFAT "blocker". At the end of the experiment, we observed that the treatment with the NFAT blocker completely suppressed the atherosclerosis in the aorta of T1D mice and did not have effects in the control mice (non-diabetic ones). In addition, NFAT blocking reduced the expression of adhesion and pro-inflammatory molecules on the arterial wall of these diabetic mice. These results led us to conclude that NFAT proteins are involved in the development of diabetes-induced atherosclerosis, in a T1D mouse model with high blood cholesterol.

Based on the observations done in article I, the next thing we wanted to know was if NFAT blocking with A-285222 would also limit the atherosclerosis in a T2D mouse model. In order to answer this question, in article II we used a novel mouse model, that has moderately high levels of glucose and insulin in blood, high cholesterol level and develops advanced and complex atherosclerotic plaques, all typical features of T2D. Four weeks after starting the experiment, half of the mice were treated with the NFAT blocker, A-285222, during the following 4 weeks. At the end of the experiment, we observed that NFAT blocking reduced the atherosclerotic plaques and the obstruction of the brachiocephalic artery lumen in A-285222 treated mice. At the same time, NFAT blocking was associated with an increase in the expression of athero-protective and antioxidants enzymes in the aortic smooth muscle cells. These results also led us to conclude that NFAT proteins are involved in the development of macrovascular complications in a T2D mouse model.

In article III, we wondered whether NFAT could also generate changes in cells from retinal microvessels (small vessels), whose modifications with time cause the complete loss of vision. In order to answer this question, we first confirmed that NFAT was present in the endothelial cells that form retinal microvessels. We also

confirmed that NFAT was activated by high glucose levels, using endothelial cell cultures and two different T1D mouse models. In one of these models, due to a spontaneous genetic alteration, mice developed diabetes at 3 or 4 weeks of age, while in the other model, diabetes was generated by injecting mice with streptozotocin. The NFAT blocker, A-285222, was administered in both models reducing the expression of adhesion and pro-inflammatory molecules in retinal vessels, as well as increasing the expression of anti-inflammatory molecules and avoiding the filtration of liquid from the blood to the eye interior in diabetic mice.

In article IV, we explored the pattern expression of all NFAT isoforms (NFATc1-NFATc4) in 13 different regions of the mouse vascular tree in normal conditions. We found that NFATc3 was by far the most abundant isoform in all vessels examined, while NFATc2 and NFATc4 were expressed at lower levels. NFATc1 was expressed in an intermediate level. We observed that NFATc2 expression was increased on the arterial wall of diabetic mice. This fact indicates that this NFAT isoform can be induced or enhanced in pathological situations like diabetes. At the same time, we found that lack of NFATc2 or NFATc3 in vascular smooth muscle cells affects in a totally opposite way the expression of genes related to the appearance and contractile function of these cells.

In summary, we arrived at two conclusions: 1) blocking NFAT is a novel and attractive approach for the treatment of macro- and microvascular complications in T1D and T2D; 2) the different expression pattern of NFAT isoforms in the vascular tree of mice and the different effects observed when NFATc2 or NFATc3 are absent in cells, makes us think that the presence of all NFAT isoforms in the same cell does not translate as a functional redundancy of NFAT.

Ciencia para todos 

Seguro que todos conocen alguna persona que fue diagnosticada con diabetes mellitus. La interpretación popular de esta enfermedad, es el hecho de tener "alto el azúcar en la sangre". En términos generales esa definición es correcta, pero no sólo en la sangre aumenta el nivel de azúcar, sino también en la orina. De ahí es que proviene su nombre de origen griego, diabetes mellitus. Diabetes es sinónimo de poliuria (aumento en la producción y eliminación de la orina) y debido al color similar al de la miel y al sabor dulce de la orina de los diabéticos, se le agregó la palabra mellitus.

En términos biomédicos, la diabetes se caracteriza por tener los niveles de glucosa en sangre igual o más altos que 7 mmol/L (126mg/dL), medidos en ayunas. La glucosa es comúnmente conocida como azúcar y proviene de los alimentos que consumimos. El valor de 7 mmol/L es considerado por la Organización Mundial de la Salud como un nivel límite para plantear un diagnóstico de diabetes. La diabetes es una enfermedad crónica e irreversible, con una distribución mundial de 415 millones de personas afectadas estimadas en el año 2015 y proyectándose para el año 2025 la existencia de 700 millones de diabéticos.

Los dos tipos más comunes de diabetes son, la diabetes tipo 1 (DT1) y la diabetes tipo 2 (DT2). La DT1 es una enfermedad autoinmune que se presenta generalmente en la niñez o adolescencia, cuando el páncreas no produce suficiente insulina. La DT2 aparece generalmente en el adulto cuando el organismo no es capaz de utilizar eficazmente la insulina que produce y en general está asociada al sobrepeso y desbalance en los lípidos sanguíneos. La insulina es una hormona producida y liberada por el páncreas, cuya acción es ayudar a que la glucosa entre en todas las células de nuestro cuerpo, y así suministrarles energía. Sin la suficiente cantidad de insulina y sin su eficiente acción, la glucosa permanece en la sangre en exceso (hiperglicemia) y genera la diabetes.

La diabetes causa complicaciones importantes a nivel de los vasos sanguíneos, tanto en los vasos pequeños (capilares) como en los grandes (arterias y venas). Los daños en las grandes arterias, conocidas como complicaciones macrovasculares, generan por ejemplo el infarto de miocardio, los accidentes cerebro-vasculares y la insuficiencia circulatoria en los miembros inferiores, mientras que los daños en los capilares (complicaciones microvasculares) generan lesiones oculares (retinopatía) que llevan a la pérdida de visión, lesiones renales (nefropatía) que culminan en

insuficiencia renal y lesiones en los nervios (neuropatía) que llevan por ejemplo a la pérdida de sensibilidad en las extremidades.

Si bien no está totalmente claro cuál es el origen de estas complicaciones vasculares, se ha identificado a la hiperglicemia como un factor de riesgo importante. Estudios previos realizados en nuestro laboratorio, han demostrado que la hiperglicemia activa las proteínas llamadas NFAT, que está presente en las células de los vasos sanguíneos (tanto en los grandes como en los pequeños vasos). La sigla NFAT proviene de su nombre en inglés, *Nuclear Factor of Activated T-cells*, ya que la presencia y actividad de esta proteína fue descubierta por primera vez en las células T del sistema inmune; un tipo de células cuya función es protegernos de partículas y agentes extraños. Con el tiempo, se supo que estas proteínas estaban presente en otras células, como por ejemplo en las células endoteliales y las de músculo liso, que forman parte de la pared vascular. Las proteínas NFAT son una familia de factores de transcripción nuclear, que cuando se activan tienen la función de unirse a porciones específicas del ADN e inducir la expresión de genes. Recordemos, que el ADN es una molécula que está en el núcleo de las células y que contiene toda la información genética. La familia NFAT está constituida por cinco versiones diferentes de la proteína NFAT, llamadas isoformas: NFATc1, NFATc2, NFATc3, NFATc4 y NFAT5. Todas ellas tiene pequeñas diferencias estructurales entre sí (excepto NFAT5, que no fue estudiada por nosotros), pero comparten la misma función y están presentes en todas las células de los vasos sanguíneos y del resto de los órganos y tejidos del cuerpo. En condiciones normales, NFAT se encuentra inactivo en el citoplasma de las células (fuera del núcleo), pero cuando se activa en respuesta a un estímulo (como lo es la hiperglicemia), NFAT pasa al núcleo y promueve la expresión de genes que están relacionados con moléculas de adhesión y moléculas pro-inflamatorias en las células de la pared vascular, así como también incrementa la contractilidad de las células de músculo liso.

El hecho de que se expresen moléculas pro-inflamatorias y de adhesión en la pared vascular, hace por ejemplo que en las arterias se acumulen y queden retenidos lípidos, mayoritariamente las partículas de LDL (conocido como "colesterol malo") y células en el interior de la pared de esos vasos. El acumulo gradual de estas células y lípidos dentro de la pared vascular es lo que genera la placa de ateroma y hace que se estreche la luz de los vasos por donde circula la sangre, generando la aterosclerosis. Una vez formada la placa de ateroma, y en ausencia tanto de medicación para reducir los lípidos, como de cambio de estilo de vida de la persona, la placa sigue creciendo y aumenta el riesgo de que se rompa. Cuando esto ocurre, el material de la placa de ateroma queda en contacto con la sangre y se forma un coágulo sanguíneo, el cual puede obstruir el pasaje de sangre por los vasos. Cuando se rompe la placa de ateroma y el coágulo se forma en los vasos del corazón (arterias coronarias), la persona sufre de un infarto, pero cuando lo mismo

ocurre en las arterias cerebrales, entonces el individuo sufre un accidente cerebro-vascular. En las personas diabéticas, el desarrollo de la aterosclerosis está acelerado y se presenta de una forma más agresiva. Por su parte, las personas diabéticas pueden tener una visión borrosa, que con el tiempo puede llevar a la ceguera. La expresión de las moléculas pro-inflamatorias y de adhesión en las células de los capilares vasculares que constituyen la retina, hace que la estructura de estos pequeños vasos se debilite, permitiendo el filtrado de liquido de la sangre hacia el interior del ojo, causando la pérdida de visión. La retina es el tejido del ojo sensible a la luz y que proporciona la visión.

El objetivo de esta tesis fue estudiar el rol que tienen las proteínas NFAT en la generación de la aterosclerosis y la retinopatía (lesiones a nivel de la retina del ojo) inducidas por la diabetes, así como también estudiar el patrón de expresión de las isoformas de NFAT en diferentes lechos vasculares y los efectos que genera a nivel celular la ausencia de NFATc2 o NFATc3 en las células vasculares.

Estos estudios dieron lugar a la generación de 4 artículos científicos, de los cuales 3 (artículos I, II y III) están publicados en revistas científicas y el cuarto (artículo IV) está en formato manuscrito y aún no fue publicado.

En el artículo I, nos preguntamos si NFAT estaba involucrado en el desarrollo de la aterosclerosis inducida por la diabetes. Para responder esa pregunta, utilizamos un modelo de ratón que tiene altos niveles de colesterol en sangre y por ello es un buen modelo animal para generar aterosclerosis. A un grupo de estos ratones se les provocó diabetes inyectándoles una sustancia (estreptozotocina) que destruye las células del páncreas encargadas de producir insulina. Al no generar insulina, la glucosa no puede ingresar a las células de los tejidos de los ratones y queda en la sangre en niveles elevados, simulando un modelo de DT1. Otro grupo de ratones fue usado como control y no se le generó diabetes. Luego de cuatro semanas de comenzado el experimento, a la mitad de los ratones de cada grupo (control y diabéticos) se les administró durante cuatro semanas más, otra sustancia (llamada A-285222) cuya función es impedir que las proteínas NFAT ingresen al núcleo, es decir que dicha sustancia funciona como un "bloqueador" de NFAT. Al finalizar el experimento, se observó que el tratamiento con el bloqueador de NFAT disminuyó completamente la aterosclerosis en la aorta de los ratones diabéticos, y no tuvo efecto en los ratones controles (no diabéticos). Además, el bloqueo de NFAT redujo la expresión de moléculas pro-inflamatorias y de adhesión en la pared arterial de esos ratones diabéticos. Estos resultados nos llevaron a concluir que la proteína NFAT estaba involucrada en el desarrollo de la aterosclerosis inducida por diabetes, en un modelo de ratón con DT1 y alto colesterol en sangre.

En base a lo observado en el artículo I, lo siguiente que quisimos saber fue si el bloqueo de NFAT con A-285222 también limitaría la aterosclerosis en un modelo de ratón con DT2. Para responder esa pregunta, en el artículo II, utilizamos un

novedoso modelo de ratón, el cual mediante modificaciones genéticas tiene niveles de glucosa e insulina en sangre moderadamente altos, el colesterol alto y desarrollan placas de ateroma complejas y avanzadas, todas éstas características de la DT2. Luego de cuatro semanas de comenzado el experimento, la mitad de los ratones fueron tratados con el bloqueador de NFAT, A-285222, durante cuatro semanas más. Al finalizar el experimento, observamos que el bloqueo de NFAT redujo las placas de ateroma y la obstrucción de la luz de la arteria braquiocefálica en los ratones tratados con A-285222. A su vez, el bloqueo de NFAT fue asociado con un aumento de la expresión de enzimas ateroprotectoras y antioxidantes en las células de músculo liso de la aorta. Estos resultados también nos llevaron a concluir que la proteína NFAT está involucrada en el desarrollo de las complicaciones macrovasculares en un modelo de DT2.

En el artículo III, nos preguntamos si NFAT también podía generar cambios en las células de los microvasos (vasos de pequeño tamaño) de la retina, cuyos cambios con el tiempo provocan la pérdida completa de visión. Para responder esta pregunta, primero confirmamos que NFAT estaba presente en las células endoteliales que forman los microvasos de la retina. A su vez, utilizando cultivo de células endoteliales y dos modelos diferentes de ratones con DT1, confirmamos que efectivamente NFAT se activaba frente a niveles altos de glucosa. En uno de los modelos, los ratones por una alteración genética espontáneamente desarrollaban diabetes a las 3 o 4 semanas de vida, mientras que en el otro modelo, la diabetes fue generada por inyecciones de estreptozotocina a los ratones. El bloqueador de NFAT, A-285222, fue administrado en ambos modelos animales y redujo la expresión de moléculas pro-inflamatorias y de adhesión en los microvasos de la retina, así como también aumentó la expresión de moléculas anti-inflamatorias y previno la filtración de líquido de la sangre hacia el interior del ojo de los ratones diabéticos.

En el artículo IV, exploramos cómo era el patrón de expresión de todas las isoformas de NFAT (NFATc1 a NFATc4) en 13 regiones del árbol vascular de ratones en condiciones normales. Encontramos que NFATc3 fue por lejos la isoforma más abundante en todos los vasos, mientras que NFATc2 y NFATc4 se expresaron en niveles bajos y NFATc1 en un nivel intermedio. Observamos que en ratones diabéticos, la expresión de NFATc2 en la pared arterial estaba aumentada, lo que nos indica que esta isoforma de NFAT se puede ver potenciada en situaciones patológicas como lo es la diabetes. A su vez, encontramos que la ausencia de las isoformas NFATc2 o NFATc3 en las células de músculo liso vascular afecta de forma totalmente opuesta la expresión de genes vinculados con la apariencia y función contráctil de dichas células.

En resumen, podemos concluir dos cosas: 1) que el bloqueo de NFAT es un novedoso y atractivo abordaje para el tratamiento de las complicaciones macro- y

microvasculares de la DT1 y DT2; 2) el patrón de expresión diferente que tienen las isoformas de NFAT en el árbol vascular y los diferentes efectos generados cuando NFATc2 o NFATc3 están ausentes, nos hace pensar que la presencia de todas las isoformas de NFAT en una misma célula, no se traduce en una redundancia funcional de NFAT.

Funding

This work has been supported by the Swedish Heart and Lung Foundation (grant numbers HLF20080843; HLF20100532, HLF20130700, HLF20160872), the Swedish Research Council (grant numbers: 2009-4120; EXODIAB 2009-1039; 2011-3900; 2014-03352), the Swedish Foundation for Strategic Research (grant number LUDC-IRC15-0067), the Swedish Medical Society, the Swedish Society for Medical Research, The Swedish Diabetes Association (Diabetesfonden), Lund University Diabetes Centre, British Heart Foundation, the Royal Physiographic Society in Lund, Skåne Hospital Research Funds, an award from the Health Sciences Center Research Allocation Committee (HSC RAC) from the University of New Mexico, the Crafoord; Lars Hierta Memorial; Edla and Eric Smedberg; Albert Påhlsson and Knut & Alice Wallenberg foundations; also by the Innovative Medicines Initiative Joint Undertaking (grant number 115006), comprising funds from the European Union's Seventh Framework Programme (grant number FP7/2007-2013) and European Federation of Pharmaceutical Industries and Associations (EFPIA) companies' in kind contribution.

I received personal support from CSIC (Comisión Sectorial de Investigación Científica), PEDECIBA (Programa de Desarrollo de las Ciencias Básicas) and the Vascular Wall Programme at Lund University.

Acknowledgements

I feel extremely fortunate to have had the opportunity to live this adventure, not only for having done the PhD work itself, but mostly for having experienced such a “gypsy” life style along these years. Yearly, I have spent roughly 183 days in a Nordic life and the other 182 days in a Latin life. Despite the big cultural difference between these two life styles, there was a common denominator which sometimes has been a reason for envying me, always living in the better seasons in each hemisphere: spring and summer!

Of course, to carry out this adventure there has been much more than only my own will. Many people have been by my side, supporting me and collaborating in different ways throughout these years, including family, friends, colleagues and I would like to express my deepest appreciation and gratitude to all of them.

I would like to thank my main supervisor **Maria Gomez**, for agreeing to supervise my "dual" PhD which has challenged us in many aspects. Thank you for encouraging me in this path, for your valuable input, for sharing your solid scientific knowledge, for inspiring me with your creativity and for always showing me the positive side of things in the not so fruitful moments that science sometimes has. Thanks for our long but productive Skype meetings. It has been a very enriching and rewarding experience for me to work in a really nice scientific team.

I would also like to acknowledge and thank my second supervisors **Lisa Berglund** and **Gustavo Brum**. **Lisa**, my "right hand" in several moments and from whom I learned a lot of things. Thanks for your patience, for always being willing to teach and to help with experimental issues. I really enjoyed and appreciated all our discussions regarding experiments, results interpretation and also all our amazing chats not work related. All of them have been very stimulating. **Gustavo**, my "right hand in Uruguay", many thanks for your continued logistic and administrative support which have been essential to carry on this study. Thanks for believing in this "project" and for supporting it.

I would like to express a deep gratitude to the committee members and the opponent for accepting to judge and revising this thesis.

I am grateful with my friend and colleague, **Anna Zetterqvist** for sharing with enthusiasm your scientific knowledge, for having introduced me in the real time-

PCR world, for having taught me many experimental protocols and for having discussed statistical issues from our data. Thanks for always conveying your positive energy to the group and for spending amazing times together in the lab and outside the CRC. Many thanks to my fellow PhD-student **Eliana** for sharing the Uruguayan ritual of drinking "mates" at the office.

My sincere thanks to **Olga** and **Anna-Maria** for their technical support and their great practical assistance all along these years. You have been a great help for me during long days of work in the animal facility when animal experiments ended. **Olga**, many thanks for your permanent assistance with cell cultures and for the coffee-breaks with interesting talks. **Anna-Maria**, your technical helpfulness in everything related to immunohistochemistry has been very important in this work, and thanks for always making me smile with your ironic humor.

To all the adorable **colleagues and technicians** from our neighbour labs, the **Jan Nilsson's** and **Nils Wierup's groups**. Many thanks for generating stimulating discussions in the seminars, for sharing interesting and fun scientific retreats, for always being available to teach protocols or to clearing up practical doubts. Thank you for the lovely *Friday training* days and for creating a warm and pleasant atmosphere at work.

My most sincere gratitude to Professor **Seppo Ylä-Herttuala**, for giving me the opportunity to visit his lab at the University of Eastern Finland in Kuopio, in a frame of collaborative work. Special mention and thanks to **Suvi** and **Erika** for having shared such pleasant and productive work days and for showing me the ultrasound biomicroscopy.

To all my **colleagues** at the **Biophysics Department**, especially all the **University Adjuncts instructors**, for having had the kindness and patience to substitute me in classes for several months. To **Ana Gabriela** for her help in paper works at the School of Medicine.

To all my **colleagues** at the **Physiology Department**, for their continuous interest in my work and for their rich contributions to it in the scientific seminars. Particularly, to all **people from Cardio** (those who are currently on the team and those who were in Cardio in the past) for so many hours of work dedicated in a super-friendly environment where friendship and camaraderie have prevailed. To **Edith** and **Paola**, women who are pillars in Cardio, for their permanent support in many aspects.

To my family in general, all **Blancos**, all **Cámeras** and especially to **my parents** and **my brothers**, for have travelling many of kilometres to meet us, give us a huge hug and travelling together around the world, during my Nordic semester.

To **Gisella** and **Úrsula** for their emotional and linguistic support, respectively, all along this path.

To the beloved Swedish family **Morales-Eriksson**, for their great affection and for always making me feel “a member of their family”. Thank you so much for the adored social gatherings shared.

Thanks to my dear Nordic friend from the South, **Andrea**, for always having been on my side, for the charming Rioplatense moments and for so many shared laughs. To my friends from **LuÑd** (**JonMi**, **Talia**, **Dani**, **Isa**, **Laura**, **Tania**, **Agi**), thanks for all the lovely Spanish moments and shared trips. To my friends **Annarita**, **Shub**, **the Natis**, **the Cardio Girls** for their warm friendship and for the unforgettable moments. To the whole **Cirkusvagen** community’s for having allowed me to reencounter myself with art and have shown me "Sweden from within";). To my friends the “**runners**” and “**swimmers**” for the kilometres of running and swimming, that have served so much to clarify ideas in this thesis; and to my coach **Tato** for having accompanied me in training plans despite the distance.

Last but not least, to each person who in one way or another has accompanied, contributed to and enjoyed this beautiful period of my life with me...and there were many.

Agradecimientos

Me siento extremadamente afortunada de haber tenido la oportunidad de vivir esta aventura, no solo por haber hecho el doctorado en sí mismo, si no por haber experimentado una vida un tanto “gitanesca” a lo largo de estos años. Anualmente he pasado aproximadamente 183 días de vida Nórdica y otros 182 días de vida Latina. A pesar de la gran diferencia cultural entre esos dos estilos vidas, hubo un denominador común, que ha sido algunas veces razón para envidiarme, vivir siempre en las mejores estaciones de cada hemisferio: primavera y verano!

Por supuesto que para llevar a cabo esta aventura, ha habido mucho más que mi propia voluntad. Muchas personas han estado a mi lado, apoyándome y colaborando de diferentes maneras a lo largo de estos años, incluidos familiares, amigos, colegas a los que quisiera expresarles mi más profundo agradecimiento y gratitud.

Quisiera agradecer a mi supervisora principal **Maria Gomez**, por haber aceptado tutorear mi “dual” PhD, el cual nos ha desafiado en muchos aspectos. Gracias por alentarme en este camino, por tus valiosos aportes, por compartir tu sólido conocimiento científico, por inspirarme con tu creatividad y por mostrarme siempre el lado positivo de las cosas en los momentos no tan fructíferos que a veces tiene la ciencia. Gracias por nuestras largas pero productivas reuniones vía Skype. Ha sido para mí una experiencia muy enriquecedora y gratificante trabajar en un grupo científico realmente agradable.

También me gustaría agradecer a mis co-supervisores, **Lisa Berglund** y **Gustavo Brum**. **Lisa**, mi "mano derecha" en varios momentos y de quien aprendí muchísimas cosas. Gracias por tu paciencia, por estar siempre dispuesta a enseñar y ayudarme con asuntos experimentales. Realmente disfruté y aprecié todas nuestras discusiones sobre experimentos, interpretación de resultados y también nuestras charlas no relacionadas con el trabajo. Todas ellas han sido muy estimulantes. **Gustavo**, mi "mano derecha en Uruguay", muchas gracias por tu continuo apoyo logístico y administrativo, que ha sido esencial para llevar a cabo este estudio. Gracias por creer en este "proyecto" y por apoyarlo.

Me gustaría expresar un profundo agradecimiento a los miembros del tribunal y a la oponente por aceptar juzgar y revisar la tesis.

Estoy muy agradecida con mi amiga y colega **Anna Zetterqvist** por haber compartido con entusiasmo su conocimiento científico, por haberme introducido al mundo del real-time PCR, por haberme enseñado muchos protocolos experimentales y por haber discutido la estadística de muchos de nuestros datos. Gracias por transmitir siempre tu energía positiva al grupo y por haber pasado juntas momentos increíbles en el laboratorio y fuera de él. Muchas gracias a mi compañera de doctorado **Eliana**, por compartir el ritual uruguayo de tomar mate en la oficina.

Mi más sincero agradecimiento a **Olga** y **Anna-Maria**, por su apoyo técnico y su gran ayuda práctica a lo largo de estos años. Han sido de gran ayuda para mí en durante los largos días de trabajo en el animalario cuando finalizaban los experimentos con animales. **Olga**, muchas gracias por ti permanente asistencia con los cultivos celulares y por los cafés con interesantes charlas. **Anna-Maria**, tu ayuda técnica en todo lo relacionado con la immunohistoquímica ha sido muy importante en este trabajo y gracias por siempre sacarme una sonrisa con tu humor irónico.

A todos los adorables **colegas** y **técnicos** de nuestros laboratorios vecinos, los **grupos de Jan Nilsson** y **Nils Wierup**. Muchas gracias por generar estimulantes discusiones en los seminarios, por compartir interesantes y divertidos retiros científicos, por siempre estar disponibles para enseñar protocolos o para evacuar dudas prácticas. Muchas gracias por los encantadores días *viernes de entrenamiento* y por crear un ambiente cálido y agradable para trabajar.

Mi sincera gratitud al Profesor **Seppo Ylä-Herttuala**, por haberme dado la oportunidad de visitar su laboratorio en la University of Eastern Finland en Kuopio, en el marco de un trabajo en colaboración. Especial mención y gracias a **Suvi** y **Erika**, por haber compartido jornadas de trabajo tan agradables y productivas y por haberme mostrado la biomicroscopía de ultrasonido.

A todos los **compañeros del Departamento de Biofísica**, en especial a los **Grados 1 y 2** por haber tenido la amabilidad y paciencia de suplantarme en las clases durante varios meses. A **Ana Gabriela** por su ayuda brindada en la logística del papeleo en Facultad de Medicina.

A los **compañeros del Departamento de Fisiología**, por su continuo interés en mi trabajo y por sus ricos aportes al mismo en los seminarios científicos. En particular, a **todos los compañeros de Cardio** (los que están hoy y los que "han paso por Cardio") por tantas horas de trabajo compartidas en un ambiente súper agradable donde ha primado la amistad y el compañerismo. A **Edith** y **Paola**, mujeres pilares en Cardio, por su permanente apoyo en muchos aspectos.

A mi **familia** en general, todos los **Blancos**, todos los **Cámeras** y en especial a **mis padres** y **hermanos**, por haberse movido miles de kilómetros para

encontrarnos, darnos un fuerte abrazo y recorrer parte del mundo juntos, durante mis semestres nórdicos.

A **Gisella** y **Úrsula** por sus soportes emocionales y lingüísticos, respectivamente, a lo largo de este camino.

A la querida familia sueca **Morales-Eriksson**, por el gran cariño, por todo el apoyo brindado y por siempre haberme hecho sentir "como en familia". Muchas gracias por las adoradas y largas tertulias compartidas.

A mi querida amiga nórdica del Sur, **Andrea**, gracias por nuestra fresca amistad, por siempre haber estado a mi lado, por los encantadores momentos Rioplatense y por tantas risas compartidas. A mis amigos de **LuÑd** (**JonMi**, **Talia**, **Dani**, **Isa**, **Laura**, **Tania**, **Agi**), gracias por todos los adorables momentos muy españoles y viajes compartidos. A mis amigos **Annarita**, **Shub**, **las Natis**, **las Chicas de Cardio** por su cálida amistad y por los inolvidables momentos vividos. A toda la comunidad del **Cirkusvagen**, por haberme permitido reencontrarme con el arte y haberme mostrado una "Suecia desde adentro" ;). A mis amigos los "**runners**" y "**swimmers**" por todos los kilómetros corridos y nadados que mucho sirvieron para aclarar ideas de esta tesis y al entrenador **Tato** por haberme acompañado en la planificación de los entrenamientos a pesar de la distancia.

Por último, pero no menos importante, a **cada persona** que de una forma u otra me acompañó, contribuyó y disfrutó junto conmigo esta linda etapa de mi vida... y fueron vari@s, eh.

References

1. WHO/IDF, Definition and diagnosis of diabetes mellitus and intermediate hyperglycaemia: Report of a WHO/IDF consultation. World Heath Organization, 2006: p. 50.
2. American Diabetes, A., 2. Classification and Diagnosis of Diabetes. Diabetes Care, 2016. **39 Suppl 1**: p. S13-22.
3. NCD-RisC, Worldwide trends in diabetes since 1980: a pooled analysis of 751 population-based studies with 4·4 million participants. The Lancet, 2016. **387**: p. 1513-30.
4. Beckman, J.A., M.A. Creager, and P. Libby, Diabetes and atherosclerosis: epidemiology, pathophysiology, and management. JAMA, 2002. **287**(19): p. 2570-81.
5. Federation, I.D., IDF Clinical Practice Recommendations for managing Type 2 Diabetes in Primary Care. International Diabetes Federation, 2017: p. 1-36.
6. Ahlqvist, E., et al., Novel subgroups of adult-onset diabetes and their association with outcomes: a data-driven cluster analysis of six variables. Lancet Diabetes Endocrinol, 2018. **6**(5): p. 361-369.
7. Paneni, F., S. Costantino, and F. Cosentino, Insulin resistance, diabetes, and cardiovascular risk. Curr Atheroscler Rep, 2014. **16**(7): p. 419.
8. Madonna, R. and R. De Caterina, Cellular and molecular mechanisms of vascular injury in diabetes--part I: pathways of vascular disease in diabetes. Vascul Pharmacol, 2011. **54**(3-6): p. 68-74.
9. Group, T.D.C.a.C.T.R., The effect of intensive treatment of diabetes on the development and progression of long-term complications in insulin-dependent diabetes mellitus. N Engl J Med, 1993. **329**: p. 977-986.
10. Nathan, D.M., et al., Intensive diabetes treatment and cardiovascular disease in patients with type 1 diabetes. N Engl J Med, 2005. **353**(25): p. 2643-53.
11. Holman, R.R., et al., 10-year follow-up of intensive glucose control in type 2 diabetes. N Engl J Med, 2008. **359**(15): p. 1577-89.
12. Bajaj, H. and B. Zinman, Diabetes: Steno-2 - a small study with a big heart. Nat Rev Endocrinol, 2016. **12**(12): p. 692-694.
13. Action to Control Cardiovascular Risk in Diabetes Study, G., et al., Effects of intensive glucose lowering in type 2 diabetes. N Engl J Med, 2008. **358**(24): p. 2545-59.
14. Group, A.C., et al., Intensive blood glucose control and vascular outcomes in patients with type 2 diabetes. N Engl J Med, 2008. **358**(24): p. 2560-72.

15. Duckworth, W., et al., Glucose control and vascular complications in veterans with type 2 diabetes. N Engl J Med, 2009. **360**(2): p. 129-39.
16. Rastogi, A. and A. Bhansali, SGLT2 Inhibitors Through the Windows of EMPA-REG and CANVAS Trials: A Review. Diabetes Ther, 2017. **8**(6): p. 1245-1251.
17. Marso, S.P., et al., Liraglutide and Cardiovascular Outcomes in Type 2 Diabetes. N Engl J Med, 2016. **375**(4): p. 311-22.
18. Duell, B., GLP-1 receptor agonist and cardiovascular prevention: insights from the LEADER trail. American College of Cardiology, 2017.
19. Hilenski, L.L.G., K.K., Vascular Smooth Muscle, in Vascular Medicine: A Companion to Braunwald's Heart Disease., M.B. Creager, J.; Loscalzo J., Editor. 2013. p. 25–42.
20. Ejaz, S., et al., Importance of pericytes and mechanisms of pericyte loss during diabetes retinopathy. Diabetes Obes Metab, 2008. **10**(1): p. 53-63.
21. Majesky, M.W., Developmental basis of vascular smooth muscle diversity. Arterioscler Thromb Vasc Biol, 2007. **27**(6): p. 1248-58.
22. straff, B.c., Medical gallery of Blausen Medical 2014. WikiJournal of Medicine, 2014.
23. Owens, G.K., M.S. Kumar, and B.R. Wamhoff, Molecular regulation of vascular smooth muscle cell differentiation in development and disease. Physiol Rev, 2004. **84**(3): p. 767-801.
24. Rzucidlo, E.M., K.A. Martin, and R.J. Powell, Regulation of vascular smooth muscle cell differentiation. J Vasc Surg, 2007. **45 Suppl A**: p. A25-32.
25. Miano, J.M., Serum response factor: toggling between disparate programs of gene expression. J Mol Cell Cardiol, 2003. **35**(6): p. 577-93.
26. House, S.J., et al., The non-excitable smooth muscle: calcium signaling and phenotypic switching during vascular disease. Pflugers Arch, 2008. **456**(5): p. 769-85.
27. Matchkov, V.V., O. Kudryavtseva, and C. Aalkjaer, Intracellular Ca(2)(+) signalling and phenotype of vascular smooth muscle cells. Basic Clin Pharmacol Toxicol, 2012. **110**(1): p. 42-8.
28. Cidad, P., et al., Characterization of ion channels involved in the proliferative response of femoral artery smooth muscle cells. Arterioscler Thromb Vasc Biol, 2010. **30**(6): p. 1203-11.
29. Lipskaia, L., Limon, I., Bobe, R. and Hajjar, R., Calcium Cycling in Synthetic and Contractile Phasic or Tonic Vascular Smooth Muscle Cells, in Current Basic and Pathological Approaches to the Function of Muscle Cells and Tissues, H. Sugi, Editor. 2012.
30. Albinsson, S., I. Nordstrom, and P. Hellstrand, Stretch of the vascular wall induces smooth muscle differentiation by promoting actin polymerization. J Biol Chem, 2004. **279**(33): p. 34849-55.
31. Orr, A.W., et al., Complex regulation and function of the inflammatory smooth muscle cell phenotype in atherosclerosis. J Vasc Res, 2010. **47**(2): p. 168-80.

32. Allahverdian, S., et al., Smooth Muscle Cell Fate and Plasticity in Atherosclerosis. Cardiovasc Res, 2018.
33. Takemoto, M., et al., Enhanced expression of osteopontin by high glucose in cultured rat aortic smooth muscle cells. Biochem Biophys Res Commun, 1999. **258**(3): p. 722-6.
34. Mori, S., et al., Hyperglycemia-induced alteration of vascular smooth muscle phenotype. J Diabetes Complications, 2002. **16**(1): p. 65-8.
35. Adhikari, N., et al., Increase in GLUT1 in smooth muscle alters vascular contractility and increases inflammation in response to vascular injury. Arterioscler Thromb Vasc Biol, 2011. **31**(1): p. 86-94.
36. Labinskyy, N., et al., Longevity is associated with increased vascular resistance to high glucose-induced oxidative stress and inflammatory gene expression in Peromyscus leucopus. Am J Physiol Heart Circ Physiol, 2009. **296**(4): p. H946-56.
37. Hien, T.T., et al., Elevated Glucose Levels Promote Contractile and Cytoskeletal Gene Expression in Vascular Smooth Muscle via Rho/Protein Kinase C and Actin Polymerization. J Biol Chem, 2016. **291**(7): p. 3552-68.
38. Sward, K., et al., Emerging roles of the myocardin family of proteins in lipid and glucose metabolism. J Physiol, 2016. **594**(17): p. 4741-52.
39. Reusch, J.E. and C.C. Wang, Cardiovascular disease in diabetes: where does glucose fit in? J Clin Endocrinol Metab, 2011. **96**(8): p. 2367-76.
40. Wang, T.a.B., J., Pathogenesis of atherosclerosis, in MINI-SYMPOSIUM: CARDIOVASCULAR PATHOLOGY. 2017, Elsevier Ltd. p. 473-478.
41. Ross, R. and J.A. Glomset, Atherosclerosis and the arterial smooth muscle cell: Proliferation of smooth muscle is a key event in the genesis of the lesions of atherosclerosis. Science, 1973. **180**(4093): p. 1332-9.
42. Witztum, J.L., The oxidation hypothesis of atherosclerosis. Lancet, 1994. **344**(8925): p. 793-5.
43. Libby, P., P.M. Ridker, and G.K. Hansson, Progress and challenges in translating the biology of atherosclerosis. Nature, 2011. **473**(7347): p. 317-25.
44. Leiva, E.W., S.; Guzmán, L.; Orrego, R., Role of Oxidized LDL in Atherosclerosis, in Hypercholesterolemia. 2015, InTech. p. 55-78.
45. Madamanchi, N.R., Z.S. Hakim, and M.S. Runge, Oxidative stress in atherogenesis and arterial thrombosis: the disconnect between cellular studies and clinical outcomes. J Thromb Haemost, 2005. **3**(2): p. 254-67.
46. Chait, A. and K.E. Bornfeldt, Diabetes and atherosclerosis: is there a role for hyperglycemia? J Lipid Res, 2009. **50 Suppl**: p. S335-9.
47. Burke, A.P., et al., Morphologic findings of coronary atherosclerotic plaques in diabetics: a postmortem study. Arterioscler Thromb Vasc Biol, 2004. **24**(7): p. 1266-71.
48. Hartge, M.M., T. Unger, and U. Kintscher, The endothelium and vascular inflammation in diabetes. Diab Vasc Dis Res, 2007. **4**(2): p. 84-8.

49. Kanter, J.E., et al., Do glucose and lipids exert independent effects on atherosclerotic lesion initiation or progression to advanced plaques? Circ Res, 2007. **100**(6): p. 769-81.
50. Bennett, M.R., S. Sinha, and G.K. Owens, Vascular Smooth Muscle Cells in Atherosclerosis. Circ Res, 2016. **118**(4): p. 692-702.
51. Nilsson-Berglund, L.M., et al., Nuclear factor of activated T cells regulates osteopontin expression in arterial smooth muscle in response to diabetes-induced hyperglycemia. Arterioscler Thromb Vasc Biol, 2010. **30**(2): p. 218-24.
52. Edsfeldt, A., et al., Sphingolipids Contribute to Human Atherosclerotic Plaque Inflammation. Arterioscler Thromb Vasc Biol, 2016. **36**(6): p. 1132-40.
53. Bengtsson, E., et al., ADAMTS-7 is associated with a high-risk plaque phenotype in human atherosclerosis. Sci Rep, 2017. **7**(1): p. 3753.
54. Erlov, T., et al., Determining carotid plaque vulnerability using ultrasound center frequency shifts. Atherosclerosis, 2016. **246**: p. 293-300.
55. Edsfeldt, A., et al., Soluble urokinase plasminogen activator receptor is associated with inflammation in the vulnerable human atherosclerotic plaque. Stroke, 2012. **43**(12): p. 3305-12.
56. Shioi, A. and Y. Ikari, Plaque Calcification During Atherosclerosis Progression and Regression. J Atheroscler Thromb, 2018. **25**(4): p. 294-303.
57. Cheung, N., P. Mitchell, and T.Y. Wong, Diabetic retinopathy. Lancet, 2010. **376**(9735): p. 124-36.
58. Yau, J.W., et al., Global prevalence and major risk factors of diabetic retinopathy. Diabetes Care, 2012. **35**(3): p. 556-64.
59. Ting, D.S., G.C. Cheung, and T.Y. Wong, Diabetic retinopathy: global prevalence, major risk factors, screening practices and public health challenges: a review. Clin Exp Ophthalmol, 2016. **44**(4): p. 260-77.
60. Antonetti, D.A., et al., Diabetic retinopathy: seeing beyond glucose-induced microvascular disease. Diabetes, 2006. **55**(9): p. 2401-11.
61. Curtis, T.M., T.A. Gardiner, and A.W. Stitt, Microvascular lesions of diabetic retinopathy: clues towards understanding pathogenesis? Eye (Lond), 2009. **23**(7): p. 1496-508.
62. Shah, M.S. and M. Brownlee, Molecular and Cellular Mechanisms of Cardiovascular Disorders in Diabetes. Circ Res, 2016. **118**(11): p. 1808-29.
63. Gardner, T.W., et al., An integrated approach to diabetic retinopathy research. Arch Ophthalmol, 2011. **129**(2): p. 230-5.
64. Navaratna, D., et al., Proteolytic degradation of VE-cadherin alters the blood-retinal barrier in diabetes. Diabetes, 2007. **56**(9): p. 2380-7.
65. Klaassen, I., C.J. Van Noorden, and R.O. Schlingemann, Molecular basis of the inner blood-retinal barrier and its breakdown in diabetic macular edema and other pathological conditions. Prog Retin Eye Res, 2013. **34**: p. 19-48.
66. Ferland-McCollough, D., et al., Pericytes, an overlooked player in vascular pathobiology. Pharmacol Ther, 2017. **171**: p. 30-42.

67. Nehls, V. and D. Drenckhahn, Heterogeneity of microvascular pericytes for smooth muscle type alpha-actin. J Cell Biol, 1991. **113**(1): p. 147-54.
68. Hamilton, N.B., D. Attwell, and C.N. Hall, Pericyte-mediated regulation of capillary diameter: a component of neurovascular coupling in health and disease. Front Neuroenergetics, 2010. **2**.
69. Moran, E.P., et al., Neurovascular cross talk in diabetic retinopathy: Pathophysiological roles and therapeutic implications. Am J Physiol Heart Circ Physiol, 2016. **311**(3): p. H738-49.
70. Kern, T.S., Contributions of inflammatory processes to the development of the early stages of diabetic retinopathy. Exp Diabetes Res, 2007. **2007**: p. 95103.
71. Duh, E.J., J.K. Sun, and A.W. Stitt, Diabetic retinopathy: current understanding, mechanisms, and treatment strategies. JCI Insight, 2017. **2**(14).
72. Barber, A.J., T.W. Gardner, and S.F. Abcouwer, The significance of vascular and neural apoptosis to the pathology of diabetic retinopathy. Invest Ophthalmol Vis Sci, 2011. **52**(2): p. 1156-63.
73. Antonetti, D.A., et al., Vascular permeability in experimental diabetes is associated with reduced endothelial occludin content: vascular endothelial growth factor decreases occludin in retinal endothelial cells. Penn State Retina Research Group. Diabetes, 1998. **47**(12): p. 1953-9.
74. Pyla, R., et al., Expression of conventional and novel glucose transporters, GLUT1, -9, -10, and -12, in vascular smooth muscle cells. Am J Physiol Cell Physiol, 2013. **304**(6): p. C574-89.
75. Haist, R.E. and C.H. Best, Factors Affecting the Insulin Content of Pancreas. Science, 1940. **91**(2365): p. 410.
76. Di Mario, U. and G. Pugliese, 15th Golgi lecture: from hyperglycaemia to the dysregulation of vascular remodelling in diabetes. Diabetologia, 2001. **44**(6): p. 674-92.
77. Alpert, E., et al., A natural protective mechanism against hyperglycaemia in vascular endothelial and smooth-muscle cells: role of glucose and 12-hydroxyeicosatetraenoic acid. Biochem J, 2002. **362**(Pt 2): p. 413-22.
78. Fernandes, R., K. Hosoya, and P. Pereira, Reactive oxygen species downregulate glucose transport system in retinal endothelial cells. Am J Physiol Cell Physiol, 2011. **300**(4): p. C927-36.
79. Kaiser, N., et al., Differential regulation of glucose transport and transporters by glucose in vascular endothelial and smooth muscle cells. Diabetes, 1993. **42**(1): p. 80-9.
80. Yang, H., et al., Oxidative stress and diabetes mellitus. Clin Chem Lab Med, 2011. **49**(11): p. 1773-82.
81. Giacco, F. and M. Brownlee, Oxidative stress and diabetic complications. Circ Res, 2010. **107**(9): p. 1058-70.
82. Cohen, G., et al., The roles of hyperglycaemia and oxidative stress in the rise and collapse of the natural protective mechanism against vascular endothelial cell dysfunction in diabetes. Arch Physiol Biochem, 2007. **113**(4-5): p. 259-67.

83. Burgoyne, J.R., et al., Redox signaling in cardiac physiology and pathology. Circ Res, 2012. **111**(8): p. 1091-106.
84. Turrens, J.F., Mitochondrial formation of reactive oxygen species. J Physiol, 2003. **552**(Pt 2): p. 335-44.
85. Du, X.L., et al., Hyperglycemia-induced mitochondrial superoxide overproduction activates the hexosamine pathway and induces plasminogen activator inhibitor-1 expression by increasing Sp1 glycosylation. Proc Natl Acad Sci U S A, 2000. **97**(22): p. 12222-6.
86. Du, X., et al., Inhibition of GAPDH activity by poly(ADP-ribose) polymerase activates three major pathways of hyperglycemic damage in endothelial cells. J Clin Invest, 2003. **112**(7): p. 1049-57.
87. Robertson, R.P., Chronic oxidative stress as a central mechanism for glucose toxicity in pancreatic islet beta cells in diabetes. J Biol Chem, 2004. **279**(41): p. 42351-4.
88. Ramasamy, R. and I.J. Goldberg, Aldose reductase and cardiovascular diseases, creating human-like diabetic complications in an experimental model. Circ Res, 2010. **106**(9): p. 1449-58.
89. Vedantham, S., et al., Human aldose reductase expression accelerates atherosclerosis in diabetic apolipoprotein E-/- mice. Arterioscler Thromb Vasc Biol, 2011. **31**(8): p. 1805-13.
90. Brownlee, M., Biochemistry and molecular cell biology of diabetic complications. Nature, 2001. **414**(6865): p. 813-20.
91. Durpes, M.C., et al., PKC-beta activation inhibits IL-18-binding protein causing endothelial dysfunction and diabetic atherosclerosis. Cardiovasc Res, 2015. **106**(2): p. 303-13.
92. Vlassara, H. and J. Uribarri, Advanced glycation end products (AGE) and diabetes: cause, effect, or both? Curr Diab Rep, 2014. **14**(1): p. 453.
93. Leurs, P. and B. Lindholm, The AGE-RAGE pathway and its relation to cardiovascular disease in patients with chronic kidney disease. Arch Med Res, 2013. **44**(8): p. 601-10.
94. Giacco, F., et al., Knockdown of glyoxalase 1 mimics diabetic nephropathy in nondiabetic mice. Diabetes, 2014. **63**(1): p. 291-9.
95. Hanssen, N.M., et al., Higher levels of advanced glycation endproducts in human carotid atherosclerotic plaques are associated with a rupture-prone phenotype. Eur Heart J, 2014. **35**(17): p. 1137-46.
96. Shinohara, M., et al., Overexpression of glyoxalase-I in bovine endothelial cells inhibits intracellular advanced glycation endproduct formation and prevents hyperglycemia-induced increases in macromolecular endocytosis. J Clin Invest, 1998. **101**(5): p. 1142-7.
97. Yao, D. and M. Brownlee, Hyperglycemia-induced reactive oxygen species increase expression of the receptor for advanced glycation end products (RAGE) and RAGE ligands. Diabetes, 2010. **59**(1): p. 249-55.

98. Brouwers, O., et al., Overexpression of glyoxalase-I reduces hyperglycemia-induced levels of advanced glycation end products and oxidative stress in diabetic rats. J Biol Chem, 2011. **286**(2): p. 1374-80.
99. Hanssen, N.M., et al., Glyoxalase 1 overexpression does not affect atherosclerotic lesion size and severity in ApoE-/- mice with or without diabetes. Cardiovasc Res, 2014. **104**(1): p. 160-70.
100. Geoffrion, M., et al., Differential effects of glyoxalase 1 overexpression on diabetic atherosclerosis and renal dysfunction in streptozotocin-treated, apolipoprotein E-deficient mice. Physiol Rep, 2014. **2**(6).
101. Wortmann, M., et al., Glyoxalase I (Glo1) and its metabolites in vascular disease. Biochem Soc Trans, 2014. **42**(2): p. 528-33.
102. Brouwers, O., et al., Glyoxalase-1 overexpression reduces endothelial dysfunction and attenuates early renal impairment in a rat model of diabetes. Diabetologia, 2014. **57**(1): p. 224-35.
103. Ullah, A., Khan, A., Khan I., Diabetes mellitus and oxidative stress—A concise review. Saudi Pharmaceutical Journal, 2016. **24**: p. 547-553.
104. Pitocco, D., et al., Oxidative stress in diabetes: implications for vascular and other complications. Int J Mol Sci, 2013. **14**(11): p. 21525-50.
105. Babior, B.M., NADPH oxidase. Curr Opin Immunol, 2004. **16**(1): p. 42-7.
106. Deliri, H. and C.A. McNamara, Nox 4 regulation of vascular smooth muscle cell differentiation marker gene expression. Arterioscler Thromb Vasc Biol, 2007. **27**(1): p. 12-4.
107. Konior, A., et al., NADPH oxidases in vascular pathology. Antioxid Redox Signal, 2014. **20**(17): p. 2794-814.
108. Langbein, H., et al., NADPH oxidase 4 protects against development of endothelial dysfunction and atherosclerosis in LDL receptor deficient mice. Eur Heart J, 2016. **37**(22): p. 1753-61.
109. Gray, S.P., et al., Reactive Oxygen Species Can Provide Atheroprotection via NOX4-Dependent Inhibition of Inflammation and Vascular Remodeling. Arterioscler Thromb Vasc Biol, 2016. **36**(2): p. 295-307.
110. Williams, C.R. and J.L. Gooch, Calcineurin Abeta regulates NADPH oxidase (Nox) expression and activity via nuclear factor of activated T cells (NFAT) in response to high glucose. J Biol Chem, 2014. **289**(8): p. 4896-905.
111. Wu, H., et al., NFAT signaling and the invention of vertebrates. Trends in Cell Biology, 2007. **17**(6): p. 251-260.
112. Rao, A., C. Luo, and P.G. Hogan, Transcription factors of the NFAT family: regulation and function. Annu Rev Immunol, 1997. **15**: p. 707-47.
113. de la Pompa, J.L., et al., Role of the NF-ATc transcription factor in morphogenesis of cardiac valves and septum. Nature, 1998. **392**(6672): p. 182-6.
114. Graef, I.A., et al., Signals transduced by Ca(2+)/calcineurin and NFATc3/c4 pattern the developing vasculature. Cell, 2001. **105**(7): p. 863-75.
115. Molkentin, J.D., et al., A calcineurin-dependent transcriptional pathway for cardiac hypertrophy. Cell, 1998. **93**(2): p. 215-28.

116. Chin, E.R., et al., A calcineurin-dependent transcriptional pathway controls skeletal muscle fiber type. Genes Dev, 1998. **12**(16): p. 2499-509.
117. Neuhofer, W., Role of NFAT5 in inflammatory disorders associated with osmotic stress. Curr Genomics, 2010. **11**(8): p. 584-90.
118. Cao, W., et al., Biomechanical Stretch Induces Inflammation, Proliferation, and Migration by Activating NFAT5 in Arterial Smooth Muscle Cells. Inflammation, 2017. **40**(6): p. 2129-2136.
119. Park, S., M. Uesugi, and G.L. Verdine, A second calcineurin binding site on the NFAT regulatory domain. Proc Natl Acad Sci U S A, 2000. **97**(13): p. 7130-5.
120. Hogan, P.G., et al., Transcriptional regulation by calcium, calcineurin, and NFAT. Genes Dev, 2003. **17**(18): p. 2205-32.
121. Vihma, H., P. Pruunsild, and T. Timmusk, Alternative splicing and expression of human and mouse NFAT genes. Genomics, 2008. **92**(5): p. 279-91.
122. Aramburu, J., A. Rao, and C.B. Klee, Calcineurin: from structure to function. Curr Top Cell Regul, 2000. **36**: p. 237-95.
123. Sorokin, A.V., E.R. Kim, and L.P. Ovchinnikov, Nucleocytoplasmic transport of proteins. Biochemistry (Mosc), 2007. **72**(13): p. 1439-57.
124. Kehlenbach, R.H. and S.A. Port, Analysis of CRM1-Dependent Nuclear Export in Permeabilized Cells. Methods Mol Biol, 2016. **1411**: p. 489-501.
125. Gomez, M.F., et al., Constitutively elevated nuclear export activity opposes Ca2+-dependent NFATc3 nuclear accumulation in vascular smooth muscle: role of JNK2 and Crm-1. J Biol Chem, 2003. **278**(47): p. 46847-53.
126. Grimes, C.A. and R.S. Jope, The multifaceted roles of glycogen synthase kinase 3beta in cellular signaling. Prog Neurobiol, 2001. **65**(4): p. 391-426.
127. Liang, Q., et al., c-Jun N-terminal kinases (JNK) antagonize cardiac growth through cross-talk with calcineurin-NFAT signaling. EMBO J, 2003. **22**(19): p. 5079-89.
128. Gomez del Arco, P., et al., A role for the p38 MAP kinase pathway in the nuclear shuttling of NFATp. J Biol Chem, 2000. **275**(18): p. 13872-8.
129. Yang, T.T., et al., Phosphorylation of NFATc4 by p38 mitogen-activated protein kinases. Mol Cell Biol, 2002. **22**(11): p. 3892-904.
130. Porter, C.M., M.A. Havens, and N.A. Clipstone, Identification of amino acid residues and protein kinases involved in the regulation of NFATc subcellular localization. J Biol Chem, 2000. **275**(5): p. 3543-51.
131. Arron, J.R., et al., NFAT dysregulation by increased dosage of DSCR1 and DYRK1A on chromosome 21. Nature, 2006. **441**(7093): p. 595-600.
132. Yang, T.T., et al., Integration of protein kinases mTOR and extracellular signal-regulated kinase 5 in regulating nucleocytoplasmic localization of NFATc4. Mol Cell Biol, 2008. **28**(10): p. 3489-501.
133. Nilsson, J., et al., High glucose activates nuclear factor of activated T cells in native vascular smooth muscle. Arterioscler Thromb Vasc Biol, 2006. **26**(4): p. 794-800.
134. Rinne, A., K. Banach, and L.A. Blatter, Regulation of nuclear factor of activated T cells (NFAT) in vascular endothelial cells. J Mol Cell Cardiol, 2009. **47**(3): p. 400-10.

135. Nilsson, L.M., et al., Nuclear factor of activated T-cells transcription factors in the vasculature: the good guys or the bad guys? Curr Opin Lipidol, 2008. **19**(5): p. 483-90.
136. Kar, P., et al., Control of NFAT Isoform Activation and NFAT-Dependent Gene Expression through Two Coincident and Spatially Segregated Intracellular Ca(2+) Signals. Mol Cell, 2016. **64**(4): p. 746-759.
137. Chen, L., et al., Structure of the DNA-binding domains from NFAT, Fos and Jun bound specifically to DNA. Nature, 1998. **392**(6671): p. 42-8.
138. Hill-Eubanks, D.C., et al., NFAT regulation in smooth muscle. Trends Cardiovasc Med, 2003. **13**(2): p. 56-62.
139. Gabriel, C.H., et al., Identification of Novel Nuclear Factor of Activated T Cell (NFAT)-associated Proteins in T Cells. J Biol Chem, 2016. **291**(46): p. 24172-24187.
140. Crabtree, G.R. and E.N. Olson, NFAT signaling: choreographing the social lives of cells. Cell, 2002. **109 Suppl**: p. S67-79.
141. Putney, J.W., Calcium signaling: deciphering the calcium-NFAT pathway. Curr Biol, 2012. **22**(3): p. R87-9.
142. Graef, I.A., et al., L-type calcium channels and GSK-3 regulate the activity of NF-ATc4 in hippocampal neurons. Nature, 1999. **401**(6754): p. 703-8.
143. Nguyen, T. and S. Di Giovanni, NFAT signaling in neural development and axon growth. Int J Dev Neurosci, 2008. **26**(2): p. 141-5.
144. Valdes, J.A., et al., NFAT activation by membrane potential follows a calcium pathway distinct from other activity-related transcription factors in skeletal muscle cells. Am J Physiol Cell Physiol, 2008. **294**(3): p. C715-25.
145. Wilkins, B.J., et al., Calcineurin/NFAT coupling participates in pathological, but not physiological, cardiac hypertrophy. Circ Res, 2004. **94**(1): p. 110-8.
146. Ono, K. and T. Iijima, Cardiac T-type Ca(2+) channels in the heart. J Mol Cell Cardiol, 2010. **48**(1): p. 65-70.
147. Makarewich, C.A., et al., Transient receptor potential channels contribute to pathological structural and functional remodeling after myocardial infarction. Circ Res, 2014. **115**(6): p. 567-580.
148. Colella, M., et al., Ca2+ oscillation frequency decoding in cardiac cell hypertrophy: role of calcineurin/NFAT as Ca2+ signal integrators. Proc Natl Acad Sci U S A, 2008. **105**(8): p. 2859-64.
149. Stevenson, A.S., et al., NFAT4 movement in native smooth muscle. A role for differential Ca(2+) signaling. J Biol Chem, 2001. **276**(18): p. 15018-24.
150. Gomez, M.F., et al., Opposing actions of inositol 1,4,5-trisphosphate and ryanodine receptors on nuclear factor of activated T-cells regulation in smooth muscle. J Biol Chem, 2002. **277**(40): p. 37756-64.
151. Bergdahl, A., et al., Plasticity of TRPC expression in arterial smooth muscle: correlation with store-operated Ca2+ entry. Am J Physiol Cell Physiol, 2005. **288**(4): p. C872-80.
152. Kumar, B., et al., Upregulated TRPC1 channel in vascular injury in vivo and its role in human neointimal hyperplasia. Circ Res, 2006. **98**(4): p. 557-63.

153. Maziere, C., et al., Oxidized low-density lipoprotein elicits an intracellular calcium rise and increases the binding activity of the transcription factor NFAT. Free Radic Biol Med, 2005. **38**(4): p. 472-80.

154. Goettsch, C., et al., Nuclear factor of activated T cells mediates oxidised LDL-induced calcification of vascular smooth muscle cells. Diabetologia, 2011. **54**(10): p. 2690-701.

155. Lipskaia, L., et al., Phosphatidylinositol 3-Kinase and Calcium-Activated Transcription Pathways Are Required for VLDL-Induced Smooth Muscle Cell Proliferation. Circ Res, 2003. **92**(10): p. 1115-1122.

156. Nilsson, L.M., et al., Novel blocker of NFAT activation inhibits IL-6 production in human myometrial arteries and reduces vascular smooth muscle cell proliferation. Am J Physiol Cell Physiol, 2007. **292**(3): p. C1167-78.

157. Liu, Z., N. Dronadula, and G.N. Rao, A novel role for nuclear factor of activated T cells in receptor tyrosine kinase and G protein-coupled receptor agonist-induced vascular smooth muscle cell motility. J Biol Chem, 2004. **279**(39): p. 41218-26.

158. Ranger, A.M., et al., The transcription factor NF-ATc is essential for cardiac valve formation. Nature, 1998. **392**(6672): p. 186-190.

159. Minami, T., et al., Vascular endothelial growth factor- and thrombin-induced termination factor, Down syndrome critical region-1, attenuates endothelial cell proliferation and angiogenesis. J Biol Chem, 2004. **279**(48): p. 50537-54.

160. Hernandez, G.L., et al., Selective Inhibition of Vascular Endothelial Growth Factor-mediated Angiogenesis by Cyclosporin A: Roles of the Nuclear Factor of Activated T Cells and Cyclooxygenase 2. J. Exp. Med., 2001. **193**(5): p. 607-620.

161. Urso, K., et al., NFATc3 regulates the transcription of genes involved in T-cell activation and angiogenesis. Blood, 2011. **118**(3): p. 795-803.

162. Minami, T., et al., Thrombin-induced autoinhibitory factor, Down syndrome critical region-1, attenuates NFAT-dependent vascular cell adhesion molecule-1 expression and inflammation in the endothelium. J Biol Chem, 2006. **281**(29): p. 20503-20.

163. Carvalho, L.D., et al., The NFAT1 transcription factor is a repressor of cyclin A2 gene expression. Cell Cycle, 2007. **6**(14): p. 1789-95.

164. Mognol, G.P., et al., Cell cycle and apoptosis regulation by NFAT transcription factors: new roles for an old player. Cell Death Dis, 2016. **7**: p. e2199.

165. Zetterqvist, A.V., et al., Inhibition of nuclear factor of activated T-cells (NFAT) suppresses accelerated atherosclerosis in diabetic mice. PLoS One, 2013. **8**(6): p. e65020.

166. Blanco, F., et al., In vivo inhibition of nuclear factor of activated T-cells leads to atherosclerotic plaque regression in IGF-II/LDLR(-/-)ApoB(100/100) mice. Diab Vasc Dis Res, 2018. **15**(4): p. 302-313.

167. Kudryavtseva, O., C. Aalkjaer, and V.V. Matchkov, Vascular smooth muscle cell phenotype is defined by Ca2+-dependent transcription factors. FEBS J, 2013. **280**(21): p. 5488-99.

168. Larrieu, D., et al., Activation of the Ca(2+)/calcineurin/NFAT2 pathway controls smooth muscle cell differentiation. Exp Cell Res, 2005. **310**(1): p. 166-75.

169. Liu, Z., et al., Blockade of Nuclear Factor of Activated T Cells Activation Signaling Suppresses Balloon Injury-induced Neointima Formation in a Rat Carotid Artery Model. J. Biol. Chem., 2005. **280**(15): p. 14700-14708.
170. Lipskaia, L., et al., Sarco/endoplasmic reticulum Ca2+-ATPase gene transfer reduces vascular smooth muscle cell proliferation and neointima formation in the rat. Circ Res, 2005. **97**(5): p. 488-95.
171. Nieves-Cintron, M., et al., Activation of NFATc3 down-regulates the beta1 subunit of large conductance, calcium-activated K+ channels in arterial smooth muscle and contributes to hypertension. J Biol Chem, 2007. **282**(5): p. 3231-40.
172. Nieves-Cintron, M., et al., The control of Ca2+ influx and NFATc3 signaling in arterial smooth muscle during hypertension. Proc Natl Acad Sci U S A, 2008. **105**(40): p. 15623-8.
173. Gonzalez Bosc, L.V., et al., Intraluminal Pressure Is a Stimulus for NFATc3 Nuclear Accumulation: ROLE OF CALCIUM, ENDOTHELIUM-DERIVED NITRIC OXIDE, AND cGMP-DEPENDENT PROTEIN KINASE. J. Biol. Chem., 2004. **279**(11): p. 10702-10709.
174. Bonnet, S., et al., The nuclear factor of activated T cells in pulmonary arterial hypertension can be therapeutically targeted. Proc Natl Acad Sci U S A, 2007. **104**(27): p. 11418-23.
175. Bierer, R., et al., NFATc3 is required for chronic hypoxia-induced pulmonary hypertension in adult and neonatal mice. Am J Physiol Lung Cell Mol Physiol, 2011. **301**(6): p. L872-80.
176. Chen, R., et al., The role of nuclear factor of activated T cells in pulmonary arterial hypertension. Cell Cycle, 2017. **16**(6): p. 508-514.
177. Szema, A.M., et al., NFATc3 and VIP in Idiopathic Pulmonary Fibrosis and Chronic Obstructive Pulmonary Disease. PLoS One, 2017. **12**(1): p. e0170606.
178. Berglund, L.M., et al., NFAT regulates the expression of AIF-1 and IRT-1: yin and yang splice variants of neointima formation and atherosclerosis. Cardiovasc Res, 2012. **93**(3): p. 414-23.
179. Li, M., et al., Sildenafil inhibits calcineurin/NFATc2-mediated cyclin A expression in pulmonary artery smooth muscle cells. Life Sci, 2011. **89**(17-18): p. 644-9.
180. Amberg, G.C., et al., NFATc3 regulates Kv2.1 expression in arterial smooth muscle. J Biol Chem, 2004. **279**(45): p. 47326-34.
181. Harper, J.V. and G. Brooks, The mammalian cell cycle: an overview. Methods Mol Biol, 2005. **296**: p. 113-53.
182. Rivard, A. and V. Andres, Vascular smooth muscle cell proliferation in the pathogenesis of atherosclerotic cardiovascular diseases. Histol Histopathol, 2000. **15**(2): p. 557-71.
183. Teixeira, L.K., et al., NFAT1 transcription factor regulates cell cycle progression and cyclin E expression in B lymphocytes. Cell Cycle, 2016. **15**(17): p. 2346-59.
184. Karpurapu, M., et al., NFATc1 targets cyclin a in the regulation of vascular smooth muscle cell multiplication during restenosis. J. Biol. Chem., 2008: p. M800423200.

185. Karpurapu, M., et al., Cyclin D1 is a bona fide target gene of NFATc1 and is sufficient in the mediation of injury-induced vascular wall remodeling. J Biol Chem, 2010. **285**(5): p. 3510-23.

186. Suzuki, T., et al., Vascular implications of the Kruppel-like family of transcription factors. Arterioscler Thromb Vasc Biol, 2005. **25**(6): p. 1135-41.

187. Zheng, B., M. Han, and J.K. Wen, Role of Kruppel-like factor 4 in phenotypic switching and proliferation of vascular smooth muscle cells. IUBMB Life, 2010. **62**(2): p. 132-9.

188. Garvey, S.M., et al., Cyclosporine up-regulates Kruppel-like factor-4 (KLF4) in vascular smooth muscle cells and drives phenotypic modulation in vivo. J Pharmacol Exp Ther, 2010. **333**(1): p. 34-42.

189. Davis-Dusenbery, B.N., et al., down-regulation of Kruppel-like factor-4 (KLF4) by microRNA-143/145 is critical for modulation of vascular smooth muscle cell phenotype by transforming growth factor-beta and bone morphogenetic protein 4. J Biol Chem, 2011. **286**(32): p. 28097-110.

190. Liu, Y., et al., Kruppel-like factor 4 abrogates myocardin-induced activation of smooth muscle gene expression. J Biol Chem, 2005. **280**(10): p. 9719-27.

191. Shi, N. and S.Y. Chen, Smooth Muscle Cell Differentiation: Model Systems, Regulatory Mechanisms, and Vascular Diseases. J Cell Physiol, 2016. **231**(4): p. 777-87.

192. Hien, T.T., et al., MicroRNA-dependent regulation of KLF4 by glucose in vascular smooth muscle. J Cell Physiol, 2018. **233**(9): p. 7195-7205.

193. Casellas, J., Inbred mouse strains and genetic stability: a review. Animal, 2011. **5**(1): p. 1-7.

194. Flecknell, P., Replacement, reduction and refinement. ALTEX, 2002. **19**(2): p. 73-8.

195. Chatzigeorgiou, A., et al., The use of animal models in the study of diabetes mellitus. In Vivo, 2009. **23**(2): p. 245-58.

196. Heinonen, S.E., et al., Animal models of diabetic macrovascular complications: key players in the development of new therapeutic approaches. J Diabetes Res, 2015. **2015**: p. 404085.

197. Kapourchali, F.R., et al., Animal models of atherosclerosis. World J Clin Cases, 2014. **2**(5): p. 126-32.

198. Getz, G.S. and C.A. Reardon, Diet and murine atherosclerosis. Arterioscler Thromb Vasc Biol, 2006. **26**(2): p. 242-9.

199. Wu, K.K. and Y. Huan, Diabetic atherosclerosis mouse models. Atherosclerosis, 2007. **191**(2): p. 241-9.

200. Getz, G.S. and C.A. Reardon, Animal models of atherosclerosis. Arterioscler Thromb Vasc Biol, 2012. **32**(5): p. 1104-15.

201. Lenzen, S., The mechanisms of alloxan- and streptozotocin-induced diabetes. Diabetologia, 2008. **51**(2): p. 216-26.

202. King, A.J., The use of animal models in diabetes research. Br J Pharmacol, 2012. **166**(3): p. 877-94.

203. Gurley, S.B., et al., Impact of genetic background on nephropathy in diabetic mice. Am J Physiol Renal Physiol, 2006. **290**(1): p. F214-22.
204. Li, J., et al., Hyperglycemia in apolipoprotein E-deficient mouse strains with different atherosclerosis susceptibility. Cardiovasc Diabetol, 2011. **10**: p. 117.
205. Nilsson-Berglund, L.M., et al., Nuclear factor of activated T cells regulates osteopontin expression in arterial smooth muscle in response to diabetes-induced hyperglycemia. Arterioscler Thromb Vasc Biol, 2009. **30**(2): p. 218-24.
206. Wang, J., et al., A mutation in the insulin 2 gene induces diabetes with severe pancreatic beta-cell dysfunction in the Mody mouse. J Clin Invest, 1999. **103**(1): p. 27-37.
207. Hsueh, W., et al., Recipes for creating animal models of diabetic cardiovascular disease. Circ Res, 2007. **100**(10): p. 1415-27.
208. Barber, A.J., et al., The Ins2Akita mouse as a model of early retinal complications in diabetes. Invest Ophthalmol Vis Sci, 2005. **46**(6): p. 2210-8.
209. Xanthoudakis, S., et al., An enhanced immune response in mice lacking the transcription factor NFAT1. Science, 1996. **272**(5263): p. 892-5.
210. Oukka, M., et al., The transcription factor NFAT4 is involved in the generation and survival of T cells. Immunity, 1998. **9**(3): p. 295-304.
211. Getz, G.S. and C.A. Reardon, Apoprotein E as a lipid transport and signaling protein in the blood, liver, and artery wall. J Lipid Res, 2009. **50 Suppl**: p. S156-61.
212. Pendse, A.A., et al., Apolipoprotein E knock-out and knock-in mice: atherosclerosis, metabolic syndrome, and beyond. J Lipid Res, 2009. **50 Suppl**: p. S178-82.
213. Jawien, J., The role of an experimental model of atherosclerosis: apoE-knockout mice in developing new drugs against atherogenesis. Curr Pharm Biotechnol, 2012. **13**(13): p. 2435-9.
214. Nakashima, Y., et al., ApoE-deficient mice develop lesions of all phases of atherosclerosis throughout the arterial tree. Arterioscler Thromb, 1994. **14**(1): p. 133-40.
215. Meir, K.S. and E. Leitersdorf, Atherosclerosis in the apolipoprotein-E-deficient mouse: a decade of progress. Arterioscler Thromb Vasc Biol, 2004. **24**(6): p. 1006-14.
216. Renard, C.B., et al., Diabetes and diabetes-associated lipid abnormalities have distinct effects on initiation and progression of atherosclerotic lesions. J Clin Invest, 2004. **114**(5): p. 659-68.
217. Heinonen, S.E., et al., Increased atherosclerotic lesion calcification in a novel mouse model combining insulin resistance, hyperglycemia, and hypercholesterolemia. Circ Res, 2007. **101**(10): p. 1058-67.
218. Farese, R.V., Jr., et al., Phenotypic analysis of mice expressing exclusively apolipoprotein B48 or apolipoprotein B100. Proc Natl Acad Sci U S A, 1996. **93**(13): p. 6393-8.
219. Devedjian, J.C., et al., Transgenic mice overexpressing insulin-like growth factor-II in beta cells develop type 2 diabetes. J Clin Invest, 2000. **105**(6): p. 731-40.

220. Lee, M. and J. Park, Regulation of NFAT activation: a potential therapeutic target for immunosuppression. Mol Cells, 2006. **22**(1): p. 1-7.
221. Sommerer, C., et al., Calcineurin inhibitors and NFAT-regulated gene expression. Clin Chim Acta, 2012. **413**(17-18): p. 1379-86.
222. Li, H., A. Rao, and P.G. Hogan, Interaction of calcineurin with substrates and targeting proteins. Trends in Cell Biology, 2011. **21**(2): p. 91-103.
223. Kipanyula, M.J., W.H. Kimaro, and P.F. Seke Etet, The Emerging Roles of the Calcineurin-Nuclear Factor of Activated T-Lymphocytes Pathway in Nervous System Functions and Diseases. J Aging Res, 2016. **2016**: p. 5081021.
224. Yu, H., T.J.C. van Berkel, and E.A.L. Biessen, Therapeutic Potential of VIVIT, a Selective Peptide Inhibitor of Nuclear Factor of Activated T cells, in Cardiovascular Disorders. Cardiovascular Drug Reviews, 2007. **25**(2): p. 175-187.
225. Umehara, H. and A. Asai, Tributylhexadecylphosphonium bromide, a novel nuclear factor of activated T cells signaling inhibitor, blocks interleukin-2 induction associated with inhibition of p70 ribosomal protein S6 kinase phosphorylation. Biol Pharm Bull, 2012. **35**(5): p. 805-9.
226. Sanghavi, M., et al., NFAT inhibitor tributylhexadecylphosphoniumbromide, ameliorates high fructose induced insulin resistance and nephropathy. Chem Biol Interact, 2015. **240**: p. 268-77.
227. Djuric, S.W., et al., 3,5-Bis(trifluoromethyl)pyrazoles: a novel class of NFAT transcription factor regulator. J Med Chem, 2000. **43**(16): p. 2975-81.
228. Trevillyan, J.M., et al., Potent inhibition of NFAT activation and T cell cytokine production by novel low molecular weight pyrazole compounds. J Biol Chem, 2001. **276**(51): p. 48118-26.
229. Nilsson-Berglund, L., Role of NFAT (nuclear factor of activated T cells) in vascular smooth muscle. Malmö: Department of Clincal Sciences, Malmö, Lund University, 2009.
230. Birsan, T., et al., Preliminary in vivo pharmacokinetic and pharmacodynamic evaluation of a novel calcineurin-independent inhibitor of NFAT. Transpl Int, 2004. **3**: p. 145-50.
231. Zetterqvist, A.V., et al., Nuclear factor of activated T cells is activated in the endothelium of retinal microvessels in diabetic mice. J Diabetes Res, 2015. **2015**: p. 428473.
232. Awla, D., et al., NFATc3 regulates trypsinogen activation, neutrophil recruitment, and tissue damage in acute pancreatitis in mice. Gastroenterology, 2012. **143**(5): p. 1352-1360 e7.
233. Fredrikson, G.N., et al., Inhibition of atherosclerosis in apoE-null mice by immunization with apoB-100 peptide sequences. Arterioscler Thromb Vasc Biol, 2003. **23**(5): p. 879-84.
234. Gan, L.M., et al., Non-invasive real-time imaging of atherosclerosis in mice using ultrasound biomicroscopy. Atherosclerosis, 2007. **190**(2): p. 313-20.
235. Zhang, X., et al., Noninvasive imaging of aortic atherosclerosis by ultrasound biomicroscopy in a mouse model. J Ultrasound Med, 2015. **34**(1): p. 111-6.

236. Gronros, J., et al., Effects of rosuvastatin on cardiovascular morphology and function in an ApoE-knockout mouse model of atherosclerosis. Am J Physiol Heart Circ Physiol, 2008. **295**(5): p. H2046-53.

237. Harmon, E.Y., et al., Ultrasound biomicroscopy for longitudinal studies of carotid plaque development in mice: validation with histological endpoints. PLoS One, 2012. **7**(1): p. e29944.

238. Murphy, H.C., The Use of Whole Animals Versus Isolated Organs or Cell Culture in Research. 1991, Nebraska Academy of Sciences at DigitalCommons@University of Nebraska - Lincoln.: http://digitalcommons.unl.edu/tnas/156. p. 105-108.

239. Bustin, S.A., et al., Quantitative real-time RT-PCR--a perspective. J Mol Endocrinol, 2005. **34**(3): p. 597-601.

240. Wong, M.L. and J.F. Medrano, Real-time PCR for mRNA quantitation. Biotechniques, 2005. **39**(1): p. 75-85.

241. Pfaffl, M.W., Quantification strategies in real-time PCR. 2004, International University Line (ILU); La Jolla, CA, USA. Editor: S.A. Bustin: A-Z of quantitative PCR. p. 87-112.

242. Suzuki, Y.J., Cell signaling pathways for the regulation of GATA4 transcription factor: Implications for cell growth and apoptosis. Cell Signal, 2011. **23**(7): p. 1094-9.

243. Rojas, A., et al., GATA4 is a direct transcriptional activator of cyclin D2 and Cdk4 and is required for cardiomyocyte proliferation in anterior heart field-derived myocardium. Mol Cell Biol, 2008. **28**(17): p. 5420-31.

244. Suzuki, Y.J., et al., Activation of GATA-4 by serotonin in pulmonary artery smooth muscle cells. J Biol Chem, 2003. **278**(19): p. 17525-31.

245. Nemer, M. and M.E. Horb, The KLF family of transcriptional regulators in cardiomyocyte proliferation and differentiation. Cell Cycle, 2007. **6**(2): p. 117-21.

246. Zhou, P., A. He, and W.T. Pu, Regulation of GATA4 transcriptional activity in cardiovascular development and disease. Curr Top Dev Biol, 2012. **100**: p. 143-69.

247. Narita, N., et al., The gene for transcription factor GATA-6 resides on mouse chromosome 18 and is expressed in myocardium and vascular smooth muscle. Genomics, 1996. **36**(2): p. 345-8.

248. Rowland, B.D. and D.S. Peeper, KLF4, p21 and context-dependent opposing forces in cancer. Nat Rev Cancer, 2006. **6**(1): p. 11-23.

249. Yellaturu, C.R., et al., A potential role for nuclear factor of activated T-cells in receptor tyrosine kinase and G-protein-coupled receptor agonist-induced cell proliferation. Biochem J, 2002. **368**(Pt 1): p. 183-90.

250. Baksh, S., et al., NFATc2-Mediated Repression of Cyclin-Dependent Kinase 4 Expression. Molecular Cell, 2002. **10**(5): p. 1071-1081.

251. Viola, J.P., et al., NFAT transcription factors: from cell cycle to tumor development. Braz J Med Biol Res, 2005. **38**(3): p. 335-44.

252. McDonald, O.G. and G.K. Owens, Programming smooth muscle plasticity with chromatin dynamics. Circ Res, 2007. **100**(10): p. 1428-41.

253. Chang, S., et al., Phenotypic modulation of primary vascular smooth muscle cells by short-term culture on micropatterned substrate. PLoS One, 2014. **9**(2): p. e88089.
254. Huber, A. and S.F. Badylak, Phenotypic changes in cultured smooth muscle cells: limitation or opportunity for tissue engineering of hollow organs? J Tissue Eng Regen Med, 2012. **6**(7): p. 505-11.
255. Han, M., et al., Smooth muscle 22 alpha maintains the differentiated phenotype of vascular smooth muscle cells by inducing filamentous actin bundling. Life Sci, 2009. **84**(13-14): p. 394-401.
256. Brozovich, F.V., et al., Mechanisms of Vascular Smooth Muscle Contraction and the Basis for Pharmacologic Treatment of Smooth Muscle Disorders. Pharmacol Rev, 2016. **68**(2): p. 476-532.
257. Gonzalez Bosc, L.V., et al., Nuclear factor of activated T cells and serum response factor cooperatively regulate the activity of an alpha-actin intronic enhancer. J Biol Chem, 2005. **280**(28): p. 26113-20.
258. Boettger, T., et al., Acquisition of the contractile phenotype by murine arterial smooth muscle cells depends on the Mir143/145 gene cluster. J Clin Invest, 2009. **119**(9): p. 2634-47.
259. Dahan, D., et al., Induction of angiotensin-converting enzyme after miR-143/145 deletion is critical for impaired smooth muscle contractility. Am J Physiol Cell Physiol, 2014. **307**(12): p. C1093-101.
260. Holmberg, J., et al., Loss of Vascular Myogenic Tone in miR-143/145 Knockout Mice Is Associated With Hypertension-Induced Vascular Lesions in Small Mesenteric Arteries. Arterioscler Thromb Vasc Biol, 2018. **38**(2): p. 414-424.
261. Shi, N. and S.Y. Chen, Mechanisms simultaneously regulate smooth muscle proliferation and differentiation. J Biomed Res, 2014. **28**(1): p. 40-6.
262. Monnier, L. and C. Colette, Glycemic Variability: Should we and can we prevent it? Diabetes Care, 2008. **31**(Supplement_2): p. S150-154.
263. Kwan, E.P., et al., Munc13-1 deficiency reduces insulin secretion and causes abnormal glucose tolerance. Diabetes, 2006. **55**(5): p. 1421-9.
264. Daly, M.E., et al., Acute effects on insulin sensitivity and diurnal metabolic profiles of a high-sucrose compared with a high-starch diet. Am J Clin Nutr, 1998. **67**(6): p. 1186-96.
265. Monnier, L. and C. Colette, Target for glycemic control: concentrating on glucose. Diabetes Care, 2009. **32 Suppl 2**: p. S199-204.
266. Yegutkin, G.G., Nucleotide- and nucleoside-converting ectoenzymes: Important modulators of purinergic signalling cascade. Biochim Biophys Acta, 2008. **1783**(5): p. 673-94.
267. Costa, G., et al., High glucose changes extracellular adenosine triphosphate levels in rat retinal cultures. Journal of Neuroscience Research, 2009. **87**(6): p. 1375-1380.
268. Loukovaara, S., et al., Increased intravitreal adenosine 5'-triphosphate, adenosine 5'-diphosphate and adenosine 5'-monophosphate levels in patients with proliferative diabetic retinopathy. Acta Ophthalmol, 2015. **93**(1): p. 67-73.

269. Lazarowski, E.R., R.C. Boucher, and T.K. Harden, Mechanisms of Release of Nucleotides and Integration of Their Action as P2X- and P2Y-Receptor Activating Molecules. Mol Pharmacol, 2003. **64**(4): p. 785-795.

270. Sima, B., et al., Extracellular Nucleotide-Induced [Ca2+]i Elevation in Rat Basilar Smooth Muscle Cells. Stroke, 1997. **28**(10): p. 2053-2059.

271. Gustavsson, C., et al., Vascular cellular adhesion molecule-1 (VCAM-1) expression in mice retinal vessels is affected by both hyperglycemia and hyperlipidemia. PLoS One, 2010. **5**(9): p. e12699.

272. Hesser, B.A., et al., Down syndrome critical region protein 1 (DSCR1), a novel VEGF target gene that regulates expression of inflammatory markers on activated endothelial cells. Blood, 2004. **104**(1): p. 149-158.

273. Park, L., et al., Suppression of accelerated diabetic atherosclerosis by the soluble receptor for advanced glycation endproducts. Nat Med, 1998. **4**(9): p. 1025-31.

274. Watson, A.M., et al., Delayed intervention with AGE inhibitors attenuates the progression of diabetes-accelerated atherosclerosis in diabetic apolipoprotein E knockout mice. Diabetologia, 2011. **54**(3): p. 681-9.

275. Averill, M.M. and K.E. Bornfeldt, Lipids versus glucose in inflammation and the pathogenesis of macrovascular disease in diabetes. Curr Diab Rep, 2009. **9**(1): p. 18-25.

276. Bochkov, V.N., et al., Oxidized phospholipids stimulate tissue factor expression in human endothelial cells via activation of ERK/EGR-1 and Ca(++)/NFAT. Blood, 2002. **99**(1): p. 199-206.

277. Norata, G.D., et al., Post-prandial endothelial dysfunction in hypertriglyceridemic subjects: molecular mechanisms and gene expression studies. Atherosclerosis, 2007. **193**(2): p. 321-7.

278. Rhee, K.J., et al., Extract of Ginkgo Biloba Ameliorates Streptozotocin-Induced Type 1 Diabetes Mellitus and High-Fat Diet-Induced Type 2 Diabetes Mellitus in Mice. Int J Med Sci, 2015. **12**(12): p. 987-94.

279. Mosca, L., E. Barrett-Connor, and N.K. Wenger, Sex/gender differences in cardiovascular disease prevention: what a difference a decade makes. Circulation, 2011. **124**(19): p. 2145-54.

280. Mathur, P., et al., Gender-Related Differences in Atherosclerosis. Cardiovasc Drugs Ther, 2015. **29**(4): p. 319-27.

281. Regensteiner, J.G., et al., Sex Differences in the Cardiovascular Consequences of Diabetes Mellitus: A Scientific Statement From the American Heart Association. Circulation, 2015. **132**(25): p. 2424-47.

282. Zhang, G., et al., Sex differences in the formation of atherosclerosis lesion in apoE(-/-)mice and the effect of 17beta-estrodiol on protein S-nitrosylation. Biomed Pharmacother, 2018. **99**: p. 1014-1021.

283. Heit, J.J., Calcineurin/NFAT signaling in the beta-cell: From diabetes to new therapeutics. Bioessays, 2007. **29**(10): p. 1011-21.

284. Schuett, H., et al., How much is too much? Interleukin-6 and its signalling in atherosclerosis. Thromb Haemost, 2009. **102**(2): p. 215-22.

285. Reiss, A.B., Siegart, N.M. and De Leon, J., Interleukin-6 in atherosclerosis: atherogenic or atheroprotective? Clinical Lipidology, 2017. **12**(10): p. 14-23.
286. Gadeau, A.P., et al., Osteopontin overexpression is associated with arterial smooth muscle cell proliferation in vitro. Arterioscler Thromb, 1993. **13**(1): p. 120-5.
287. Lund, S.A., C.M. Giachelli, and M. Scatena, The role of osteopontin in inflammatory processes. J Cell Commun Signal, 2009.
288. Wolak, T., Osteopontin - a multi-modal marker and mediator in atherosclerotic vascular disease. Atherosclerosis, 2014. **236**(2): p. 327-37.
289. Doganay, S., et al., Comparison of serum NO, TNF-alpha, IL-1beta, sIL-2R, IL-6 and IL-8 levels with grades of retinopathy in patients with diabetes mellitus. Eye, 2002. **16**(2): p. 163-70.
290. Hernandez, C., et al., Interleukin-8, monocyte chemoattractant protein-1 and IL-10 in the vitreous fluid of patients with proliferative diabetic retinopathy. Diabet Med, 2005. **22**(6): p. 719-22.
291. Petrovic, M.G., et al., Vitreous levels of interleukin-8 in patients with proliferative diabetic retinopathy. Am J Ophthalmol, 2007. **143**(1): p. 175-6.
292. Kawashima, M., et al., Soluble IL-6 receptor in vitreous fluid of patients with proliferative diabetic retinopathy. Jpn J Ophthalmol, 2007. **51**(2): p. 100-4.
293. Elner, S.G., et al., Cytokines in proliferative diabetic retinopathy and proliferative vitreoretinopathy. Curr Eye Res, 1995. **14**(11): p. 1045-53.
294. Adamiec-Mroczek, J. and J. Oficjalska-Mlynczak, Assessment of selected adhesion molecule and proinflammatory cytokine levels in the vitreous body of patients with type 2 diabetes--role of the inflammatory-immune process in the pathogenesis of proliferative diabetic retinopathy. Graefes Arch Clin Exp Ophthalmol, 2008. **246**(12): p. 1665-70.
295. Kase, S., et al., Increased osteopontin levels in the vitreous of patients with diabetic retinopathy. Ophthalmic Res, 2007. **39**(3): p. 143-7.
296. Cockerill, G.W., et al., Regulation of granulocyte-macrophage colony-stimulating factor and E- selectin expression in endothelial cells by cyclosporin A and the T- cell transcription factor NFAT. Blood, 1995. **86**(7): p. 2689-2698.
297. Kahles, F., H.M. Findeisen, and D. Bruemmer, Osteopontin: A novel regulator at the cross roads of inflammation, obesity and diabetes. Mol Metab, 2014. **3**(4): p. 384-93.
298. Wakabayashi, Y., et al., Increased levels of monokine induced by interferon-gamma (Mig) in the vitreous of patients with diabetic retinopathy. Diabet Med, 2008. **25**(7): p. 875-7.
299. Mysliwiec, M., et al., The role of vascular endothelial growth factor, tumor necrosis factor alpha and interleukin-6 in pathogenesis of diabetic retinopathy. Diabetes Res Clin Pract, 2008. **79**(1): p. 141-6.
300. Smallie, T., et al., IL-10 inhibits transcription elongation of the human TNF gene in primary macrophages. J Exp Med, 2010. **207**(10): p. 2081-8.
301. Lee, C.G., et al., A distal cis-regulatory element, CNS-9, controls NFAT1 and IRF4-mediated IL-10 gene activation in T helper cells. Mol Immunol, 2009. **46**(4): p. 613-21.

302. Didion, S.P., et al., Endogenous Interleukin-10 Inhibits Angiotensin II-Induced Vascular Dysfunction. Hypertension, 2009. **54**(3): p. 619-624.
303. Huang, H., et al., TNFalpha is required for late BRB breakdown in diabetic retinopathy, and its inhibition prevents leukostasis and protects vessels and neurons from apoptosis. Invest Ophthalmol Vis Sci, 2011. **52**(3): p. 1336-44.

Paper I

OPEN ACCESS Freely available online

PLOS ONE

Inhibition of Nuclear Factor of Activated T-Cells (NFAT) Suppresses Accelerated Atherosclerosis in Diabetic Mice

Anna V. Zetterqvist, Lisa M. Berglund, Fabiana Blanco, Eliana Garcia-Vaz, Maria Wigren, Pontus Dunér, Anna-Maria Dutius Andersson, Fong To, Peter Spegel, Jan Nilsson, Eva Bengtsson, Maria F. Gomez*

Department of Clinical Sciences in Malmö, Lund University, Malmö, Sweden

Abstract

Objective of the Study: Diabetic patients have a much more widespread and aggressive form of atherosclerosis and therefore, higher risk for myocardial infarction, peripheral vascular disease and stroke, but the molecular mechanisms leading to accelerated damage are still unclear. Recently, we showed that hyperglycemia activates the transcription factor NFAT in the arterial wall, inducing the expression of the pro-atherosclerotic protein osteopontin. Here we investigate whether NFAT activation may be a link between diabetes and atherogenesis.

Methodology and Principal Findings: Streptozotocin (STZ)-induced diabetes in apolipoprotein $E^{-/-}$ mice resulted in 2.2 fold increased aortic atherosclerosis and enhanced pro-inflammatory burden, as evidenced by elevated blood monocytes, endothelial activation- and inflammatory markers in aorta, and pro-inflammatory cytokines in plasma. *In vivo* treatment with the NFAT blocker A-285222 for 4 weeks completely inhibited the diabetes-induced aggravation of atherosclerosis, having no effect in non-diabetic mice. STZ-treated mice exhibited hyperglycemia and higher plasma cholesterol and triglycerides, but these were unaffected by A-285222. NFAT-dependent transcriptional activity was examined in aorta, spleen, thymus, brain, heart, liver and kidney, but only augmented in the aorta of diabetic mice. A-285222 completely blocked this diabetes-driven NFAT activation, but had no impact on the other organs or on splenocyte proliferation or cytokine secretion, ruling out systemic immunosuppression as the mechanism behind reduced atherosclerosis. Instead, NFAT inhibition effectively reduced IL-6, osteopontin, monocyte chemotactic protein 1, intercellular adhesion molecule 1, CD68 and tissue factor expression in the arterial wall and lowered plasma IL-6 in diabetic mice.

Conclusions: Targeting NFAT signaling may be a novel and attractive approach for the treatment of diabetic macrovascular complications.

Citation: Zetterqvist AV, Berglund LM, Blanco F, Garcia-Vaz E, Wigren M, et al. (2013) Inhibition of Nuclear Factor of Activated T-Cells (NFAT) Suppresses Accelerated Atherosclerosis in Diabetic Mice. PLoS ONE 8(6): e65020. doi:10.1371/journal.pone.0065020

Editor: Karin Jandeleit-Dahm, Baker IDI Heart and Diabetes Institute, Australia

Received November 20, 2012; **Accepted** April 21, 2013; **Published** June 3, 2013

Funding: This work was supported by the Swedish Heart and Lung Foundation [HLF20080843; HLF20100532]; the Swedish Research Council [#2009-4120; #2011-3900; #2009-1039], Lund University Diabetes Centre, the Swedish Medical Society; the Swedish Society for Medical Research, the Royal Physiographic Society in Lund, Skåne Hospital Research Funds, and Crafoord; Albert Påhlsson; Lars Hierta Memorial; and the Knut & Alice Wallenberg foundations. This work was also supported by Innovative Medicines Initiative Joint Undertaking [#115006], comprising funds from the European Union's Seventh Framework Programme [FP7/2007-2013] and EFPIA companies' in kind contribution. The funders had no role in study design, data collection and analysis, decision to publish, or preparation of the manuscript.

Competing Interests: The authors have declared that no competing interests exist.

* E-mail: maria.gomez@med.lu.se

Introduction

A much more widespread and aggressive form of atherosclerosis is observed in the coronary arteries, lower extremities and extracranial carotid arteries of diabetic patients, causing nearly 80% of all deaths and much of their disability [1]. Both diabetes type 1 and type 2 are independent risk factors for myocardial infarction, peripheral vascular disease and stroke. Despite vast clinical experience linking diabetes and atherosclerosis, it is still unclear how diabetes accelerates the clinical course of the disease. A wealth of epidemiologic evidence demonstrate that hyperglycemia increases cardiovascular event rates and worsens outcome [2]. Recent studies also show a causal association between elevated glucose levels and increased carotid intima-media thickness, a surrogate marker of subclinical atherosclerosis [3]. Intensive glycemic control early in the course of the disease lowers cardiovascular events in the long term [4]. Despite all this evidence, very little is understood about the molecular mechanisms connecting hyperglycemia to atherosclerosis.

The nuclear factor of activated T-cells (NFATc1-c4) are a family of Ca^{2+}/calcineurin-dependent transcription factors first characterized in T-lymphocytes as inducers of cytokine gene expression. Since then, NFAT proteins have been shown to play various roles outside immune cells, including in the cardiovascular system. We have previously shown that hyperglycemia effectively activates NFATc3 in the arterial wall [5,6] and once activated, NFATc3 induces the expression of the pro-inflammatory matrix protein osteopontin (OPN), a cytokine that promotes atherosclerosis and diabetic vascular disease [6]. Diabetes increased OPN expression in the aorta of normolipidemic mice and this was prevented by pharmacological inhibition of NFAT with the NFAT-blocker A285222 or by lack of NFATc3 protein in

NFATc3 deficient mice [6]. Additional experimental evidence supports a role for NFAT as a regulator of genes able to promote vascular dysfunction and potentially, a pro-atherogenic vascular phenotype [7,8,9]. NFAT promotes vascular smooth muscle cell (VSMC) proliferation and migration [7,10], and plays a role in neointima formation and in the regulation of cyclooxygenase 2 (Cox2) expression after vascular injury [11,12,13]. NFAT contributes to the development of angiotensin II-induced hypertension, via down-regulation of potassium channel expression [14,15]. Moreover, NFAT controls the alternative splicing of allograft inflammatory factor-1 (AIF-1), resulting in products differentially associated to parameters defining human plaque phenotype and stability [16].

Together, these observations led us to hypothesize that NFAT may act as a glucose-sensor in the vessel wall, translating changes in Ca^{2+} signals into changes in gene expression that lead to macrovascular disease in diabetes. To more directly test this hypothesis and in the context of an atherosclerosis-prone experimental model, we investigate the effects of NFAT-signaling inhibition on atherosclerotic plaque formation and inflammatory burden in diabetic and non-diabetic apolipoprotein (Apo)E deficient mice.

Materials and Methods

Animals

This study was carried out in strict accordance with the recommendations in the Guide for the Care and Use of Laboratory Animals of the National Institutes of Health. All protocols were approved by the local ethics review board at Lund University and the Malmö/Lund Animal Care and Use Committee (Permit Number: M29-12). Animals were anaesthetized with ketamine hydrochloride and xylazine (i.p.; 2.5 mg and 7.5 mg/100 g body weight, respectively) and euthanized by exsanguination through cardiac puncture for blood collection. Depth of anesthesia was assessed by the toe-pinch reflex procedure and absence of muscular tone. All efforts were made to minimize suffering. Adult $ApoE^{-/-}$ (B6.129P2-Apoe^{tm1Unc}/J; Charles River, Sulzfeld, Germany; n = 196), C57BL/6J (stock number 000664; Charles River; n = 25) and FVBN 9x-NFAT-luciferase reporter mice (NFAT-luc; n = 72) [17] were used.

Study Design

Treatment protocols are summarized in Figure 1. **Protocol I**: 22 weeks old $ApoE^{-/-}$ mice received intraperitoneal (i.p.) injections of streptozocin (STZ; Sigma-Aldrich, Stockholm, Sweden; 60 mg/kg body weight, pH 4.5) or vehicle (citrate buffer) once a day for 5 days at the start of the experiments, as previously described [6]. One group of mice (n = 24) was euthanized 4 weeks after the first STZ/vehicle injection, while additional 2 groups received daily i.p. injections of the NFAT blocker A-285222 (0.29 mg/kg body weight) or vehicle (saline) for 1 (n = 81) or 4 weeks (n = 43) until termination. **Protocols II** and **III:** NFAT-luc mice were used. In protocol II (n = 29), diabetes was induced as in protocol I and mice received daily i.p. injections of A-285222 (0.15 mg/kg body weight) or saline until termination at day 16. In protocol III (n = 36), mice were fed a normal chow (R3; Lantmännen, Kimstad, Sweden) or a high fat diet (HFD; R638:0.15% cholesterol, 21% fat; Lantmännen) during 4 or 8 weeks. **Protocol IV**: C57BL/6J mice (n = 25) received daily i.p. injections of A-285222 (0.29 mg/kg body weight) or vehicle for 4 weeks until termination.

A-285222 inhibits all NFAT family members and was provided by Abbott Laboratories (Abbott Park, IL). Body weight and blood glucose, measured in whole venous blood (One-Touch, LifeScan Inc., Milipitas, CA) were monitored once a week. Animals had free access to tap water, fed normal chow diet (except in protocol III). For *en face* and cross sectional measurements of plaque (4- and 8-weeks groups), the aorta and heart were dissected out after whole body perfusion with phosphate-buffered saline (PBS) and stored in Histochoice (Amresco Inc, Solon, OH) at 4°C for fixation until further processing. For mRNA expression measurements in the aortic arch and experiments involving splenocytes and monocytes (5-weeks group), whole body perfusion with PBS was performed, after which aortas were dissected free of connective tissue and snap frozen, and whole spleens were weighed and stored in ice cold PBS until further processing. The 8-week version of protocol I was repeated in an additional group of diabetic mice (n = 25) for mRNA and protein expression measurements in the aortic arch and for liver histology. For the pharmacokinetics of A-285222, additional $ApoE^{-/-}$ (n = 23) and FVBN (n = 7) mice were used.

Histological Evaluation of Atherosclerosis, Spleen and Liver

En face preparations of the aorta were performed as described before [18]. Briefly, aortas were fixed in Histochoice, dipped in 78% methanol and stained for 40 min in 0.16% Oil Red O (ORO) dissolved in 78% methanol/0.2 mol/L NaOH, after which they were washed in 78% methanol and distilled water. Cover slips were mounted with water-soluble mounting media L-550A (Histolab, Göteborg, Sweden). Lipids are stained red, which makes the plaques bordeaux-colored. Lipid (ORO), macrophages (Moma-2; monocyte/macrophage 2), α-smooth muscle actin (α-SMA) and collagen contents were evaluated in cross-sections (10 μm) of the aortic root as described before [18]. Rat anti-Moma-2 primary antibody (1 μg/mL; BMA Biomedicals, Augst, Switzerland), mouse anti-alpha-SMA (0.42 μg/mL, Sigma-Aldrich) and biotinylated secondary IgG antibodies (Vector Laboratories, Burlingame, CA) were used. Sections were counterstained with Harris hematoxylin for determination of subvalvular lesion area, expressed both in μm^2 and as percentage of total cross sectional area to correct for potential structural differences in the arterial wall between groups [19]. Media and lumen areas were also determined based on the Harris hematoxylin staining. Specificity of immune staining was confirmed by the absence of staining when primary or secondary antibodies were omitted from the protocol. Sections (5–6 per mouse) were analyzed under blind conditions by computer-aided morphometry (Image-Pro Plus, Media Cybernetics, Bethesda, MD and BioPix iQ 2.0 software, Biopix AB, Gothenburg, Sweden, for *en face* and cross sections respectively). Expression of tissue factor (TF) and osteopontin (OPN) was also evaluated in the aortic root using confocal immunofluorescence microscopy as described before [6]. Sections were stained with primary rabbit antibodies, anti-OPN (0.5 μg/mL, IBL, Hamburg, Germany) or anti-TF (10 μg/mL, American Diagnostica, Stamford, CT) and secondary antibody, DyLight 649 anti-rabbit IgG (1:400 and 1:500, for OPN and TF, respectively; Jackson ImmunoResearch, West Grove, PA); and counterstained with the nucleic acid dye SYTOX Green (1:3000, Molecular Probes, Invitrogen, Paisley, UK). Sections (3–6 per mouse) were examined under blind conditions at 20X in a Zeiss LSM 5 Pascal laser scanning confocal microscope and mean fluorescence intensities of OPN and TF in the plaque were quantified using the Zeiss LSM 5 analysis software and ImageJ (version 1.47 m), respectively.

Spleen and liver cryosections (10 μm) were fixed with Histochoice and stained with hematoxylin and eosin (H&E). Liver sections were also stained with ORO and hematoxylin. For

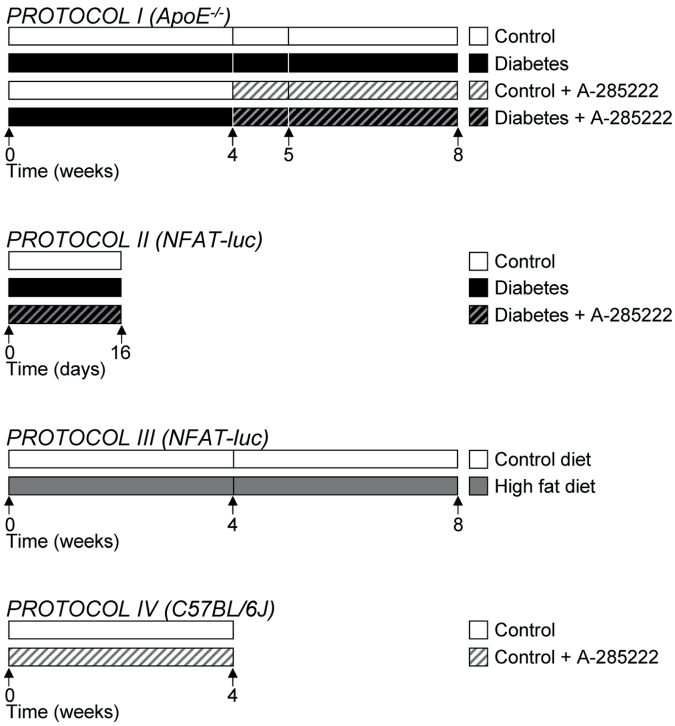

Figure 1. Study design. Protocol I: 22 weeks old ApoE$^{-/-}$ mice received intraperitoneal (i.p.) injections of STZ or vehicle as previously described [6]. One group of mice was euthanized 4 weeks after the first STZ/vehicle injection, while additional 2 groups received daily i.p. injections of the NFAT blocker A-285222 (0.29 mg/kg body weight) or vehicle (saline) for 1 or 4 weeks until termination. **Protocols II** and **III:** NFAT-luc mice were used. In protocol II, diabetes was induced as in protocol I and mice received daily i.p. injections of A-285222 (0.15 mg/kg body weight) or saline until termination at day 16. In protocol III, mice were fed a normal chow or a high fat diet (HFD; 0.15% cholesterol, 21% fat) during 4 or 8 weeks. **Protocol IV:** C57BL/6J mice received daily i.p. injections of A-285222 (0.29 mg/kg body weight) or vehicle for 4 weeks until termination. Arrows indicate time of termination; diabetes (black bars), control (white bars), A-285222-treated (hatched bars) and high fat diet (grey bars).
doi:10.1371/journal.pone.0065020.g001

quantification of liver fat content (ORO), three sections per mouse were analyzed under blind conditions by computer-aided morphometry (BioPix iQ 2.0 software, Biopix AB, Gothenburg, Sweden).

Luciferase Reporter Assay

Luciferase activity was measured in tissue homogenates from the aortic arch, spleen, thymus, brain, heart, liver and kidney. Assays were performed as previously described [5,7]. Optical density was measured using a Tecan Infinite M200 instrument (Tecan Nordic AB, Mölndal, Sweden) and data expressed as relative luciferase units (RLU) per µg protein. Protein concentration was determined with the EZQ protein quantification kit (Molecular Probes, Invitrogen, Paisley, UK) or the DC Protein Assay (Bio-Rad Laboratories Sundbyberg, Sweden).

Plasma Cholesterol, Triglycerides and Cytokines

Plasma cholesterol and triglycerides were measured by colorimetric assays (Infinity^{TM}-Cholesterol and Infinity^{TM}-Triglyceride; Thermo Scientific, Middletown, VA) as described before [20]. Plasma cytokines were measured using a pro-inflammatory 7-plex kit (Meso Scale Discovery, Rockville, MD). The lower detection limit for each cytokine was within the range described by the manufacturer. Plasma OPN and soluble (s) vascular cell adhesion molecule 1 (VCAM-1) levels were assayed using Quantikine mouse OPN and sVCAM-1 ELISA kits (R&D Systems, Abingdon UK). Absorbance was measured at 450 nm and the lower limits of detection were 5.7 pg/mL and 0.31 ng/mL, respectively. All assays were performed according to the manufacturers' instructions.

Quantitative RT-PCR (qRT-PCR)

RNA was extracted from the aortic arch using TRI Reagent BD (Sigma-Aldrich) and a protocol for simultaneous isolation of RNA, DNA and protein, according to the manufacturer's instructions. cDNA synthesis and real-time PCR were performed as previously described [21], using TaqMan Gene Expression assays for IL-6 (Mm00446190_m1), OPN (Mm00436767_m1), monocyte chemotactic protein 1 (MCP-1; Mm00441242_m1), intercellular adhesion molecule 1 (ICAM-1; Mm00516023_m1), VCAM-1 (Mm01320970_m1), IL-1β (Mm01336189_m1), Cox-2 (Mm00478374_m1), IL-10 (Mm00439614_m1), TF

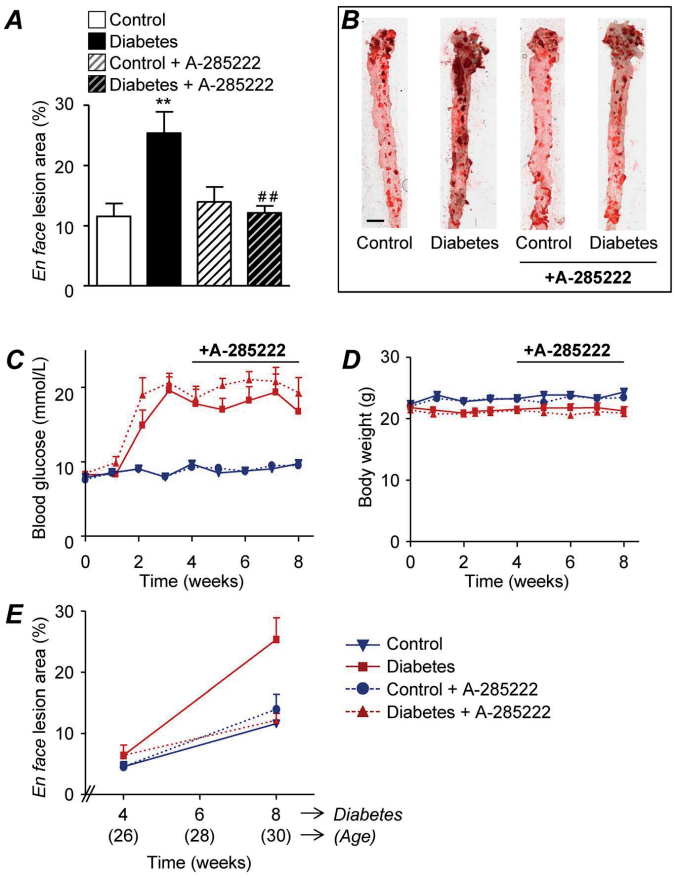

Figure 2. NFAT inhibition suppresses accelerated atherosclerosis in diabetes. (**A**) *En face* lesion area in the aortic arch of control and diabetic female ApoE$^{-/-}$ mice treated for 4 weeks with A-285222 or saline (protocol I). Mice were 30 weeks old at the time of analysis, 8 weeks after the first STZ or vehicle injection. Data is expressed as percentage of total aortic arch area (n = 9–12 mice/group). Two-way ANOVA for the effect of diabetes and the drug revealed significant interaction between factors (*$P<0.005$). Bonferroni post-test yielded **$P<0.01$ vs. non-diabetic control mice and ##$P<0.01$ vs. diabetic saline-treated mice. (**B**) Representative *en face* preparations of aortas from ApoE$^{-/-}$ mice treated as in A and stained with ORO (bordeaux-colored). Scale = 2 mm. (**C**) Blood glucose (mmol/L) and (**D**) body weight (g) values for mice in panel A. (**E**) Merged data from the measurements in panel A and *en face* data obtained 4 weeks after the first STZ or vehicle injection (n = 9–13 mice/group). Control non-diabetic (blue); diabetic (red); A-285222-treated (dotted lines); saline treated (unbroken lines).
doi:10.1371/journal.pone.0065020.g002

(Mm00436948_m1), CD68 (Mm03047340_m1) with HPRT (Mm00446968_m1) and β-actin (Mm00607939_s1) as endogenous controls.

Western Blotting

Following RNA extraction from the aortic arch, protein was precipitated from the phenol-ethanol supernatant obtained after sedimentation of the DNA pellet. After a series of washes, the protein-containing pellet was dried and dissolved in SDS sample buffer (62.5 mmol/L Tris-HCl pH 6.8, 2% SDS, 10% glycerol, 5% 2-mercaptoethanol and 0.001% bromophenol blue). Alternatively, arteries were homogenized directly in SDS sample buffer as previously described [6]. Protein concentration was determined with the EZQ protein quantification kit (Molecular Probes). An equal amount of protein was loaded onto 12.5% Tris-HCl gels (Bio-Rad Laboratories) and separated by gel electrophoresis. Proteins were transferred to polyvinylidene difluoride membranes (Bio-Rad Laboratories), blocked in 3% BSA/5% non-fat dry milk and incubated with primary anti-TF (2 μg/mL in 3% BSA, American Diagnostica, Stamford, CT) or to nitrocellulose membranes (Bio-Rad Laboratories), blocked in 5% BSA and incubated with anti-CD68 (0.82 μg/mL in 5% milk, DakoCytomation, Glostrup, Denmark). HRP-conjugated secondary antibody (Cell Signaling, Danvers, MA) was used and bands detected with chemiluminescence (Supersignal West Dura, Pierce Biotechnology, Rockford, IL). β-actin (1:3000) or α-tubulin (1:5000; both

Table 1. Blood glucose, body weight, plasma cholesterol and triglyceride values in mice undergoing the different experimental protocols.

Genotype and treatment	Blood glucose (mmol/L)	Body weight (g)	Total cholesterol (mmol/L)	Triglycerides (mmol/L)
Protocol I (ApoE$^{-/-}$)				
4 weeks:				
Control (n = 13)	8.8±0.8	22.9±1.4	10.8±1.5	0.48±0.13
Diabetes (n = 11)	19.6±4.7***	21.6±1.9	16.9±3.5***	0.55±0.22
5 weeks:				
Control (n = 9)	9.1±1.1	30.2±2.0	10.6±1.4	1.44±0.36
Diabetes (n = 11)	23.4±5.5***	29.4±1.7	17.9±2.4**	2.71±1.02
Control+A-285222 (n = 8)	9.6±0.5	30.6±2.1	13.6±3.2	2.14±1.03
Diabetes+A-285222 (n = 11)	23.2±5.8***	28.3±2.6*	17.2±5.6	2.57±1.56
8 weeks:				
Control (n = 12)	9.0±1.6	24.3±1.7	10.2±1.3	0.65±0.22
Diabetes (n = 10)	17.7±5.5***	21.3±2.2***	15.6±4.4***	1.04±0.38**
Control+A-285222 (n = 12)	9.0±0.4	23.4±1.3	11.7±1.4	0.68±0.19
Diabetes+A-285222 (n = 9)	19.8±3.5***	20.8±1.0**	16.0±4.7**	0.93±0.25
Protocol II (NFAT-luc)				
Control (n = 11)	8.9±1.0	22.5±3.0	2.30±0.33	1.74±0.39
Diabetes (n = 8)	15.4±7.2*	21.9±1.4	2.49±0.33	2.20±0.30
Diabetes+A-285222 (n = 10)	14.7±5.4*	22.7±2.3	2.45±0.36	1.91±0.75
Protocol III (NFAT-luc)				
4 weeks:				
Control (n = 12)	10.3±1.2	30.8±4.3	3.19±0.34	1.31±0.56
High fat diet (n = 8)	11.4±1.6	39.0±7.7**	5.59±1.25***	0.80±0.38
8 weeks:				
Control (n = 9)	9.7±0.7	35.9±5.6	3.39±0.67	1.24±0.53
High fat diet (n = 7)	12.7±3.0**	43.7±5.0*	6.00±1.01***	1.04±0.40
Protocol IV (C57Bl6/J)				
Control (n = 13)	12.8±2.7	25.2±3.4	2.75±0.73	0.50±0.13
Control+A-285222 (n = 12)	11.7±1.9	26.0±4.5	2.42±0.46	0.49±0.15

Values represent mean ± SD. Blood glucose values are averaged during the experiments (from week 2 until termination). Body weight and lipids values were measured at termination. For protocol 1 (4 weeks), student's t-test yielded ***$p<0.001$ vs. non-diabetic mice. For protocol 1 (5 and 8 weeks), two-way ANOVA (for the effects of diabetes and A-285222) revealed no interactions between factors. Bonferroni post-tests yielded *<0.05, **$p<0.01$, ***$p<0.001$ for comparisons between control and diabetic mice receiving the same treatment. For protocol 2, one-way ANOVA and Bonferroni post-tests yielded *<0.05, vs non-diabetic control. For protocol 3, two-way ANOVA (for the effects of high fat diet and diet duration) revealed no interactions. Bonferroni post-tests yielded *<0.05, **$p<0.01$, ***$p<0.001$ for comparisons between mice fed high fat diet and controls.

doi:10.1371/journal.pone.0065020.t001

from GenScript Corporation, Piscataway, NJ) were used as loading controls.

Splenocyte Proliferation and Cytokine Production

Splenocytes were isolated as previously described [22]. Briefly, single cell suspensions were prepared by pressing spleens through a 70-µm cell strainer (BD Falcon, Franklin Lakes, NJ). Erythrocytes were removed using red blood cell lysing buffer (Sigma-Aldrich). Cells were cultured in culture medium containing 10% heat-inactivated FCS, 1 mmol/L sodium pyruvate, 10 mmol/L Hepes, 50 U of penicillin, 50 µg/mL streptomycin, 0.05 mmol/L β-mercaptoethanol, and 2 mmol/L L-glutamine (RPMI 1640, GIBCO, Paisley, UK) in 96-well round bottom plates (Sarstedt, Nümbrecht, Germany). For proliferation assay, 2×10^5 cells/well were cultured with or without Dynabeads® coupled to anti-CD3 and anti-CD28 antibodies for T-cell activation and expansion (bead to cell ratio 1:1, Invitrogen, Life Technologies, Carlsbad, CA); alternatively, with or without 2.5 µg/mL concanavalin A (ConA; Sigma-Aldrich) for 88 hours. To measure DNA synthesis, the cells were pulsed with 1 µCi [methyl-^{3}H]thymidine (Amersham Biosciences, Uppsala, Sweden); during the last 16 hours, macromolecular material was harvested on glass fiber filters using a Filter Mate Harvester (Perkin Elmer, Buckinghamshire, UK) and analyzed using a liquid scintillation counter (Wallac 1450 MicroBeta, Ramsey, MN). For cytokine production, 1×10^6 cells/well were cultured in 48-well plates (Sarstedt, Nümbrecht, Germany) with or without anti-CD3/CD28 dynabeads (bead to cell ratio 1:1, Invitrogen) for 48 hours, after which cytokine concentrations in the culture media were measured using a Th1/Th2 9-plex ultra-sensitive kit (Meso Scale Discovery). The lower detection limit for each cytokine was within the range described by the manufacturer.

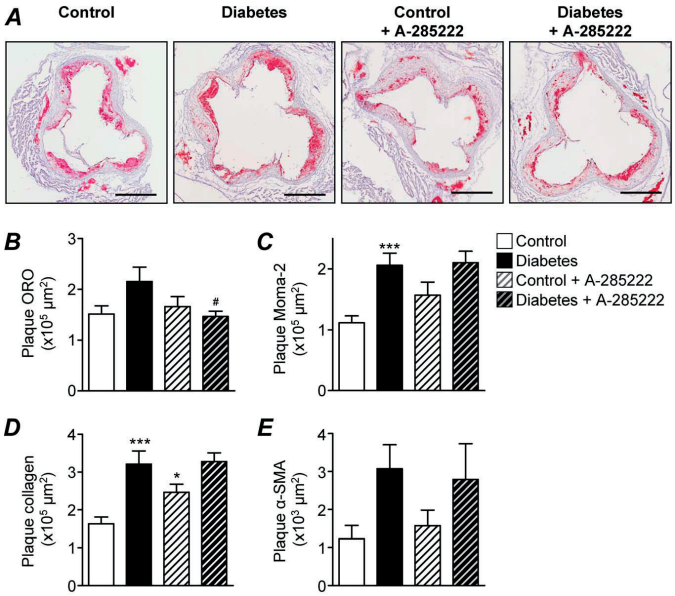

Figure 3. Inhibition of NFAT reduces the lipid contents in the plaque of diabetic mice. (**A**) ORO stained cross-sections of the aortic root from control and diabetic female ApoE$^{-/-}$ mice treated with or without A-285222 for 4 weeks (Protocol I). Sections were counter-stained with Harris hematoxylin. Scale = 500 µm. (**B**) Summarized morphometric data from sections stained as in A showing ORO positive area in the plaques. Two-way ANOVA for the effect of diabetes and the drug revealed significant interaction between factors ($P<0.05$). Post-test yielded $^{\#}P<0.05$ vs. diabetic saline-treated mice (n = 9–12 mice/group). (**C–E**) Summarized morphometric data from the same animals as in B showing monocytes/macrophages-2 (Moma-2, C), collagen (D) and α-smooth muscle actin (α-SMA, E) positive areas in the plaques. Two-way ANOVA revealed significant effect of diabetes ($P<0.001$ for Moma-2 and collagen; $P<0.05$ for α-SMA), Bonferroni post-test yielded $^{*}P<0.05$ and $^{***}P<0.001$ vs. non-diabetic saline-treated mice (n = 9–12 mice/group).
doi:10.1371/journal.pone.0065020.g003

Flow Cytometry Analysis

Cells from blood and splenocytes were analyzed as previously described [23,24,25]. Blood cells were stained with the following fluorochrome-conjugated antibodies after blocking of FC receptors for 5 minutes: PerCP/Cy5.5-anti-CD62L (L-selectin), PE/Cy7-anti-Ly-6c, (BioLegend, San Diego, CA) and APC-anti-CD115 (eBioscience, San Diego, CA). Splenocytes were stained for PE/Cy7-anti-CD3, Pacific Blue-anti-CD4, APC-anti-CD25 after blocking of FC receptors for 5 minutes. Cells where then permeabilized and thereafter stained with PE-anti-Foxp3 (Biolegend). For interferon (IFN)-γ measurements, splenocytes (5×10^5 cells/cell culture well) were incubated with phorbol 12-myristate 13-acetate (PMA; 10 ng), ionomycin (0.2 µg), and brefeldin A (1 µg, all from Sigma) for 4 hours at 37°C. Stimulated cells were then stained for CD3 and CD4 (as above). Cells were thereafter permeabilized and stained with PE-anti-IFN-γ (Biolegend). Measurements were performed using a CyAn ADP flow cytometer (Beckman Coulter, Brea, CA) and analyzed with FlowJo7.6 software (Tree Star, Ashland, OR). Mononuclear leukocytes were gated from the forward scatter (FSC)/side scatter (SSC). Single stained samples were used to correct for fluorescence spillover in multicolor analyses, and gate boundaries were set by fluorescence-minus-one (FMO) controls.

Gas Chromatography Mass Spectroscopy (GC/MS)

For the pharmacokinetics of A-285222, blood was collected from adult ApoE$^{-/-}$ mice (n = 23) by cardiac puncture at different time points (30 min, 1, 2, 4, 6, 12 and 24 hours) after i.p. injection of A-285222 (0.29 mg/kg body weight in saline solution). Plasma was isolated and a known concentration (2.5 µmol/L) of the analogous inactive compound A-216491 (Abbott Park, IL) was added as an internal standard to all samples. Samples were randomized and run in duplicates. Samples (300 µL) were extracted twice with ethyl acetate (400 µL), followed by evaporation. The dried residues were finally re-dissolved in chloroform (30 µL) and analyzed by GC/MS on an Agilent 6890N gas chromatograph (Agilent, Santa Clara, CA) coupled to a Leco Pegasus III TOFMS electron impact TOF (time-of-flight) mass spectrometer (Leco Corp., St. Joseph, MI). Identification was based on mass spectra and retention indexes, calculated from the injection of a homologous series of n-alkanes. The concentration of A-285222 in plasma was determined using a calibration curve calculated from analyses of plasma from untreated mice, spiked with known concentrations of A-285222 and A-216491. Plasma A-285222 levels were also determined in mice from protocols I (5 and 8 weeks), II and IV, from blood collected at the time of euthanasia (i.e.~24 h after the last i.p. injection of A-285222). These measurements were performed in duplicate using pooled plasma from 6–12 mice for each experimental condition. Plasma from the groups treated with saline served as negative controls. In

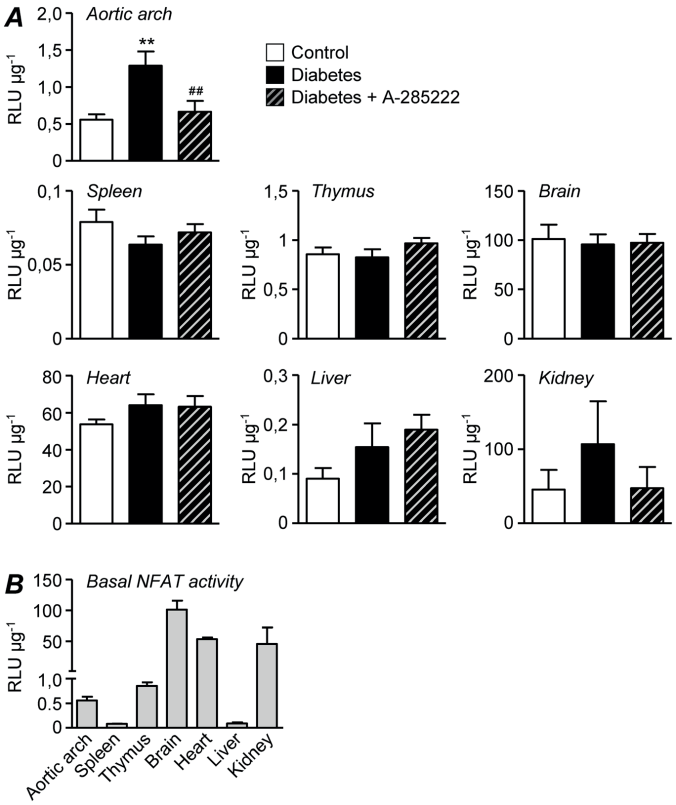

Figure 4. *In vivo* treatment with A-285222 effectively blocks diabetes-induced NFAT-dependent transcriptional activity. (**A**) NFAT-luciferase activity in the aortic arch, spleen, thymus, brain, heart, liver and kidney from control and diabetic female NFAT-luc mice treated with A-285222 or saline (Protocol II). Values are expressed as relative luciferase units (RLU) per µg protein (n = 8–11 mice/group for aortic arch, spleen and thymus; n = 4–8 mice/group for brain, heart, liver and kidney). $^{**}P<0.01$ vs. non-diabetic control mice and $^{\#\#}P<0.01$ vs. diabetic saline-treated group. (**B**) Basal (non-diabetic) NFAT-dependent transcriptional activity (RLU μg^{-1}) in the different tissues examined (n = 4–11 mice/group).
doi:10.1371/journal.pone.0065020.g004

a separate experiment to evaluate efficacy of i.p. administration, plasma levels of A-285222 after intracardiac (i.c.) injection of the drug were compared to levels after i.p. administration (n = 7 mice).

Statistics

Results are expressed as means ± SEM if not otherwise specified. Statistical analysis was performed using GraphPad software (Prism 5.0). For parametric data, significance was determined using Student's t-test, one- or two-way ANOVA as specified in the text, followed by Bonferroni post hoc tests. Non-parametric data was analyzed using Mann-Whitney or Kruskal-Wallis test followed by Dunn's post-test.

Results

In vivo Inhibition of NFAT Prevents the Diabetes-induced Aggravation of Atherosclerosis in the Aortic Arch

Atherosclerosis prone 22 week old ApoE$^{-/-}$ mice were treated as outlined in PROTOCOL I (Figure 1). A 2.2 fold increase in atherosclerotic plaque area (25.4% vs. 11.6%; $p<0.01$) was observed in the aortic arch of diabetic mice when compared to aged-matched non-diabetic controls, as assessed by *en face* measurements of ORO stained area eight weeks after the first STZ-injection (Figure 2A–B). *In vivo* treatment with the NFAT blocker A-285222 for the last 4 weeks of the experiment completely abrogated ($p<0.01$) the effect of diabetes on lesion area (Figure 2A–B). There was no effect of A-285222 on atherosclerosis in non-diabetic ApoE$^{-/-}$ mice. As expected, STZ-treated mice had higher blood glucose and lower weight gain than control mice, but A-285222 had no impact on these parameters (Figure 2C–D and Table 1). A similar effect of diabetes was observed in the descending aorta (2.1 fold increase in plaque area), but the overall plaque area was lower than in the arch and the effect of A-285222 less pronounced (Figure S1).

Lesion area was also evaluated in a separate group of control and diabetic mice 4 weeks after the first STZ or vehicle injection, when mice were 26 weeks of age. At this earlier time point diabetes had no evident effect on lesion size in the aortic arch (Figure 2E). Figure 2E also shows the accelerated development of plaque in the

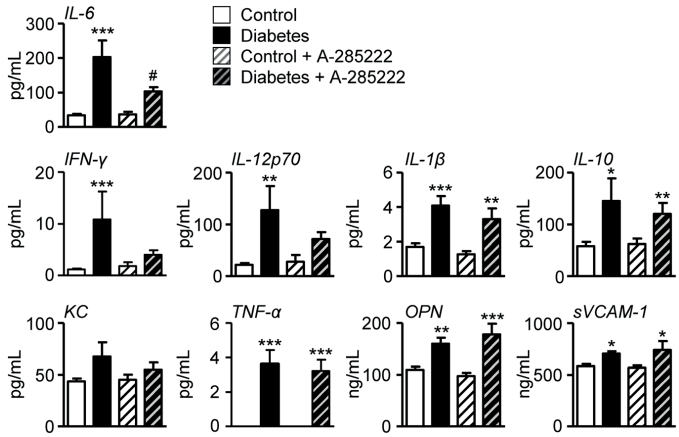

Figure 5. ***In vivo*** **NFAT inhibition reduces diabetes-induced elevation of plasma IL-6 levels.** The effect of diabetes and NFAT inhibition on plasma IL-6, IFN-γ, IL-12p70, IL-1β, IL-10, KC, TNF-α, OPN and sVCAM-1 was studied 8 weeks after the first STZ/vehicle injection in female ApoE$^{-/-}$ mice treated with A-285222 or saline for the last 4 weeks of the experiment (Protocol I, n = 9–12 mice/group). Only for IL-6, two-way ANOVA for the effect of diabetes and the drug revealed a significant interaction between factors (*$P<0.05$). Bonferroni post-test yielded ***$P<0.001$ vs. non-diabetic control and $^{\#}P<0.05$ vs. diabetic saline-treated group. All other cytokines except KC were increased by diabetes. For parametrically distributed data (IL-1β and OPN), two-way ANOVA followed by Bonferroni post-test yielded **$P<0.01$ and ***$P<0.01$ vs. corresponding non-diabetic groups. For the rest of the cytokines, which were non-parametrically distributed, Kruskal-Wallis followed by Dunn's post-test yielded *$P<0.05$, **$P<0.01$ and ***$P<0.01$ vs. corresponding non-diabetic groups.
doi:10.1371/journal.pone.0065020.g005

diabetic mice, which is completely prevented by NFAT inhibition, and the well-recognized effect of age on atherosclerosis [26] in the non-diabetic groups.

Atherosclerosis was also examined in cross-sections of the aortic root from the same animals used for the *en face* measurements shown in Figure 2A–B. Total cross sectional area calculated from the hematoxylin staining was larger in diabetic than non-diabetic mice (1.68×10^6 um^2 vs. 1.23×10^6 um^2; $P<0.001$). This increased area in the diabetic mice is the combined result of increased plaque (6.59×10^5 um^2 vs. 4.03×10^5 um^2; $P<0.001$) and lumen (9.04×10^5 um^2 vs. 6.65×10^5 um^2; $P<0.001$) area, while a concomitant thinning of the media was observed (1.15×10^5 um^2 vs. 1.83×10^5 um^2; $P<0.001$), especially in regions beneath the atherosclerotic plaques. Erosion and focal dilatation of the medial layer have been described in the aortic root of ApoE$^{-/-}$ mice when fed an atherogenic diet with cholate or when bred on specific backgrounds (C3H or 128SvJ) [27,28]. Our results show that diabetes (without the atherogenic diet or specific background) is a sufficient drive for medial wall erosion; in line with work showing structural modifications and disruption of the arterial media as a result of diabetes in STZ-treated C56B/J6 mice [19]. When the subvalvular plaque area was expressed as percentage of total cross sectional area, it was 16.5% larger in diabetic than in control untreated mice ($p<0.05$); whereas the effect of diabetes was attenuated in A-285222-treated mice (9.6% increase, n.s.). Interestingly, inhibition of NFAT resulted in reduced lipid contents in the plaque of diabetic mice (Figure 3A–B). Even though plaque macrophage, collagen and α-SMA contents were increased in the aortic root of diabetic mice when compared to non-diabetic controls, values were not affected by A-285222 treatment (Figure 3C–E and Figure S2A). Higher expression of OPN, but not of TF was observed in aortic root sections from diabetic mice when compared to non-diabetic controls; but values were not affected by A-285222 treatment either (Figure S2A–B).

In agreement with previous studies [20], total plasma cholesterol was significantly elevated in diabetic ApoE$^{-/-}$ mice when compared to non-diabetic controls at 4, 5 and 8 weeks (Table 1). Plasma triglycerides were also elevated after 8 weeks. However, the reduced atherosclerosis is less likely due to a lipid lowering effect, since A-285222 had no effect on plasma lipids, regardless if the mice were diabetic or not (Table 1). In agreement to what others have reported [29], ApoE$^{-/-}$ mice on chow diet had very little fat accumulation in the liver (<2%). No signs of liver steatosis were observed after treatment of ApoE$^{-/-}$ mice with A-285222 (Figure S3).

In vivo Treatment with A-285222 Effectively Blocks Diabetes-induced NFAT-dependent Transcriptional Activity

Previous studies from our group have shown that A-285222 is a potent blocker of glucose-induced NFAT-dependent transcriptional activity and NFAT-target genes [6,7] in VSMCs and intact vessels *in vitro* [5,6]. Here we demonstrate that *in vivo* treatment with A-285222 completely blocks the diabetes-induced NFAT-dependent transcriptional activity in the aortic arch of NFAT-luc mice (Figure 4A, PROTOCOL II). Of all organs examined, NFAT was selectively activated in the aorta of diabetic mice, with a tendency to increased activation in kidneys, but no effect in spleen, thymus, brain, heart or liver. A-285222 treatment was effective only if NFAT had been previously activated as in the aortic arch, and possibly in the kidneys. Diabetic mice had significant hyperglycemia at this time-point, but unchanged body weight and plasma lipids (Table 1). A-285222 had no effect on any of these parameters (Table 1). As shown in Figure 4B, basal levels of NFAT activity varied depending on the organ. Consistent with what others have reported, the highest levels were observed in brain, kidney and heart; and the lowest in spleen and liver [17].

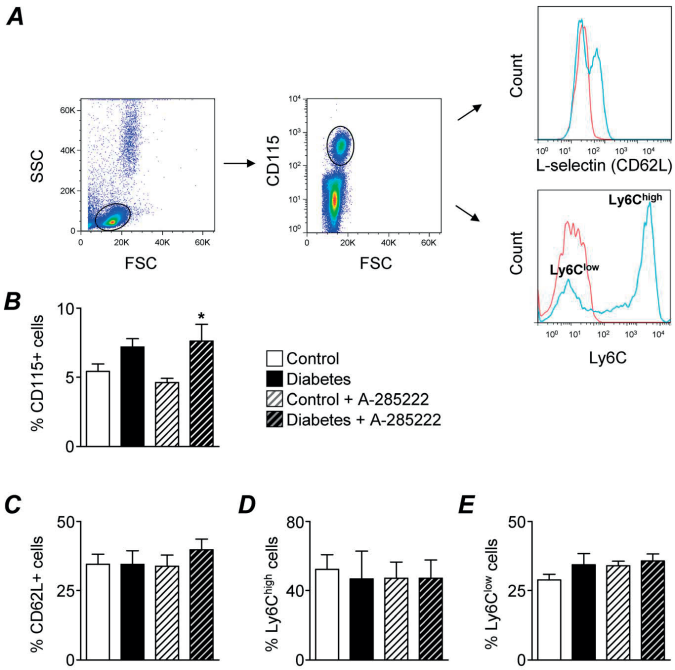

Figure 6. Circulating monocyte levels are increased in diabetic ApoE$^{-/-}$ mice but not affected by NFAT inhibition. (**A**) Left and middle panels: Dot plots showing the gating strategy for monocyte identification from blood mononuclear cells based on the expression of CD115 (M-CSF receptor). Right panels: Identification of monocytes expressing CD62L (L-selectin) and of Ly6C^{high} and Ly6C^{low} subsets (blue lines); fluorescence-minus-one controls (red lines). (**B**) Summarized data from flow cytometry experiments showing percentages of CD115+ monocytes in total blood mononuclear cells from control and diabetic ApoE$^{-/-}$ mice treated with the NFAT blocker A-285222 or saline for one week (Protocol I, n = 9–11 mice/group). Two-way ANOVA revealed a significant effect of diabetes ($P<0.01$). Bonferroni post-test yielded $^{*}P<0.05$ vs. non-diabetic control mice. (**C–E**) No differences in the percentages of CD115+ mononuclear cells expressing CD62L+ (C) Ly6C^{high} (D) or Ly6C^{low} (E) were found between treatment groups.

doi:10.1371/journal.pone.0065020.g006

A separate set of NFAT-luc mice were fed HFD or chow diet for 4 or 8 weeks and NFAT-luciferase activity measured in the aorta (PROTOCOL III). Even though plasma cholesterol levels were significantly higher in mice fed HFD when compared to controls (Table 1), no differences in NFAT-luciferase activity were observed (Figure S4). Body weight increased with HFD, and a small (3 mmol/L) but significant increase in blood glucose was observed after 8 weeks of HFD, while triglycerides were not significantly affected (Table 1).

Effect of Diabetes and NFAT-signaling Inhibition on Systemic and Plaque Inflammation

Plasma cytokines, levels and phenotype of circulating monocytes and expression of inflammatory genes in the aortic arch were examined in ApoE$^{-/-}$ mice undergoing PROTOCOL I. Plasma IL-6, IFN-γ, IL-12p70, IL-1β, IL-10, tumor necrosis factor (TNF)α, OPN and sVCAM-1 were significantly increased in diabetic mice 8 weeks after the first STZ injection, whereas keratinocyte-derived chemokine (KC) was not affected (Figure 5). Treatment with A-285222 for 4 weeks blunted the effect of diabetes on IL-6 levels, but had no significant effects on the other plasma cytokines (Figure 5). Already early after the onset of diabetes, circulating monocytes were elevated in diabetic ApoE$^{-/-}$ mice when compared to non-diabetic controls, as evidenced by higher percentages of CD115 (M-CSF receptor) expressing blood mononuclear cells (Figure 6B). Treatment with A-285222 had no effect on blood monocyte levels. Neither diabetes nor NFAT inhibition had any impact on the fraction of CD115 positive cells expressing the adhesion molecule CD62L (L-selectin) or on the fractions of inflammatory (CD115+ Ly6C^{high}) or patrolling (CD115+ Ly6C^{low}) blood monocytes (Figure 6C–E).

Also early after the onset of diabetes, several markers of inflammation and endothelial activation including MCP-1, VCAM-1, IL-1β, Cox2 and TF were significantly increased at the mRNA level in the aortic wall of diabetic mice when compared to controls; and trends towards increased IL-6 and ICAM-1 were observed (Figure S5). Treatment with A-285222 for 4 weeks significantly reduced IL-6, OPN, MCP-1 and ICAM-1 mRNA in the aortic arch of diabetic mice, while levels of VCAM-1, IL-1β, Cox2 and IL-10 were not affected (Figure 7A). Expression of the macrophage marker CD68 and cellular TF were significantly lowered after A-285222 treatment in diabetic mice, both at the mRNA and protein level (Figure 7B–C).

To determine whether NFAT signaling inhibition affected the capacity of immune cells to proliferate, splenocytes were isolated from ApoE$^{-/-}$ mice 5 weeks after the first STZ injection, after

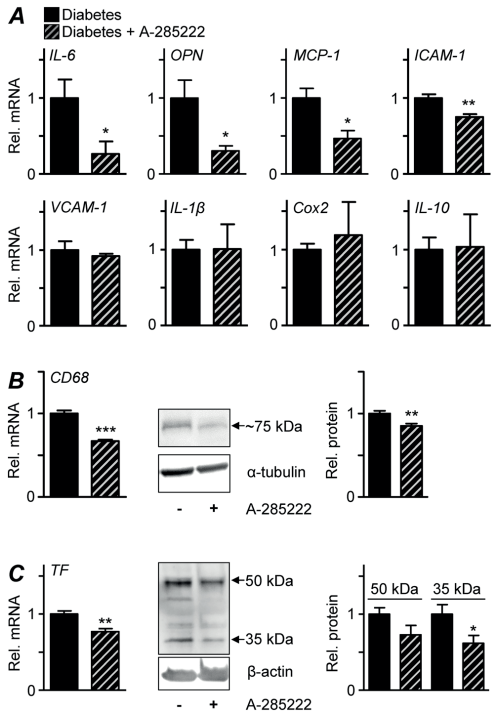

Figure 7. *In vivo* inhibition of NFAT reduces the expression of markers of inflammation and endothelial activation and macrophage infiltration in the aortic arch of diabetic mice. (**A**) Gene expression analyses by qRT-PCR in the aortic arch of diabetic ApoE$^{-/-}$ mice treated with A-285222 or saline for 4 weeks (Protocol I, hatched and black bars, respectively). HPRT and β-actin were used as endogenous controls and data (Rel. mRNA) is expressed in relation to the diabetic saline-treated group. (**B**) CD68 and (**C**) TF mRNA and protein levels were decreased after treatment with A-285222. Left graphs show relative CD68 and TF mRNA from the same animals as in A. Middle panels show representative immunoblots for CD68 and TF (50 and 35 kDa) and loading controls. Right graphs show summarized results from western blot experiments, with CD68 expression normalized to α-tubulin and TF expression normalized to β-actin. Data (Rel. protein) is expressed in relation to the diabetic saline treated group. $^{*}P<0.05$, $^{**}P<0.01$ and $^{***}P<0.001$; n = 5–13 mice/group.
doi:10.1371/journal.pone.0065020.g007

receiving daily i.p. injections of A-285222 or vehicle for one week (PROTOCOL I, 5 weeks group). No differences in their proliferative capacity were found between groups, as assessed by measurements of thymidine incorporation under non-stimulated conditions or after stimulation with either anti-CD3/CD28 beads or Con A (Figure S6A–B). Similar observations were made using splenocytes isolated from control C57BL/6 mice treated with A-285222 for 4 weeks (Figure S6C). Blood glucose, body weight and plasma lipids were not affected in these animals (Table 1). We also examined the effects of diabetes and A-285222 treatment on cytokine secretion capacity of splenocytes under control non-stimulated conditions and after stimulation with anti-CD3/CD28 beads (Table S1). Diabetes had no impact on the levels of cytokines produced by non-stimulated splenocytes, but resulted in significantly increased levels of TNF-α in cells stimulated with anti-CD3/CD28 beads. A-285222 treatment on the other hand resulted in decreased secretion of IL-2 in non-stimulated splenocytes from non-diabetic mice and no effects in stimulated splenocytes (Table S1). Percentages of CD3+CD4+CD8- splenocytes expressing IFN-γ after stimulation with PMA and ionomycin were not affected by diabetes or NFAT inhibition (Figure S6E). Moreover, no differences in spleen histology or size were detected between treatment groups (Figure S6F–G).

Pharmacokinetics of A-285222

Previous studies in cynomolgus monkeys have demonstrated that A-285222 is well tolerated when the plasma concentration is maintained below 4 μg/mL (9.6 μmol/L), a level achieved by oral administration of the drug twice daily at 5–7.5 mg/kg body weight [30]. In our hands, a lower dose was sufficient for changes in vascular OPN expression in normolipidemic BalB/c mice [6] and for the effects on NFAT-transcriptional activity and on diabetes-induced atherosclerosis described here (0.15–0.29 mg/kg body weight). In previous *ex vivo* experiments using mouse arteries, A-285222 blocked NFAT-transcriptional activity at 1 μmol/L [5]. To assess the actual plasma concentration of A-285222 after *in vivo* treatment of ApoE$^{-/-}$ mice, we collected blood by cardiac puncture at different time points (30 min, 1, 2, 4, 6, 12 and 24 hours) after i.p. injection of the drug (0.29 mg/kg body weight). A-285222 was identified and quantified with GC/MS, based on its mass spectra and retention indexes (Figure S5). Plasma A-285222 levels peaked at 2 hours, were between 100–200 nmol/L for the first six hours and no longer detected at 12 or 24 hours. We failed to detect any A-285222 in mice from protocols I (5 and 8 weeks), II and IV, from blood collected at the time of euthanasia (i.e.~24 h after the last i.p. injection of A-285222), ruling out an accumulation of the drug in the circulation. A comparison between plasma levels of A-285222 measured 5 min after i.p. injection of the drug (0.15 and 1.5 mg/kg) and after direct injection into the circulation (i.c.), showed that levels were within the same range regardless administration route (430 nmol/L vs. 480 nmol/L for the low dose; 770 nmol/L vs. 675 nmol/L for the high dose), indicating high bioavailability.

Discussion

The present study demonstrates that inhibition of NFAT-signaling completely suppresses accelerated atherosclerosis in the aortic arch of diabetic ApoE$^{-/-}$ mice and that this effect is independent of changes in plasma glucose or lipid levels. This finding suggests that NFAT may play a role in the development of atherosclerosis in diabetes and identifies this signaling pathway as a novel therapeutic target for the treatment of diabetic macrovascular complications.

The ApoE-deficient mouse is a well-established model for the study of atherosclerosis. Mice develop spontaneous hypercholesterolemia and mimic the initial phases of human atherosclerosis, even when fed a regular chow diet as in this study. The extent and severity of the lesions increase with age, displaying all known phases of atherogenesis. Monocyte adhesion takes place between 8–10 weeks of age, lipid deposition and development of fatty-streaks starts at approximately 9 weeks of age, and progression to intermediate and more mature fibrous plaques at ~15–20 weeks of age [31]. As shown in Figure 2E, at the age when mice were treated with the NFAT blocker A-285222 (26–30 weeks of age), plaque size in the aortic arch was still increasing, and this was clearly accelerated by diabetes. Interestingly, NFAT inhibition did only affect the diabetes-driven aggravation of atherosclerosis, but

had no impact on atherosclerosis in non-diabetic mice, suggesting potentially different mechanisms underlying plaque formation under diabetic and non-diabetic conditions. The increased lesion size observed in the aortic arch is in line with what others have described in STZ-treated ApoE$^{-/-}$ mice [32]. However, the effect of diabetes on plaque area at the level of the aortic root was modest when compared to those observed when mice are treated with STZ at younger age (6 weeks [32] vs. 22 weeks in this study). Along these lines, A-285222 treatment had a more distinct impact on the aortic arch than in the aortic root, as exemplified by decreased macrophage infiltration, TF and OPN expression in the arch (Figure 7) but not in the root of the aorta (Figure S2). These results highlight differential susceptibility to diabetes-induced atherosclerosis in these two segments of the aorta and the need for a diabetes-driven process for NFAT-inhibition to play a role.

Previous work from our group established that high extracellular glucose (>15 mmol/L) activates NFATc3 in intact arteries *ex vivo* by a mechanism involving the release of extracellular nucleotides (i.e. UTP, UDP) acting on P2Y receptors, leading to increased intracellular Ca^{2+} and subsequent activation of the calcineurin/NFATc3 signaling pathway [5]. High glucose also decreases the export of NFATc3 from the nucleus by inhibiting the otherwise constitutively elevated kinase activity of glycogen synthase kinase (GSK)-3β and c-Jun N-terminal kinase in the arterial wall [5]. In a follow-up study, we demonstrated that hyperglycemia readily activated NFATc3 in the arterial wall *in vivo*, as evidenced by increased NFATc3 nuclear accumulation in cerebral arteries after an i.p. glucose-tolerance test and by increased NFATc3-dependent transcriptional activity in aorta 2 weeks after the induction of diabetes with STZ [6]. Here we show that this diabetes-induced activation of NFAT in the aorta is completely inhibited by *in vivo* treatment with A-285222 (Figure 4A), demonstrating that A-285222 is an effective blocker of NFAT-transcriptional activity in this tissue. Even though NFAT is expressed in many tissues and basal (non-diabetic) NFAT-luciferase activity was detected in all tissues examined, the diabetes-induced NFAT activation is not a generalized phenomenon. At least at this time point after the onset of diabetes (2 weeks), NFAT-luciferase activity seemed only elevated in the aorta, whereas no changes were observed in the other organs examined (Figure 4), an advantageous difference from the therapeutic point of view.

Not only hyperglycemia, but hyperlipidemia, or the combination of both could be driving the accelerated atherosclerosis in diabetes. To our knowledge, the effect of hyperlipidemia on NFAT-transcriptional activity in the vasculature has never been studied *in vivo*. A number of *in vitro* studies though, demonstrated that NFAT activation can be triggered by lipids. Exposure to triglyceride-rich very low-density lipoproteins increases NFATc3 nuclear accumulation in cultured rat aortic VSMCs [33], and postprandial triglyceride-rich lipoproteins collected after an oral fat load activate several transcription factors including NFAT in cultured endothelial cells [34]. Also, incubation of T-lymphocytes, macrophages, fibroblasts and endothelial cells with copper-oxidized or monocyte-oxidized low-density lipoproteins increases NFAT binding to DNA [35,36]. Here we show that a ~2-fold increase in total cholesterol induced by HFD, had no effect on NFAT-transcriptional activity in the aortas of NFAT-luc mice (Figure S4). Interestingly, after 8 weeks of HFD mice had a mild but still significant increase in blood glucose (from 9.7 to 12.7 mmol/L; Table 1), which did not translate in enhanced luciferase activity. This is in line with previous data showing that glucose levels >15 mmol/L are required for NFAT activation in the vasculature [5,6]. Even though high cholesterol *per se* had no effect on NFAT-transcriptional activity *in vivo*, it is still possible that high triglycerides instead, or even higher absolute levels of cholesterol (such as those observed in ApoE-deficient mice), or higher degree of lipid oxidation as it may occur in the context of diabetes, could trigger NFAT activation.

Inflammation is recognized as a critical regulator of atherosclerotic plaque formation and progression. Along these lines, the accelerated atherosclerosis in diabetic ApoE$^{-/-}$ mice was preceded by elevated blood monocytes and higher expression of endothelial activation- and inflammatory markers in the aorta. Already after 4 weeks of diabetes, a time-point when no changes in aortic plaque size had yet occurred, expression of VCAM-1, MCP-1, IL-1β, Cox2, TF and maybe also IL-6 and ICAM-1 (borderline significance) were higher than in control non-diabetic mice. The enhanced pro-inflammatory burden in diabetic mice is also reflected by the overall increased levels of circulating plasma cytokines (IL-6, IFN-γ, IL-12p70, IL-1β, IL-10, TNFα, OPN and sVCAM-1; Figure 5) after 8 weeks of diabetes. One important observation in this study was that A-285222 treatment for 4 weeks significantly reduced the diabetes-driven IL-6 levels in plasma as well as mRNA expression in the aortic arch. IL-6 is one of the most prominent pro-inflammatory cytokines, extensively studied in the context of atherogenesis [37]. It can be generated locally by cells within the lesions or released by adipose tissue into the circulation, promoting endothelial dysfunction, VSMC proliferation and migration as well as recruitment and activation of inflammatory cells, hence amplifying the inflammatory response. Moreover, IL-6 stimulates the expression of scavenger receptors SR-A and CD36, involved in the uptake of modified LDL and formation of foam cells [38]. Lack of this positive stimulation due to reduced IL-6 levels could explain the reduced plaque lipids observed in diabetic mice after A-285222 treatment (Figures 2 and 3A). The reduced IL-6 expression after treatment with A-285222 is in line with previous studies by us and other investigators, showing NFAT-dependent regulation of IL-6 gene expression in VSMCs [10,39] and in human resistance arteries [7].

The NFAT blocker A-285222 belongs to a series of 3,5-bis (trifluoromethyl)pyrazole (BTP) derivatives originally developed in a search for safer immunosuppressive drugs. These drugs maintain NFAT in a phosphorylated state, blocking its nuclear import and subsequent transcription, without affecting NF-κB or AP-1 activation, or calcineurin phosphatase activity [40]. *In vivo* administration of A-285222 completely blocked diabetes-induced NFAT-transcriptional activity in the aorta, leading to reduced expression of IL-6, OPN, MCP-1, ICAM-1, CD68 and TF, all established players in atherogenesis, as well as to reduced diabetes-induced atherosclerosis. This was achieved without any effect on body weight, blood glucose or lipid levels and at concentrations that had no impact on NFAT activity in spleen or thymus, on T-cell proliferation rates or cytokine secretion capacity, ruling out systemic immunosuppression as the mechanism behind reduced atherosclerosis. A-285222 did not affect the number or phenotype of circulating blood monocytes, nor did it alter the numbers of T-regulatory cells in the spleen. The reduction of TF was particularly interesting, given the lack of available systemic strategies that target TF expression [41]. The dose of A-285222 used here and plasma levels achieved upon treatment were far below those required in cynomolgus monkeys for inhibition of T-cell cytokine production, which is consistent with the negative T-cell cytokine data presented here. Furthermore, non-diabetic ApoE$^{-/-}$ mice exhibited measurable levels of plasma cytokines, reflecting a low-grade inflammation typical of this hyperlipidemic model, however, A-285222 had no effect on these levels (Figure 5), speaking against a general immunosuppressant effect of A-285222. Together,

results suggest that NFAT inhibition affects the plaque phenotype at the level of the plaque itself and not via systemic immunosuppression.

Calcineurin inhibitors (i.e. CsA and FK506) are commonly used to prevent host-versus graft disease, a therapy often associated with side effects, including increased risk of atherosclerosis. While the immunosuppressive effects of these drugs are directly related to the inhibition of NFAT in immune cells, the adverse cardiovascular effects seem to be NFAT-independent and mediated via intracellular cyclophilin and chaperone activities, extracellular cyclophilin A and NFAT-independent transcriptional effects [42]. The degrees to which these NFAT-independent pathways are engaged seem to be dose-dependent [43]. Low-dose FK506 (~0.2 ng/mL) inhibited collar-induced atherosclerosis progression and promoted plaque stability in ApoE$^{-/-}$ mice, whereas higher doses similar to those given to transplant patients engaged instead NF-κB in macrophages and consequently increased production of cytokines. Other serious side effects associated with CsA treatment are hyperlipidemia and diabetes [42]; but these were not observed after treatment with A-285222.

Despite major advances in the treatment of cardiovascular disease during the past decades, with the introduction of lipid lowering, anti-thrombotic and anti-hypertensive drugs, there is still no available therapy that specifically targets macrovascular diabetic complications. Our data reveals the NFAT-signaling pathway as a promising target for the treatment of accelerated atherosclerosis in diabetes.

Supporting Information

Figure S1 Diabetes increases atherosclerosis in the descending aorta, but the overall plaque area is lower than in the aortic arch. Summarized data from measurements of en face lesion area in the descending aorta for comparison with the aortic arch data from the same animals included in Figure 2. Results are from control and diabetic female ApoE−/− mice that had been treated for 4 weeks with the NFAT blocker A-285222 or saline. Mice were 30 weeks old at the time of analysis, performed 8 weeks after the first STZ or vehicle injection. Data is expressed as percentage of total aortic area (n = 9–12 mice/group). Two-way analysis of variance for the effect of diabetes and the drug revealed significant effect of diabetes ($P<0.001$). Bonferroni post-test yielded $^{**}P<0.01$ vs non-diabetic saline-treated group. The inset shows corresponding data for the total aorta (i.e. arch and descending).
(PDF)

Figure S2 Histological examination of subvalvular plaques. (**A**) Representative cross-sections of the aortic root from control and diabetic female ApoE−/− mice treated with or without A-285222 for 4 weeks (Protocol I) stained for monocytes/macrophages (Moma-2), collagen, α-smooth muscle actin (α-SMA), tissue factor (TF, red) and osteopontin (OPN, red). Moma-2 and α-SMA stained sections were counter-stained with Harris hematoxylin; TF and OPN stained sections were counter-stained with SYTOX Green. Scale = 500 μm (Moma-2); = 100 μm (collagen, TF, OPN); = 50 μm (α-SMA). (**B, C**) Summarized data from confocal immunofluorescence experiments showing mean fluorescence intensity for plaque TF and OPN. Three to six sections for each animal were analyzed (n = 9–12 mice/group). Two-way ANOVA revealed significant effect of diabetes on OPN expression ($P<0.0001$). Bonferroni post-test yielded $^{*}P<0.05$ and $^{**}P<0.01$ vs corresponding non-diabetic groups.
(PDF)

Figure S3 Lipid deposition in the liver is not affected by NFAT inhibition. (**A**) Representative liver sections from diabetic female ApoE−/− mice treated with or without A-285222 for 4 weeks (Protocol I) were stained with hematoxylin-eosin (H&E) and oil red O (ORO). Scale = 100 μm. (**B**) Lipid deposition in the liver was evaluated from three ORO-stained sections per mouse using computer-assisted image analysis (n = 6–7 mice/group).
(PDF)

Figure S4 High fat diet does not affect NFAT-dependent transcriptional activity in the aorta. NFAT-luciferase activity in the thoracic aorta from mice fed normal chow diet (white bars) or a high fat diet (grey bars) during 4 or 8 weeks (Protocol III). Values are expressed as RLU per μg protein (n = 7–12 mice/group).
(PDF)

Figure S5 Diabetes leads to increased expression of inflammatory and endothelial activation markers in the aortic arch. Gene expression analyses by qRT-PCR in the aortic arch of control and diabetic ApoE−/− mice analyzed after 4 weeks of diabetes (Protocol I, n = 7–10 mice/group). HPRT and β-actin were used as endogenous controls. Data (Rel. mRNA) is expressed in relation to diabetic mice. $^{*}P<0.05$ and $^{**}P<0.01$.
(PDF)

Figure S6 In vivo A-285222 treatment does not affect splenocyte proliferative capacity. (**A–B**) [Methyl-3H]thymidine incorporation (counts per minute, cpm) after stimulation with or without anti-CD3/CD28 beads (**A**) or 2.5 μg/mL ConA (**B**) in splenocytes isolated from control and diabetic ApoE−/− mice treated for 1 week with the NFAT blocker A-285222 or saline (Protocol I; n = 9–11 mice/group) (**C**). Proliferation after stimulation with or without 2.5 μg/mL ConA in splenocytes from control mice treated for 4 weeks with the NFAT blocker A-285222 or saline (Protocol IV; n = 12–13 mice/group). (**D**) Flow cytometry data showing percentages of CD4+CD25+Foxp3+ regulatory T-cells (of total CD3+ splenocytes) in the same mice as in A. Two-way ANOVA revealed significant effect of diabetes ($P<0.001$). Bonferroni post-test yielded $^{*}P<0.05$ vs. corresponding non-diabetic groups. (**E**) Percentages of CD3+CD4+D8- splenocytes expressing IFN-γ after stimulation with phorbol myristate acetate (PMA) and ionomycin in the same mice as in A. (**F**) Representative spleen sections stained for hematoxylin-eosin and (**G**) spleen weight in relation to tibia length from the same mice as in A. Scale = 500 μm.
(PDF)

Figure S7 Identification and quantification of A-285222 with GC/MS. A-285222 and the inactive analog A-216491 were identified from their mass spectra and retention indexes. (**A**) Total ion chromatogram showing substances present in a plasma sample from a mouse injected i.c. with 1.5 mg A-285222 per kg body weight. (**B**) Reconstructed ion chromatogram from the same sample as in A, showing retention indexes (s) of A-216491 (left peak, m/z = 295) and A-285222 (right peak, m/z = 416). (**C**) Mass spectra for A-285222 including the molecular ion (m/z = 416). Only the molecular ion was selective and used for quantification. (**D**) Quantification of A-285222 in plasma samples collected at different time points after i.p. injection of 0.29 mg A-285222 per kg body weight (n = 2–4 mice/time point).
(PDF)

Table S1 Effects of diabetes and A-285222 on splenocyte cytokine production. Splenocytes were isolated from control and diabetic mice that had been treated for 1 week with the

NFAT blocker A-285222 or saline (Protocol I; n = 8–11 mice/group) after which they were cultured either under control non-stimulated conditions or with anti-CD3/CD28 beads for 48 hours. Levels of interferon (IFN)-γ, interleukin (IL)-1β, IL-2, IL-4, IL-5, KC/GRO (keratinocyte chemoattractant; keratinocyte-derived chemokine/growth related oncogene), IL-10, IL-12total and tumor necrosis factor (TNF)-α. were measured in the culture media collected at the end of the experiments. Data was analyzed by two-way ANOVA (for the effects of diabetes and A-285222). Values represent mean ± SD; significant differences after Bonferroni post-tests are indicated in the table. Diabetes had no impact on the levels of cytokines produced by non-stimulated splenocytes, while A-285222 treatment resulted in decreased IFN-γ and IL-2 (both $P<0.05$). Bonferroni post-test yielded *$P<0.05$ only for IL-2. CD3/CD28 stimulated cells from diabetic mice produced lower levels of IFN-γ ($P<0.05$) and IL-5 ($P<0.01$) but higher TNF-α. ($P<0.05$). Bonferroni post-test yielded #$P<0.05$ for TNF-α. A-285222 treatment had no impact on the ability of splenocytes to respond to CD3/CD28 stimulation. (PDF)

Acknowledgments

We thank Irena Ljungkrantz and Ingrid Söderberg for skillful technical assistance.

Author Contributions

Conceived and designed the experiments: AVZ MFG. Performed the experiments: AVZ LMB FB EGV MW PD AMDA FT PS MFG. Analyzed the data: AVZ LMB FB EGV MW AMDA FT PS JN EB MFG. Contributed reagents/materials/analysis tools: PS EB JN MFG. Wrote the paper: AVZ LMB MFG. Critical revision and final approval of submitted version: AVZ LMB FB EGV MW PD AMDA FT PS JN EB MFG.

References

1. Rahman S, Rahman T, Ismail AA, Rashid AR (2007) Diabetes-associated macrovasculopathy: pathophysiology and pathogenesis. Diabetes Obes Metab 9: 767–780.
2. Coutinho M, Gerstein HC, Wang Y, Yusuf S (1999) The relationship between glucose and incident cardiovascular events. A metaregression analysis of published data from 20 studies of 95,783 individuals followed for 12.4 years. Diabetes Care 22: 233–240.
3. Rasmussen-Torvik LJ, Li M, Kao WH, Couper D, Boerwinkle E, et al. (2011) Association of a Fasting Glucose Genetic Risk Score With Subclinical Atherosclerosis. Diabetes 60: 331–335.
4. Brown A, Reynolds LR, Bruemmer D (2010) Intensive glycemic control and cardiovascular disease: an update. Nat Rev Cardiol 7: 369–375.
5. Nilsson J, Nilsson LM, Chen Y-W, Molkentin JD, Erlinge D, et al. (2006) High Glucose Activates Nuclear Factor of Activated T Cells in Native Vascular Smooth Muscle. Arterioscler Thromb Vasc Biol 26: 794–800.
6. Nilsson-Berglund LM, Zetterqvist AV, Nilsson-Ohman J, Sigvardsson M, Gonzalez Bosc LV, et al. (2009) Nuclear factor of activated T cells regulates osteopontin expression in arterial smooth muscle in response to diabetes-induced hyperglycemia. Arterioscler Thromb Vasc Biol 30: 218–224.
7. Nilsson LM, Sun ZW, Nilsson J, Nordstrom I, Chen YW, et al. (2007) Novel blocker of NFAT activation inhibits IL-6 production in human myometrial arteries and reduces vascular smooth muscle cell proliferation. Am J Physiol Cell Physiol 292: C1167–1178.
8. Orr AW, Lee MY, Lemmon JA, Yurdagul A, Gomez MF, et al. (2008) Molecular Mechanisms of Collagen Isotype-Specific Modulation of Smooth Muscle Cell Phenotype. Arterioscler Thromb Vasc Biol 29: 225–231.
9. Nilsson LM, Nilsson-Ohman J, Zetterqvist AV, Gomez MF (2008) Nuclear factor of activated T-cells transcription factors in the vasculature: the good guys or the bad guys? Curr Opin Lipidol 19: 483–490.
10. Liu Z, Dronadula N, Rao GN (2004) A Novel Role for Nuclear Factor of Activated T Cells in Receptor Tyrosine Kinase and G Protein-coupled Receptor Agonist-induced Vascular Smooth Muscle Cell Motility. J Biol Chem 279: 41218–41226.
11. Karpurapu M, Wang D, Van Quyen D, Kim T-K, Kundumani-Sridharan V, et al. (2010) Cyclin D1 Is a Bona Fide Target Gene of NFATc1 and Is Sufficient in the Mediation of Injury-induced Vascular Wall Remodeling. Journal of Biological Chemistry 285: 3510–3523.
12. Lipskaia L, del Monte F, Capiod T, Yacoubi S, Hadri L, et al. (2005) Sarco/endoplasmic reticulum Ca2+-ATPase gene transfer reduces vascular smooth muscle cell proliferation and neointima formation in the rat. Circ Res 97: 488–495.
13. Lee MY, Garvey SM, Baras AS, Lemmon JA, Gomez MF, et al. (2009) Integrative genomics identifies DSCR1 (RCAN1) as a novel NFAT-dependent mediator of phenotypic modulation in vascular smooth muscle cells. Hum Mol Genet 19: 468–479.
14. Amberg GC, Rossow CF, Navedo MF, Santana LF (2004) NFATc3 regulates Kv2.1 expression in arterial smooth muscle. J Biol Chem 279: 47326–47334.
15. Nieves-Cintron M, Amberg GC, Nichols CB, Molkentin JD, Santana LF (2007) Activation of NFATc3 down-regulates the beta1 subunit of large conductance, calcium-activated K+ channels in arterial smooth muscle and contributes to hypertension. J Biol Chem 282: 3231–3240.
16. Berglund LM, Kotova O, Osmark P, Grufman H, Xing C, et al. (2011) NFAT regulates the expression of AIF-1 and IRT-1: yin and yang splice variants of neointima formation and atherosclerosis. Cardiovasc Res 93: 414–423.
17. Wilkins BJ, Dai YS, Bueno OF, Parsons SA, Xu J, et al. (2004) Calcineurin/NFAT coupling participates in pathological, but not physiological, cardiac hypertrophy. Circ Res 94: 110–118.
18. Fredrikson GN, Soderberg I, Lindholm M, Dimayuga P, Chyu KY, et al. (2003) Inhibition of atherosclerosis in apoE-null mice by immunization with apoB-100 peptide sequences. Arterioscler Thromb Vasc Biol 23: 879–884.
19. Prévost G, Bulckaen H, Gaxatte C, Boulanger E, Béraud G, et al. (2011) Structural modifications in the arterial wall during physiological aging and as a result of diabetes mellitus in a mouse model: Are the changes comparable? Diabetes & Metabolism 37: 106–111.
20. Gustavsson C, Agardh CD, Zetterqvist AV, Nilsson J, Agardh E, et al. (2010) Vascular cellular adhesion molecule-1 (VCAM-1) expression in mice retinal vessels is affected by both hyperglycemia and hyperlipidemia. PLoS One 5: e12699.
21. Awla D, Zetterqvist AV, Abdulla A, Camello C, Berglund LM, et al. (2012) NFATc3 Regulates Trypsinogen Activation, Neutrophil Recruitment, and Tissue Damage in Acute Pancreatitis in Mice. Gastroenterology: Jul 27. [Epub ahead of print].
22. Wigren M, Bengtsson D, Duner P, Olofsson K, Bjorkbacka H, et al. (2009) Atheroprotective effects of Alum are associated with capture of oxidized LDL antigens and activation of regulatory T cells. Circ Res 104: e62–70.
23. Wigren M, BjÄrkbacka H, Andersson L, Ljungcrantz I, Fredrikson GN, et al. (2012) Low Levels of Circulating CD4+FoxP3+ T Cells Are Associated With an Increased Risk for Development of Myocardial Infarction But Not for Stroke. Arteriosclerosis, Thrombosis, and Vascular Biology 32: 2000–2004.
24. Engelbertsen D, Andersson L, Ljungcrantz I, Wigren M, Hedblad B, et al. (2013) T-Helper 2 Immunity Is Associated With Reduced Risk of Myocardial Infarction and Stroke. Arteriosclerosis, Thrombosis, and Vascular Biology 33: 637–644.
25. Kolbus D, Ramos OH, Berg KE, Persson J, Wigren M, et al. (2010) CD8+ T cell activation predominate early immune responses to hypercholesterolemia in Apoe(-)(/)(-) mice. BMC Immunol 11: 58.
26. Reddick RL, Zhang SH, Maeda N (1994) Atherosclerosis in mice lacking apo E. Evaluation of lesional development and progression. Arterioscler Thromb 14: 141–147.
27. Carmeliet P, Moons L, Lijnen R, Baes M, Lemaitre V, et al. (1997) Urokinase-generated plasmin activates matrix metalloproteinases during aneurysm formation. Nat Genet 17: 439–444.
28. Shi W, Brown MD, Wang X, Wong J, Kallmes DF, et al. (2003) Genetic Backgrounds but Not Sizes of Atherosclerotic Lesions Determine Medial Destruction in the Aortic Root of Apolipoprotein Eâ€"Deficient Mice. Arteriosclerosis, Thrombosis, and Vascular Biology 23: 1901–1906.
29. Lohmann C, Schafer N, von Lukowicz T, Sokrates Stein MA, Boren J, et al. (2009) Atherosclerotic mice exhibit systemic inflammation in periadventitial and visceral adipose tissue, liver, and pancreatic islets. Atherosclerosis 207: 360–367.
30. Birsan T, Dambrin C, Marsh KC, Jacobsen W, Djuric SW, et al. (2004) Preliminary in vivo pharmacokinetic and pharmacodynamic evaluation of a novel calcineurin-independent inhibitor of NFAT. Transpl Int 3: 145–150.
31. Nakashima Y, Plump AS, Raines EW, Breslow JL, Ross R (1994) ApoE-deficient mice develop lesions of all phases of atherosclerosis throughout the arterial tree. Arterioscler Thromb 14: 133–140.
32. Park L, Raman KG, Lee KJ, Lu Y, Ferran EJ, et al. (1998) Suppression of accelerated diabetic atherosclerosis by the soluble receptor for advanced glycation endproducts. Nat Med 4: 1025–1031.
33. Lipskaia L, Pourci M-L, Delomenie C, Combettes L, Goudouneche D, et al. (2003) Phosphatidylinositol 3-Kinase and Calcium-Activated Transcription Pathways Are Required for VLDL-Induced Smooth Muscle Cell Proliferation. Circ Res 92: 1115–1122.
34. Norata GD, Grigore L, Raselli S, Redaelli L, Hamsten A, et al. (2007) Post-prandial endothelial dysfunction in hypertriglyceridemic subjects: molecular mechanisms and gene expression studies. Atherosclerosis 193: 321–327.

35. Bochkov VN, Mechtcheriakova D, Lucerna M, Huber J, Malli R, et al. (2002) Oxidized phospholipids stimulate tissue factor expression in human endothelial cells via activation of ERK/EGR-1 and Ca(++)/NFAT. Blood 99: 199–206.
36. Maziere C, Morliere P, Massy Z, Kamel S, Louandre C, et al. (2005) Oxidized low-density lipoprotein elicits an intracellular calcium rise and increases the binding activity of the transcription factor NFAT. Free Radic Biol Med 38: 472–480.
37. Schuett H, Luchtefeld M, Grothusen C, Grote K, Schieffer B (2009) How much is too much? Interleukin-6 and its signalling in atherosclerosis. Thromb Haemost 102: 215–222.
38. Takeda N, Manabe I, Shindo T, Iwata H, Iimuro S, et al. (2006) Synthetic retinoid Am80 reduces scavenger receptor expression and atherosclerosis in mice by inhibiting IL-6. Arterioscler Thromb Vasc Biol 26: 1177–1183.
39. Abbott KL, Loss JR, Robida AM, Murphy TJ (2000) Evidence that Galpha(q)-coupled receptor-induced interleukin-6 mRNA in vascular smooth muscle cells involves the nuclear factor of activated T cells. Mol Pharmacol 58: 946–953.
40. Trevillyan JM, Chiou XG, Chen YW, Ballaron SJ, Sheets MP, et al. (2001) Potent inhibition of NFAT activation and T cell cytokine production by novel low molecular weight pyrazole compounds. J Biol Chem 276: 48118–48126.
41. Breitenstein A, Camici GG, Tanner FC (2010) Tissue factor: beyond coagulation in the cardiovascular system. Clin Sci (Lond) 118: 159–172.
42. Kockx M, Jessup W, Kritharides L (2010) Cyclosporin A and atherosclerosis–cellular pathways in atherogenesis. Pharmacol Ther 128: 106–118.
43. Donners MM, Bot I, De Windt LJ, van Berkel TJ, Daemen MJ, et al. (2005) Low-dose FK506 blocks collar-induced atherosclerotic plaque development and stabilizes plaques in ApoE−/− mice. Am J Transplant 5: 1204–1215.

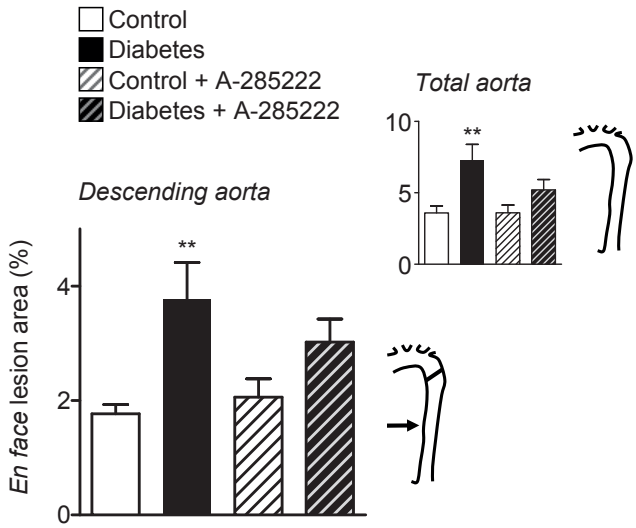
Control
Diabetes
Control + A-285222
Diabetes + A-285222
Descending aorta
Total aorta
En face lesion area (%)
**
**
0
2
4
0
5
10

Figure S1

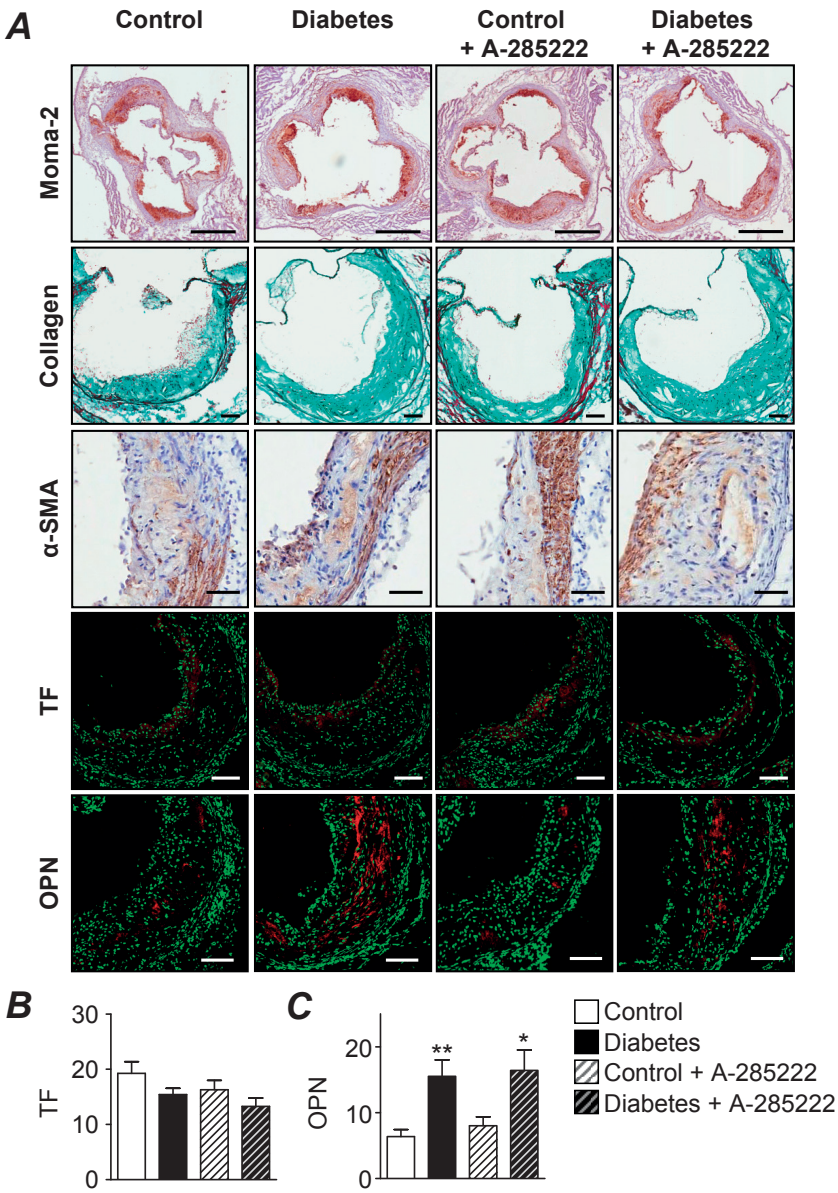
A
Control
Diabetes
Control
+ A-285222
Diabetes
+ A-285222
Moma-2
Collagen
α-SMA
TF
OPN
B
TF
30
20
10
0
C
OPN
20
10
0
**
*
Control
Diabetes
Control + A-285222
Diabetes + A-285222

Figure S2

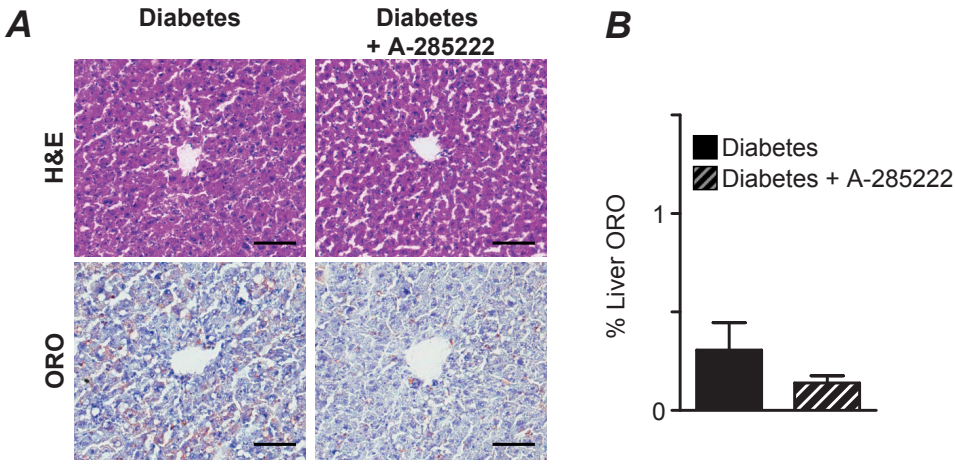
A
Diabetes
Diabetes
+ A-285222
H&E
ORO
B
Diabetes
Diabetes + A-285222
% Liver ORO
1
0

Figure S3

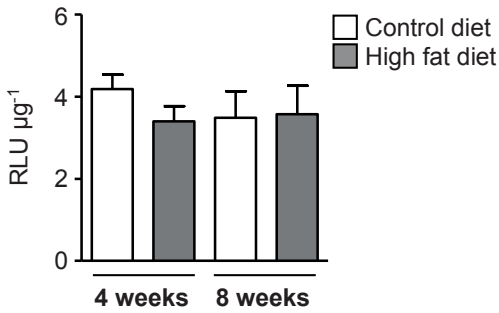

Figure S4

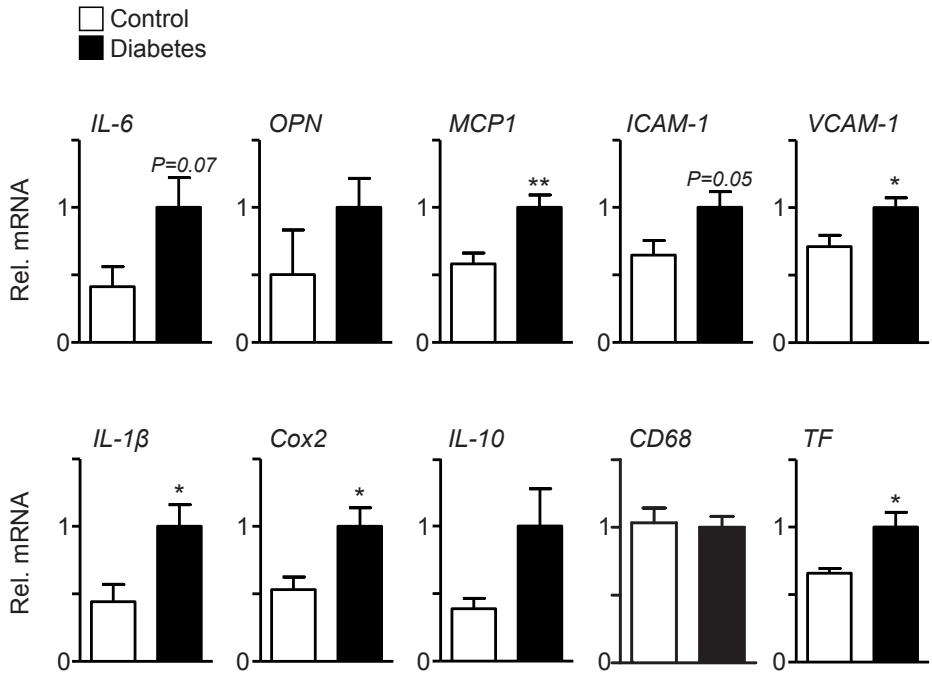
Control
Diabetes
IL-6
P=0.07
OPN
MCP1
**
ICAM-1
P=0.05
VCAM-1
*
Rel. mRNA
1
0
IL-1β
*
Cox2
*
IL-10
CD68
TF
*

Figure S5

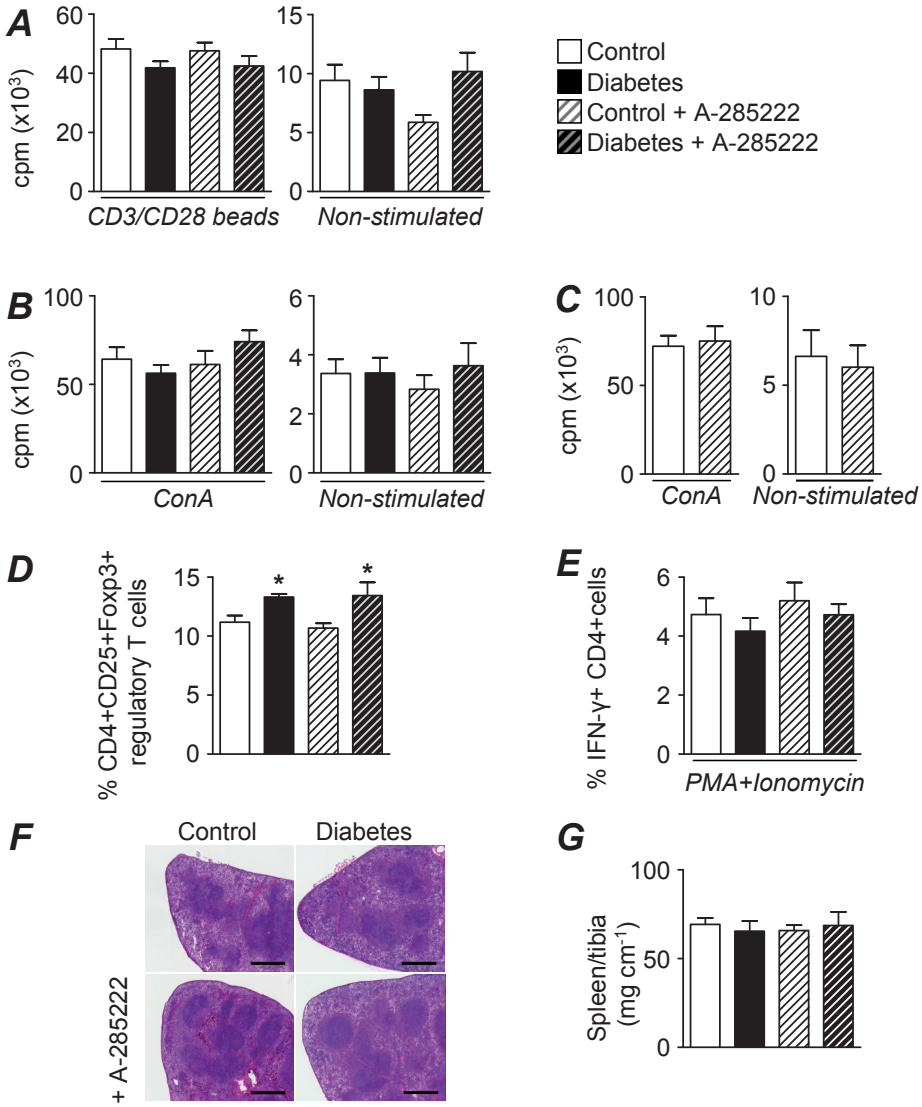
A
cpm (x10³)
60
40
20
0
15
10
5
0
CD3/CD28 beads
Non-stimulated
Control
Diabetes
Control + A-285222
Diabetes + A-285222
B
cpm (x10³)
100
50
0
6
4
2
0
ConA
Non-stimulated
C
cpm (x10³)
100
50
0
10
5
0
ConA
Non-stimulated
D
% CD4+CD25+Foxp3+ regulatory T cells
15
10
5
0
*
*
E
% IFN-γ+ CD4+cells
6
4
2
0
PMA+Ionomycin
F
Control
Diabetes
+ A-285222
G
Spleen/tibia (mg cm⁻¹)
100
50
0

Figure S6

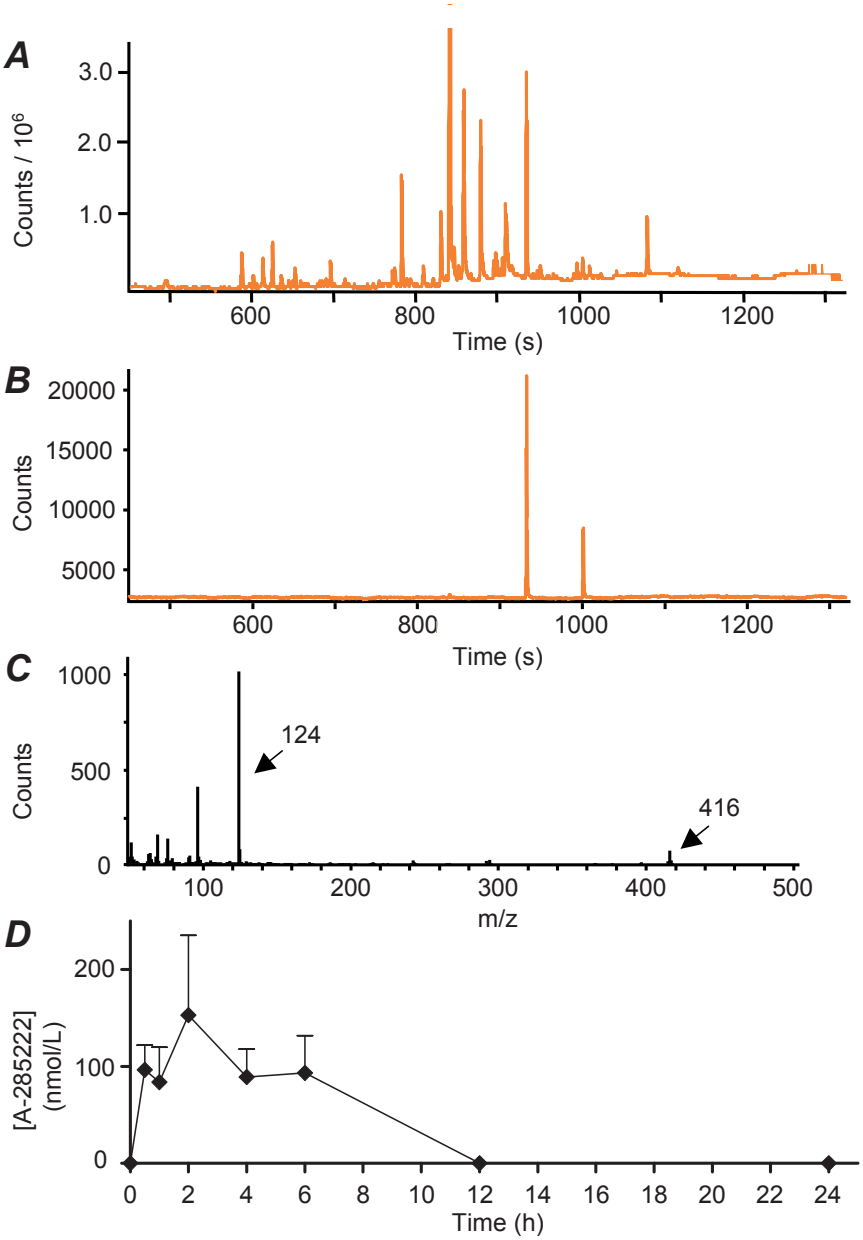
A
Counts / 10^6
3.0
2.0
1.0
600
800
1000
1200
Time (s)
B
Counts
20000
15000
10000
5000
600
800
1000
1200
Time (s)
C
Counts
1000
500
0
124
416
100
200
300
400
500
m/z
D
[A-285222] (nmol/L)
200
100
0
0
2
4
6
8
10
12
14
16
18
20
22
24
Time (h)

Figure S7

TABLE S1.

Cytokine (pg/mL)	Control (n=11)	Diabetes (n=11)	Control + A-285222 (n=10)	Diabetes + A-285222 (n=8)
Non-stimulated				
IFN-γ	1.36±1.22	1.06±0.30	0.78±0.56	0.33±0.17
IL-1β	0.62±0.54	0.45±0.38	0.41±0.28	0.80±0.35
IL-2	33.0±23.8	18.7±11.1	15.3±8.9*	12.1±7.04
IL-4	1.04±0.87	0.87±0.83	0.40±0.55	0.70±0.61
IL-5	0.20±0.17	0.24±0.31	0.25±0.25	0.21±0.12
KC/GRO	3.25±1.90	3.24±2.14	4.52±4.12	4.70±2.69
IL-10	11.9±8.63	12.2±5.73	11.1±10.5	13.3±4.24
IL-12total	184±84.8	190±116	148±74.5	160±36.5
TNF-α	0.43±0.86	0.79±1.51	0.26±0.62	0.29±0.54
CD3/CD28 stimulated				
IFN-γ	4197±941	3523±1110	4202±823	3408±889
IL-1β	23.4±12.0	25.2±16.9	28.2±11.6	24.0±21.4
IL-2	74.2±28.1	106.2±44.3	116.9±47.4	92.8±35.4
IL-4	31.4±11.2	35.9±22.6	46.4±15.2	30.8±20.4
IL-5	62.1±39.3	35.9±14.4	58.6±35.9	29.7±11.6
KC/GRO	32.0±9.37	39.1±19.8	38.4±10.4	44.4±27.0
IL-10	282±129	203±59.3	242±65.0	214±78.1
IL-12total	287±89.3	269±93.1	243±56.6	256±67.0
TNF-α	110.7±31.0	125.2±33.5	98.4±37.7	138.5±42.0#

Paper II

In vivo inhibition of nuclear factor of activated T-cells leads to atherosclerotic plaque regression in IGF-II/LDLR$^{-/-}$ ApoB$^{100/100}$ mice

Diabetes & Vascular Disease Research
2018, Vol. 15(4) 302–313

DOI: 10.1177/1479164118759220
journals.sagepub.com/home/dvr


Fabiana Blanco[1,2], Suvi E Heinonen[3], Erika Gurzeler[4], Lisa M Berglund[1], Anna-Maria Dutius Andersson[1], Olga Kotova[1], Ann-Cathrine Jönsson-Rylander[3], Seppo Ylä-Herttuala[4,5] and Maria F Gomez[1]

Abstract

Aims: Despite vast clinical experience linking diabetes and atherosclerosis, the molecular mechanisms leading to accelerated vascular damage are still unclear. Here, we investigated the effects of nuclear factor of activated T-cells inhibition on plaque burden in a novel mouse model of type 2 diabetes that better replicates human disease.

Methods & Results: IGF-II/LDLR$^{-/-}$ApoB$^{100/100}$ mice were generated by crossbreeding low-density lipoprotein receptor–deficient mice that synthesize only apolipoprotein B100 (LDLR$^{-/-}$ApoB$^{100/100}$) with transgenic mice overexpressing insulin-like growth factor-II in pancreatic β cells. Mice have mild hyperglycaemia and hyperinsulinaemia and develop complex atherosclerotic lesions. *In vivo* treatment with the nuclear factor of activated T-cells blocker A-285222 for 4 weeks reduced atherosclerotic plaque area and degree of stenosis in the brachiocephalic artery of IGF-II/LDLR$^{-/-}$ApoB$^{100/100}$ mice, as assessed non-invasively using ultrasound biomicroscopy prior and after treatment, and histologically after termination. Treatment had no impact on plaque composition (i.e. muscle, collagen, macrophages). The reduced plaque area could not be explained by effects of A-285222 on plasma glucose, insulin or lipids. Inhibition of nuclear factor of activated T-cells was associated with increased expression of atheroprotective NOX4 and of the anti-oxidant enzyme catalase in aortic vascular smooth muscle cells.

Conclusion: Targeting the nuclear factor of activated T-cells signalling pathway may be an attractive approach for the treatment of diabetic macrovascular complications.

Keywords

Atherosclerosis, oxidative stress, type 2 diabetes, nuclear factor of activated T-cells, hyperglycaemia, ApoB100

Introduction

Diabetes-induced macro- and microvascular complications are the major cause of morbidity and mortality in diabetic patients. Based on current trends, the rising incidence of diabetes (expected to reach 700 million people worldwide by 2025) will undoubtedly equate to increased cardiovascular mortality.[1] Diabetic patients have a much more widespread and aggressive form of atherosclerosis and, therefore, higher risk for myocardial infarction, peripheral vascular disease and stroke, but the molecular mechanisms leading to accelerated damage are still unclear.[2,3]

Previous studies from our laboratory identified the calcium/calcineurin-dependent transcription factor nuclear

[1]Department of Clinical Sciences, Malmö, Lund University Diabetes Centre (LUDC), Lund University, Malmö, Sweden
[2]Departamento de Biofísica, Facultad de Medicina, Universidad de la República, Montevideo, Uruguay
[3]Bioscience, Cardiovascular, Renal and Metabolic diseases, Innovative Medicines and Early Development Biotech Unit, AstraZeneca Gothenburg, Sweden
[4]A.I. Virtanen Institute for Molecular Sciences, University of Eastern Finland, Kuopio, Finland
[5]Heart Center, Kuopio University Hospital, Kuopio, Finland

Corresponding author:
Maria F Gomez, Department of Clinical Sciences, Malmö, Lund University Diabetes Centre (LUDC), Lund University, Jan Waldenströms gata 35, CRC 91-12, Malmö 21428, Sweden.
Email: maria.gomez@med.lu.se

factor of activated T-cells (NFAT) as a potential mediator of vascular disease in the context of hyperglycaemia. NFAT is expressed in the vascular wall and is readily activated by modest elevations of extracellular glucose in conduit[4] and medium-sized resistance arteries[5] as well as in the microvasculature.[6] Once activated, NFAT induces the expression of the pro-atherogenic cytokine osteopontin (OPN) in the arterial wall, as well as the expression of inflammatory mediators, such as cyclooxygenase-2 (COX-2), interleukin 6 (IL-6), vascular cell adhesion molecule 1 (VCAM-1), tissue factor (TF) and allograft inflammatory factor-1 (AIF-1).[4,7–11] Clinical and experimental studies have implicated all these NFAT-targets in the development of vascular disease.[4,7–11] More recently, we showed that *in vivo* treatment of streptozotocin (STZ)-induced diabetic female ApoE$^{-/-}$ mice with the NFAT blocker A-285222 for 4 weeks abrogated- hyperglycaemia induced atherosclerosis in the aorta.[10]

A large number of studies over the past years have focused on the generation of oxidative stress as the pathogenic mechanism linking diabetes to atherosclerosis.[12] A shift in the balance between oxidant [i.e. reactive oxygen and nitrogen species (ROS and RNS)] and anti-oxidant or detoxifying agents [i.e. catalase and glyoxalase I (GLO1)] results in chronically elevated oxidative stress levels in diabetes.[13] Key players in the generation of ROS in the arterial wall are the vascular isoforms of the NADPH oxidase (NOX) family of proteins.[14] In particular, NOX1 and NOX2 have been shown to be induced and promote atherosclerosis in the context of diabetes, while NOX4 has recently emerged as an atheroprotective isoform in both humans and in mouse.[15,16] Interestingly, in mouse kidney fibroblasts, the calcineurin/NFAT pathway has been shown to regulate NOX expression and activity in response to high glucose.[17]

Here, we investigated whether inhibition of NFAT had any impact on atherosclerosis in the context of type 2 diabetes, using a novel mouse model with a metabolic profile and plaque characteristics that better mimic human disease than other mouse models currently available.[18] Moreover, we explore the potential link between NFAT signalling and oxidative stress in this setting.

Methods

Animals

IGF-II/LDLR$^{-/-}$ApoB$^{100/100}$ mice were originated by crossbreeding low-density lipoprotein (LDL) receptor–deficient mice expressing only apolipoprotein B100 (LDLR$^{-/-}$ApoB$^{100/100}$; C57BL/6x129/SvJae background) with C57BL6/SJL mice overexpressing IGF-II in pancreatic β-cells.[19] Mice were either bred at the National Laboratory Animal Centre at the University of Eastern Finland or at Taconic Europe (Ejby, Denmark) after re-derivation from the University of Eastern Finland. Mice are characterized by hyperglycaemia, mild hyperinsulinaemia, a human-like hypercholesterolaemic lipid profile, and advanced and complex atherosclerotic lesions, hence representing a model that better replicates human disease and a more appropriate model for the study of macrovascular complications in the context of type 2 diabetes.[19] Animals were housed in groups and maintained in a temperature- and humidity-controlled environment with a 12-h light/dark cycle. This study was carried out in strict accordance with the recommendations in the Guide for the Care and Use of Laboratory Animals of the National Institutes of Health. All protocols were approved by the local ethics review board at Lund University and Malmö/Lund Animal Care and Use Committee (M29-12; M9-15), and by the National Animal Experiment Board in Finland (ESAVI-2012-001260).

Study protocol

The study protocol was carried out twice and referred to as Study I and Study II throughout the article (Figure 1(a)). Study I: Young (15–16 weeks old, $N=30$) IGF-II/LDLR$^{-/-}$ApoB$^{100/100}$ mice bred at Taconic Europe were used at Lund University. Study II: Young (10 weeks old, $N=10$) and old (46–74 weeks old, $N=17$) IGF-II/LDLR$^{-/-}$ApoB$^{100/100}$ mice were bred and used at the University of Eastern Finland. Mice at Lund University, but not at the University of Eastern Finland were housed in individually ventilated cages. All animals were fed ad libitum and switched from a normal chow to high fat Western diet (TD 88137, Harlan Tekland: 42% of calories from fat and 0.15% from cholesterol) at the start of the experiments. After 4 weeks on high-fat diet, mice were randomized based on blood glucose, body weight and plasma cholesterol to receive daily intraperitoneal (i.p.) injections of the NFAT blocker A-285222 (0.29 mg/kg body weight) or vehicle (saline) for an additional 4 weeks. In Study II, brachiocephalic artery plaque size measured by ultrasound biomicroscopy (see below) before the start of A-285222 treatment was also included as parameter in the randomization. A-285222 inhibits all NFAT family members and was kindly provided by Abbott Laboratories (Abbott Park, IL). This drug belongs to a series of 3,5-bis (trifluoromethyl) pyrazole (BTP) derivatives demonstrated to maintain NFAT in a phosphorylated state, blocking its nuclear import and subsequent transcription, without affecting NF-kB or AP-1 activation, or calcineurin phosphatase activity.[20] Body weight, fasting (16 h) and non-fasting venous blood glucose (saphenous or tail vein) were measured using Contour Glucometer (Bayer) before, during and at termination of the experiments. All fluid and tissue processing and analyses for both studies

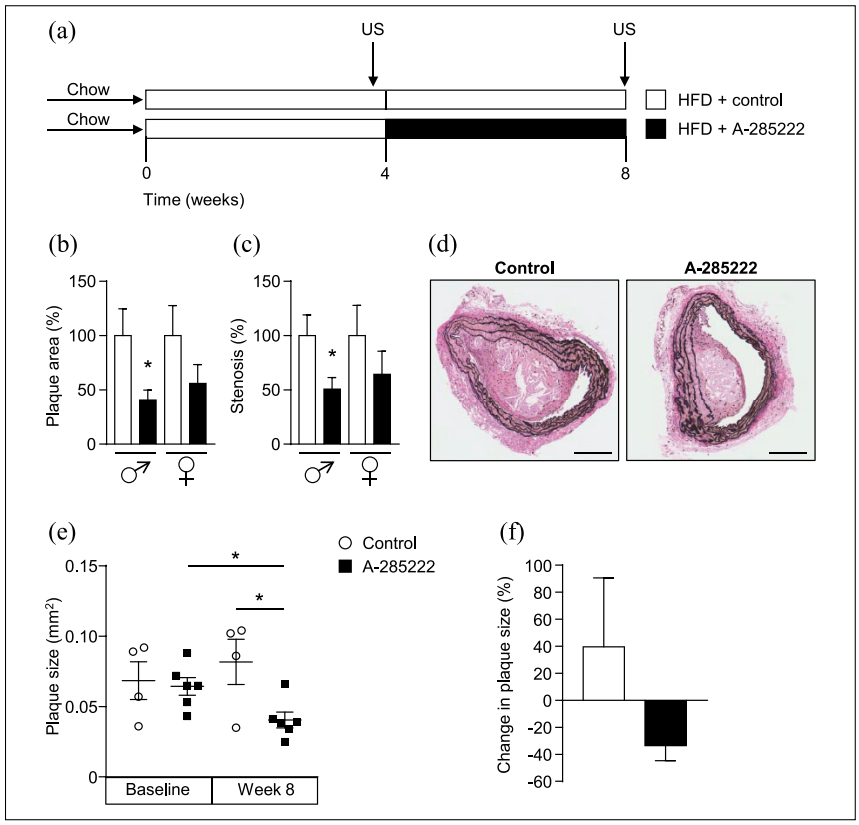

Figure 1. NFAT inhibition reduces plaque area and degree of stenosis in IGF-II/LDLR$^{-/-}$ApoB$^{100/100}$ mice. (a) Study protocol used for all conducted *in vivo* experiments (both for Study I and II): IGF-II/LDLR$^{-/-}$ApoB$^{100/100}$ mice were fed high-fat diet (HFD, 42% of calories from fat and 0.15% from cholesterol) for 8 weeks and received daily i.p. injections of A-285222 (0.29 mg/kg body weight) or vehicle (saline; control) for the last 4 weeks of the HFD period. Arrows indicate the time of the ultrasound biomicroscopy measurements (US) performed in Study II. (b–c) Histologically determined plaque size and degree of stenosis in the brachiocephalic arteries of young (10–16 weeks old) mice. Data represent merged results from Studies I and II, normalized to each control ($N = 10$ mice/condition, except $N = 9$ in control females). (d) Representative Elastin van Gieson stained sections from the brachiocephalic artery of young male mice in Study II after treatment with A-285222 or vehicle. Scale bar = 200 µm. (e) Plaque size determined non-invasively by ultrasound biomicroscopy in young mice before and after treatment with A-285222. (f) Change in plaque size from week 4 to week 8 for control and A-285222 treated mice. $N = 4$–6 mice/group; *$p < 0.05$.

I and II were done at Lund University to avoid inter-lab variability.

Ultrasound measurements

Brachiocephalic artery plaque size and lesion progression were assessed non-invasively using ultrasound biomicroscopy as previously described and validated[21,22] (Vevo2100, Visualsonics, Toronto, Canada), with a transducer frequency of 40MHz (providing a theoretical resolution of 40 µm at a frame rate of 32Hz). Prior to the scan, animals were anaesthetized with isoflurane (4.5% isoflurane 450 mL air for induction, 2% isoflurane 200 mL air for maintenance; Baxter International Inc., IL, USA). The brachiocephalic artery was visualized in a cross-sectional short axis view and atherosclerotic lesion size was measured within the proximal 200 µm from its bifurcation from the aortic arch. All measurements were performed blinded by one operator (intra-individual coefficient of variance = 2.7%). Loops of at least 100 frames were stored and the frame with the largest plaque was chosen for off-line, blinded measurements. At the end of the experimental protocol, mice were

anaesthetized with ketamine hydrochloride and xylazine (i.p.; 7.5 mg and 2.5 mg/100 g body weight, respectively) and euthanized by exsanguination through cardiac puncture for blood collection and perfused with phosphate-buffered saline before tissue harvesting. Depth of anaesthesia was assessed by toe-pinch procedure and absence of muscular tone. All efforts were made to minimize suffering.

Plasma cholesterol, triglycerides, insulin and OPN measurements

Total plasma cholesterol and triglycerides levels were measured in overnight fasting blood samples before and after treatment by colorimetric assays (Infinity™-Cholesterol and Infinity™-Triglyceride; Thermo Scientific, Middletown, VA, USA). Plasma insulin and OPN were determined after overnight fasting at the end of the treatment using Mercodia mouse insulin enzyme-linked immunosorbent assay (ELISA) kit (Mercodia AB, Uppsala, Sweden) and Quantikine mouse OPN ELISA kit (R&D Systems, Abingdon UK), respectively. All assays were performed according to the manufacturer's instructions and the lower limits of detection were 0.2 µg/L for insulin and 5.7 pg/mL for OPN.

Histological evaluations of plaque size and plaque composition

Brachiocephalic arteries and hearts were immersion-fixed with 4% buffered paraformaldehyde (PFA, pH 7.4) and thereafter embedded in paraffin. Plaque and media contents of smooth muscle, collagen and elastin were evaluated in cross-sections (5 µm) stained with haematoxylin and eosin (H&E), as well as with Elastin van Gieson (EvG). Plaque macrophage contents were evaluated both in cross-sections (5 µm) of the brachiocephalic artery and of the subvalvular region of the aortic root, using rat anti-MOMA-2 (monocytes/macrophage 2) primary antibody (1 µg/mL, BMA Biomedicals, Augst, Switzerland), biotinylated rabbit anti-rat secondary IgG antibody (1:70, BA-40011, Vector Laboratories, Burlingame, CA) and immPACT-DAB (Vector Laboratories, Burlingame, CA) for visualization. No staining was detected when primary or secondary antibodies were omitted from the protocols. Sections were counterstained with Mayer's haematoxylin. Plaque and media areas (mm^2), degree of stenosis and media thickness (µm) were measured under blinded conditions using computer-aided morphometry (BioPix iQ2.3.1 software, Biopix AB, Gothenburg, Sweden). Stenosis is expressed as the percentage of area within the internal elastic lamina occupied by atherosclerotic plaque. For media thickness, tiff-files were imported into NIS Elements BR Analysis 3.2 64-bit software and a wheel (Rose binary) grid with 16 spokes was centred in the lumen. An average of the media thickness measured at each of the 16 positions where the spokes met the media was calculated.

Cell culture

Vascular smooth muscle cells (VSMCs) were obtained by outgrowth from aorta explants from BalB/c NFATc3$^{-/-}$ and wild-type (WT; NFATc3$^{+/+}$) mice[23] as previously described.[8] Briefly, mice were anaesthetized with ketamine hydrochloride and xylazine (i.p.; 7.5 mg and 2.5 mg/100 g body weight, respectively) and euthanized by cervical dislocation. After reaching confluence, VSMCs (passages 10–15) were seeded in 24-well plates (7.5×10^4 cells/well) and cultured for 24 h in Dulbecco's Modified Eagle Medium (DMEM) containing 5 mmol/L D-glucose and supplemented with 10% FBS before stimulations. Hydrogen peroxide (H_2O_2, 500 µmol/L; Sigma-Aldrich, Darmstadt, Germany) or 3-Morpholinosydnonimine hydrochloride (SIN-1, 100 µmol/L, Sigma-Aldrich) were used to induce oxidative stress. After stimulation, cells were harvested for gene expression analyses. Oxidative stress levels were measured in culture media using OxiSelect™ *In Vitro* ROS/RNS Assay Kit (Cells Biolab, Inc., San Diego, CA, USA), according to the manufacturer's instructions. H_2O_2 levels were determined in culture medium using Amplex Red Hydrogen Peroxide/Peroxidase Assay Kit [Molecular probes, Eugene, OR, USA] in VSMCs cultured as above or in human microvascular endothelial cells [HMEC-1, Centers for Disease Control and Prevention (CDC)/Emory University] cultured in M200 medium supplemented with low serum growth supplement (LSGS).

RT-qPCR

Total RNA was extracted from intact, snap-frozen aortas from IGF-II/LDLR$^{-/-}$ApoB$^{100/100}$ mice using TRI Reagent BD (Sigma-Aldrich, St Louis, MO, USA) or from cultured VSMCs using RNeasy® Plus Mini Kit (Qiagen, Hilden, Germany) according to the manufacturer's instructions. cDNA synthesis (RevertAid M-MuLV Reverse Transcriptase; Fermentas GMBH, St Leon-Rot, Germany) and real-time PCR were performed as previously described[24] using TaqMan Gene Expression assays for OPN (Mm00436763), IL-6 (Mm00446190_m1), ICAM (Mm00516023), CD68 (Mm03047340_m1), TF (Mm00436948_m1), GLO1 (Mm00844954_s1), NOX1 (Mm00549170_m1), NOX2 (Mm01287743_m1), NOX4 (Mm00479246_m1) and catalase (Mm00437992_m1) with HPRT (Mm0046968_m1) and β-actin (Mm00607939_s1) as endogenous controls.

Statistics

Results are expressed as mean ± SEM unless otherwise specified. Analyses of distributions were performed before statistical tests were performed using GraphPad software (Prism 7.0). For parametric data, significance was determined using Student's *t*-test, one- or two-way analysis of variance (ANOVA), followed by Bonferroni post-tests.

Table 1. Metabolic parameters of young IGF-II/LDLR$^{-/-}$ApoB$^{100/100}$ mice on HFD.

		Control	A-285222
Glucose (mmol/L)			
Fasted	Males	7.16 ± 0.99	8.92 ± 2.09*
	Females	6.77 ± 1.19	6.69 ± 0.93
Fed	Males	9.47 ± 3.14	9.17 ± 1.80
	Females	8.46 ± 1.79	7.96 ± 1.69
Insulin (µg/L)			
	Males	0.549 ± 0.37	0.492 ± 0.37
	Females	0.383 ± 0.12	0.323 ± 0.18
Triglycerides (mmol/L)			
	Males	2.39 ± 0.99	2.28 ± 1.35
	Females	1.55 ± 0.50	1.28 ± 0.62
Cholesterol (mmol/L)			
	Males	33.9 ± 6.81	33.7 ± 9.00
	Females	34.8 ± 9.44	33.9 ± 7.43
OPN (ng/mL)			
	Males	151 ± 37	135 ± 25
	Females	136 ± 23	122 ± 19
Body weight (g)			
	Males	34.4 ± 2.7	33.1 ± 2.5
	Females	24.5 ± 3.3	24.7 ± 2.6

HFD: high-fat diet; OPN: osteopontin.
Values are expressed as mean ± SD ($N = 8$–11 mice/group from Study I and II) and represent values after overnight fasting measured at the end of the treatment (week 8 of study protocol). Blood glucose values under non-fasting conditions are also shown (measured during week 7 of study protocol).
*$p < 0.05$ versus control. Two-way ANOVA for the effect of gender and treatment revealed significant effects of gender on plasma triglycerides ($p = 0.0035$) and body weight ($p < 0.0001$).

Non-parametric data were analysed using Mann–Whitney or Kruskal–Wallis test followed by Dunn's post-test.

Results

In vivo *inhibition of NFAT effectively leads to plaque regression in the brachiocephalic artery of IGF-II/LDLR$^{-/-}$ApoB$^{100/100}$ mice*

Histological evaluation of the brachiocephalic arteries of young mice revealed reduced plaque area and degree of stenosis after 4 weeks of treatment with the NFAT blocker A-285222 (Figure 1(b) to (d)). The effects of the blocker were significant in the males only (Figure 1(b) to (d)). The same pattern was observed in Study I and II (Supplemental Figure 1(A) and (B)). No significant differences in media area or thickness were observed after NFAT inhibition (Supplemental Figure 1(C) to (H)). Male IGF-II/LDLR$^{-/-}$ApoB$^{100/100}$ mice exhibited larger atherosclerotic plaques than female mice. Interestingly, despite being younger, male mice in Study II had considerably larger plaques than males in Study I, maybe due to different breeding or housing environments.

Non-invasive longitudinal ultrasound measurements in Study II revealed that the effects of NFAT inhibition on atherosclerosis may not only be due to limited plaque progression but also to plaque regression, as evidenced by smaller plaque size after treatment with A-285222 when compared to plaque size in the same mice before treatment (Figure 1(e) and (f)). Ultrasound experiments also showed significantly smaller brachiocephalic artery plaque size in mice treated with A-285222 when compared to control mice (Figure 1(e)), in line with the histological results.

The reduction in plaque size was unlikely due to lowering effects of A-285222 on plasma glucose, cholesterol or triglyceride levels, since these were not significantly reduced by the treatment (Table 1). In male mice, we even observed a small elevation in fasting blood glucose in the A-285222 treated group (Table 1), which would instead counteract any beneficial effect of the NFAT blocker. We have seen a similar effect of the NFAT blocker on blood glucose in STZ-induced diabetic BalB/c mice: an effect that was no longer evident after lowering the dose of A-285222 from 0.29 to 0.15 mg/kg.[4] We have not observed this effect in other diabetic mouse models or strains.[10] This could potentially be attributed to direct effects of A-285222 on pancreatic β-cells, where the involvement of NFAT in the regulation of insulin transcription is well established.[25] This effect was only evident under fasting conditions and no effects on plasma insulin or body weight were detected after treatment with A-285222 (Table 1). Male mice had higher body weight than female mice and higher plasma

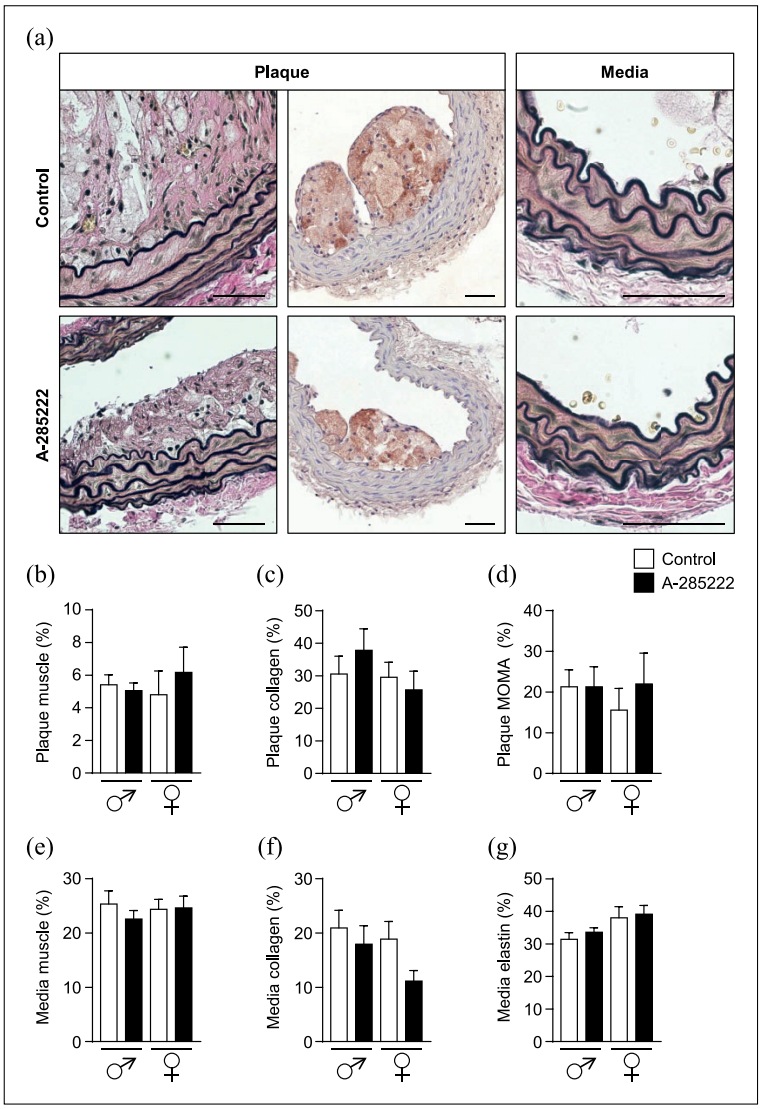

Figure 2. Composition of atherosclerotic plaques. (a) Representative images showing plaque and media regions of brachiocephalic arterial sections from young mice in Study I, stained with Elastin van Gieson (left and right panels in each row) and MOMA-2 (middle panels). Sections from control mice are shown in the upper row, while sections from A-285222 treated mice are shown in the lower row. Graphs summarize morphometric data showing plaque (b) to (d) and media (e) and (f) composition. Muscle (b) and (e), collagen (c) and (f), macrophage (d) and elastin (g) contents in μm^2 are expressed as percentage of plaque area. $N = 7–8$ mice/group; scale bars = 50 µm.

triglycerides: this last, potentially contributing to their larger atherosclerotic plaques (Table 1).

We also evaluated if inhibition of NFAT had any impact on plaque composition, but we did not detect any differences in plaque muscle, collagen or macrophage contents after treatment with A-285222 in Study I (Figure 2(a) to (d)). No significant differences were observed regarding media muscle, collagen or elastin contents (Figure 2(a) and (e) to (g)).

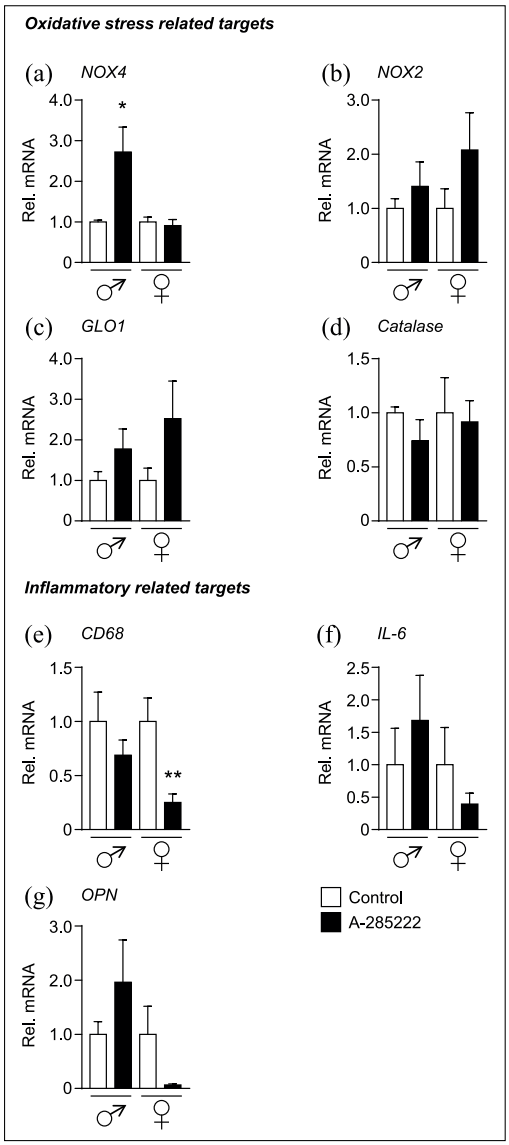

Figure 3. *In vivo* inhibition of NFAT modifies the expression of oxidative stress and inflammatory markers in the aorta of young IGF-II/LDLR$^{-/-}$ApoB$^{100/100}$ mice. Gene expression of oxidative stress targets (a) NOX4, (b) NOX2, (c) GLO1 and (d) catalase, as well as inflammatory targets (e) CD68, (f) IL-6 and (g) OPN were quantified by qPCR in the aortas of young IGF-II/LDLR$^{-/-}$ApoB$^{100/100}$ mice from Study I and II. HPRT and β-actin were used as endogenous controls and data were expressed relative to each control group. $N = 5$ and 7 for control and treated males, respectively; $N = 8$ for female groups.
*$p < 0.05$ and **$p < 0.01$.

Similarly, no significant differences were observed when corresponding measurements were performed in vessels from Study II (Supplemental Figure 2).

In vivo *inhibition of NFAT signalling induces changes in the expression of oxidative stress and inflammatory targets in the arterial wall of IGF-II/LDLR$^{-/-}$ApoB$^{100/100}$ mice*

In agreement with previous work, both NOX2 and NOX4 were expressed in mouse aorta.[16] Treatment with the NFAT blocker A-285222 for 4 weeks significantly increased the expression of the atheroprotective isoform NOX4 in the aorta of male mice (Figure 3(a)), while changes in NOX2 were not significant (Figure 3(b)). We also examined the expression of the detoxifier protein glyoxalase I (GLO1), which metabolizes methylglyoxal (MG), a major source of intracellular and plasmatic advanced glycation end product (AGE) formation, into the unreactive D-lactate. But neither changes in GLO1 expression (Figure 3(c)) nor in the expression of another detoxifier enzyme, catalase (Figure 3(d)), were significant. Consistent with results obtained in our previous studies in which STZ-induced diabetic ApoE$^{-/-}$ female mice were treated with A-285222,[10] expression of the macrophage marker CD68 was significantly reduced by NFAT inhibition in the aortas of IGF-II/LDLR$^{-/-}$ApoB$^{100/100}$ female mice (Figure 3(e)), along with tendencies to reduced IL-6 and OPN (Figure 3(f) to (g)). In line with previous studies,[10] plasma OPN was not affected by treatment with A-285222 (Table 1), suggesting the effects of the blocker are targeted to the vessel wall and not due to lower systemic inflammation.

The analysis of the expression data also revealed sex-dependent differences in the IGF-II/LDLR$^{-/-}$ApoB$^{100/100}$ model, as assessed in the aortas of vehicle treated mice. Levels of NOX2 were relatively higher in males than in females, while arteries from female mice expressed relatively higher levels of atheroprotective NOX4, catalase and GLO1 (Supplemental Figure 3): maybe underlying the differences in overall plaque burden observed between sexes (Supplemental Figure 1(A) and (B)).

NFAT modulates the expression of NOX4 and catalase in a powerful oxidative stress environment

Next, we explored whether inhibition of NFAT could alter the expression of oxidative stress related genes in VSMCs cultured under controlled oxidative stress conditions. VSMCs were incubated either with hydrogen peroxide (H_2O_2; 500 µmol/L) or with peroxynitrite donor 3-morpholinosydnonimine (SIN-1; 100 µmol/L) for 48 h to induce oxidative stress, in the presence or absence of A-285222 (1 µmol/L). Figure 4 shows that inhibition of

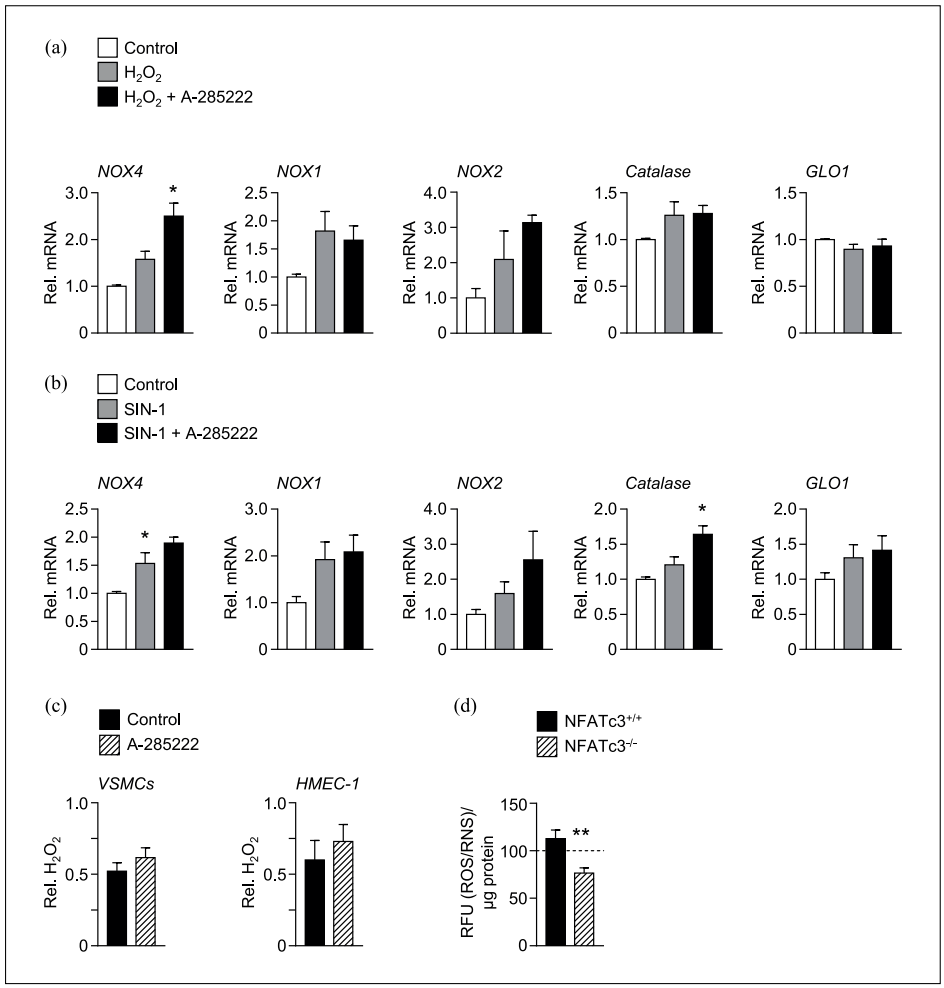

Figure 4. *In vitro* inhibition of NFAT increased the expression of the anti-oxidant enzymes NOX4 and catalase in VSMCs. Mouse VMSCs were incubated with (a) H_2O_2 (500 µmol/L) or (b) SIN-1 (100 µmol/L) for 48 h in the presence or absence of A-285222 (1 µmol/L). The expression of oxidative stress targets NOX4, NOX1, NOX2, catalase and GLO1 was measured using qPCR and are expressed relative to untreated control cells. $N = 4–7$ experiments/condition $^*p < 0.05$. (c) H_2O_2 levels were measured in the medium of VSMCs and HMEC-1 cells after 24 h in high glucose (25 mmol/L; HG) in the presence or absence of A-285222 (1 µmol/L). H_2O_2 levels were normalized to protein and expressed relative to control without A-285222 ($N = 6–16$ experiments/condition). (d) ROS/RNS levels, expressed as relative fluorescence units (RFU) were measured in the cell culture medium of VSMCs from NFATc3 competent ($NFATc3^{+/+}$) and knockout ($NFATc3^{-/-}$) mice in the presence of high glucose concentration (25 mmol/L) during 48 h. The dashed line shows ROS/RNS levels measured under low glucose conditions (5 mmol/L) as a reference ($N = 9$ experiments/condition).

NFAT effectively increased expression of NOX4 in VSMCs exposed to H_2O_2 and of catalase in VSMCs exposed to SIN-1, suggesting involvement of NFAT in the modulation of these genes under strong oxidative stress conditions. Inhibition of NFAT with A-285222 had no impact on H_2O_2 levels measured during culture of VSMCs or endothelial cells (Figure 4(c)). Interestingly, ROS/RNS levels are significantly lower in the culture medium of VSMCs from NFATc3 knockout ($NFATc3^{-/-}$) mice cultured in high glucose (25 mmol/L) for 48 h, when compared to levels measured in the medium of NFATc3 competent ($NFATc3^{+/+}$) cells (Figure 4(d)). H_2O_2 levels

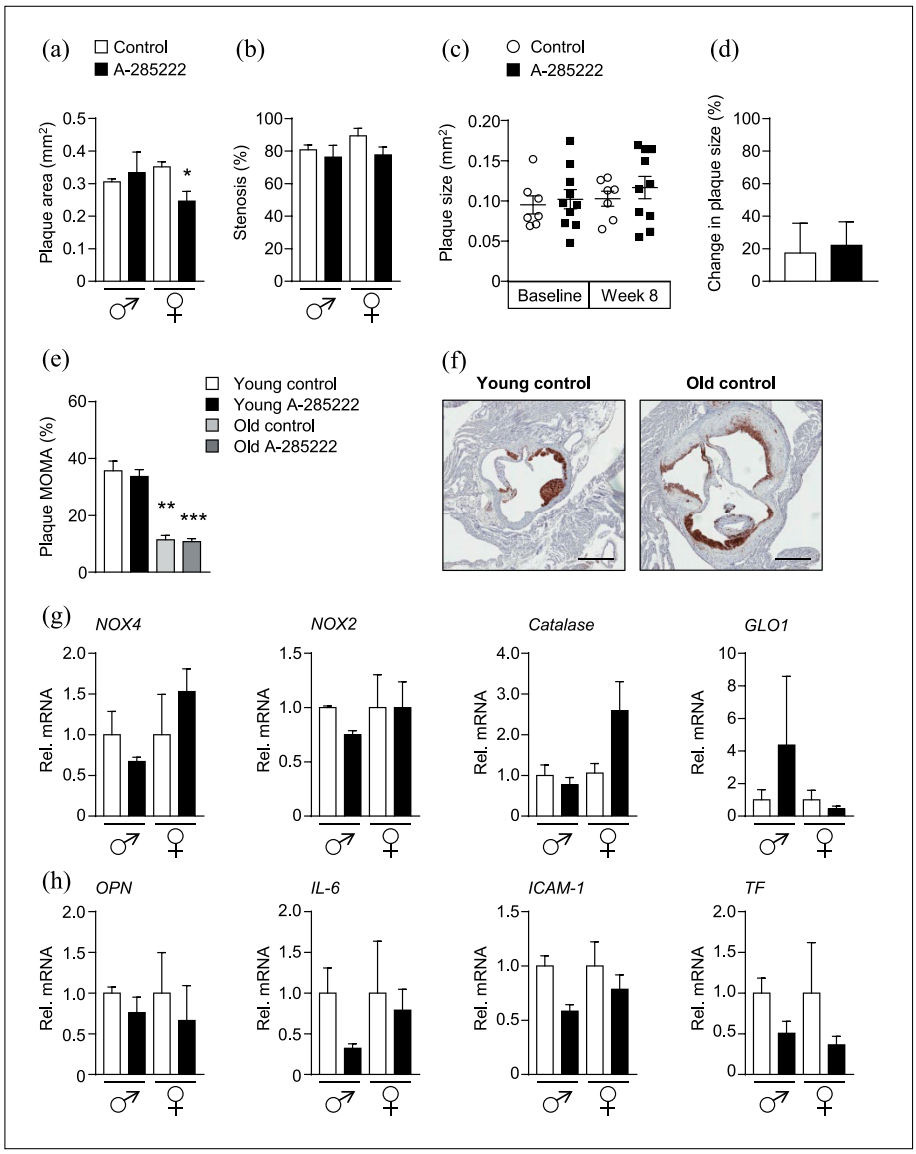

Figure 5. *In vivo* treatment with the NFAT blocker A-285222 reduces plaque size in the brachiocephalic artery of old female IGF-II/LDLR$^{-/-}$ApoB$^{100/100}$ mice. (a) Histologically determined plaque size and (b) stenosis in the brachiocephalic artery of old mice treated with A-285222 (0.29 mg/kg) or vehicle (saline) for 4 weeks according to the same protocol detailed in Figure 1(a). $N = 3$ males, $N = 4$–7 females; *$p < 0.05$. (c) and (d) Plaque size determined non-invasively by ultrasound biomicroscopy before (baseline, week 4 of the experiment) and after treatment (week 8 of the experiment; $N = 7$–10 mice/group). (d) Change in plaque size from week 4 to week 8 for each group. (e) Young IGF-II/LDLR$^{-/-}$ApoB$^{100/100}$ mice had higher proportion of macrophage infiltration in subvalvular aortic plaques when compared to old mice ($N = 4$–6 young mice, $N = 7$–10 old mice). (f) Representative MOMA-2 stained sections of the subvalvular aorta from untreated young and old mice. Scale bar = 400 μm. (g) and (h) Gene expression of oxidative stress targets NOX4, NOX2, catalase and GLO1 (g) and inflammatory targets OPN, IL6, ICAM-1 and TF (h) in the aorta of old mice ($N = 2$–7 mice/group and sex). HPRT and β-actin were used as endogenous controls. *$p < 0.05$; **$p < 0.01$; and ***$p < 0.001$.

were below detection in the culture media of VSMCs from NFATc3$^{-/-}$ mice.

In vivo *inhibition of NFAT signalling in old IGF-II/LDLR$^{-/-}$ApoB$^{100/100}$ mice have modest effects on plaque size*

Treatment of older mice for 4 weeks with A-285222 (0.29 mg/kg) resulted in reduced histologically assessed plaque area only in female mice (Figure 5(a)). This smaller plaque size was not translated in a significantly larger arterial lumen (Figure 5(b)). We were not able to detect differences in plaque size by ultrasound biomicroscopy (Figure 5(c) and (d)), maybe due to the lower sensitivity of the method when compared to histology. Old IGF-II/LDLR$^{-/-}$ApoB$^{100/100}$ mice had significantly lower macrophage infiltration in subvalvular aortic plaques than young mice, as expected to be the case during later phases of the atherogenic process (Figure 5(e) and (f)), but higher circulating levels of OPN (222 ± 70 ng/mL and 185 ± 42 ng/mL for males and females, respectively; Supplemental Table 1) reflecting increased plasma inflammatory burden when ageing.

Despite reduced expression of CD68 in the aortas of younger mice (Figure 3(e)), treatment with A-285222 did not translate into reduced macrophage infiltration in subvalvular plaques regardless the age of the mice (Figure 5(e)). This lack of effect at the level of the aortic root is in line with previous data in diabetic ApoE$^{-/-}$ mice.[10] Treatment with the NFAT blocker had no impact on elastin or collagen contents in the subvalvular plaques (data not shown) or on elastin and collagen contents or vessel morphometry in the brachiocephalic arteries (Supplemental Figure 4). No significant differences in gene expression were found in the aortas of older mice treated with A-285222 when compared to vehicle-treated mice (Figure 5(g) and (h)). In line with findings in the young mice, no significant effects on body weight or on metabolic parameters that could explain changes in plaque size were found after treatment with A-285222 (Supplemental Table 1).

Discussion

This study demonstrates that inhibition of NFAT signalling in IGF-II/LDLR$^{-/-}$ApoB$^{100/100}$ mice reduces atherosclerosis in the brachiocephalic artery, a particularly disease-prone vascular segment in mice, independently of changes in plasma glucose, insulin or lipid levels. This may not only be due to limited plaque progression but also due to plaque regression, as evidenced in the ultrasound biomicroscopy experiments by smaller plaque size after treatment with A-285222 when compared to plaque size in the same mice before treatment. These findings are in line with previous work from our laboratory showing abrogation of diabetes-induced aggravation of atherosclerosis in the aortic arch of STZ-induced diabetic ApoE$^{-/-}$ mice. This study goes beyond a toxin-induced type 1 diabetes model and supports a role for NFAT in the development of atherosclerosis in the context of type 2 diabetes and in an animal model that better replicates human disease than the STZ model.

Experimental models of atherosclerosis and diabetes are very susceptible to the housing environment, often translating into differences in the severity of the disease phenotype (i.e. atherosclerotic plaque size, degree of hyperglycaemia) when the same strain is studied in different animal facilities.[18] This issue adds to the complexity of using animal models in medical research, potentially having an impact on study results and their interpretation, and to some extent, contributing to the poor translation of preclinical *in vivo* results into successful clinical trials and higher approval rates of new drug candidates. Among other explanations for this limited translational value [e.g. shortcomings in the design of clinical trials, over-optimistic conclusions from methodologically flawed animal studies, animal models that do not reflect human disease (reviewed in Van der Worp et al.[26])] is the fact that validation studies are not traditionally conducted in the animal experimental field (when it is an absolute requirement for all other steps leading to the establishment of new therapies). A strength of this study is that the inhibitory effect of the NFAT blocker on atherosclerosis was replicated in two independent mice cohorts undergoing the same experimental protocol at different animal facilities.

Plaque size is the preferred primary readout in animal models and is typically determined histologically at the end of the experiments. Advances in ultrasound techniques have made possible the measurement of plaque progression/regression non-invasively in rodents, allowing for longitudinal studies which help reduce the number of animals required for statistical power. At termination, complementary evaluations of plaque area have shown good correlation between the histological and the non-invasive measurements in the brachiocephalic artery, the aorta and carotid arteries.[22,27] Here, we also found a good correlation between the two techniques in the brachiocephalic arteries of young mice but were not able to dissect the histological difference in plaque size observed in the old female mice (Figure 5), probably because the effect size of the NFAT blocker was smaller in older mice than in younger mice and due to lower number of mice in the older cohort. Nevertheless, ultrasound biomicroscopy should be considered as an attractive non-invasive method to assess the effects of interventions in rodents.

In the ApoE-deficient mouse, it is well established that atherosclerotic lesions progress with age through all phases of atherogenesis, from monocyte adhesion, then lipid deposition and formation of fatty streaks to more mature and fibrous plaques;[28,29] and that the pace at which this happens can vary depending on the vascular segment (e.g. more advanced lesions in the aortic root vs the aortic arch;[10] slowest progressing lesions in the coronary arteries[29]). Our previous work highlighted differential susceptibility to STZ-induced atherosclerosis depending

on the age of the lesions, with more pronounced effects of hyperglycaemia on plaque size in early stage lesions, such as those in the aortic arch, when compared to the effects on more advanced plaques such as those in the aortic root.[10] In line with NFAT being activated by hyperglycaemia as we previously established,[4,5] the effects of A-285222 had a more distinct impact on the aortic arch than on the aortic root of STZ-diabetic ApoE$^{-/-}$ mice, stressing the need for a diabetes-driven process for NFAT-inhibition to play a role.[10] Here, we found in the IGF-II/LDLR$^{-/-}$ApoB$^{100/100}$ mice, a model in which the extent and severity of the lesions progress with age,[19] a clear effect of A-285222 in the younger cohorts but only modest effects of NFAT-inhibition in the older mice (Figure 1 vs 5). Young mice exhibited more dynamic lesions characterized by an active inflammatory process with higher degree of macrophage infiltration than old mice (Figure 5(e) and (f)). It is possible that the reduction in plaque size observed after inhibition of NFAT signalling could be, at least in part, driven by reduced inflammation. Even though the proportion of the plaque occupied by macrophages was not affected by A-285222 treatment (Figure 2(d)), the reduction in plaque size observed in the males inevitably translated into reduced total macrophage content (from $7474 \pm 2497\,\mu m^2$ to $2239 \pm 939\,\mu m^2$ in males, $p = 0.08$).

IGF-II/LDLR$^{-/-}$ApoB$^{100/100}$ mice included in this study have elevated fasting blood glucose levels in line with previously reported values;[19,30,31] however, they exhibited only moderate non-fasting hyperglycaemia compared to the values originally reported when the model was generated (~16 mmol/L)[19]. This discrepancy could be attributed to genetic drift, which should not be neglected even in inbred strains. The combination of impaired glucose tolerance and impaired fasting glucose[31] makes the IGF-II/LDLR$^{-/-}$ApoB$^{100/100}$ mice a relevant model of pre-diabetes, a condition associated with higher risk of developing type 2 diabetes and cardiovascular disease. In previous work, we showed a clear dose-dependency of glucose-induced NFAT transcriptional activity, with modest elevations of a few mmol/L of extracellular glucose being sufficient for significant NFATc3 activation in the arterial wall.[5] In light of this dose-dependency and the need of a hyperglycaemia-driven process to occur for NFAT-inhibition to have effects, it was reasonable to find that the same treatment with A-285222 had a more profound inhibitory effect on the expression of inflammatory markers in the aorta of STZ-diabetic ApoE$^{-/-}$ mice (a model characterized by profound hyperglycaemia) than of IGF-II/LDLR$^{-/-}$ApoB$^{100/100}$ mice with their milder hyperglycaemic phenotype.

NOX4 has recently been shown to protect against endothelial dysfunction and atherosclerosis in LDLR deficient mice.[32] It was suggested that hydrogen peroxide derived from NOX4 acted via pAKT1 phosphorylation on eNOS activation. Here, we showed that inhibition of NFAT signalling in VSMCs exposed to a strong oxidative stress environment, significantly increased NOX4 expression (Figure 4(a)). The cell experiments also suggest that the observed upregulation of NOX4 expression in the aorta of male IGF-II/LDLR$^{-/-}$ApoB$^{100/100}$ mice (Figure 3(a)) after treatment with A-285222 could at least in part be due to direct effects of the NFAT blocker on the vascular cells. A similar NFAT-dependent regulation of NOX4 has been demonstrated in immortalized human podocytes stimulated with insulin using three complementary approaches to inhibit NFAT-signalling (tacrolimus, cyclosporine A and VIVIT peptide).[33] Using another inducer of oxidative stress (SIN-1), we also found that inhibition of NFAT signalling resulted in enhanced catalase expression in VSMCs (Figure 4(b)).

This study shows that inhibition of NFAT signalling in IGF-II/LDLR$^{-/-}$ApoB$^{100/100}$ mice not only limits the progression of atherosclerosis but, more importantly, it leads to atherosclerosis plaque regression. The effects are not due to changes in plasma glucose, insulin or lipid levels but may be attributed to reduced inflammatory burden and improved anti-oxidant defences such as NOX4 and catalase. Vascular NFAT may be considered as a novel therapeutic target for the treatment of diabetic macrovascular complications.

Acknowledgements

The authors would like to thank Anna Zetterqvist for valuable input on the project and manuscript and Anne-Christine Andréasson for histological assistance.

Declaration of conflicting interests

The author(s) declared no potential conflicts of interest with respect to the research, authorship and/or publication of this article.

Funding

This work was supported by the Swedish Heart and Lung Foundation (grant numbers 20130700, 20160872), the Swedish Research Council (grant numbers 2011-3900, 2014-03352), the Swedish Foundation for Strategic Research (grant number IRC15-0067), the Swedish Society for Medical Research, the Crafoord, Albert Påhlsson and Knut & Alice Wallenberg foundations: also by the Innovative Medicines Initiative Joint Undertaking (grant number 115006), comprising funds from the European Union's Seventh Framework Programme (grant number FP7/2007-2013) and European Federation of Pharmaceutical Industries and Associations (EFPIA) companies' in kind contribution. F.B. received support from CSIC (Comisión Sectorial de Investigación Científica) and PEDECIBA (Programa de Desarrollo de Ciencias Básicas).

ORCID iDs

Lisa M Berglund https://orcid.org/0000-0001-6440-116X

Maria F Gomez https://orcid.org/0000-0001-6210-3142

References

1. NCD-RisC. Worldwide trends in diabetes since 1980: a pooled analysis of 751 population-based studies with 4.4 million participants. *Lancet* 2016; 387: 1513–1530.
2. Madonna R and De Caterina R. Cellular and molecular mechanisms of vascular injury in diabetes – part I: pathways of vascular disease in diabetes. *Vascul Pharmacol* 2011; 54: 68–74.
3. Paneni F, Costantino S and Cosentino F. Insulin resistance, diabetes, and cardiovascular risk. *Curr Atheroscler Rep* 2014; 16: 419.
4. Nilsson-Berglund LM, Zetterqvist AV, Nilsson-Ohman J, et al. Nuclear factor of activated T cells regulates osteopontin expression in arterial smooth muscle in response to diabetes-induced hyperglycemia. *Arterioscler Thromb Vasc Biol* 2010; 30: 218–224.
5. Nilsson J, Nilsson LM, Chen YW, et al. High glucose activates nuclear factor of activated T cells in native vascular smooth muscle. *Arterioscler Thromb Vasc Biol* 2006; 26: 794–800.
6. Zetterqvist AV, Blanco F, Öhman J, et al. Nuclear factor of activated T cells is activated in the endothelium of retinal microvessels in diabetic mice. *J Diabetes Res* 2015; 2015: 428473.
7. Lee MY, Garvey SM, Baras AS, et al. Integrative genomics identifies DSCR1 (RCAN1) as a novel NFAT-dependent mediator of phenotypic modulation in vascular smooth muscle cells. *Hum Mol Genet* 2010; 19: 468–479.
8. Nilsson LM, Sun ZW, Nilsson J, et al. Novel blocker of NFAT activation inhibits IL-6 production in human myometrial arteries and reduces vascular smooth muscle cell proliferation. *Am J Physiol Cell Physiol* 2007; 292: C1167–C1178.
9. Orr AW, Lee MY, Lemmon JA, et al. Molecular mechanisms of collagen isotype-specific modulation of smooth muscle cell phenotype. *Arterioscler Thromb Vasc Biol* 2008; 29: 225–231.
10. Zetterqvist AV, Berglund LM, Blanco F, et al. Inhibition of nuclear factor of activated T-cells (NFAT) suppresses accelerated atherosclerosis in diabetic mice. *PLoS ONE* 2013; 8: e65020.
11. Berglund LM, Kotova O, Osmark P, et al. NFAT regulates the expression of AIF-1 and IRT-1: yin and yang splice variants of neointima formation and atherosclerosis. *Cardiovasc Res* 2012; 93: 414–423.
12. Yamagishi SI, Nakamura K, Matsui T, et al. Role of postprandial hyperglycaemia in cardiovascular disease in diabetes. *Int J Clin Pract* 2007; 61: 83–87.
13. Lubrano V and Balzan S. Enzymatic antioxidant system in vascular inflammation and coronary artery disease. *World J Exp Med* 2015; 5: 218–224.
14. Lassègue B and Griendling KK. NADPH oxidases: functions and pathologies in the vasculature. *Arterioscler Thromb Vasc Biol* 2010; 30: 653–661.
15. Konior A, Schramm A, Czesnikiewicz-Guzik M, et al. NADPH oxidases in vascular pathology. *Antioxid Redox Signal* 2014; 20: 2794–2814.
16. Gray SP, Di Marco E, Kennedy K, et al. Reactive oxygen species can provide atheroprotection via NOX4-dependent inhibition of inflammation and vascular remodeling. *Arterioscler Thromb Vasc Biol* 2016; 36: 295–307.
17. Williams CR and Gooch JL. Calcineurin Aβ regulates NADPH oxidase (Nox) expression and activity via nuclear factor of activated T cells (NFAT) in response to high glucose. *J Biol Chem* 2014; 289: 4896–4905.
18. Heinonen SE, Genove G, Bengtsson E, et al. Animal models of diabetic macrovascular complications: key players in the development of new therapeutic approaches. *J Diabetes Res* 2015; 2015: 404085.
19. Heinonen SE, Leppanen P, Kholova I, et al. Increased atherosclerotic lesion calcification in a novel mouse model combining insulin resistance, hyperglycemia, and hypercholesterolemia. *Circ Res* 2007; 101: 1058–1067.
20. Trevillyan JM, Chiou XG, Chen YW, et al. Potent inhibition of NFAT activation and T cell cytokine production by novel low molecular weight pyrazole compounds. *J Biol Chem* 2001; 276: 48118–48126.
21. Gan LM, Gronros J, Hagg U, et al. Non-invasive real-time imaging of atherosclerosis in mice using ultrasound biomicroscopy. *Atherosclerosis* 2007; 190: 313–320.
22. Gronros J, Wikstrom J, Brandt-Eliasson U, et al. Effects of rosuvastatin on cardiovascular morphology and function in an ApoE-knockout mouse model of atherosclerosis. *Am J Physiol Heart Circ Physiol* 2008; 295: H2046–H2053.
23. Oukka M, Ho IC, de la Brousse FC, et al. The transcription factor NFAT4 is involved in the generation and survival of T cells. *Immunity* 1998; 9: 295–304.
24. Awla D, Zetterqvist AV, Abdulla A, et al. NFATc3 regulates trypsinogen activation, neutrophil recruitment, and tissue damage in acute pancreatitis in mice. *Gastroenterology* 2012; 143: 1352–1360.
25. Heit JJ. Calcineurin/NFAT signaling in the beta-cell: from diabetes to new therapeutics. *Bioessays* 2007; 29: 1011–1021.
26. Van der Worp HB, Howells DW, Sena ES, et al. Can animal models of disease reliably inform human studies? *PLoS Med* 2010; 7: e1000245.
27. Gronros J, Wikstrom J, Hagg U, et al. Proximal to middle left coronary artery flow velocity ratio, as assessed using color Doppler echocardiography, predicts coronary artery atherosclerosis in mice. *Arterioscler Thromb Vasc Biol* 2006; 26: 1126–1131.
28. Ross R. Atherosclerosis – an inflammatory disease. *N Engl J Med* 1999; 340: 115–126.
29. Nakashima Y, Plump AS, Raines EW, et al. ApoE-deficient mice develop lesions of all phases of atherosclerosis throughout the arterial tree. *Arterioscler Thromb* 1994; 14: 133–140.
30. Heinonen SE, Merentie M, Hedman M, et al. Left ventricular dysfunction with reduced functional cardiac reserve in diabetic and non-diabetic LDL-receptor deficient apolipoprotein B100-only mice. *Cardiovasc Diabetol* 2011; 10: 59.
31. Kinnunen K, Heinonen SE, Kalesnykas G, et al. LDLR-/-ApoB100/100 mice with insulin-like growth factor II overexpression reveal a novel form of retinopathy with photoreceptor atrophy and altered morphology of the retina. *Mol Vis* 2013; 19: 1723–1733.
32. Langbein H, Brunssen C, Hofmann A, et al. NADPH oxidase 4 protects against development of endothelial dysfunction and atherosclerosis in LDL receptor deficient mice. *Eur Heart J* 2016; 37: 1753–1761.
33. Xia S, Liu Y, Li X, et al. Insulin increases expression of TRPC6 channels in podocytes by a calcineurin-dependent pathway. *Cell Physiol Biochem* 2016; 38: 659–669.

Supplemental Table 1. Metabolic parameters in old IGF-II/LDLR$^{-/-}$ApoB$^{100/100}$ mice on HFD

		Control	A-285222
Glucose (mmol/L)			
Fasted	Males	6.23 ± 0.38	6.93 ± 0.57
	Females	6.73 ± 0.93	6.44 ± 0.65
Fed	Males	7.87 ± 0.65	9.63 ±1.51
	Females	6.35 ± 0.42	6.99 ± 1.17
Insulin (µg/L)			
	Males	0.671 ± 1.77	0.638 ± 0.26
	Females	0.494 ± 0.31	0.446 ± 0.17
Triglycerides (mmol/L)			
	Males	2.24 ± 1.61	1.41 ± 0.24
	Females	0.933 ± 0.063	1.88 ± 1.77
Cholesterol (mmol/L)			
	Males	27.7 ± 7.41	31.0 ± 19.9
	Females	21.6 ± 3.25	23.2 ± 8.33
OPN (ng/mL)			
	Males	222 ± 70.3	209 ± 38.9
	Females	185 ± 42.0	234 ± 101
Body weight (g)			
	Males	41.3 ± 4.0	36.4 ± 3.2
	Females	28.2 ± 4.5	27.4 ± 5.4

Blood glucose was monitored at week 7 (fed conditions) and at week 8 (fasted conditions) of the experimental protocol. Insulin, triglycerides, total plasma cholesterol and OPN were measured at the termination of the experiment (all fasted conditions), after four weeks treatment with A-285222 (0.29 mg/kg body weight). Values are expressed as mean ± SD (n=3 males/group; n=4-7 females/group).

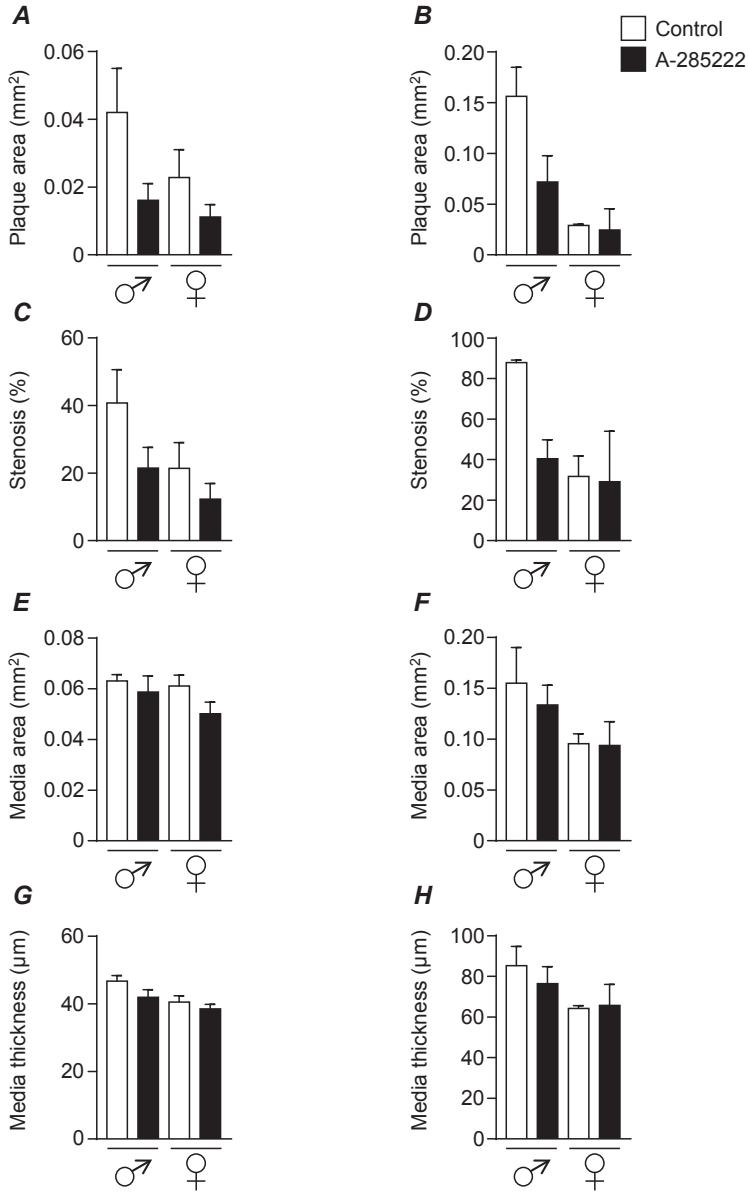

Supplemental figure 1. Summarized morphometric data showing plaque size **(A-B)**, degree of stenosis **(C-D)**, media area **(E-F)** and media thickness **(G-H)** determined histologically in the brachiocephalic arteries of young mice from study I (left graphs A, C, E and G; N=7-8 mice/group) and from study II (right graphs B, D, F and H; N=2-3 mice/group). *p<0.05.

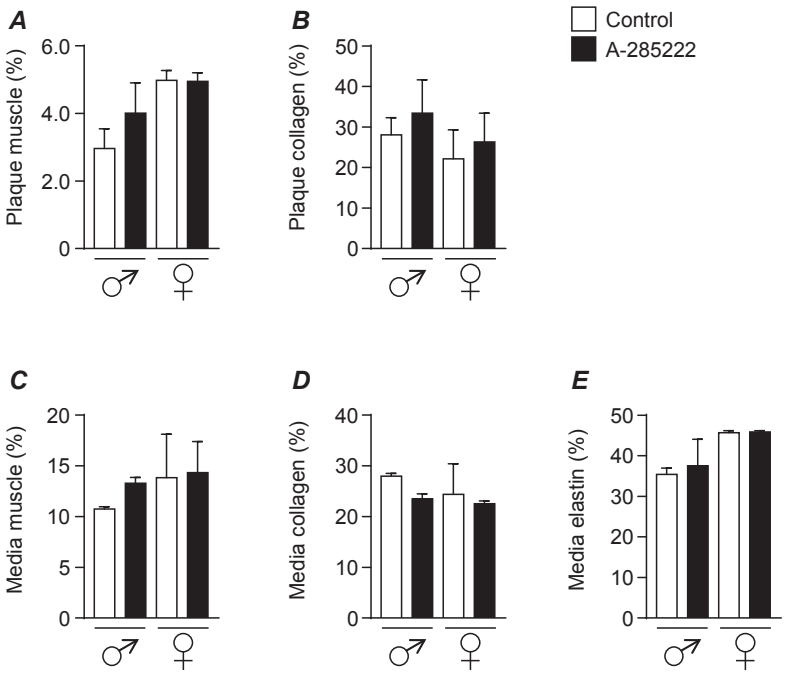

Supplemental figure 2. Summarized histological data showing muscle and collagen contents in plaques (A-B), and muscle, collagen and elastin contents in the media (C-E) of brachiocephalic arteries from young mice in study II, determined in sections stained with Elastin van Gieson (N=2-3 mice/group).

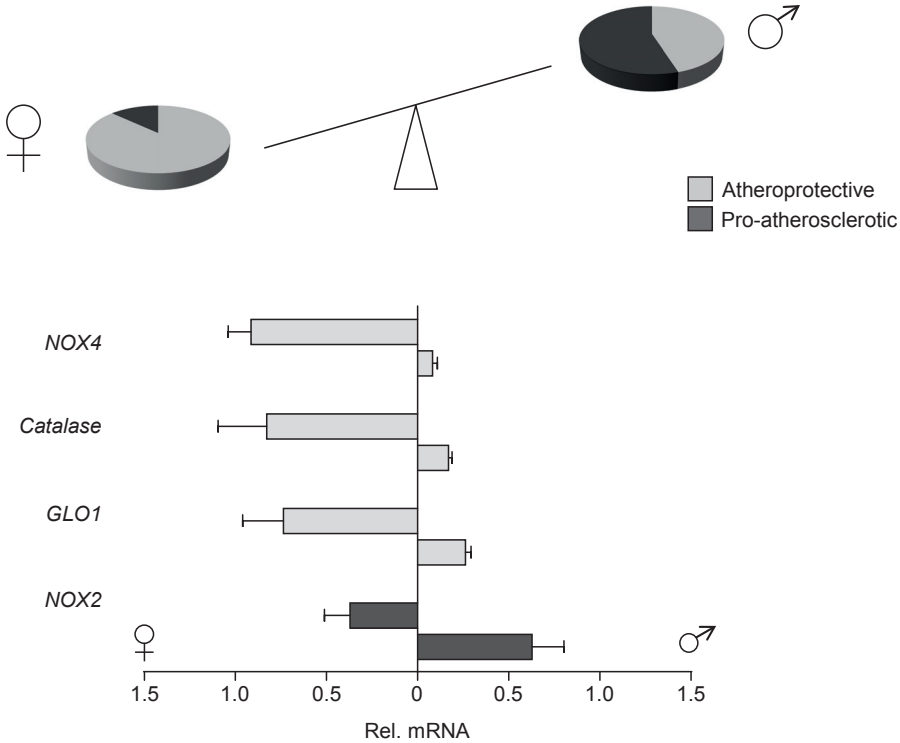

Supplemental figure 3. Sex-dependent differences in oxidative stress burden in mouse aorta. The bar graph shows the relative mRNA expression of the oxidative stress targets NOX4, catalase, GLO1 and NOX2 in the aortas of female (left side of x-axis) and male (right side of x-axis) IGF-II/LDLR-/-ApoB100/100 mice from studies I and II. HPRT and β-actin were used as endogenous controls (N=5-8 mice/group). For comparison of expression between genders, the sum of female and male expression levels is set to 1 for each target. The pie charts in the upper part of the figure are for visualization purposes only and show the abundance of the pro-atherosclerotic oxidative stress target NOX2 relative to the three measured atheroprotective targets (NOX4, catalase and GLO1) for each gender.

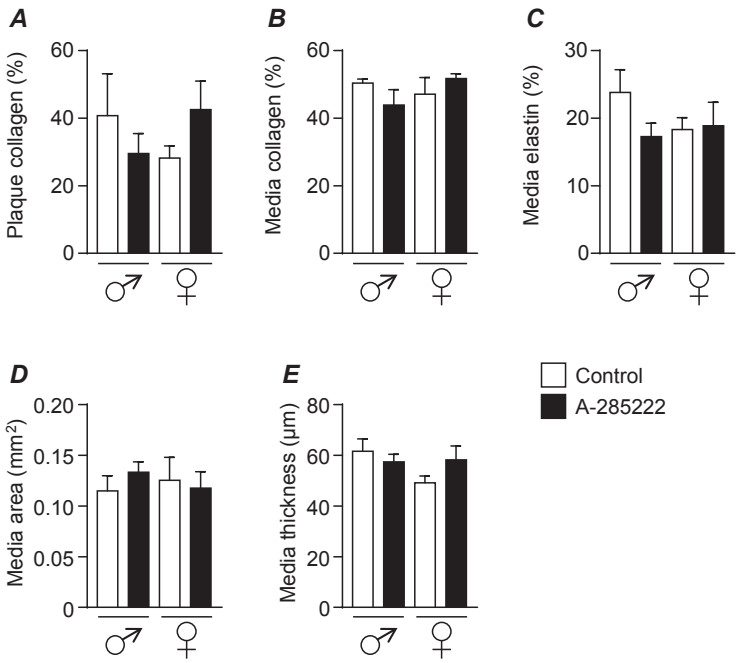

Supplemental figure 4. Summarized histological data showing collagen contents in plaques (A), collagen and elastin contents in the media (B-C), as well as media area and media thickness (D-E) of brachiocephalic arteries from old mice, determined in sections stained with Elastin van Gieson (N=2-3 mice/group).

Paper III

Hindawi Publishing Corporation
Journal of Diabetes Research
Volume 2015, Article ID 428473, 14 pages
http://dx.doi.org/10.1155/2015/428473

Research Article

Nuclear Factor of Activated T Cells Is Activated in the Endothelium of Retinal Microvessels in Diabetic Mice

Anna V. Zetterqvist,[1] Fabiana Blanco,[1,2] Jenny Öhman,[1] Olga Kotova,[1] Lisa M. Berglund,[1] Sergio de Frutos Garcia,[3] Raed Al-Naemi,[1] Maria Wigren,[1] Paul G. McGuire,[3] Laura V. Gonzalez Bosc,[3] and Maria F. Gomez[1]

[1]*Department of Clinical Sciences in Malmö, Lund University, 20502 Malmö, Sweden*
[2]*Departamento de Biofísica, Facultad de Medicina, Universidad de la República, 11800 Montevideo, Uruguay*
[3]*Department of Cell Biology and Physiology, University of New Mexico Health Sciences Center, Albuquerque, NM 87131, USA*

Correspondence should be addressed to Maria F. Gomez; maria.gomez@med.lu.se

Received 28 November 2014; Revised 25 February 2015; Accepted 25 February 2015

Academic Editor: Ute Christine Rogner

The pathogenesis of diabetic retinopathy (DR) remains unclear but hyperglycemia is an established risk factor. Endothelial dysfunction and changes in Ca^{2+} signaling have been shown to precede the onset of DR. We recently demonstrated that high extracellular glucose activates the Ca^{2+}/calcineurin-dependent transcription factor NFAT in cerebral arteries and aorta, promoting the expression of inflammatory markers. Here we show, using confocal immunofluorescence, that NFAT is expressed in the endothelium of retinal microvessels and is readily activated by high glucose. This was inhibited by the NFAT blocker A-285222 as well as by the ectonucleotidase apyrase, suggesting a mechanism involving the release of extracellular nucleotides. Acute hyperglycemia induced by an IP-GTT (intraperitoneal glucose tolerance test) resulted in increased NFATc3 nuclear accumulation and NFAT-dependent transcriptional activity in retinal vessels of NFAT-luciferase reporter mice. In both Akita (*Ins2*$^{+/-}$) and streptozotocin- (STZ-) induced diabetic mice, NFAT transcriptional activity was elevated in retinal vessels. *In vivo* inhibition of NFAT with A-285222 decreased the expression of *OPN* and *ICAM-1* mRNA in retinal vessels, prevented a diabetes driven downregulation of anti-inflammatory IL-10 in retina, and abrogated the increased vascular permeability observed in diabetic mice. Results identify NFAT signaling as a putative target for treatment of microvascular complications in diabetes.

1. Introduction

Diabetic retinopathy (DR) is still one of the leading causes of vision loss worldwide. Even though the underlying pathogenesis is not clear, hyperglycemia is an important risk factor [1]. We have recently demonstrated that modest elevations of extracellular glucose activate the Ca^{2+}/calcineurin-dependent transcription factor NFAT (nuclear factor of activated T cells) in smooth muscle cells of conduit and resistance arteries [2, 3]. The effect of glucose involved the local release of extracellular nucleotides, such as ATP and UTP, acting on P2Y receptors, leading to increased intracellular Ca^{2+} ($[Ca^{2+}]_i$) and subsequent activation of calcineurin and NFAT [2]. ATP and UTP are vasoactive signals able to increase $[Ca^{2+}]_i$ in the retina, via stimulation of purinergic receptors including P2Y4 [4]. Also, high glucose has been shown to increase extracellular ATP in rat retinal cell cultures [5]. Therefore, we hypothesize that hyperglycemia may activate NFAT in retinal microvessels.

Inflammation and endothelial activation are important early steps in the development of DR, leading to leukostasis, platelet activation, and upregulation of inflammatory cytokines [6]. The NFAT family (NFATc1–c4) plays a central role in the production of cytokines in immune cells and in the regulation of T-cell proliferation. We and others have shown that in conduit and resistance arteries and in cultured vascular cells NFAT regulates the expression of inflammatory genes, such as IL-6, allograft inflammatory factor 1 (AIF-1), tissue factor (TF), cyclooxygenase 2 (Cox-2), and osteopontin (OPN) [3, 7–9]. Expression of endothelial activation markers, such as VCAM-1 and E-selectin, is also dependent on NFAT signaling in cultured smooth muscle

and endothelial cells, respectively [10, 11]. More recently, we showed that *in vivo* inhibition of NFAT signaling reduces *ICAM-1* mRNA expression in the aortas of diabetic Apoe$^{-/-}$ mice [9], a leukocyte adhesion molecule that is elevated in retinal vessels from diabetic mice and patients [6, 12].

Another early feature of DR is the breakdown of the blood-retinal barrier (BRB) [13], which results in vascular leakage and development of retinal edema. Earlier investigations focused on vascular endothelial growth factor (VEGF), shown to induce rapid phosphorylation of tight junction proteins and increased retinal permeability [14]. However, recent *in vivo* kinetic data show that the retinal barrier function is compromised before VEGF levels are increased and use of a neutralizing anti-VEGF antibody is not effective at reducing permeability at early stages of diabetes (8 weeks) [15]. In the context of angiogenesis [16, 17], VEGF appears to be an upstream activator of NFAT, but both VEGF and its receptor VEGFR2 are also downstream targets of NFAT in endothelial cells [18, 19]. Hence, a role of NFAT in the early changes of DR cannot be ruled out.

Here, we investigated the effects of high glucose and diabetes on NFAT activation in a streptozotocin (STZ) model of diabetes and in hyperglycemic Akita (*Ins2*$^{+/-}$) mice. We also explored the effects of *in vivo* NFAT-signaling inhibition on the expression of inflammatory mediators, endothelial adhesion molecules, and vascular permeability in diabetic mice.

2. Research Design and Methods

2.1. Animals. All animal protocols in this study were reviewed and approved by Institutional Animal Care and Use Committees, University of New Mexico, School of Medicine and Lund University, Sweden. The following mice strains (number of animals per strain indicated) were bred in our animal facilities: FVBN 9x-NFAT-luciferase reporter (NFAT-luc [2, 7, 20]; $N = 133$), Akita (*Ins2*$^{+/-}$), and wild-type (*Ins2*$^{+/+}$) littermates (stock number 003548, C57Bl/6J background, Jackson Laboratories, Maine, here referred to as Akita and WT; $N = 31$). We also generated Akita/NFAT-luc mice and WT/NFAT-luc littermates ($N = 43$), which were backcrossed at least four generations into the C57Bl/6J background. Wild-type adult BALB/c ($N = 76$), C57Bl/6 (Taconic, Europe; $N = 12$), and ApoE$^{-/-}$ (B6.129P2-Apoe^{tm1Unc}/J; Charles River, Sulzfeld, Germany; $N = 22$) mice were also used. Animals had free access to tap water and were fed normal chow diet. Retinas, cerebral arteries, aortas, and plasma were used. Both eyes were enucleated from all mice included in this study; however, not always both eyes were used (some were stored for future studies). If both eyes were used, each eye was processed differently for the various types of measurements detailed below. For *in vivo* experiments using A-285222, the drug was administered intraperitoneally (i.p.) once a day for the duration of the experiments, at 0.15–0.29 mg/kg body weight depending on the mouse strain and based on previous studies [3]. A-285222 is a low molecular weight (461 daltons), cell permeable organic compound that inhibits all NFAT family members and was provided by Abbott Laboratories (Abbott Park, IL). For experiments involving collection of blood at termination, mice were anaesthetized by i.p. injection of 7.5 mg ketamine hydrochloride and 2.5 mg xylazine per 100 mg body weight and euthanized by exsanguination through cardiac puncture. For all other experiments, mice were euthanized by cervical dislocation or pentobarbital injection (200 mg/kg) followed by decapitation.

2.2. Isolation of Retinal Vessels. Eyes were enucleated and retinas dissected in ice-cold Ca^{2+}-free physiological saline solution (PSS; in mmol/L: NaCl, 135; KCl, 5.9; $MgCl_2$, 1.2; Hepes, 11.6; glucose, 2.0; pH 7.4). Retinal vessels were isolated from one eye as previously described [21]; the second eye was used for measurements in whole retina (see below). A total of 194 eyes were used for isolation of retinal vessels. Vessel integrity after isolation was confirmed by staining the vessel networks with smooth muscle α-actin antibody and the fluorescent nucleic acid dye SYTOX green (1 : 3000, Molecular Probes, Invitrogen, Paisley, UK). Intact retinal endothelial and smooth muscle cells were visualized by confocal microscopy as described below. Potential residual levels of neuronal and glial contamination were assessed by quantitative RT-PCR measuring *Tau* and *GFAP* expression, respectively, using *18S* as endogenous control.

2.3. RNA Isolation, Conventional RT-PCR, and Quantitative Real Time PCR. Total RNA was extracted from whole retinas, isolated retinal vessels, and aortas from mice and from human retinal microvessel endothelial cells (HRMVECs) as previously described [3, 21]. HRMVECs (catalog number ACBRI 181) were purchased from Cell Systems (Kirkland, WA) and grown in Medium 131 containing microvascular growth supplement (Gibco, Life Technologies Corp., Carlsbad, CA), 50 U/mL penicillin, and 50 μg/mL streptomycin at 37°C, 95% air, and 5% CO_2. For conventional RT-PCR, RNA extraction was followed by reverse transcription using RevertAid (Fermentas GMBH, St. Leon-Rot, Germany) and oligo-dT primers. cDNA was amplified (HotStarTaq Master Mix Kit, Qiagen) using NFAT isoform specific primers as previously described [7]. PCR products were separated by agarose gel electrophoresis and confirmed by sequencing. Equal amounts of RNA for whole retina and isolated retinal vessel preparations were used for the reverse transcription reactions. For quantitative real time PCR, cDNA was synthesized using random hexamer primers and amplified on a 7900HT TaqMan system (Applied Biosystems, Carlsbad, CA) using TaqMan Gene Expression assays for *Tau* (Mm00521988_m1), *GFAP* (Mm01253033_m1), *OPN* (Mm00436767_m1), *ICAM-1* (Mm00516023_m1) with *18S* (Hs999999021_s1), *HPRT* (Mm00446968_m1), *Cyclophilin B* (Mm00478295_m), and *GAPDH* (4352339E) as endogenous controls. Relative quantities of target genes were calculated using the comparative threshold method ($\Delta\Delta C_t$) and experiments were performed in triplicate.

2.4. Intraperitoneal Glucose Tolerance Test (IP-GTT). BALB/c mice fasted for 16 hours followed by i.p. injection of glucose (2 g/kg body weight) or saline (vehicle). Blood glucose was

measured in whole venous blood from the tail vein (One-Touch glucometer, LifeScan, Inc., CA). Mice were euthanized 30 minutes or 6 hours after the glucose bolus, after which eyes were enucleated and retinas were dissected free and used for measurements of NFATc3 nuclear accumulation by confocal immunofluorescence microscopy or for measurements of luciferase activity as explained below, respectively.

2.5. Streptozotocin (STZ) Treatment. Mice were injected i.p. with STZ (60 mg/kg body weight in citrate buffer, pH 4.5) or vehicle (citrate buffer), once a day during 4 or 6 days, for NFAT-luc and BALB/c, respectively, as previously described [3]. Mice were weighed and glucose levels measured at various time points. NFAT-luc mice (control, diabetic, and diabetic treated with the NFAT blocker A-285222) were euthanized at different time points as specified in the results. BALB/c mice (control and diabetic with or without A-285222, resp.) were euthanized 4 weeks after the first STZ/vehicle injections.

2.6. Confocal Immunofluorescence. For measurements of NFATc3 nuclear accumulation, retinas and cerebral arteries from BALB/c mice were dissected in ice-cold Ca^{2+}-free PSS and treated *ex vivo* as described in Results section. Alternatively, retinas were fixed directly after IP-GTT. Whole retinas were fixed with Histochoice MB (AMRESCO Inc., Solon, OH), blocked and permeabilized with 2% BSA containing 0.2% Triton X-100 in PBS for 2 hours, and incubated with rabbit polyclonal anti-NFATc3 (1 : 100, Santa Cruz Biotechnology, Santa Cruz, CA) overnight at 4°C and with Cy5-anti-rabbit IgG (1 : 500, Jackson ImmunoResearch, West Grove, PA) for 2 hours at room temperature. Human umbilical vein endothelial cells (HUVEC; Gibco, Life Technologies Corp., Carlsbad, CA) and HRMVECs were grown on glass coverslips and stained with goat polyclonal anti-NFATc2 (Santa Cruz Biotechnology, Santa Cruz, CA) and with Cy5-anti-goat IgG (1 : 500, Jackson ImmunoResearch, West Grove, PA). Nuclei were stained with SYTOX Green. Cerebral arteries were processed as previously described [2, 3]. NFATc3 or NFATc2 and nuclear regions were detected by monitoring Cy5 and green fluorescence, respectively, on a Zeiss LSM 5 laser scanning confocal microscope. Images were obtained at 63x magnification and mean fluorescence intensity of nuclear NFATc3 or NFATc2 was quantified using the Zeiss LSM 5 analysis software as previously described [3, 7]. Orientation of the nuclei was used to distinguish endothelial from smooth muscle cells. For visualization of colocalized image regions or double tagged regions (red: NFATc3 tagged with Cy5 and green: nuclear regions tagged with SYTOX Green), the crosshair function of the LSM program was used. This tool leads to the distribution of all image pixels over 4 quadrants in a scattergram according to their intensity levels, with the background pixels sorted into the bottom left quadrant, the single-tagged pixels (either red or green) into the upper left and bottom right quadrants, and the pixels having an intensity above the background in both channels (i.e., colocalized pixels) represented by the upper right quadrant. The image pixels corresponding to the upper right quadrant are then color-coded white in the original image to allow fast identification of colocalized areas. Also, staining of retinal whole-mounts with antibodies against von Willebrand factor (1 : 400, DAKO), smooth muscle α-actin (1 : 400, Sigma), and platelet-derived growth factor β-receptor (PDGFRβ, 1 : 100, Santa Cruz) was performed to identify endothelial, smooth muscle cells and pericytes, respectively (see Supplementary Figure 1 in the Supplementary Material available online at http://dx.doi.org/10.1155/2015/428473). For quantification, multiple fields for each retina, vessels, or coverslips were imaged and analyzed under blind conditions.

2.7. Luciferase Reporter Assay. Luciferase activity was measured in intact retinas and in isolated retinal vessels as previously described [2, 7]; optical density was measured using a Tecan Infinite M200 instrument (Tecan Nordic AB, Mölndal, Sweden) and data was expressed as relative light units per microgram protein.

2.8. Cytokines in Plasma and Retina Homogenates. Cytokine concentrations were measured in plasma and retina homogenates using an inflammation 7-Plex kit (Meso Scale Discovery, Rockville, MD). The lower detection limits were within the range specified by the manufacturer. Plasma OPN was assayed using Quantikine Mouse OPN ELISA kit (R&D Systems, Abingdon, UK). Absorbance was measured at 450 nm and the lower limit of detection was 5.7 pg/mL. Plasma from $OPN^{-/-}$ mice [22] (kindly provided by Anna Hultgårdh, Lund University) was used as negative control.

2.9. Quantitative Assessment of Blood-Retinal Barrier Permeability. FITC-labelled albumin (45 mg/kg; Sigma) was administered i.v. and 1 hour later, mice were anesthetized, and a blood sample was collected from the left ventricle. Mice were perfused with PBS and euthanized by cardiac puncture. The fluorescence of retinal extracts and a 1 : 1000 dilution of plasma were measured at 485 nm (Ex) and 515 nm (Em). The concentration of FITC-albumin was calculated from a standard curve of FITC-labelled albumin in PBS and the blood-retinal barrier permeability was calculated as follows and was expressed as (μL/mg$*$hr/eye):

$$\frac{\text{FITC} - \text{albumin retina (mg)} / \text{Retina dry weight (mg)}}{[\text{FITC} - \text{albumin}] \text{ (mg)} / \text{Plasma (ul)} \times \text{Circulation time (h)}}. \quad (1)$$

2.10. Statistics. Results are expressed as means ± SEM unless otherwise specified. Statistical analysis was performed using GraphPad software (Prism 5.01). The use of parametric or nonparametric tests was based on results from analyses of distributions. Statistical significance was determined using Student's t-test; Kruskal-Wallis followed by Dunn's multiple comparison test for nonparametric data; or one- or two-way ANOVA as stated in the figure legends, followed by Bonferroni post hoc tests ($^{*}P < 0.05$, $^{**}P < 0.01$, and $^{***}P < 0.001$). Pearson's test was used for correlation analyses.

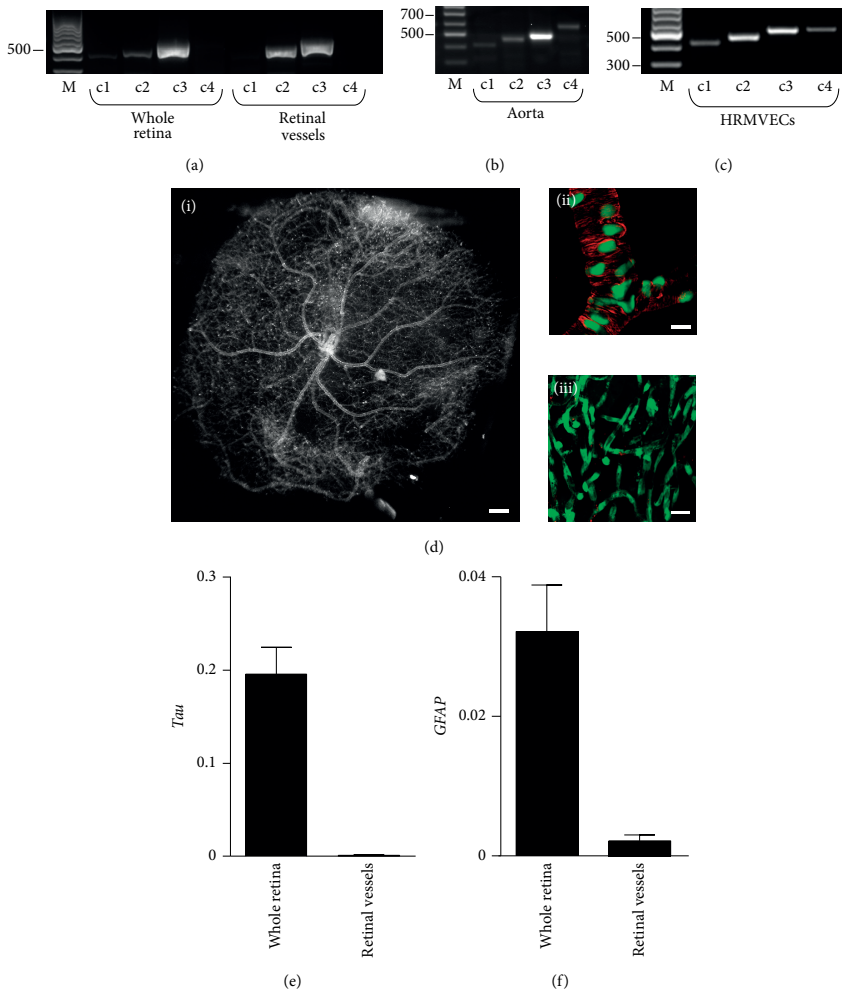

Figure 1: Expression of NFATc transcription factor genes in whole retina and in retinal microvessels. (a) RT-PCR analysis of NFAT isoform (c1–c4) expression in whole retinas and isolated retinal vessels from nondiabetic FVBN mice ($N = 8$). ((b)-(c)) All NFAT family members are expressed in mouse aorta (b) and in cultured human retinal microvascular endothelial cells (HRMVECs, (c)). Markers (M) for 300, 500, and 700 bp are indicated. (d)(i) Dark field/side illumination of a vascular network isolated from whole retina as described in material and methods (Section 2.2). (d)(ii) Confocal image showing smooth muscle α-actin positive staining (red) and nuclei (green) of an isolated retinal vessel preparation. Note the lack of surrounding nonvascular tissue (black background). (d)(iii) Confocal image of a smaller caliber vessel network stained as in (d)(ii) showing the absence of smooth muscle α-actin positive cells. Scale bars = 500 μm for (d)(i); 20 μm for (d)(ii)-(d)(iii). (e)-(f) Quantitative RT-PCR data showing expression levels of neuronal maker Tau (e) and glial marker GFAP (f) in whole retina and in isolated retinal vessels, both normalized to 18S. $N = 6$ retinas/group.

3. Results

3.1. Expression of NFATc Transcription Factors in Mouse Retina. RT-PCR was used to examine the expression of NFATc transcription factors in mouse retina. *NFATc2* and *NFATc3* were readily detected in whole retina from mouse, whereas expression of *NFATc1* was very low and of *NFATc4* very low to undetectable (Figure 1(a)). Using the same primer pairs as for retina, all four NFAT family members were detected in intact mouse aorta (Figure 1(b)) and in cultured human retinal microvascular endothelial cells (HRMVECs; Figure 1(c)). In intact mouse retinal vessels (Figure 1(d)),

virtually devoid of neuronal and glial cells (Figures 1(e)-1(f)), both *NFATc2* and *NFATc3* were detected (Figure 1(a)). Although the level of expression is not a determinant of transcription factor activity, we chose to focus on NFATc3, given that we previously established that this family member is glucose sensitive and activated in aorta and cerebral arteries in diabetic mice [2, 3, 9].

3.2. Acute Hyperglycemia Increases NFATc3 Nuclear Accumulation and NFAT-Dependent Transcriptional Activity in Retinal Microvessels. Raising the extracellular glucose concentration *ex vivo* from 2 mmol/L to 20 mmol/L for 30 min significantly increased NFATc3 nuclear accumulation in the endothelium of retinal vessels (Figures 2(a)-2(b)). Exposure to high glucose results in a 115% increase in mean fluorescence intensity of nuclear NFATc3 when compared to vessels incubated under low glucose conditions (Figure 2(c)). This increase was prevented by the NFAT blocker A-285222 (1 μmol) and also by the ectonucleotidase apyrase (3.6 U/mL), implicating extracellular nucleotides in the activation of NFATc3 (Supplementary Figures 2(a)-2(b)). Mannitol and L-glucose failed to induce NFATc3 nuclear accumulation, ruling out a possible osmotic effect of glucose and indicating that glucose needs to be metabolized in order to activate NFAT signaling (Supplementary Figures 2(c)-2(d)). For comparison, in Figure 2(d), a less dramatic NFATc3 activation is observed in the endothelium of mouse intact cerebral arteries after 30 min stimulation with HG, which was prevented by the NFAT blocker.

We have not been able to perform a quantitative analysis of NFATc2 activation in retinal whole-mounts due to substantial nonspecific binding of the antibodies tested, resulting in less reliable immunostaining. However, using HUVEC and HRMVECs, we have not seen any significant effect of glucose on NFATc2 nuclear accumulation (Supplementary Figure 3).

To test the effect of acute hyperglycemia on NFATc3 activation *in vivo*, i.p. glucose tolerance tests (IP-GTT) were performed and NFATc3 nuclear accumulation was determined in retinal vessels by confocal microscopy. Blood glucose levels were significantly higher in mice after the IP-GTT (Figure 3(a)), and this was accompanied by a 110% increase in mean fluorescence intensity of nuclear NFATc3 in the endothelium of mouse retinal microvessels (Figure 3(b)) compared to vehicle-injected mice. Levels of NFATc3 nuclear accumulation correlated with blood glucose concentrations ($r = 0.600$; $P = 0.017$). Nuclear accumulation of NFAT translated into increased NFAT-dependent transcriptional activity, as evidenced by significantly increased luciferase activity in isolated retinal vessels of transgenic NFAT-luc reporter mice after an IP-GTT (Figures 3(c)-3(d)). Interestingly, we could not detect any effect of acute hyperglycemia on NFAT-dependent transcriptional activity when measured in whole retina (Figure 3(e)), suggesting selective glucose-dependent activation of NFAT in the vascular retina.

3.3. Chronic Hyperglycemia Increases NFAT-Dependent Transcriptional Activity in Retinal Vessels in Two Different Models of Diabetes. NFAT-luc mice were injected with STZ or vehicle once a day for 4 days and euthanized one week after the last injection (day 12). At this time point, blood glucose levels were significantly elevated in diabetic mice when compared to controls (Figure 4(a)). This resulted in a 68% increase in NFAT-dependent transcriptional activity in isolated retinal microvessels (Figure 4(b)), which correlated with blood glucose ($r = 0.696$, $P = 0.037$). NFAT-luciferase activity was also measured in whole retinas at day 12, but no differences were observed between diabetic and control mice (Figure 4(c)), not even at earlier or later time points (days 7 and 16; data not shown). Akita mice have a single amino acid substitution in the insulin 2 gene that causes misfolding of the insulin protein, progressive loss of β-cell function, and significant hyperglycemia as early as 4-5 weeks of age [23]. In our hands, at 6 weeks of age Akita/NFAT-luc mice had significantly increased blood glucose levels compared to WT/NFAT-luc mice (Figure 4(d)) and this was accompanied by a 148% increase in luciferase activity in isolated retinal microvessels (Figure 4(e)). Together, these results demonstrate activation of NFAT signaling in retinal vessels in two different models of type 1 diabetes.

Table 1: A-285222 treatment does not affect plasma cytokine levels in diabetic NFAT-luc mice.

Cytokine (pg/mL)	Control ($N = 10$)	STZ ($N = 13$)	STZ + A-285222 ($N = 8$)
IL-10	22.0 ± 3.6	28.1 ± 7.0	29.4 ± 21.1
TNF-α	0.7 ± 0.3	0.6 ± 0.5	0.2 ± 0.5
IFN-γ	1.3 ± 1.3	1.2 ± 0.5	1.4 ± 0.8
IL-12p70	3.9 ± 5.5	8.2 ± 9.0	32.7 ± 56.2
IL-1β	1.0 ± 0.4	1.2 ± 0.5	1.1 ± 0.8
IL-6	13.3 ± 5.7	16.6 ± 5.8	25.0 ± 22.4
KC	51.4 ± 27.5	56.5 ± 17.7	64.1 ± 53.6

Data expressed as mean ± SD. Plasma cytokine levels (pg/mL) in control and STZ-treated NFAT-luc mice that had been treated with the NFAT inhibitor A-285222 (0.15 mg/kg/day) or saline, measured 2 weeks after the first STZ/vehicle injection. One-way ANOVA revealed no significant differences between groups. Interleukin- (IL-) 10, tumor necrosis factor- (TNF-) α, interferon- (IFN-) γ, IL-12p70, IL-1β, IL-6, and keratinocyte chemoattractant (KC) were measured using multiplex technology.

3.4. Effect of NFAT-Signaling Inhibition on Inflammatory Cytokines and Endothelial Activation. Nondiabetic (control) and STZ-induced diabetic NFAT-luc mice received daily i.p. injections of the NFAT blocker A-285222 (0.15 mg/kg body weight) or vehicle and were euthanized 16 days after the first injections. Diabetes resulted in significantly reduced levels of the anti-inflammatory cytokine IL-10 in whole-retina homogenates, which were completely restored in mice treated with A-285222 (Figure 5(a)). Blood glucose levels were significantly higher in STZ-treated mice when compared to control mice (Figure 5(b)) but were not affected by treatment with A-285222 (Figure 5(b)). The levels of other cytokines such as IFN-γ, IL-12p70, IL-1β, IL-6, GROα/keratinocyte-derived chemokine (KC), and TNFα in whole-retina homogenates were not significantly affected by diabetes or treatment with A-285222 (Figures 5(c)–5(h)). When the same cytokines were examined in plasma, no differences were detected between diabetic mice treated with or without A-285222 (Table 1),

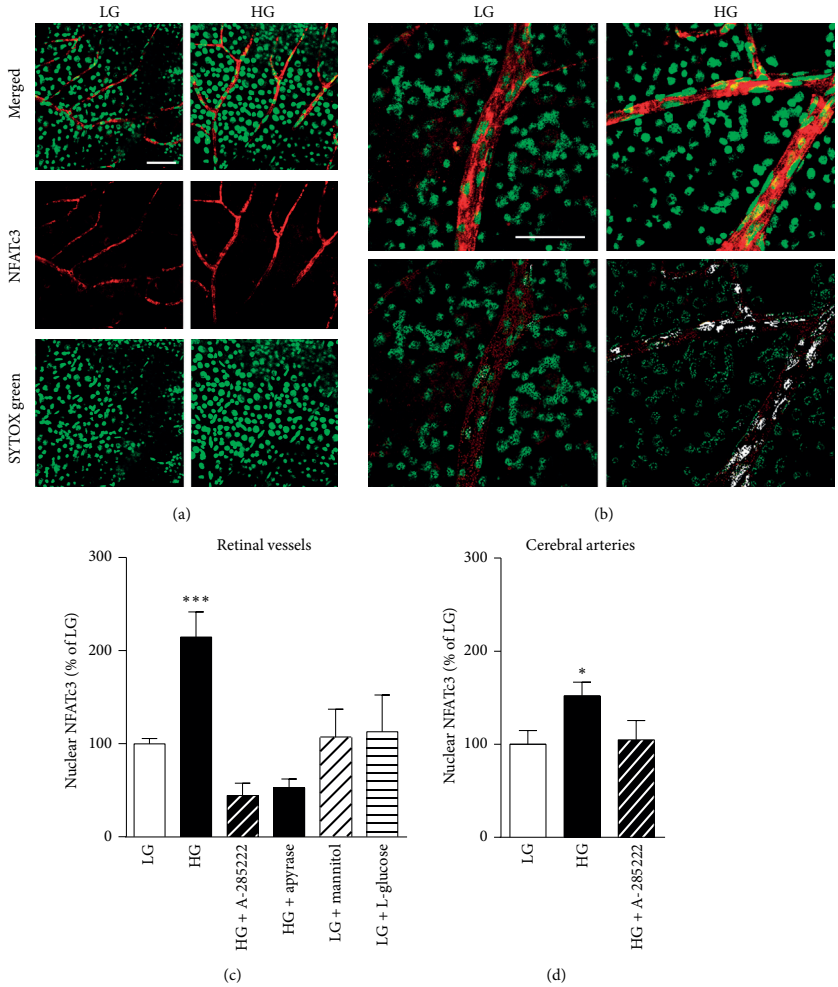

Figure 2: High glucose activates NFATc3 in the endothelium of retinal vessels. (a) Representative confocal immunofluorescence images of retinal whole-mounts, stimulated for 30 min in low (LG; 2 mmol/L; left panels) or high (HG; 20 mmol/L; right panels) extracellular glucose and stained for NFATc3 (red) and SYTOX green for identification of nuclei (green). Merged and individual channel images are shown. Endothelial cells were identified by the orientation of their nuclei. (b) Higher magnification confocal images of retinal whole-mounts stimulated and stained as in ((a), upper panels) and pseudocolored images to visualize colocalization of NFATc3 and SYTOX green (white; lower panels). Scale bars = 50 μm. (c) Summarized mean fluorescence intensity data from experiments as in (a), showing NFATc3 nuclear accumulation after 30 min stimulation in LG or HG in the presence or absence of A-285222 (1 μmol), or apyrase (3.6 U/mL), or after stimulation with LG plus mannitol (18 mmol/L), or LG plus L-glucose (18 mmol/L). $N = 21$ and 22 retinas for LG and HG, respectively; 5–7 retinas for the other stimulatory conditions. $^{***}P < 0.001$ versus all other groups. (d) Summarized mean fluorescence intensity data showing NFATc3 nuclear accumulation in mouse cerebral arteries after 30 min stimulation in LG or HG in the presence or absence of A-285222 (1 μmol). $N = 5$/group. $^{*}P < 0.05$ versus LG.

suggesting that the effect on retinal IL-10 is local, rather than systemic.

In a separate set of experiments using BALB/c mice and contrary to expectations, one month after the first STZ injection we did not detect enhanced *OPN* or *ICAM-1* mRNA in the retinal vessels of diabetic mice (Figures 6(a)-6(b)). OPN levels in the aortas of these same diabetic mice were elevated when compared to controls [3], suggesting

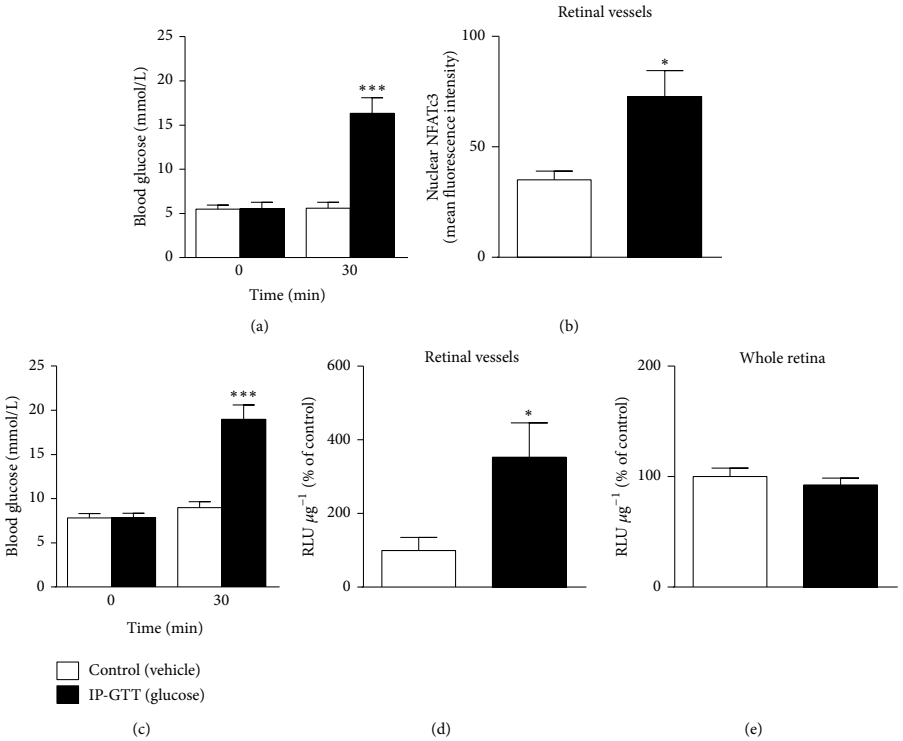

Figure 3: Acute hyperglycemia increases NFATc3 nuclear accumulation and NFAT-dependent transcriptional activity in retinal microvessels. (a) Blood glucose levels measured before and 30 min after an i.p. injection of glucose (2 g/kg; IP-GTT, black bars) or saline (control, white bars) in BALB/c mice, $N = 7$-8 mice/group. (b) Summarized data from confocal immunofluorescence experiments in the mice described in (a), showing increased NFATc3 nuclear accumulation in the retinal endothelium of hyperglycemic mice when compared to controls. (c) Blood glucose levels measured before and 30 min after an i.p. injection of glucose (2 g/kg; IP-GTT, black bars) or saline (control, white bars) NFAT-luc mice. (d)-(e) NFAT-dependent transcriptional activity in isolated retinal vessels (d) and whole retinas (e) in the NFAT-luc mice described in (c) measured 6 hours after i.p. injection of glucose or saline. Relative light units (RLU) in (d) and (e) were normalized to protein content and expressed as percentage of vehicle-treated control. $N = 7$–12 mice/group. $^{*}P < 0.05$ and $^{***}P < 0.001$ versus normoglycemic control group.

differential regulation of OPN expression depending on the vascular bed. Similar to what we observed in retinal vessels from BALB/c mice, neither *OPN* mRNA in retinal vessels (Supplementary Figure 4(a)) nor OPN protein levels in whole-retina homogenates (data not shown) were changed in NFAT-luc mice after 2 weeks of diabetes. Furthermore, *OPN* mRNA in retinal vessels of Akita mice was not changed (Supplementary Figure 4(b)). STZ-induced diabetes in hyperlipidemic *Apoe*$^{-/-}$ mice, on the other hand, resulted in a 2.1-fold increase in *OPN* mRNA in retinal vessels, 8 weeks after the first STZ injection (Supplementary Figure 4(c)), highlighting potential differences in the regulation of OPN depending on mice strain, duration of diabetes, and/or blood lipid levels. Despite the lack of diabetes-induced *OPN* and *ICAM-1* expression in BALB/c mice, daily injections with A-285222 lowered the levels of *OPN* and *ICAM-1* mRNA (Figures 6(a)-6(b)). No changes in plasma levels of OPN, IL-10, TNFα, IL-12p70, IL-1β, IL-6, and KC were observed in response to diabetes or NFAT inhibition; however plasma IFN-γ was reduced in diabetic animals that had been treated with A-285222 (Supplementary Table S1).

3.5. In Vivo Inhibition of NFAT Reduces Diabetes-Induced Vascular Permeability. Vascular permeability was measured in the retinas of 8-week-old Akita and WT mice that had been treated with i.p. injections of A-285222 or saline (control) for 2 weeks. Mean blood glucose was 10.0 mmol/L and 18.5 mmol/L for control and Akita mice, respectively. Vascular permeability was increased 2.1-fold in diabetic versus control mice (Figure 7). Inhibition of NFAT signaling with A-285222 completely abrogated the diabetes-induced permeability (Figure 7).

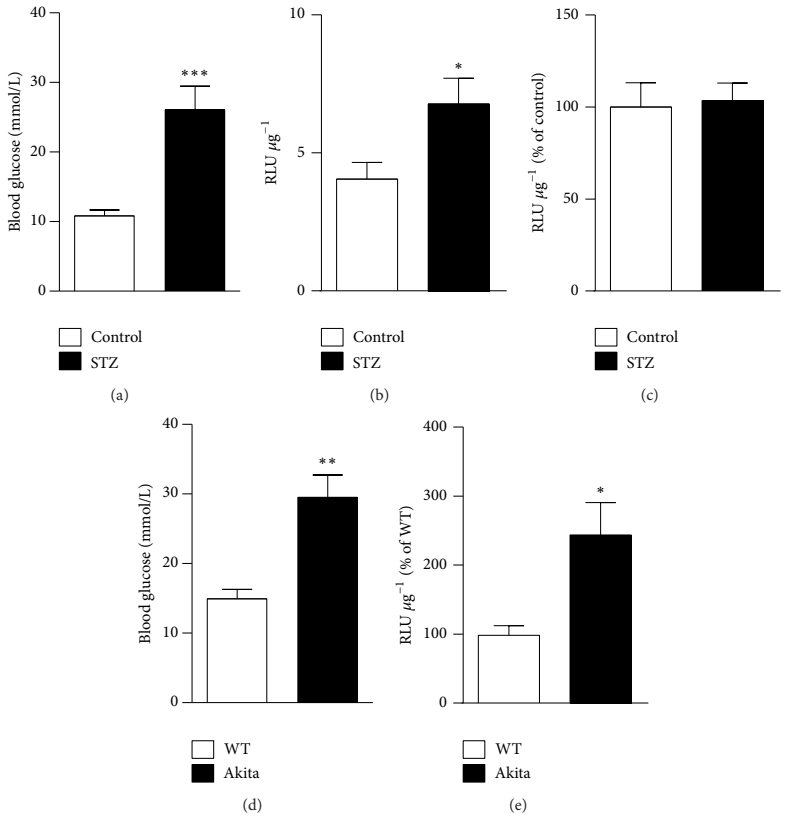

Figure 4: Chronic hyperglycemia increases NFAT-dependent transcriptional activity in retinal vessels from two different mouse models of diabetes. (a) Blood glucose levels in NFAT-luc mice, treated with STZ (60 mg/kg; black bars) or vehicle (citrate buffer; white bars), measured 12 days after the first injection. (b) NFAT-dependent transcriptional activity (RLU μg^{-1}) in isolated retinal vessels (N = 6-7 mice/group) and (c) in whole retinas (N = 4–7) from the mice in (a). Data is expressed as percentage of activity in normoglycemic control mice. (d) Blood glucose levels in Akita/NFAT-luc mice (black bars) and WT/NFAT-luc mice (white bars) at 6 weeks of age. (e) NFAT-dependent transcriptional activity (RLU μg^{-1}) in isolated retinal vessels from the same mice as in (d). Data is expressed as percentage of activity in WT control mice. N = 11–15 mice/group. $^{*}P < 0.05$; $^{**}P < 0.01$; and $^{***}P < 0.001$ versus corresponding normoglycemic control groups.

4. Discussion

In this study we show that mouse retinal vessels express NFATc3 and that this transcription factor is sensitive to changes in extracellular glucose levels. In two mouse models of diabetes, STZ-induced, and Akita mice, diabetes results in increased NFAT-dependent transcriptional activity in retinal vessels. Interestingly, levels of the potent anti-inflammatory cytokine IL-10 were decreased in the retina of diabetic mice and these were restored by treatment with the NFAT blocker A-285222 for 2 weeks. The effects on retinal IL-10 were achieved without any impact on blood glucose or on the levels of circulating plasma cytokines (IL-10, IFN-γ, IL-12p70, IL-1β, IL-6, KC, and TNFα). Moreover, inhibition of NFAT for 4 weeks resulted in decreased expression of basal *OPN* and *ICAM-1* mRNA levels in retinal vessels. We also demonstrate that inhibition of NFAT abrogates the increased vascular permeability observed in diabetic Akita mice. Therefore, we suggest that NFAT inhibition may exert a protective effect in the retina of diabetic mice.

The pattern of expression of *NFATc* transcription factors seems to vary depending on the vascular bed, with arteries such as the aorta that express all NFATc family members (Figure 1(c)), myometrial arteries expressing *NFATc1*, *NFATc3,* and *NFATc4* [7], or cerebral arteries which express *NFATc3* and *NFATc4* [24]. NFAT transcription factors were initially considered to have redundant functions, but differential activation of NFAT proteins within a cell [25] and varied expression profiles among cell types have been observed, suggesting functions specific to the different NFAT

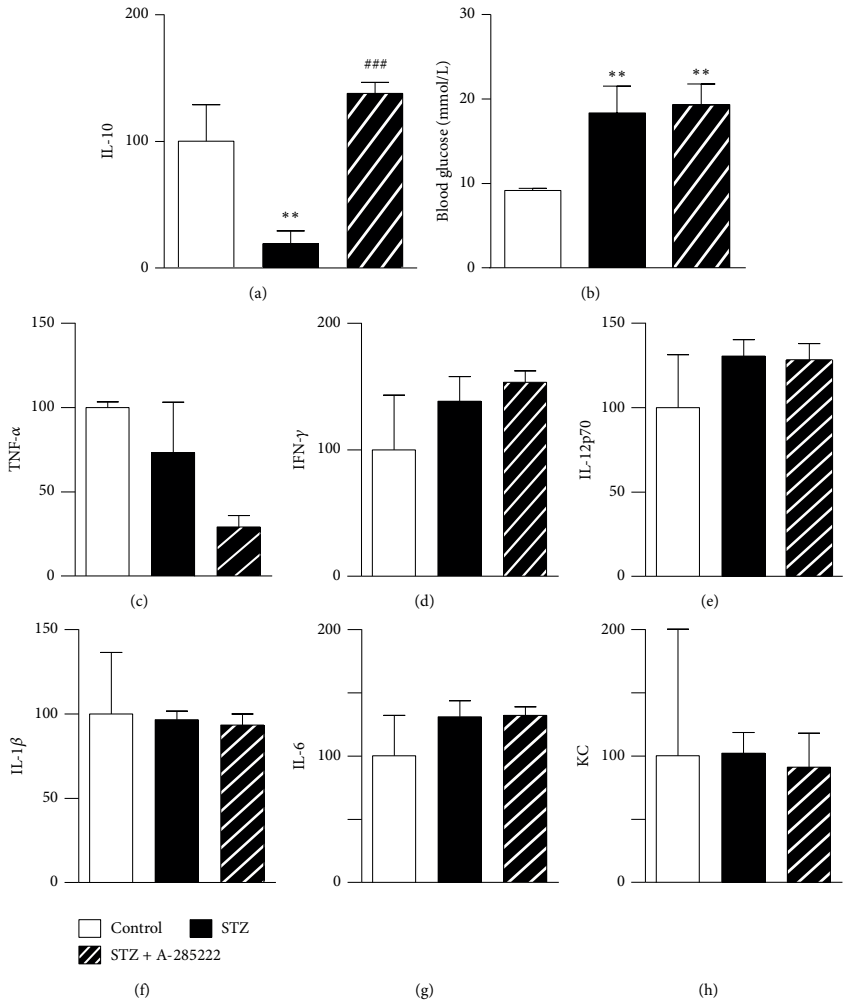

Figure 5: *In vivo* inhibition of NFAT restores levels of anti-inflammatory IL-10 in the retina of diabetic mice. (a) Levels of IL-10 in whole-retina homogenates from NFAT-luc mice, treated with STZ (60 mg/kg) or vehicle (citrate buffer). Mice received daily i.p. injections of A-285222 (0.15 mg/kg) or vehicle (saline) for two weeks ($N = 2, 7$, and 9 for control, STZ, and STZ + A-285222, resp.). $^{**}P < 0.01$ versus control and $^{###}P < 0.001$ versus STZ. (b) Blood glucose levels in mice treated as in (a) ($^{**}P < 0.01$ versus control; $N = 7$–12 mice/group). (c)–(h) TNFα, IFN-γ, IL-12p70, IL-1β, IL-6, and KC levels were determined in whole-retina homogenates from the same mice as in (a). Cytokines levels were normalized to protein content and are expressed as percentage of control. No significant differences were observed between the groups.

family members. In the intact mouse retina, all four isoforms could be detected, whereas in isolated retinal vessels only *NFATc2* and *NFATc3* were demonstrated. This suggests that NFATc1 and NFATc4 may be of neuronal origin [26, 27] or may be upregulated in culture, given that primary retinal endothelial cells expressed all four isoforms. Our previous work in conduit and resistance arteries focused on the effects of glucose on NFATc3 in vascular smooth muscle cells [2], but here we show that endothelial NFATc3 seems to be sensitive to changes in extracellular glucose as well. NFATc2, on the other hand, did not seem sensitive to glucose, at least in cells (Supplementary Figure 2).

Diabetes is characterized by both sustained hyperglycemia and acute glucose fluctuations. There is cogent evidence for the deleterious effects of sustained hyperglycemia, but the role of glucose variability is less well documented

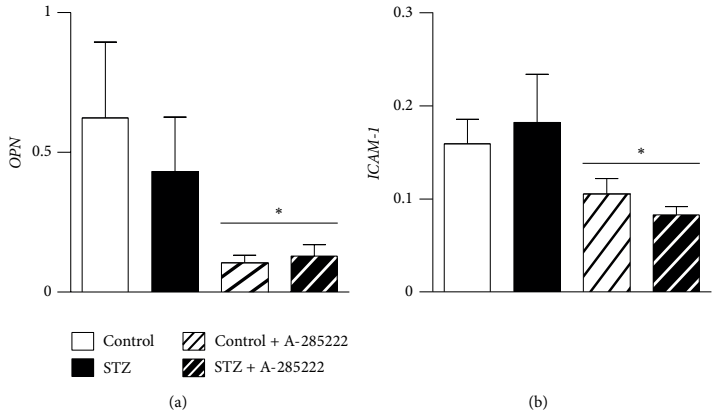

Figure 6: *In vivo* inhibition of NFAT reduces the expression of *OPN* and *ICAM-1* in retinal vessels. mRNA expression of (a) OPN and (b) *ICAM-1* in isolated retinal vessels from BALB/c mice treated with STZ (60 mg/kg) or vehicle (citrate buffer). Mice received for 4 weeks daily i.p. injections of A-285222 (0.29 mg/kg for 2 weeks followed by 0.15 mg/kg until termination) or vehicle (saline). Expression levels were determined by quantitative RT-PCR and *HPRT* was used as endogenous control. $N = 7$-8 mice/group. Two-way ANOVA revealed a significant effect of A-285222 on *OPN* and *ICAM-1* expression; $^{*}P < 0.05$.

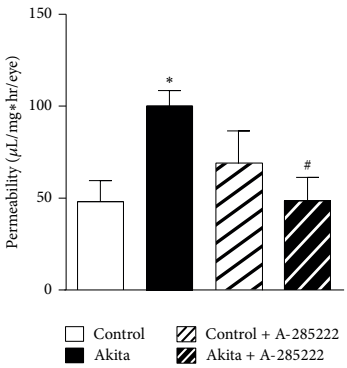

Figure 7: *In vivo* inhibition of NFAT reduces diabetes-induced vascular permeability. Vascular permeability (μL/mg$*$hr/eye) in the retinas of 8-week-old Akita mice and WT mice that had been treated for 2 weeks with daily i.p. injections of A-285222 (0.29 mg/kg) or saline (control). $N = 8$, 10, 7, and 7 for WT, Akita, WT + A-285222, and Akita + A-285222, respectively. Two-way ANOVA with Bonferroni post hoc test revealed $^{*}P < 0.05$ versus WT and $^{\#\#}P < 0.05$ versus Akita.

[28]. To our knowledge, nothing is known regarding the effect of glycemic peaks and nadirs on transcriptional activity in intact arteries. In mice, blood glucose reaches a maximum value upon a single IP-GTT after 30 minutes and returns to control levels after 120 minutes [29]. The results from this study show that acute elevations in blood glucose, as those induced by IP-GTT, efficiently induced NFAT nuclear accumulation and NFAT-dependent transcriptional activity in retinal vessels. Sustained hyperglycemia in STZ-treated mice resulted in increased NFAT transcriptional activity in retinal vessels. In contrast, NFAT transcriptional activity in whole retinas was not changed after an IP-GTT or after sustained hyperglycemia, suggesting different activation requirements of NFAT proteins in the nonvascular retina. Results also emphasize the importance of isolating retinal vessels rather than using whole-retina preparations for the study of pathological changes in the microvasculature.

The contribution of different cell types in the retina, as well as the chronology of events in the pathogenesis of DR, is still a matter of debate [6, 30, 31]. However, accumulating evidence suggests that localized inflammatory processes play a role in the early phases of DR [6], including increased expression of adhesion molecules, cytokines, and growth factors. For cytokine level quantification we chose a multiplex assay designed to measure IL-10, IFN-γ, IL-12p70, IL-1β, IL-6, KC, and TNFα. Except for KC, all of these cytokines have been implicated in the pathogenesis of human diabetic retinopathy [32–41]. In our study, 2 or 4 weeks of STZ-induced diabetes had no significant effect on the levels of circulating cytokines, despite the fact that animals had significantly higher blood glucose levels. The reason why this model fails to affect plasma cytokines as it could be predicted from previous studies may be due to differences between species. Rodents and in particular mice are known to be resilient to hyperglycemia-induced changes and only mimic early stages of diabetic retinopathy [42]. The plasma cytokine results presented here for FVBN and BALB/c mice are however in line with previous data obtained in C57BL/6, where we showed that 8 weeks of STZ-induced diabetes does not increase the levels of circulating inflammatory cytokines

[43]. Treatment with A-285222 for 2 weeks had no effect on plasma cytokine levels, but 4-week treatment significantly reduced plasma IFN-γ concentration in diabetic animals (Table S1).

To better resolve potential local changes in cytokine production in the retina, we measured the same cytokines in retina homogenates. In the STZ-mouse model of diabetes that we used here, 2 weeks of diabetes resulted in decreased levels of IL-10. The same results were obtained after 4 weeks of diabetes in other strains (FVBN and BALB/c; data not shown). This cytokine is produced by numerous immune cells (i.e., T-helper cells, regulatory T cells, B cells, monocytes, macrophages, and dendritic cells [44]) and plays a central nonredundant role in limiting inflammation *in vivo* [45]. Also local production of endogenous IL-10 has been suggested to limit angiotensin-II-induced oxidative stress and vascular dysfunction in mouse carotid arteries [46]. Our results demonstrate that *in vivo* treatment for 2 weeks with A-285222 restores IL-10 levels, suggesting that NFAT inhibition may be protective for the retina. Apart from IL-10, no other changes in cytokine levels in retina or in the expression of *ICAM-1* mRNA in retinal vessels were observed in response to diabetes, at least at these early time points and in these mice strains. This contrasts with previous findings in C57Bl/6 mice at later time points after 8 weeks of diabetes, in which we were able to detect increased *ICAM-1* mRNA in retinal vessels and enhanced levels of *TNF*α, *IL-6,* and *IL-1*β mRNA in whole-retina homogenates [21].

We have recently shown that hyperglycemia induces the proinflammatory cytokine OPN in mouse aorta by direct binding of NFATc3 to the OPN promoter [3]. OPN protein was increased in subvalvular aortic sections and in plasma of STZ-treated diabetic mice 8 weeks after the onset of hyperglycemia [3]. OPN has been reported to be increased in the vitreous of patients with DR compared to nondiabetic patients [47] and in retinal endothelial cells after *in vitro* stimulation with high glucose, resulting in enhanced endothelial cell migration [48]. However, in the STZ-model used here, no changes in the expression of *OPN* in retinal vessels were observed at early time points, after 2 or 4 weeks of diabetes. Hyperglycemia in Akita mice also failed to induce *OPN* expression. In contrast, a 2.1-fold increase in retinal microvessel *OPN* mRNA was observed in hyperlipidemic $Apoe^{-/-}$ mice at 8 weeks after the first STZ injection, indicating that diabetes duration or metabolic state is of importance for regulation of OPN in retinal microvessels. However, despite the lack of diabetes-induced OPN expression in BALB/c mice after 4 weeks of diabetes, in agreement with previous results in larger vessels [3], *in vivo* NFAT-inhibition for the duration of the experiment reduced the levels of OPN mRNA in retinal vessels regardless of the diabetic condition, indicating a potential NFAT-dependent regulation of OPN under basal conditions in this tissue. NFAT inhibition also reduced *ICAM-1* mRNA levels in retinal microvessels, highlighting a potential mechanism by which NFAT inhibition may prevent leukostasis and inflammation in diabetic retinopathy.

An early feature of diabetic retinopathy is the breakdown of the BRB which results in vascular leakage and development of retinal edema. Clinical evidence from fluorescein angiography in patient with diabetic retinopathy indicates that the inner BRB, which is formed by junctions between endothelial cells of the retinal capillaries, is the primary site of vascular leakage. In agreement with previous studies [49], we demonstrate that increased vascular leakage is an early event in Akita mice. The fact that *in vivo* treatment with A-285222 for 2 weeks prevented diabetes-induced changes in retinal permeability suggests NFAT signaling to play a role in the regulation of the BRB. In diabetes, increased BRB permeability is associated with reduced expression of tight junction (claudin-5, ZO-1, and occludin) and adherens (VE-cadherin) proteins [50]. Interestingly, a high number of NFAT consensus binding sites were found in the promoter region of claudin-5 (26 sites), theoretically making it a possible direct target of NFAT regulation.

A-285222 is a low molecular weight (416 daltons) organic compound [51]. Given its lipophilic nature and small size, it crosses both the plasma membrane and the nuclear envelope by simple diffusion. We have previously studied the pharmacokinetics of A-285222 after i.p. administration in mice using gas chromatography/mass spectroscopy (GC/MS) [9]. A comparison between plasma levels of A-285222 measured 5 min after i.p. injection of the drug and after direct injection into the circulation (intracardiac) showed that levels were within the same range regardless of administration route, indicating high bioavailability and confirming transport across several membranes. Studies in cynomolgus monkeys also confirm the cell-permeable nature of the compound, as A-285222 was readily detected in plasma after oral administration [52]. As a cell-permeable compound A-285222 is expected to reach the retinal circulation and enter the cells in the vessel wall. The effects of treatment on vascular permeability could therefore be due to direct effects of A-285222 on vascular NFATc3 activation; however, indirect effects cannot be ruled out.

In conclusion, these results suggest that NFAT acts as a glucose-sensor in the wall of retinal microvessels, translating changes in extracellular glucose concentration into changes in gene expression leading to enhanced inflammation, endothelial activation, and vascular permeability. Even though tight blood glucose and blood pressure control are key in preventing and/or slowing down the development of diabetic macular edema and retinopathy, these are therapeutic goals difficult to achieve. Standard of care still relies on laser photocoagulation and intravitreal injections of corticosteroids or more recently anti-VEGF but these are invasive procedures that can have complications [53]. Therefore, new approaches beyond current standards of diabetes care are necessary. Here, we have identified the NFAT signaling as a putative target for treatment of microvascular complications in diabetes.

Conflict of Interests

The authors declare that there is no conflict of interests regarding the publication of this paper.

Authors' Contribution

Anna V. Zetterqvist designed and performed experiments, analyzed the data, and wrote and edited the paper. Fabiana Blanco designed and performed experiments and analyzed the data; Jenny Öhman designed and performed experiments, analyzed the data, and contributed to the writing of the paper; Olga Kotova performed experiments and analyzed the data; Lisa M. Berglund designed and performed experiments and analyzed the data; and Sergio de Frutos Garcia and Raed Al-Naemi performed experiments and analyzed the data. Maria Wigren performed experiments. Paul G. McGuire and Laura V. Gonzalez Bosc designed and performed experiments and analyzed the data. Maria F. Gomez conceived, designed, and performed experiments, analyzed the data, wrote and edited the paper, and supervised the project. All authors read and approved the final version of the paper. Maria F. Gomez is the guarantor of this work and, as such, had full access to all the data in the study and takes the responsibility for the integrity of the data and the accuracy of the data analysis.

Acknowledgments

The authors would like to thank Bodil Israelsson and Ann-Helen Thorén-Fischer, both of the Department of Clinical Sciences, Lund University, for skillful technical assistance; and Dr. Faisel Khan, University of Dundee for valuable discussions. This work was supported by the Swedish Heart and Lung Foundation (HLF20080843; HLF20100532); the Swedish Research Council (no. 2009-4120; no. 2011-3900; no. 2009-1039), British Heart Foundation, Lund University Diabetes Centre, the Swedish Medical Society; the Swedish Society for Medical Research, the Royal Physiographic Society in Lund, Skåne Hospital Research Funds, the Vascular Wall Programme at Lund University, and Crafoord; Albert Påhlsson; Lars Hierta Memorial; Edla and Eric Smedberg; Knut & Alice Wallenberg Foundations; and an award from the Health Sciences Center Research Allocation Committee (HSC RAC) from the University of New Mexico. It was supported also by Innovative Medicines Initiative Joint Undertaking (no. 115006), comprising funds from the European Union's Seventh Framework Programme (FP7/2007–2013) and EFPIA companies in kind contribution.

References

[1] M. Brownlee, "Biochemistry and molecular cell biology of diabetic complications," *Nature*, vol. 414, no. 6865, pp. 813–820, 2001.

[2] J. Nilsson, L. M. Nilsson, Y.-W. Chen, J. D. Molkentin, D. Erlinge, and M. F. Gomez, "High glucose activates nuclear factor of activated T cells in native vascular smooth muscle," *Arteriosclerosis, Thrombosis, and Vascular Biology*, vol. 26, no. 4, pp. 794–800, 2006.

[3] L. M. Nilsson-Berglund, A. V. Zetterqvist, J. Nilsson-Öhman et al., "Nuclear factor of activated T cells regulates osteopontin expression in arterial smooth muscle in response to diabetes-induced hyperglycemia," *Arteriosclerosis, Thrombosis, and Vascular Biology*, vol. 30, no. 2, pp. 218–224, 2010.

[4] H. Kawamura, T. Sugiyama, D. M. Wu et al., "ATP: a vasoactive signal in the pericyte-containing microvasculature of the rat retina," *The Journal of Physiology*, vol. 551, no. 3, pp. 787–799, 2003.

[5] G. Costa, T. Pereira, A. M. Neto, A. J. Cristóvão, A. F. Ambrósio, and P. F. Santos, "High glucose changes extracellular adenosine triphosphate levels in rat retinal cultures," *Journal of Neuroscience Research*, vol. 87, no. 6, pp. 1375–1380, 2009.

[6] T. S. Kern, "Contributions of inflammatory processes to the development of the early stages of diabetic retinopathy," *Experimental Diabetes Research*, vol. 2007, Article ID 95103, 14 pages, 2007.

[7] L. M. Nilsson, Z.-W. Sun, J. Nilsson et al., "Novel blocker of NFAT activation inhibits IL-6 production in human myometrial arteries and reduces vascular smooth muscle cell proliferation," *The American Journal of Physiology—Cell Physiology*, vol. 292, no. 3, pp. C1167–C1178, 2007.

[8] M. Y. Lee, S. M. Garvey, A. S. Baras et al., "Integrative genomics identifies DSCR1 (RCAN1) as a novel NFAT-dependent mediator of phenotypic modulation in vascular smooth muscle cells," *Human Molecular Genetics*, vol. 19, no. 3, pp. 468–479, 2009.

[9] A. V. Zetterqvist, L. M. Berglund, F. Blanco et al., "Inhibition of nuclear factor of activated T-cells (NFAT) suppresses accelerated atherosclerosis in diabetic mice," *PLoS ONE*, vol. 8, no. 6, Article ID e65020, 2013.

[10] B. A. Hesser, X. H. Liang, G. Camenisch et al., "Down syndrome critical region protein 1 (DSCR1), a novel VEGF target gene that regulates expression of inflammatory markers on activated endothelial cells," *Blood*, vol. 104, no. 1, pp. 149–158, 2004.

[11] A. W. Orr, M. Y. Lee, J. A. Lemmon et al., "Molecular mechanisms of collagen isotype-specific modulation of smooth muscle cell phenotype," *Arteriosclerosis, Thrombosis, and Vascular Biology*, vol. 29, no. 2, pp. 225–231, 2008.

[12] D. S. McLeod, D. J. Lefer, C. Merges, and G. A. Lutty, "Enhanced expression of intracellular adhesion molecule-1 and P-selectin in the diabetic human retina and choroid," *The American Journal of Pathology*, vol. 147, no. 3, pp. 642–653, 1995.

[13] J. Cunha-Vaz, J. R. Faria de Abreu, A. J. Campos, and G. M. Figo, "Early breakdown of the blood retinal barrier in diabetes," *British Journal of Ophthalmology*, vol. 59, no. 11, pp. 649–656, 1975.

[14] D. A. Antonetti, A. J. Barber, L. A. Hollinger, E. B. Wolpert, and T. W. Gardner, "Vascular endothelial growth factor induces rapid phosphorylation of tight junction proteins occludin and zonula occluden 1. A potential mechanism for vascular permeability in diabetic retinopathy and tumors," *The Journal of Biological Chemistry*, vol. 274, no. 33, pp. 23463–23467, 1999.

[15] A. Cerani, N. Tetreault, C. Menard et al., "Neuron-derived semaphorin 3A is an early inducer of vascular permeability in diabetic retinopathy via neuropilin-1," *Cell Metabolism*, vol. 18, no. 4, pp. 505–518, 2013.

[16] G. L. Hernández, O. V. Volpert, M. A. Íñiguez et al., "Selective inhibition of vascular endothelial growth factor-mediated angiogenesis by cyclosporin A: roles of the nuclear factor of activated T cells and cyclooxygenase 2," *Journal of Experimental Medicine*, vol. 193, no. 5, pp. 607–620, 2001.

[17] C. A. Bretz, S. Savage, M. Capozzi, and J. S. Penn, "The role of the NFAT signaling pathway in retinal neovascularization," *Investigative Ophthalmology & Visual Science*, vol. 54, no. 10, pp. 7020–7027, 2013.

[18] W. Dong, Y. Li, X. Li et al., "P85alpha mediates NFAT3-dependent VEGF induction in the cellular UVB response," *Journal of Cell Science*, vol. 126, no. 6, pp. 1317–1322, 2013.

[19] M. Jinnin, D. Medici, L. Park et al., "Suppressed NFAT-dependent VEGFR1 expression and constitutive VEGFR2 signaling in infantile hemangioma," *Nature Medicine*, vol. 14, no. 11, pp. 1236–1246, 2008.

[20] B. J. Wilkins, Y.-S. Dai, O. F. Bueno et al., "Calcineurin/NFAT coupling participates in pathological, but not physiological, cardiac hypertrophy," *Circulation Research*, vol. 94, no. 1, pp. 110–118, 2004.

[21] C. Gustavsson, C.-D. Agardh, A. V. Zetterqvist, J. Nilsson, E. Agardh, and M. F. Gomez, "Vascular cellular adhesion molecule-1 (VCAM-1) expression in mice retinal vessels is affected by both hyperglycemia and hyperlipidemia," *PLoS ONE*, vol. 5, no. 9, Article ID e12699, 2010.

[22] A. Strom, A. Franzen, C. Wangnerud et al., "Altered vascular remodeling in osteopontin-deficient atherosclerotic mice," *Journal of Vascular Research*, vol. 41, no. 4, pp. 314–322, 2004.

[23] A. J. Barber, D. A. Antonetti, T. S. Kern et al., "The Ins2Akita mouse as a model of early retinal complications in diabetes," *Investigative Ophthalmology and Visual Science*, vol. 46, no. 6, pp. 2210–2218, 2005.

[24] M. F. Gomez, L. V. G. Bosc, A. S. Stevenson, M. K. Wilkerson, D. C. Hill-Eubanks, and M. T. Nelson, "Constitutively elevated nuclear export activity opposes Ca^{2+}-dependent NFATc3 nuclear accumulation in vascular smooth muscle: role of JNK2 and Crm-1," *Journal of Biological Chemistry*, vol. 278, no. 47, pp. 46847–46853, 2003.

[25] A. Rinne, K. Banach, and L. A. Blatter, "Regulation of nuclear factor of activated T cells (NFAT) in vascular endothelial cells," *Journal of Molecular and Cellular Cardiology*, vol. 47, no. 3, pp. 400–410, 2009.

[26] E. O. Hernández-Ochoa, M. Contreras, Z. Cseresnyés, and M. F. Schneider, "Ca^{2+} signal summation and NFATc1 nuclear translocation in sympathetic ganglion neurons during repetitive action potentials," *Cell Calcium*, vol. 41, no. 6, pp. 559–571, 2007.

[27] Y. Xu, L. Yang, S. Yu et al., "Spatiotemporal changes in NFATc4 expression of retinal ganglion cells after light-induced damage," *Journal of Molecular Neuroscience*, vol. 53, no. 1, pp. 69–77, 2014.

[28] L. Monnier and C. Colette, "Glycemic variability: should we and can we prevent it?" *Diabetes Care*, vol. 31, no. supplement 2, pp. S150–S154, 2008.

[29] E. P. Kwan, L. Xie, L. Sheu et al., "Munc13-1 deficiency reduces insulin secretion and causes abnormal glucose tolerance," *Diabetes*, vol. 55, no. 5, pp. 1421–1429, 2006.

[30] E. L. Fletcher, J. A. Phipps, M. M. Ward, T. Puthussery, and J. L. Wilkinson-Berka, "Neuronal and glial cell abnormality as predictors of progression of diabetic retinopathy," *Current Pharmaceutical Design*, vol. 13, no. 26, pp. 2699–2712, 2007.

[31] J. Cunha-Vaz, "Characterization and relevance of different diabetic retinopathy phenotypes," *Developments in Ophthalmology*, vol. 39, pp. 13–30, 2007.

[32] M. G. Petrovič, P. Korošec, M. Košnik, and M. Hawlina, "Vitreous levels of interleukin-8 in patients with proliferative diabetic retinopathy," *The American Journal of Ophthalmology*, vol. 143, no. 1, pp. 175–176, 2007.

[33] A. M. A. El-Asrar, L. Missotten, and K. Geboes, "Expression of hypoxia-inducible factor-1α and the protein products of its target genes in diabetic fibrovascular epiretinal membranes," *British Journal of Ophthalmology*, vol. 91, no. 6, pp. 822–826, 2007.

[34] Y. Wakabayashi, Y. Usui, Y. Okunuki et al., "Increased levels of monokine induced by interferon-gamma (Mig) in the vitreous of patients with diabetic retinopathy," *Diabetic Medicine*, vol. 25, no. 7, pp. 875–877, 2008.

[35] M. Myśliwiec, K. Zorena, A. Balcerska, J. Myśliwska, P. Lipowski, and K. Raczyńska, "The activity of N-acetyl-beta-d-glucosaminidase and tumor necrosis factor-alpha at early stage of diabetic retinopathy development in type 1 diabetes mellitus children," *Clinical Biochemistry*, vol. 39, no. 8, pp. 851–856, 2006.

[36] K. Zorena, J. Myśliwska, M. Myśliwiec, A. Balcerska, P. Lipowski, and K. Raczyńska, "Interleukin-12 and tumour necrosis factor-alpha equilibrium is a prerequisite for clinical course free from late complications in children with type 1 diabetes mellitus," *Scandinavian Journal of Immunology*, vol. 67, no. 2, pp. 204–208, 2008.

[37] R. A. Kowluru and S. Odenbach, "Role of interleukin-1β in the pathogenesis of diabetic retinopathy," *British Journal of Ophthalmology*, vol. 88, no. 10, pp. 1343–1347, 2004.

[38] J. A. Vincent and S. Mohr, "Inhibition of caspase-1/interleukin-1beta signaling prevents degeneration of retinal capillaries in diabetes and galactosemia," *Diabetes*, vol. 56, no. 1, pp. 224–230, 2007.

[39] E. Shimizu, H. Funatsu, H. Yamashita, T. Yamashita, and S. Hori, "Plasma level of interleukin-6 is an indicator for predicting diabetic macular edema," *Japanese Journal of Ophthalmology*, vol. 46, no. 1, pp. 78–83, 2002.

[40] H. Funatsu, H. Yamashita, E. Shimizu, R. Kojima, and S. Hori, "Relationship between vascular endothelial growth factor and interleukin-6 in diabetic retinopathy," *Retina*, vol. 21, no. 5, pp. 469–477, 2001.

[41] A. M. Joussen, V. Poulaki, N. Mitsiades et al., "Nonsteroidal anti-inflammatory drugs prevent early diabetic retinopathy via TNF-alpha suppression," *The FASEB Journal*, vol. 16, no. 3, pp. 438–440, 2002.

[42] A. K. W. Lai and A. C. Y. Lo, "Animal models of diabetic retinopathy: summary and comparison," *Journal of Diabetes Research*, vol. 2013, Article ID 106594, 29 pages, 2013.

[43] J. Nilsson-Öhman, G. N. Fredrikson, L. M. Nilsson-Berglund et al., "Tumor necrosis factor-alpha does not mediate diabetes-induced vascular inflammation in mice," *Arteriosclerosis, Thrombosis, and Vascular Biology*, vol. 29, no. 10, pp. 1465–1470, 2009.

[44] C.-G. Lee, K.-H. Kang, J.-S. So et al., "A distal cis-regulatory element, CNS-9, controls NFAT1 and IRF4-mediated IL-10 gene activation in T helper cells," *Molecular Immunology*, vol. 46, no. 4, pp. 613–621, 2009.

[45] T. Smallie, G. Ricchetti, N. J. Horwood, M. Feldmann, A. R. Clark, and L. M. Williams, "IL-10 inhibits transcription elongation of the human TNF gene in primary macrophages," *The Journal of Experimental Medicine*, vol. 207, no. 10, pp. 2081–2088, 2010.

[46] S. P. Didion, D. A. Kinzenbaw, L. I. Schrader, Y. Chu, and F. M. Faraci, "Endogenous interleukin-10 inhibits angiotensin II-induced vascular dysfunction," *Hypertension*, vol. 54, no. 3, pp. 619–624, 2009.

[47] S. Kase, M. Yokoi, W. Saito et al., "Increased osteopontin levels in the vitreous of patients with diabetic retinopathy," *Ophthalmic Research*, vol. 39, no. 3, pp. 143–147, 2007.

[48] Q. Huang and N. Sheibani, "High glucose promotes retinal endothelial cell migration through activation of Src, PI3K/Akt1/

eNOS, and ERKs," *The American Journal of Physiology—Cell Physiology*, vol. 295, no. 6, pp. C1647–C1657, 2008.

[49] H. Huang, J. K. Gandhi, X. Zhong et al., "TNFalpha is required for late BRB breakdown in diabetic retinopathy, and its inhibition prevents leukostasis and protects vessels and neurons from apoptosis," *Investigative Ophthalmology and Visual Science*, vol. 52, no. 3, pp. 1336–1344, 2011.

[50] D. Navaratna, P. G. McGuire, G. Menicucci, and A. Das, "Proteolytic degradation of VE-cadherin alters the blood-retinal barrier in diabetes," *Diabetes*, vol. 56, no. 9, pp. 2380–2387, 2007.

[51] J. M. Trevillyan, X. G. Chiou, Y.-W. Chen et al., "Potent inhibition of NFAT activation and T cell cytokine production by novel low molecular weight pyrazole compounds," *The Journal of Biological Chemistry*, vol. 276, no. 51, pp. 48118–48126, 2001.

[52] T. Bîrsan, C. Dambrin, K. C. Marsh et al., "Preliminary in vivo pharmacokinetic and pharmacodynamic evaluation of a novel calcineurin-independent inhibitor of NFAT," *Transplant International*, vol. 17, no. 3, pp. 145–150, 2004.

[53] R. Simó, J. M. Sundstrom, and D. A. Antonetti, "Ocular anti-VEGF therapy for diabetic retinopathy: the role of VEGF in the pathogenesis of diabetic retinopathy," *Diabetes Care*, vol. 37, no. 4, pp. 893–899, 2014.

Online Supplemental Material

Table S1. Plasma cytokines

Cytokine	Control (n=7)	STZ (n=8)	Control+A-285222 (n=8)	STZ+A-285222 (n=8)
OPN	81.0±11.4	94.2±32.5	76.5±12.1	84.9±20.7
IL-10	13.8±8.4	15.8±10.4	14.4±4.2	12.7±7.7
TNF-α	n.d.	0.2±0.7	0.2±0.4	n.d.
IFN-γ	1.9±0.9	3.4±3.3	2.1±1.0	1.0±0.6*
IL-12p70	6.7±8.9	8.7±8.5	4.8±7.8	16.6±27.6
IL-1β	0.6±0.3	1.1±0.8	0.8±0.2	0.7±0.4
IL-6	2.9±1.9	7.8±1.4	4.6±4.4	3.3±3.9
KC	39.0±5.6	60.6±41.5	68.2±17.1	68.1±27.5

Cytokine levels are expressed in ng/ml for OPN and in pg/ml for all other cytokines. Values represent mean ± SD. Plasma cytokine levels in control and STZ-treated BALB/c mice that have been treated with the NFAT inhibitor A-285222 (0.29 mg/kg for 2 weeks followed by 0.15 mg/kg for last 2 weeks) or saline, measured 4 weeks after the first STZ/vehicle injection. Interleukin (IL)-10, tumor necrosis factor (TNF)-α, interferon (IFN)-γ, IL-12p70, IL-1β, IL-6 and keratinocyte chemoattractant (KC) were measured using multiplex technology. n.d.; not detectable. Two-way ANOVA revealed no significant interactions, except for IFN-γ. For IFN-γ, one-way ANOVA and Bonferroni post-test revealed $^{*}P<0.05$ vs STZ-treated saline group.

Supplementary figure 1. Confocal immunofluorescence images showing staining of retinal whole-mounts with antibodies against von Willebrand factor (**A**; 1:400), smooth muscle α-actin (**B**; 1:400) and platelet-derived growth factor β-receptor (**C**; PDGFRβ, 1:100) for

identification of endothelial, smooth muscle cells and pericytes, respectively. **D**. Smooth muscle α-actin and PDGFRβ double staining of retinal whole-mounts.

Supplementary Figure 2. Representative confocal immunofluorescence images of retinal whole mounts, stimulated for 30 min in high extracellular glucose (HG; 20 mmol/l) in the presence of A-285222 (**A**; 1μmol), or apyrase (**B**; 3.6 U/ml), or after stimulation with low D-glucose (LG; 2 mmol/l) plus mannitol (**C**; 18 mmol/l), or LG plus L-glucose (**D**; 18 mmol/l). Preparations were stained for NFATc3 (red) and SYTOX Green for identification of nuclei (green). Endothelial cells were identified by the orientation of their nuclei. Scale bars=50 μm.

Supplementary Figure 3. No significant effects of high glucose on NFATc2 nuclear accumulation in endothelial cells. A. Representative confocal immunofluorescence images of HUVEC stimulated for 30 min in low (LG; 2 mmol/l) or high (HG; 20 mmol/l; right panels) extracellular glucose with or without A-285222 (1μmol), stained for NFATc2 (red) and SYTOX Green for identification of nuclei (green). **B.** Summarized data from experiments as in (A), showing NFATc2 nuclear accumulation after 30 min stimulation in LG or HG in the presence or absence of A-285222 (1μmol), or after stimulation with LG plus mannitol (18 mmol/l). **C**. Summarized data from corresponding confocal experiments in HRMVECs, stimulated as in (A) and with VEGF (25 ng/ml) with or without A-285222 (1μmol).

Supplementary Figure 4. Expression of *OPN* mRNA in isolated retinal microvessels from normolipidemic (A-B) and dyslipidemic (C) diabetic mice, determined by quantitative RT-PCR. **A**. No differences between *OPN* mRNA expression levels in retinal vessels from diabetic and control NFAT-luc mice, measured 2 weeks after the first STZ/vehicle injection. *HPRT* was used as endogenous control. N=19 mice/group. **B.** No differences between *OPN*

mRNA expression in retinal vessels from Akita and WT littermate control mice**.** *18S* and *Cyklophilin B* were used as endogenous controls. N=12 and 4 for WT and Akita, respectively. **C.** *OPN* mRNA expression was significantly higher in diabetic *Apoe*$^{-/-}$ mice when compared to non-diabetic *Apoe*$^{-/-}$ mice measured 8 weeks after the first STZ/vehicle injection. *HPRT* and *GAPDH* were used as endogenous controls. N=11 mice/group, $^{*}P<0.05$.

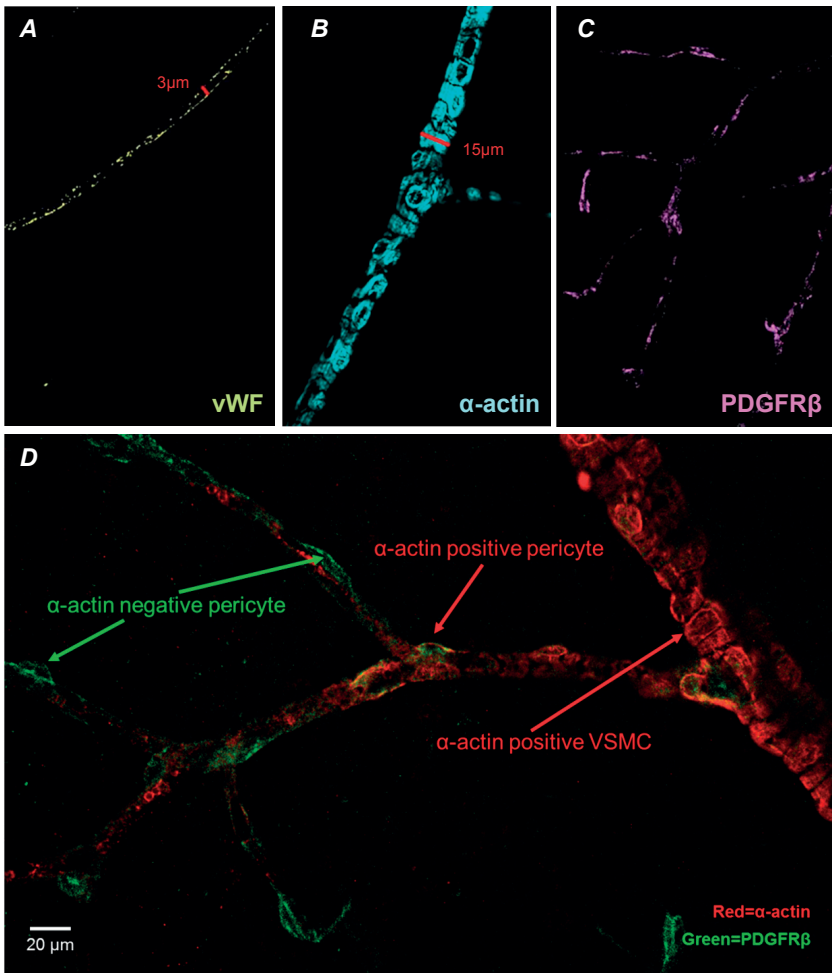

Supplemental figure 1

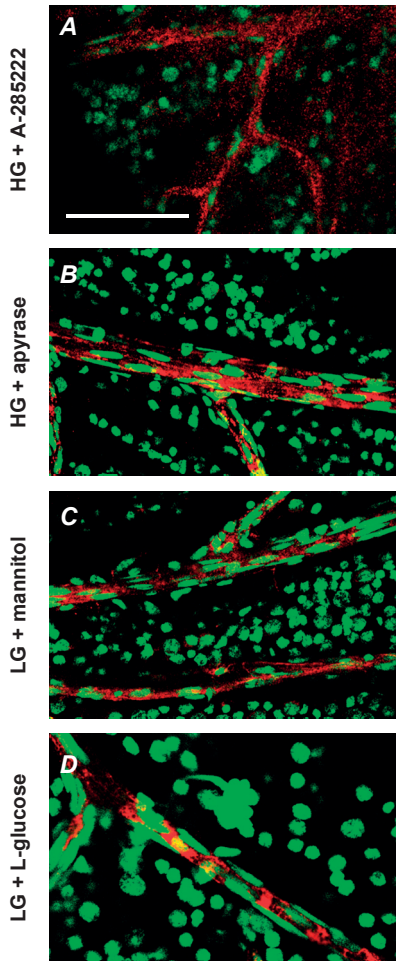

Supplemental figure 2

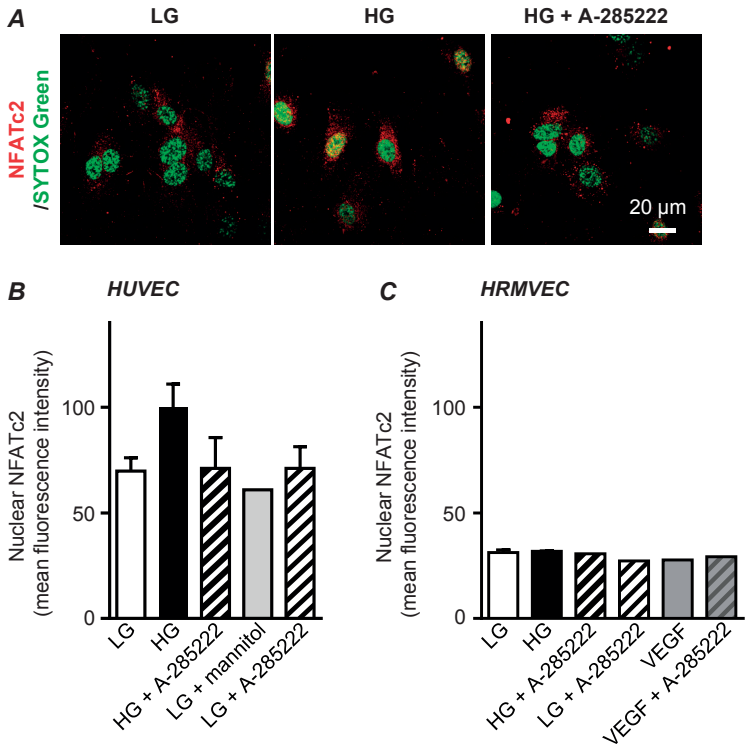

Supplemental figure 3

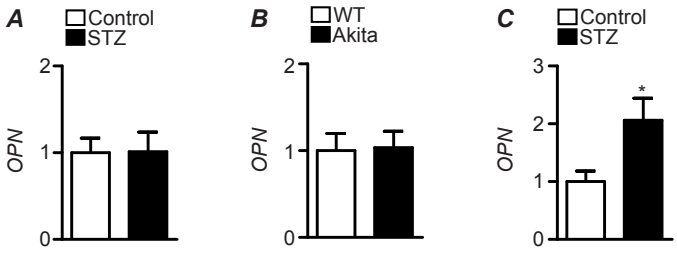

Supplemental figure 4

Paper IV

DIFFERENTIAL EFFECTS OF NFATc2 AND NFATc3 DELETION ON VASCULAR SMOOTH MUSCLE GENE EXPRESSION AND PROLIFERATION

Fabiana Blanco[1,2], Lisa M. Berglund[1], Olga Kotova[1], Anna-Maria Dutius Andersson[1], Petr Volkov[1], Maria F. Gomez[1]✉

[1]Department of Clinical Sciences in Malmö, Lund University Diabetes Centre, Lund University, Sweden;
[2]Departamento de Biofísica, Facultad de Medicina, Universidad de la República, Uruguay

Address correspondence to: Maria F. Gomez, Dept. of Clinical Sciences in Malmö, Lund University, Diabetic Complications, CRC 91:12; Box 50332, 202 13 Malmö, Sweden
Phone: +46-40-391058/ Fax: +46-40-391212 / E-mail: maria.gomez@med.lu.se

Proteins of the NFAT family consist of four calcium (Ca^{2+})/calcineurin-sensitive transcription factors (NFATc1-c4) known to play a role in several cells types outside the immune system, including those of the cardiovascular system. NFAT signaling seems to be engaged in the development of vascular diseases, such as systemic and pulmonary hypertension, restenosis and vascular complications of diabetes, but little effort has been made to dissect potential NFATc isoform-specific functions in the vasculature. Here, we performed a systematic mapping of the pattern of NFATc isoform expression in 13 different regions of the mouse vascular tree using absolute qPCR quantification. We found that NFATc3 is by far the predominant isoform in all vessels examined (~800-4000 million copies/µg total/µg total RNA), while NFATc2 and NFATc4 are expressed at substantially lower levels (~10 million copies/ and NFATc1 is expressed at an intermediate level (~150 million copies/µg total/µg total RNA). Further, only NFATc2 expression was increased in the aortic wall of diabetic mice, suggesting that this isoform can be induced or enhanced in pathological situations or under certain stimulatory conditions. We also found that genetic deletion of NFATc2 or NFATc3 differentially affected the expression of Kruppel-like factor 4 (Klf4), Kruppel-like factor 5 (Klf5) and Gata4, genes that have been implicated in the regulation of VSMC phenotypic modulation. Moreover, deletion of NFATc3 resulted in increased expression of angiotensin I converting enzyme (peptidyl-dipeptidase A) 1 (Ace) and of smooth muscle marker genes calponin 1 (Cnn1) and transgelin (Tagnl), as well as in higher VSMC proliferation. In summary, the differential isoform expression and effects observed upon NFATc2 and NFATc3 deletion support the idea of functional non-redundancy of NFAT isoforms in the vasculature.

Proteins of the NFAT family consist of four well characterized calcium (Ca^{2+})/calcineurin-sensitive transcription factors (NFATc1-c4), originally described as transcriptional activators of cytokine and immunoregulatory genes in T cells (1) but now known to play a role in several cells types outside the immune system. (2,3) NFAT signaling controls multiple steps during the development of the cardiovascular system, including the formation of heart valves and the proper assembly of peripheral vessels.(4) Postnatally, it is well recognized that this signaling pathway plays a key role in the pathogenesis of cardiac hypertrophy (5) and more recent work implicates NFAT as an important regulator of cardiac myofibroblast differentiation and extracellular matrix production in the pressure overloaded heart. (6) We and others have provided experimental evidence for the involvement of NFAT signaling in the development of vascular diseases, such as systemic (7,8) and pulmonary hypertension, (9-11) restenosis (12-14) and vascular complications of diabetes. (15-18)

Vascular smooth muscle cells (VSMCs) are the main constitutive cellular component in the vascular wall. They not only provide structural integrity to blood vessels but perform a variety of physiological functions. Owing to their intrinsic plasticity and ability to adopt different shapes and roles, VSMCs are involved in all the pathological processes that lead to vascular disease. (19) In response to acute or chronic stimuli (i.e. mechanical stress or injury, growth factors, changes in metabolic or inflammatory environment), VSMCs are capable to undergo phenotypic modulation by virtue of re-programming their gene expression pattern. The concept of phenotypic switching is widely accepted, (20-22) and we understand today that VSMCs not only can assume a proliferative synthetic

or a quiescent contractile phenotype as two ends of a linear spectrum, but they can gain distinct and not necessarily mutually exclusive phenotypes (i.e. the ability to produce extracellular matrix proteins, migrate, proliferate, secrete inflammatory mediators, promote calcification). (23) (24) Although a large body of work has helped identify several regulatory circuits that control differentiation of VSMCs, how these circuits relate and cross-talk with transcriptional programs that promote phenotypic modulation and are active in the context of disease, such as the NFAT-signaling pathway, is still unclear.

NFATc isoforms were initially considered to have redundant functions, but differential activation of isoforms within the same cell and varied expression profiles among cell types have been observed, suggesting isoform-specific functions (25) NFAT isoforms co-expressed in the same cell type can be differentially regulated by the same stimuli and much of what determines the efficiency of the stimulus is the ability to deliver an appropriate pattern of intracellular calcium signaling in combination with precise regulation of NFAT export kinases (26-29). In pancreatic acinar cells for example, we have shown that NFATc3 but not NFATc1 is readily activated by cholecystokinin or by ACh (30) Another example of differential control of NFAT isoforms is illustrated by the dramatic NFATc3 activation in the endothelium of retinal microvessels after acute hyperglycemia and the complete lack of NFATc2 response to elevated extracellular glucose in retinal endothelial cells (18). Despite these observations suggesting functional nonredundancy of NFAT isoforms, a more systematic characterization of the patterns of NFAT isoform expression in different types of vessels or regions of the vascular tree is missing. Most vascular related NFAT studies in the past have focused on one isoform at a time without monitoring concomitant changes in the expression or activation state of the other NFATc isoforms. (Reviewed in (25))

In this paper we determined the pattern of NFATc isoform expression in various regions of the vascular tree by means of absolute quantification. We found NFATc3 to be the most abundant isoform in all blood vessels examined and NFATc2 to be readily induced in the arteries of diabetic mice. We explored the impact of NFATc2 or NFATc3 deletion on vascular smooth muscle gene expression and proliferation.

MATERIALS & METHODS

Animals — All animal protocols were performed in accordance with the Malmö / Lund Animal Care and Use Committee (Permits M29-12 and M9-15) and abided by the Guide for the Care and Use of Laboratory Animals published by the Directive 2010/63/EU of the European Parliament. For figures 1 and S1A, C57BL/6J control mice were used (The Jackson Laboratory, Maine). For all other figures, NFATc2 and NFATc3 deficient and corresponding control competent mice were used. B6.129-*Nfatc2*^{tm1Rao}/Mmnc embryos originally generated by Dr. Anjana Rao (31) (Center for Blood Research, Harvard University) were purchased from the Mutant Mouse Resource & Research Centers (https://www.mmrrc.org, RRID: MMRRC_000197-UNC). Founders on a mixed 129/SvJ and C57BL/6J background were crossed to C57BL/6 mice for at least 4 generations. These mice were generated using a targeting vector designed to delete a large portion of an exon encoding amino acids near the NH_2-terminus of the DNA binding domain, a region critical for DNA-binding activity. However, the deletion resulted in an aberrant splice between the flanking exons and a predicted mutant fragment that is either not made or rapidly degraded, rendering the mice deficient of NFATc2 protein (NFATc2$^{-/-}$). (31) NFATc3 deficient mice (NFATc3$^{-/-}$) were originally generated by Dr. Laurie Glimcher (Harvard Medical School) using a targeting construct containing the neomycin drug resistance (neo) gene to replace a region in the NFATc3 gene encoding the DNA-binding domain, rendering the mice deficient of NFATc3 protein. (32) Mice are on a Balb/C background and have been used routinely in our lab. (15,30) All mice were bred in our animal facilities and used at adult age. Mice were housed in groups and maintained in a temperature- and humidity-controlled environment with a 12-hour light/dark cycle, with free access to tap water and fed *ad libitum* with normal chow diet. For tissue harvesting, mice were anaesthetized with ketamine hydrochloride and xylazine (i.p.; 7.5 mg and 2.5 mg/100 g body weight, respectively) and euthanized either by exsanguination through cardiac puncture or by cervical dislocation. Depth of anesthesia was assessed by toe-pinch procedure and absence of muscular tone. All efforts were made to minimize suffering.

Streptozotocin (STZ) treatment — Adult male NFAT competent mice (C57BL/6J) were injected intraperitoneally (i.p.) with streptozotocin (STZ, 60 mg/kg body weight in citrate buffer, pH 4.5) or equal volume of vehicle (citrate buffer), once a day during 5 days. Mice were weighed and glucose levels measured in whole venous blood (Contour Glucometer, Bayer) before the STZ treatment and regularly until the mice were euthanized two weeks after the first STZ injection. Diabetes was defined by blood glucose >13.9 mmol/L (250 mg/dL) and animals with lower blood glucose value at the end of the experiment were excluded from the study. After termination, the thoracic aorta was isolated and dissected free from surrounding tissue in ice-cold Ca^{2+}-free physiological saline solution (PSS; containing in mmol/L: NaCl, 135; KCl, 5.9; $MgCl_2$, 1.2; Hepes, 11.6; glucose, 2.0; pH 7.4) and frozen in liquid nitrogen for further analyses.

Cell Culture — VSMCs cells were obtained from thoracic aorta explants from NFATc2$^{+/+}$ and NFATc2$^{-/-}$ mice as well as from NFATc3$^{+/+}$ and NFATc3$^{-/-}$ mice as previously described. (33) VSMCs were cultured in full culture medium consisting of DMEM/HAM's F-12 (1:1) supplemented with 15% fetal bovine serum (FBS, Biochrom AG), 2 mM L-glutamine, 50 U/mL penicillin and 50 µg/mL streptomycin. Cells were cultured in a water-jacketed incubator at 37°C and 5% CO_2.

NFATc2 and NFATc3 transfections — On the day prior to transfection, aortic VSMCs of the different genotypes (NFATc2$^{+/+}$, NFATc2$^{-/-}$, NFATc3$^{+/+}$ and NFATc3$^{-/-}$) were seeded in 24-well plates in antibiotic free culture medium

($5x10^4$ cells/well; passages 4-11). Confluent VSMCs were transfected either with pNFATc2-EGFP or with pNFATc3-pEGFP plasmids (0.8 µg and 1 µg of plasmid DNA, respectively; GenScript), complexed with Lipofectamine 2000 (1.6 µL or 2 µL, respectively; Invitrogen) in antibiotic and serum-free culture medium. After 4 hours, transfection complexes were removed and cells were incubated for another 20 hours in fresh antibiotic and serum-free culture medium. Twenty-four hours after transfection, cells received full culture medium and were incubated for another 7 days. Seven days after transfection start, approximately 90% of the cells were positive for EGFP, as determined using a Zeiss LSM 5 laser scanning confocal microscope.

VSMC proliferation — Seven days after transfection, VSMCs were reseeded in 96-well plates ($5x10^3$ cells/well) and cultured in full culture medium for 48 hours. To measure DNA synthesis, cells were pulsed with 1µCi thymidine [methyl-^{3}H] (PerkinElmer) during the last 24 hours of culture, after which cells were harvested on glass fiber filters (Printed Filtermat A; Wallac Oy, Turku, Finland) using a FilterMate harverster (Perkin Elmer, Buckinghamshire, UK). Filters were air-dried and the bound radioactivity was measured using a liquid scintillation counter (Wallac, TRILUX 6DET1450021) and expressed as counts per minute (cpm).

RNA isolation — Retinas, cerebral arteries, carotid arteries, aorta, hepatic artery, renal arteries, portal vein, mesenteric arteries, femoral arteries, tail artery and thymus were dissected out from adult collected from adult NFAT competent mice (C57BL/6J). Blood vessels and thymus were dissected free from surrounding tissue in ice-cold Ca^{2+}-free PSS. Retinal vessels were isolated from the intact retinas as previously described. (34) Total RNA was extracted from the blood vessels and thymus using TRI Reagent BD (Sigma-Aldrich, St. Louis, MO, USA) according to the manufacturer's instructions. From cultured VSMCs, total RNA was isolated using RNeasy® Plus Mini Kit (Qiagen, Hilden, Germany) according to the manufacturer's instructions. Purity and concentration of RNA was determined spectrophotometrically (NanoDrop ND-1000; NanoDrop Technologies, Wilmington, DE).

RT^2 Profiler PCR Arrays — Reverse transcription was performed using RT^2 First Strand Kit (Qiagen, Hilden, Germany) according to the manufacturer's instructions. For each experimental condition, RNA was pooled using equal amounts from two different experiments in one cDNA reaction, with 125 ng total RNA from each sample. The expression of mRNA was analyzed using a custom-designed RT^2 Profiler PCR Array (Qiagen) including 42 genes that have previously been demonstrated to be involved in the regulation of VSMC phenotype and function, 3 housekeeping genes and 3 technical controls, all run in duplicates (see Supplementary table 1 for the complete list of genes). Samples were run on 96-well array plates in a StepOnePlus qPCR cycler (Applied Biosystems, Foster City, CA), using RT^2 SYBR Green ROX qPCR Mastermix (Qiagen). The housekeeping genes included were Gapdh, Rn18s and Hsp90ab1. Target gene expression was normalized to the geometric mean of the three housekeeping genes, using the comparative threshold method ($\Delta\Delta C_t$) of the GeneGlobe Data Analysis Center provided by Qiagen. Genomic DNA control (GDC) wells showed no contamination of genomic DNA. Reverse-transcription control (RTC) wells revealed consistent and efficient reverse transcription in all samples. The positive PCR control (PPC) varied less than 0.3 cycles between plates to be compared. Genes below detection limit ($C_t > 35$) in both samples were not included in the analysis (Prom1, Sgcg, Myocd, Thbs4, Kcnmb1 and Mef2c).

Quantitative RT-PCR — For quantitative PCR, cDNA was synthesized using RevertAid First Strand cDNA kit (Thermo Fisher Scientific, Stockholm, Sweden) and amplified in triplicates using TaqMan gene expression assays for Nfatc1 Mm00479445_m1; Nfatc2 Mm00477776_m1; Nfatc3 Mm01249195_m1; Nfatc4 Mm00452375_m1; Cnn1 Mm00487032_m1; Klf4 Mm00516104_m1; Klf5 Mm00456521_m1; Tagln Mm00441661_g1; Ace Mm00802048_m1; Gata4 Mm00484689_m1; Nox4 Mm00479246_m1; Cat Mm00437992_m1; Ccna2 Mm00438063_m1; Ccnd1 Mm00432359_m1; Cdk4 Mm00726334_s1; Gapdh 4352339 and Ppib Mm00478295_m1 on a Quant Studio 7 Flex System instrument (Applied Biosystems, Carlsbad, CA). Relative expression of target genes was calculated using the comparative threshold method ($\Delta\Delta C_t$) with Gapdh and/or cyclophilin B as housekeeping genes.

For absolute quantification of NFAT isoform expression in different vessels and VSMCs, thymus cDNA was first amplified using TaqMan gene expression assays for Nfatc1-c4 specified above. PCR products were isolated using NucleoSpin Gel and PCR Clean-up kit (Macherey-Nagel, Düren, Germany) and DNA concentration determined spectrophotometrically (NanoDrop ND-1000; NanoDrop Technologies, Wilmington, DE). The number of copies per µl for each NFAT isoform was calculated using the formula [X * $6.022x10^{23}$ molecules/mole] / [N * 660 g/mole] where X is the concentration of isolated PCR fragments in g/µl and N is the length of the PCR product in base pairs. (35) Ten-fold serial dilutions from 10^9 to 10 copies per µl were prepared and amplified in triplicates to generate absolute standard curves for each isoform, from where copy numbers for vessel samples and VSMCs, expressed per µg of total RNA input, were determined by reading off their threshold cycle (C_t) values after amplification in triplicates.

Statistical analysis — Results are expressed as means ± SEM unless otherwise specified. Analyses of distributions were performed before statistical tests were performed, using GraphPad software (Prism 7.0). For parametric data, significance was determined using Student's t-test, or one-way ANOVA followed by Bonferroni's multiple comparison post-test. Non-parametric data was analyzed using Mann-Whitney or Kruskal-Wallis test followed by Dunn's post-test.

RESULTS

Pattern of NFATc isoform expression in various regions of the mouse vascular tree. Previous studies have used RT-PCR, Western blotting or immunohistochemistry to demonstrate the presence of one or several NFAT isoforms in several arteries and in vascular cells. However, these techniques only determine presence or absence of the transcript or protein, and/or relative expression changes in response to an intervention. To our knowledge, the absolute

levels of basal NFATc isoform expression have not been determined in any given blood vessel, nor has the pattern of NFATc isoform expression been systematically compared throughout the vascular tree. Using absolute qPCR quantification we determined the transcript copy number of each NFATc isoform in various regions of the mouse vascular tree, including retinal microvessels, cerebral and carotid arteries, the aortic arch, thoracic and abdominal portions of the aorta, hepatic artery, portal vein, renal, mesenteric and femoral arteries and tail artery. As shown in **Figure 1**, NFATc3 is by far the most abundantly expressed NFATc isoform, with expression levels ranging from as low as 800 million copies per µg total RNA in the hepatic artery and as close to 4000 million copies per ug total RNA in the tail and cerebral arteries. In contrast, NFATc2 and NFATc4 were expressed at substantially lower levels with ~10 million copies per µg total RNA in most vessels examined. NFATc1 was expressed at an intermediate level with approximately 150 million copies per µg total RNA. Interestingly, retinal microvessels were characterized by the lowest NFATc1 expression (19 million copies per µg total RNA) and the highest NFATc2 expression (34 million copies per µg total RNA) of all vessels examined (**Figure 1**).

Plasticity of NFATc2 expression in the arterial wall. Previous studies in our group had shown that NFATc2 expression could be induced under certain stimulatory conditions. (33) While in native unstimulated human myometrial arteries NFATc2 expression was either absent or too low to be detected, it was readily amplified after arteries had been cultured for 4 days under conditions favoring a proliferating and less differentiated phenotype. (33) Moreover, increased NFATc2 expression and activation (assessed by measurements of NFATc2 nuclear localization) was found in pulmonary arteries from patients with pulmonary arterial hypertension when compared to healthy individuals and in experimental models of pulmonary hypertension. (36) Here, we sought to determine whether NFATc2 expression could be affected in the context of diabetes. For this, we measured NFATc isoform expression in mouse aortas from diabetic and non-diabetic mice. Two weeks after the first streptozotocin (STZ) injection, mice were diabetic and had significantly higher blood glucose

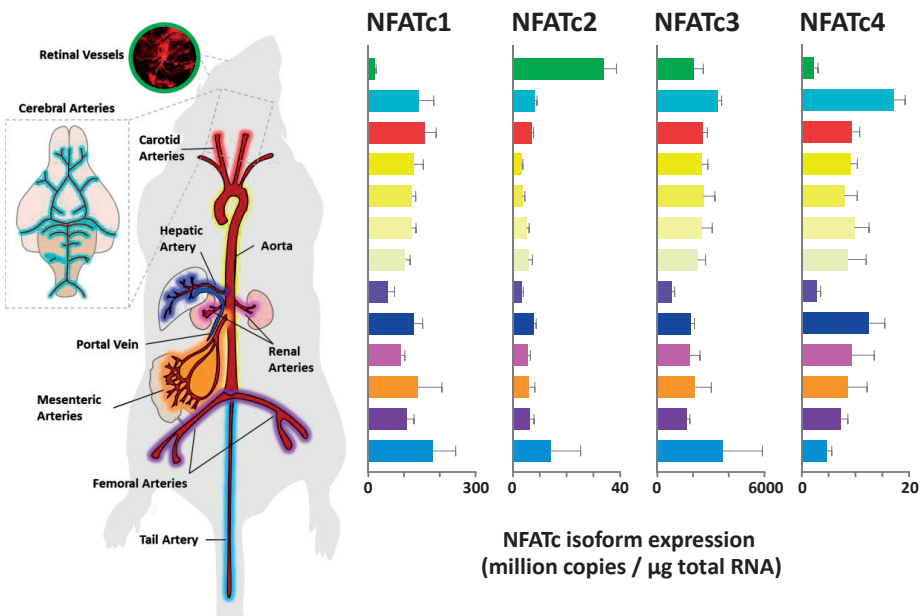

Figure 1. NFAT isoform expression in the mouse vasculature. Absolute quantification of NFATc isoforms in blood vessels was performed using qPCR and is expressed as 10^6 copies/µg total RNA. The colors of the bars in each of the graphs represent expression levels in the various regions of the vascular tree, which are highlighted with corresponding colors in the mouse schematic. The order of the bars (from upper to lower bar) is: retinal microvessels (green), cerebral arteries (turquoise), carotid arteries (red), aortic arch, descending thoracic aorta, suprarenal abdominal aorta, infrarenal aorta (four nuances of yellow), hepatic artery (lilac), portal vein (blue), renal arteries (pink), mesenteric arteries (orange), femoral arteries (violet), tail artery (light blue). N=3 mice for each vessel type.

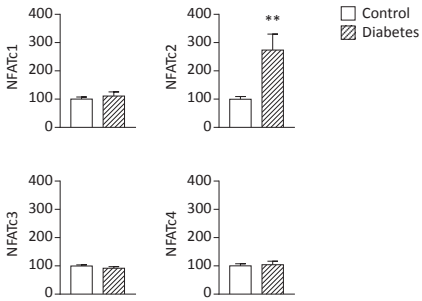

Figure 2. STZ-induced diabetes increases NFATc2 expression in mouse aorta. Expression of NFATc1-c4 isoforms measured using qRT-PCR in the aorta of control and diabetic mice (C57BL/6) 2 weeks after the first STZ-injection. NFAT expression was normalized to Ppib and is expressed as percentage of non-diabetic control. N=8-9 mice per group; **p<0.01.

levels than vehicle-injected control mice (8.9±0.62 mmol/L vs. 23.2±1.85 mmol/L; p=0.0088). At that time point, NFATc2 expression was significantly higher in the aortas from diabetic mice when compared to expression in control non-diabetic mice (**Figure 2**). No differences in the levels of expression of NFATc1, NFATc3 or NFATc4 were detected between groups (**Figure 2**). Taken together, results suggest that NFATc2 expression can be induced or enhanced in pathological situations or under certain stimulatory conditions.

Genetic deletion of NFATc2 and NFATc3 differentially affects gene expression in VSMCs. Expression of genes that have been implicated in the regulation of vascular smooth muscle phenotypic modulation (i.e. transcriptional activators and co-activators of smooth muscle specific gene expression, regulators of actin polymerization, miR-143/145 target genes) and of smooth muscle marker genes was examined in aortic VSMCs from NFAT competent mice and from mice lacking either NFATc3 or NFATc2 proteins. A complete list of the genes included in the custom-designed PCR Profiler Array used for these experiments is presented in Supplementary table 1. **Figure 3** summarizes results for all genes examined with expression levels above the detection threshold. Fold change differences in gene expression between NFATc3 deficient and competent cells are plotted in the horizontal bar graph in the upper part of **Figure 3**, while corresponding comparison for NFATc2 is plotted in the vertical bar graph in the left part of Figure 3. In

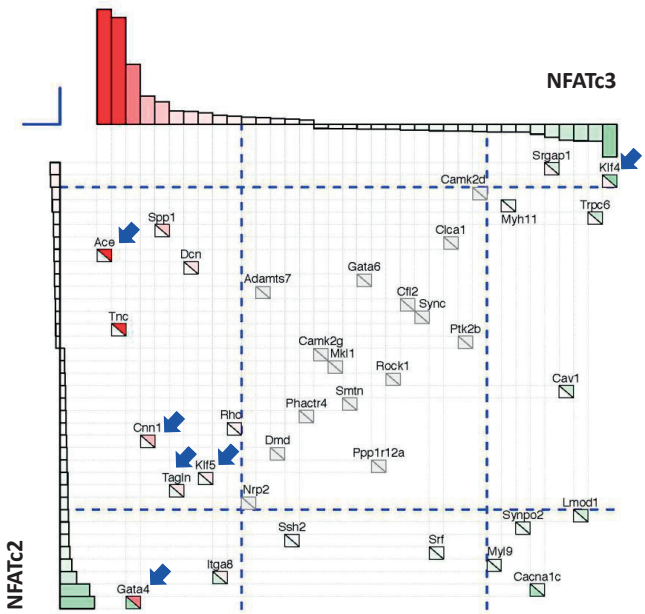

Figure 3. Differential regulation of target genes by NFATc2 and NFATc3. Vascular smooth muscle cells from NFATc2 and NFATc3 wildtype (WT) and knockout (KO) mice were cultured and gene expression of selected genes analyzed. The bars show fold change in KO vs WT cells for NFATc2 and NFATc3. Each gene is represented by a square with the upper right corner reflecting expression ratio for NFATc3 KO/WT and the lower left corner reflecting expression ratio for NFATc2 KO/WT. The dashed blue lines indicate 2-fold up- or down regulated. Scale bar=10 fold difference.

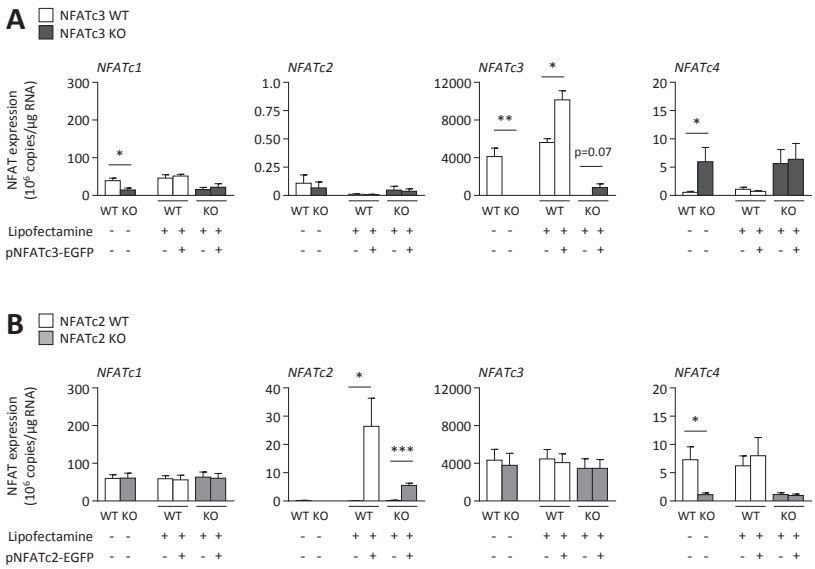

Figure 4. Absolute quantification of NFATc isoforms in VSMCs from **A)** NFATc3 WT and KO mice and **B)** NFATc2 WT and KO mice. VSMCs were used untreated or after transfection with NFATc2-EGFP or NFATc3-EGFP plasmids complexed with Lipofectamine, or Lipofectamine only as mock treatment. Absolute quantification was performed using qPCR and is expressed as 10^6 copies/µg total RNA. N=2-6 experiments per condition; *p<0.05, **p<0.01, ***p<0.001.

each bar graph, genes are ranked based on fold change sizes, with the color intensity of the bars also reflecting the size of the differences. Red colors represent higher gene expression in VSMCs lacking either NFATc2 or NFATc3 protein vs. NFATc competent cells, while green colors represent lower gene expression instead. Genes were then projected onto a 2-dimensional matrix for easier visualization of genes that were regulated both in cells lacking NFATc2 and NFATc3, either in the same or in opposite direction, as well as of genes that were exclusively affected by the lack of one of the isoforms only. Dashed lines in the matrix indicate thresholds for >2-fold up- or downregulation of gene expression.

We found that lack of NFATc3 resulted in a larger number of >2-fold regulated genes and larger fold changes than lack of NFATc2. The overall most affected gene was Angiotensin I converting enzyme (peptidyl-dipeptidase A) 1 (Ace), showing 31-fold higher expression in cells lacking NFATc3 than in control cells. Lack of NFATc2 had no impact on Ace expression. Other genes that were also upregulated in cells lacking NFATc3 were the extracellular matrix glycoprotein Tenascin C (Tnc), Gata4, Calponin 1 (Cnn1), Osteopontin (Spp1), Transgelin (Tagln), Decorin (Dcn), Kruppel-like factor 5 (Klf5), Integrin alpha 8 (Itga8) and Rhodopsin (Rho). Interestingly, of these up-regulated genes, both Gata4 and Itga8 (projected in the lower left corner of the 2-dimensional matrix), were instead >2-fold down-regulated in cells lacking NFATc2. In the opposite upper right corner of the matrix, we can find Kruppel-like factor 4 (Klf4) and SLIT-ROBO Rho GTPase activating protein 1 (Srgap1); two genes that were down-regulated in cells lacking NFATc3 and up-regulated in cells lacking NFATc2. Among all 9 genes that were >2-fold down-regulated in cells lacking NFATc3, the alpha 1C subunit of the voltage-dependent L-type calcium channel (Cacna1c), Myosin regulatory light chain 9 (Myl9), Synaptopodin (Synpo2) and smooth muscle leiomodin 1 (Lmod1) were also down-regulated >2-fold in cells lacking NFATc2. Serum response factor (Srf) and Slingshot homolog 2 (Ssh2) were >2-fold down-regulated in cells lacking NFATc2 but unaffected in cells lacking NFATc3. Blue arrows in **Figure 3** point at target genes that were validated in subsequent experiments.

Compensatory changes in NFATc isoform expression in NFATc2 and NFATc3 knockout cells. Absolute quantification of NFATc isoforms confirmed the absence of NFATc3 mRNA expression in aortic VSMCs from NFATc3$^{-/-}$ mice (**Figure 4A**). VSMCs from NFATc2$^{-/-}$ mice still expressed a low level of NFATc2 transcript (0.018 million copies per µg total RNA vs 0.16 in NFATc2$^{+/+}$ cells; **Figure 4B**), which is consistent with studies describing the production of a rapidly degraded mutant transcript in NFATc2$^{-/-}$ mice.

(31) Deletion of NFATc3 resulted in a compensatory decrease in NFATc1 expression, no effect on NFATc2 expression and a compensatory increase in NFATc4 expression (**Figure 4A**). Deletion of NFATc2 had no impact on NFATc1 or NFATc3 expression but resulted instead in a compensatory decrease in NFATc4 expression (**Figure 4B**).

The pattern of NFATc isoform expression in cultured VSMCs originated from explants from the aortas of control NFATc3$^{+/+}$ and NFATc2$^{+/+}$ mice was similar to that observed in freshly dissected intact aortas in terms of relative abundance of each of the isoforms. However cultured cells had lower NFATc1 and NFATc2, and higher NFATc3 expression than that observed in native aorta (**Supplemental figure 1**).

To further investigate the potential impact of altered NFATc2 and NFATc3 expression on smooth muscle gene expression, VSMCs were transfected with plasmids encoding NFATc2 or NFATc3. While transfection with pNFATc2-EGFP resulted in significant overexpression of NFATc2 in both NFATc2 competent and deficient cells (**Figure 4B**), transfection with pNFATc3-EGFP resulted in significant overexpression of NFATc3 competent cells but less efficient overexpression in NFATc3 deficient cells (**Figure 4A**). Overexpression of NFATc2 or NFATc3 had no impact on the expression of the other NFATc isoforms (**Figure 4**).

Differential effects of NFATc2 and NFATc3 deletion on Klf4, Klf5 and Gata4 gene expression. As shown in **Figure 3**, expression of Gata4 and Klf4 seem to be differentially affected in cells lacking NFATc2 or NFATc3 protein. While Gata4 was up-regulated in cells lacking NFATc3, it was downregulated in cells lacking NFATc2. A similar pattern was observed for Klf5, while the opposite was true for Klf4. These results obtained using the custom-designed PCR Profiler Array were confirmed in a larger number of samples using quantitative RT-PCR. **Figure 5A** shows significantly higher levels of Gata4 and Klf5 expression, as well as significantly lower levels of Klf4 expression in cells lacking NFATc3 when compared to NFATc competent cells. **Figure 5B** shows the opposite effects in cells lacking NFATc2. Despite confirmed overexpression of NFATc3 and NFATc2 after transfection with pNFATc3-EGFP and pNFATc2-EGFP (**Figure 4**), no significant changes in Gata4 or Klf5 were observed and only a minor increase in Klf4 expression was observed upon overexpression of NFATc2 in NFATc2$^{+/+}$ cells.

Deletion of NFATc3 leads to higher expression of Ace, Cnn1 and Tagln in VSMCs. Using quantitative RT-PCR, the results regarding Ace, Cnn1 and Tagln obtained using the custom-designed PCR Profiler Array were confirmed in a larger number of samples.

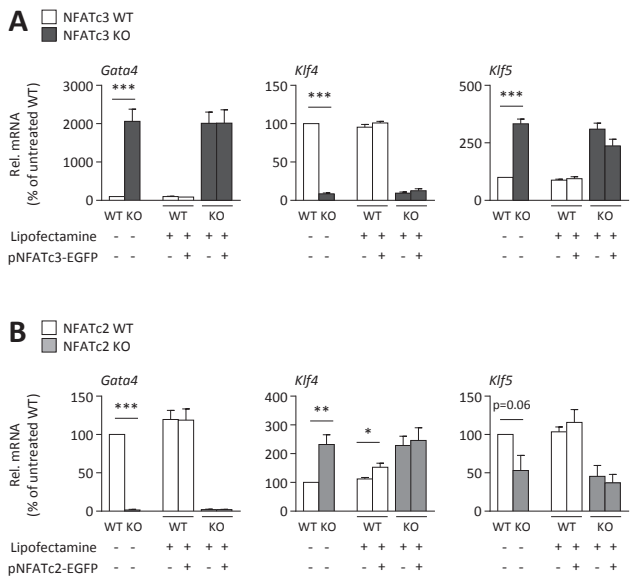

Figure 5. Gata4 and Klf4 are differentially affected in NFATc2 and NFATc3 KO cells. Gene expression analyses of Gata4, Klf4 and Klf5 in VSMCs from **A)** NFATc3 WT and KO mice and **B)** NFATc2 WT and KO mice. VSMCs were used untreated or after transfection with NFATc2-EGFP or NFATc3-EGFP plasmids complexed with Lipofectamine, or Lipofectamine only as mock treatment. Target gene expression was normalized to Ppib and Gapdh and expressed as percentage of the control untreated WT group in each genotype. N=2-5 experiments per condition; *p<0.05, **p<0.01, ***p<0.001.

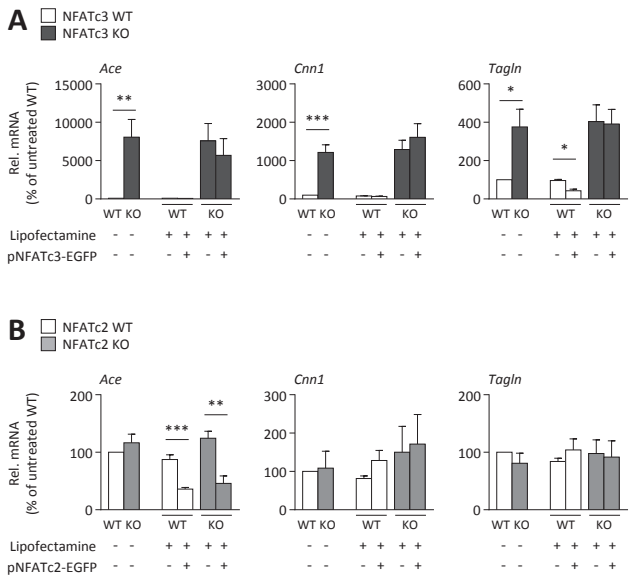

Figure 6. Ace is increased in VSMCs from NFATc3 KO mice. Gene expression analyses of Ace, Cnn1 and Tagln in VSMCs from **A)** NFATc3 WT and KO mice and **B)** NFATc2 WT and KO mice. VSMCs were used untreated or after transfection with NFATc2-EGFP or NFATc3-EGFP plasmids complexed with Lipofectamine, or Lipofectamine only as mock treatment. Target gene expression was normalized to Ppib and Gapdh and expressed as percentage of the control untreated WT group in each genotype. N=2-5 experiments per condition; *p<0.05, **p<0.01, ***p<0.001.

As shown in **Figure 6A**, expression of these 3 genes was higher in cells lacking NFATc3 when compared to NFATc competent cells. In agreement with the results from the Arrays, no impact of NFATc2 deletion was observed on the expression of these 3 genes (**Figure 6B**). Overexpression of NFATc3 resulted in significantly decreased Tagln expression in NFAT competent cells, while no effect was observed in NFATc3 deficient cells (**Figure 6A**). Interestingly, overexpression of NFATc2 significantly decreased Ace expression in both NFAT competent and NFATc2 deficient cells (**Figure 6B**).

Lack of NFATc3 renders VSMCs with higher proliferative capacity. NFAT has been implicated in the regulation of VSMC proliferation and the regulation of cell cycle markers. (33,37-39) (40-42) Here we show that NFATc3 deficient cells have significantly higher proliferating capacity (**Figure 7A**) and this is associated to higher expression of CCna2 (**Figure 7B**). Lack of NFATc2 had no impact on VSMC proliferation (**Figure 7C**), even though cells had higher levels of Ccnd1 expression when compared to control cells (**Figure 7D**). Overexpression of NFATc3 had no effect on VSMC proliferation or on the expression of cell cycle markers (**Figures 7A-B**), while overexpression of NFATc2 resulted in significant inhibition of proliferation in control cells (**Figure 7C**) and a minor increase in Ccnd1 expression (**Figure 7D**). No differences in Cdk4 expression were observed between NFATc competent and NFATc2 or NFATc3 deficient cells; nor were differences observed after overexpression of any of the isoforms (**Figure 7B and D**).

DISCUSSION

In this study we determined the pattern of NFATc isoform expression in various regions of the mouse vascular tree. Absolute qPCR quantification of the NFATc isoforms in 13 different blood vessels or areas of the vasculature revealed that NFATc3 is by far the most abundantly expressed isoform, while NFATc2 and NFATc4 are expressed at substantially lower levels and NFATc1 is expressed at an intermediate level. Two interesting observations from this systematic characterization of isoform expression were: 1) that retinal vessels deviated from the more generalized pattern of expression in that they had the lowest NFATc1 expression and the highest NFATc2 expression of all vessels examined and 2) cultured VSMCs had lower NFATc1 and NFATc2, and higher NFATc3 expression than the levels observed in native aorta. In agreement with what we and others have

described in the past in human myometrial arteries (33) and in human and experimental models of pulmonary hypertension (36), we observed increased NFATc2 expression in the aortic wall of diabetic mice when compared to non-diabetic controls, suggesting that NFATc2 expression can be induced or enhanced in pathological situations or under certain stimulatory conditions.

Other main finding of this study was that despite significant differences in the abundance of NFATc3 and NFATc2 transcripts in the vascular wall and in VSMCs (on average ~400-fold lower NFATc2 than NFATc3 expression for the vessels examined), lack of the much less abundant NFATc2 in VSMCs of NFATc2$^{-/-}$ mice still had a clear and measurable impact on the expression of several transcriptional activators and co-activators of smooth muscle specific gene expression.

Maybe the most interesting finding of this study is the opposite impact of NFATc2 and NFATc3 deletion on the expression of Klf4, Kl5 and Gata4 gene expression. It is well established that Klf4 is a potent inhibitor of cell proliferation, primarily via regulation of the cell cycle regulator p21 (43), while Klf5 instead has been shown to have the opposite effect, promoting cell proliferation. (44) Klf4 acts also as repressor of smooth muscle specific gene expression via inhibition of myocardin/SRF-dependent transcription as well as transcriptional silencing via epigenetic changes of smooth muscle marker loci. (24,45,46) Conditional deletion of Klf4 in smooth muscle results in delayed loss of smooth muscle differentiation but accelerated neointimal growth following vascular injury. (47) Klf4 has also been shown to play a role in the trans-differentiation of smooth muscle cells to macrophage- or mesenchymal stem cell-like phenotypes (48) of relevance, given that ~16% of macrophage-like cells in atherosclerotic lesions seemed to be derived from smooth muscle cells. (49) Klf5 instead has been shown to induce VSMC proliferation and to activate many genes inducible during cardiovascular remodeling (i.e. PDGF-A/B, Egr-1, plasminogen activator inhibitor-1, and VEGF receptors). (44) As we demonstrate in **Figure 5A**, lack of NFATc3 resulted in significantly lower expression of Klf4 and higher expression of Klf5, which could potentially explain the increased proliferative rate and expression of smooth muscle specific markers Calponin 1 (Cnn1) and Transgelin/SM22 (Tagln) observed in these NFATc3 deficient cells (**Figures 7A and 6B**, respectively). Lack of NFAc2 on the other hand resulted in the opposite effects on Klf4 and Klf5 expression, although the magnitude of the effects were less pronounced and did

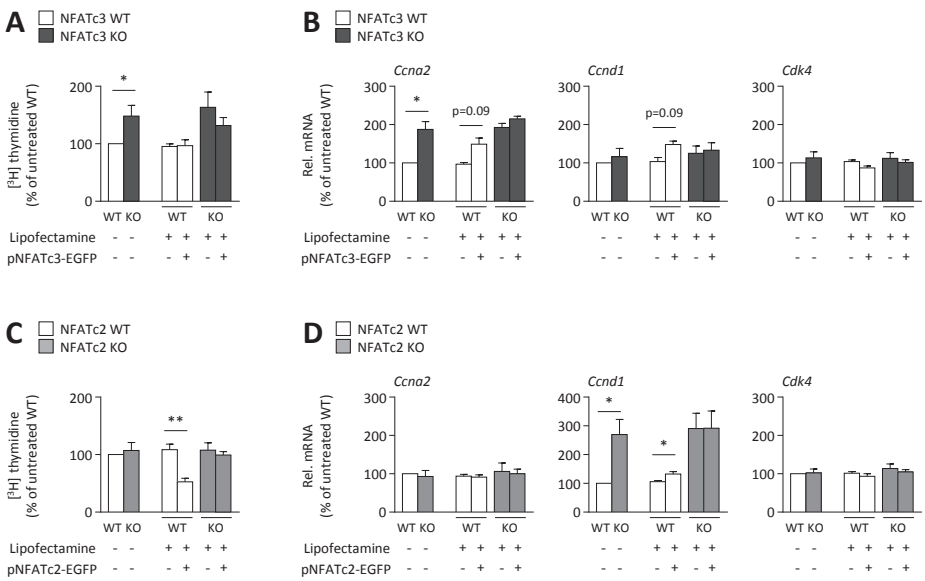

Figure 7. Overexpression of NFATc2 reduces VSMC proliferation. A and C. Thymidine incorporation in VSMCs from NFATc3 WT and KO mice and (A) from NFATc2 WT and KO mice (C). **B and D.** Gene expression analyses of proliferation markers Ccna2, Ccnd1 and Cdk4 in VSMCs from NFATc3 WT and KO mice (B) and NFATc2 WT and KO mice (D). VSMCs were used untreated or after transfection with NFATc2-EGFP or NFATc3-EGFP plasmids complexed with Lipofectamine, or Lipofectamine only as mock treatment. Target gene expression was normalized to Ppib and Gapdh. Both thymidine incorporation and gene expression are expressed as percentage of the control untreated WT group in each genotype. N=2-6 experiments per condition; *p<0.05.

not translate into changes in VSMC proliferation or expression of smooth muscle gene markers.

Gata4 is a member of the GATA family of zinc finger transcription factors originally described as a regulator of cardiac hypertrophy, for which it cooperatively interacts with NFAT. (50,51) Gata4 activity can be enhanced or decreased by changes in Gata4 expression. (50) Gata4 has been shown to be expressed in pulmonary artery smooth muscle cells and to regulate VSMC growth; inducers of pulmonary hypertension (i.e. serotonin and endothelin-1) affectively activate Gata4 via the MEK-ERK pathway. (52) Outside the heart, low or undetected levels of Gata4 have been described in the vascular tree, with low amounts of Gata4 in the root of the aorta and branches of the pulmonary artery but no expression in the descending aorta, carotid, umbilical and femoral arteries, (53), so we were surprised to find such dramatic induction in Gata4 expression in cells lacking NFATc3 (**Figure 5A**). Given the role of Gata4 in promoting pulmonary artery smooth muscle proliferation, it can be speculated that this increased Gata4 expression in NFATc3 deficient cells can also potentially contribute to the observed increased cell proliferation in **Figure 7A**. As for Klf4 and Klf5, Gata4 was also differentially impacted by NFATc2, with dramatically decreased levels of Gata4 expression in cells lacking NFATc2 (**Figure 5B**).

The role of microRNAs (miRNAs) in the control of VSMC differentiation and function has gained increasing attention in the past few years. In particular, the miR-143/145 cluster, which becomes confined to smooth muscle cells during embryonic development, has proven central for the maintenance of the contractile phenotype and expression of contractile proteins. (54,55) Using an unbiased high-throughput, quantitative, mass spectrometry–based proteomics approach, the angiotensin converting enzyme (Ace) was identified among other miR-143/145 specific targets. (54) We found a significant up-regulation of Ace expression in cells lacking NFATc3 when compared to NFATc3 competent cells (**Figure 6A**). It has been postulated that increased Ace in VSMCs favors acquisition of a synthetic phenotype and results in desensitization of G protein-coupled signaling, explaining the reduced contractile responses observed in vessels of miR143/145 mutant mice. (54,56)

The differential effects observed upon NFATc2 and NFATc3 deletion on Klf4, Klf5 and Gata4 gene expression support the idea of functional non-redundancy of NFAT isoforms in VSMCs. Along these lines, it was shown in human retinal microvascular endothelial cells that silencing of NFATc2 and NFATc3 have opposing effects on the expression of leukocyte adhesion proteins chemokine ligand 1 (CX3CL1) and E-selectin (SELE). (57) These studies highlight the importance of examining and dissecting the role of individual NFAT isoforms and of cautiously interpreting results relying on the use of pharmacological agents known to inhibit all isoforms indistinctly.

It is not only the expression or relative abundance of these two isoforms that differs, but NFATc2 and NFATc3 have been recently shown to have very different activation and deactivation requirements. (58) Kar et al found that NFATc2 is activated by Ca^{2+} micro domains in the vicinity of plasma membrane store-operated CRAC channels, whereas NFATc3 activation additionally requires nuclear Ca^{2+} and engagement of IP_3R in the inner nuclear membrane, with sustained NFATc3 activation being strongly linked to oscillations in nuclear Ca^{2+}. The authors also show that these isoforms have very different deactivation kinetics and that the slower inactivation of NFATc2 works as a form of short-term memory to gene expression. Although the study by Kar et al was conducted in HEK293, RBL-1 and HBE cells, we have reported another example of differential control of these 2 NFAT isoforms in the endothelium of retinal microvessels after acute hyperglycemia (18). The study by Kar et al also suggests that while NFATc2 activation might be governed only by Ca^{2+} microdomains near store-operated CRAC channels, a more robust stimulus may be required for NFATc3 activation, given that IP_3 has to overcome breakdown by cytoplasmic enzymes in order to reach the nucleus and promote the release of nuclear Ca^{2+}. Interestingly, we do see a characteristic accumulation of NFATc3 at the nuclear poles of smooth muscle cells after minutes of agonist stimulation and prior to nuclear translocation (25) This strategic localization of NFATc3 would seem logic if NFATc3 activation was dependent on nuclear Ca^{2+} release also in VSMCs.

Our results here showing increased NFATc2 expression in the aortic wall of diabetic mice, along with previous data obtained in human myometrial arteries (33) and in the context of pulmonary hypertension, (36) suggest that NFATc2 expression can be induced or enhanced in pathological situations or under certain stimulatory conditions leading to phenotypic modulation. Under these circumstances, the switch in the repertoire of ion channels expressed in the plasma membrane of VSMCs that involves, among other changes, (59) the loss of the L-type voltage-gated calcium channel and the concomitant increase in store-operated Ca^{2+} channels, (60-62) would favor the activation of this particular NFATc2 isoform, which otherwise based on its relatively low abundance could be anticipated to play a minor role. Future studies will be needed to test if these differences in activation requirements between NFATc2 and NFATc3 do take place in VSMCs and have functional or pathophysiological relevance.

ACKNOWLEDGEMENTS

This work was supported by the Swedish Heart and Lung Foundation [#20160872]; the Swedish Research Council [#2014-03352; EXODIAB #2009-1039], the Swedish Society for Medical Research, the Swedish Foundation for Strategic Research (LUDC-IRC #15-0067), the Swedish Diabetes Association (Diabetesfonden), the Crafoord, Albert Påhlsson and Knut & Alice Wallenberg foundations. FB received support from CSIC (Comisión Sectorial de Investigación Científica) and PEDECIBA (Programa de Desarrollo de Ciencias Básicas).

REFERENCES

1. Rao, A., Luo, C., and Hogan, P. G. (1997) *Annual Review of Immunology* 15, 707-747
2. Crabtree, G. R., and Olson, E. N. (2002) *Cell* 109 Suppl, S67-79
3. Wu, H., Peisley, A., Graef, I. A., and Crabtree, G. R. (2007) *Trends in cell biology* 17, 251-260
4. Schulz, R. A., and Yutzey, K. E. (2004) *Developmental Biology* 266, 1-16
5. Clerk, A., Cullingford, T. E., Fuller, S. J., Giraldo, A., Markou, T., Pikkarainen, S., and Sugden, P. H. (2007) *Journal of Cellular Physiology* 212, 311-322
6. Herum, K. M., Lunde, I. G., Skrbic, B., Florholmen, G., Behmen, D., Sjaastad, I., Carlson, C. R., Gomez, M. F., and Christensen, G. (2013) *Journal of molecular and cellular cardiology* 54, 73-81
7. Amberg, G. C., Rossow, C. F., Navedo, M. F., and Santana, L. F. (2004) *J. Biol. Chem.* 279, 47326-47334
8. Nieves-Cintron, M., Amberg, G. C., Nichols, C. B., Molkentin, J. D., and Santana, L. F. (2007) *The Journal of biological chemistry* 282, 3231-3240
9. de Frutos, S., Spangler, R., Alo, D., and Bosc, L. V. (2007) *The Journal of biological chemistry* 282, 15081-15089
10. de Frutos, S., Duling, L., Alo, D., Berry, T., Jackson-Weaver, O., Walker, M. K. P. D., Kanagy, N. L., and Gonzalez Bosc, L. V. (2008) *American journal of physiology*, 00132.02008
11. Chen, R., Yan, J., Liu, P., Wang, Z., Wang, C., Zhong, W., and Xu, L. (2017) *Cell cycle* 16, 508-514
12. Lipskaia, L., del Monte, F., Capiod, T., Yacoubi, S., Hadri, L., Hours, M., Hajjar, R. J., and Lompre, A. M. (2005) *Circulation research* 97, 488-495
13. Liu, Z., Zhang, C., Dronadula, N., Li, Q., and Rao, G. N. (2005) *J. Biol. Chem.* 280, 14700-14708
14. Berglund, L. M., Kotova, O., Osmark, P., Grufman, H., Xing, C., Lydrup, M. L., Goncalves, I., Autieri, M. V., and Gomez, M. F. (2012) *Cardiovascular research* 93, 414-423
15. Nilsson-Berglund, L. M., Zetterqvist, A. V., Nilsson-Ohman, J., Sigvardsson, M., Gonzalez Bosc, L. V., Smith, M. L., Salehi, A., Agardh, E., Fredrikson, G. N., Agardh, C. D., Nilsson, J., Wamhoff, B. R., Hultgardh-Nilsson, A., and Gomez, M. F. (2010) *Arteriosclerosis, thrombosis, and vascular biology* 30, 218-224
16. Zetterqvist, A. V., Berglund, L. M., Blanco, F., Garcia-Vaz, E., Wigren, M., Duner, P., Andersson, A. M., To, F., Spegel, P., Nilsson, J., Bengtsson, E., and Gomez, M. F. (2013) *PloS one* 8, e65020
17. Blanco, F., Heinonen, S. E., Gurzeler, E., Berglund, L. M., Dutius Andersson, A. M., Kotova, O., Jonsson-Rylander, A. C., Yla-Herttuala, S., and Gomez, M. F. (2018) *Diabetes & vascular disease research*, 1479164118759220
18. Zetterqvist, A. V., Blanco, F., Öhman, J., Kotova, O., Berglund, L. M., de Frutos Garcia, S., Al-Naemi, R., Wigren, M., McGuire, P. G., Gonzalez Bosc, L. V., and Gomez, M. F. (2015) *Journal of diabetes research* 2015, 14
19. Lacolley, P., Regnault, V., Nicoletti, A., Li, Z., and Michel, J. B. (2012) *Cardiovascular research* 95, 194-204
20. Chamley-Campbell, J., Campbell, G. R., and Ross, R. (1979) *Physiological reviews* 59, 1-61
21. Majesky, M. W., Dong, X. R., Regan, J. N., and Hoglund, V. J. (2011) *Circulation research* 108, 365-377
22. Gomez, D., Swiatlowska, P., and Owens, G. K. (2015) *Arteriosclerosis, thrombosis, and vascular biology* 35, 2508-2516
23. Owens, G. K., Kumar, M. S., and Wamhoff, B. R. (2004) *Physiol. Rev.* 84, 767-801
24. Gomez, D., and Owens, G. K. (2012) *Cardiovascular research* 95, 156-164
25. Nilsson, L. M., Nilsson-Ohman, J., Zetterqvist, A. V., and Gomez, M. F. (2008) *Current opinion in lipidology* 19, 483-490
26. Sumit, M., Neubig, R. R., Takayama, S., and Linderman, J. J. (2015) *Integrative biology : quantitative biosciences from nano to macro* 7, 1378-1386
27. Tomida, T., Hirose, K., Takizawa, A., Shibasaki, F., and Iino, M. (2003) *The EMBO journal* 22, 3825-3832
28. Stevenson, A. S., Gomez, M. F., Hill-Eubanks, D. C., and Nelson, M. T. (2001) *The Journal of biological chemistry* 276, 15018-15024
29. Gomez, M. F., Bosc, L. V., Stevenson, A. S., Wilkerson, M. K., Hill-Eubanks, D. C., and Nelson, M. T. (2003) *The Journal of biological chemistry* 278, 46847-46853
30. Awla, D., Zetterqvist, A. V., Abdulla, A., Camello, C., Berglund, L. M., Spegel, P., Pozo, M. J., Camello, P. J., Regner, S., Gomez, M. F., and Thorlacius, H. (2012) *Gastroenterology* 143, 1352-1360 e1351-1357
31. Xanthoudakis, S., Viola, J. P., Shaw, K. T., Luo, C., Wallace, J. D., Bozza, P. T., Luk, D. C., Curran, T., and Rao, A. (1996) *Science* 272, 892-895
32. Oukka, M., Ho, I. C., de la Brousse, F. C., Hoey, T., Grusby, M. J., and Glimcher, L. H. (1998) *Immunity* 9, 295-304
33. Nilsson, L. M., Sun, Z. W., Nilsson, J., Nordstrom, I., Chen, Y. W., Molkentin, J. D., Wide-Swensson, D., Hellstrand, P., Lydrup, M. L., and Gomez, M. F. (2007) *American journal of physiology. Cell physiology* 292, C1167-1178
34. Gustavsson, C., Agardh, C. D., Zetterqvist, A. V., Nilsson, J., Agardh, E., and Gomez, M. F. (2010) *PloS one* 5, e12699
35. Dhanasekaran, S., Doherty, T. M., Kenneth, J., and Group, T. B. T. S. (2010) *Journal of immunological methods* 354, 34-39
36. Bonnet, S., Rochefort, G., Sutendra, G., Archer, S. L., Haromy, A., Webster, L., Hashimoto, K., Bonnet, S. N., and Michelakis, E. D. (2007) *Proceedings of the National Academy of Sciences of the United States of America* 104, 11418-11423
37. Liu, Z., Dronadula, N., and Rao, G. N. (2004) *J. Biol. Chem.* 279, 41218-41226

38. Yellaturu, C. R., Ghosh, S. K., Rao, R. K., Jennings, L. K., Hassid, A., and Rao, G. N. (2002) *The Biochemical journal* 368, 183-190
39. Lipskaia, L., Pourci, M.-L., Delomenie, C., Combettes, L., Goudouneche, D., Paul, J.-L., Capiod, T., and Lompre, A.-M. (2003) *Circulation research* 92, 1115-1122
40. Karpurapu, M., Wang, D., Singh, N. K., Li, Q., and Rao, G. N. (2008) *J. Biol. Chem.*, M800423200
41. Karpurapu, M., Wang, D., Van Quyen, D., Kim, T.-K., Kundumani-Sridharan, V., Pulusani, S., and Rao, G. N. (2010) *Journal of Biological Chemistry* 285, 3510-3523
42. Mognol, G. P., Carneiro, F. R., Robbs, B. K., Faget, D. V., and Viola, J. P. (2016) *Cell death & disease* 7, e2199
43. Rowland, B. D., and Peeper, D. S. (2005) *Nature Reviews Cancer* 6, 11
44. Suzuki, T., Aizawa, K., Matsumura, T., and Nagai, R. (2005) *Arteriosclerosis, thrombosis, and vascular biology* 25, 1135-1141
45. Yoshida, T., Gan, Q., and Owens, G. K. (2008) *American journal of physiology. Cell physiology* 295, C1175-1182
46. Hien, T. T., Garcia-Vaz, E., Stenkula, K. G., Sjögren, J., Nilsson, J., Gomez, M. F., and Albinsson, S. (2018) *Journal of Cellular Physiology* 233, 7195-7205
47. Yoshida, T., Kaestner, K. H., and Owens, G. K. (2008) *Circulation research* 102, 1548-1557
48. Shankman, L. S., Gomez, D., Cherepanova, O. A., Salmon, M., Alencar, G. F., Haskins, R. M., Swiatlowska, P., Newman, A. A., Greene, E. S., Straub, A. C., Isakson, B., Randolph, G. J., and Owens, G. K. (2015) *Nature medicine* 21, 628-637
49. Albarran-Juarez, J., Kaur, H., Grimm, M., Offermanns, S., and Wettschureck, N. (2016) *Atherosclerosis* 251, 445-453
50. Suzuki, Y. J. (2011) *Cellular signalling* 23, 1094-1099
51. Molkentin, J. D. (2000) *The Journal of biological chemistry* 275, 38949-38952
52. Suzuki, Y. J., Nagase, H., Wong, C. M., Kumar, S. V., Jain, V., Park, A. M., and Day, R. M. (2007) *American journal of respiratory cell and molecular biology* 36, 678-687
53. Narita, N., Heikinheimo, M., Bielinska, M., White, R. A., and Wilson, D. B. (1996) *Genomics* 36, 345-348
54. Boettger, T., Beetz, N., Kostin, S., Schneider, J., Kruger, M., Hein, L., and Braun, T. (2009) *The Journal of clinical investigation* 119, 2634-2647
55. Holmberg, J., Bhattachariya, A., Alajbegovic, A., Rippe, C., Ekman, M., Dahan, D., Hien, T. T., Boettger, T., Braun, T., Sward, K., Hellstrand, P., and Albinsson, S. (2018) *Arteriosclerosis, thrombosis, and vascular biology* 38, 414-424
56. Dahan, D., Ekman, M., Larsson-Callerfelt, A. K., Turczynska, K., Boettger, T., Braun, T., Sward, K., and Albinsson, S. (2014) *American journal of physiology. Cell physiology* 307, C1093-1101
57. Bretz, C. A., Savage, S. R., Capozzi, M. E., Suarez, S., and Penn, J. S. (2015) *Scientific reports* 5, 14963
58. Kar, P., Mirams, G. R., Christian, H. C., and Parekh, A. B. (2016) *Molecular cell* 64, 746-759
59. Cidad, P., Moreno-Dominguez, A., Novensa, L., Roque, M., Barquin, L., Heras, M., Perez-Garcia, M. T., and Lopez-Lopez, J. R. *Arteriosclerosis, thrombosis, and vascular biology*
60. Bergdahl, A., Gomez, M. F., Wihlborg, A. K., Erlinge, D., Eyjolfson, A., Xu, S. Z., Beech, D. J., Dreja, K., and Hellstrand, P. (2005) *American journal of physiology. Cell physiology* 288, C872-880
61. Beech, D. J. (2007) *Biochemical Society transactions* 35, 890-894
62. Kumar, B., Dreja, K., Shah, S. S., Cheong, A., Xu, S. Z., Sukumar, P., Naylor, J., Forte, A., Cipollaro, M., McHugh, D., Kingston, P. A., Heagerty, A. M., Munsch, C. M., Bergdahl, A., Hultgardh-Nilsson, A., Gomez, M. F., Porter, K. E., Hellstrand, P., and Beech, D. J. (2006) *Circulation research* 98, 557-563

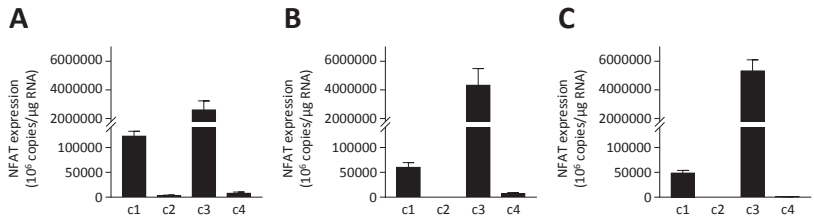

Supplemental figure 1. Absolute quantification of NFATc isoforms in **A)** freshly dissected thoracic aorta from NFAT competent mice (corresponding to data plotted in Figure 1), **B)** cultured VSMCs originated from thoracic aorta explants from NFATc2 WT mice and **C)** cultured VSMCs originated from thoracic aorta explants from NFATc3 WT mice. Absolute quantification was performed using qPCR and the copy number is expressed as 10^6 copies/µg total RNA. N=2-6 mice or experiments per condition.

Supplementary table 1. Genes included in the RT² Profiler PCR Array.

Gene Symbol	Refseq	Full Name
Srf	NM_020493	Serum response factor
Myocd	NM_145136	Myocardin
Mkl1	NM_153049	MKL (megakaryoblastic leukemia)/myocardin-like 1
Gata6	NM_010258	GATA binding protein 6
Gata4	NM_008092	GATA binding protein 4
Cnn1	NM_009922	Calponin 1
Myh11	NM_013607	Myosin, heavy polypeptide 11, smooth muscle
Cacna1c	NM_009781	Calcium channel, voltage-dependent, L type, alpha 1C subunit
Prom1	NM_008935	Prominin 1
Clca1	NM_009899	Chloride channel calcium activated 1
Dcn	NM_007833	Decorin
Adamts7	NM_001003911	A disintegrin-like and metallopeptidase (reprolysin type) with thrombospondin type 1 motif, 7
Trpc6	NM_013838	Transient receptor potential cation channel, subfamily C, member 6
Sync	NM_023485	Syncoilin
Nrp2	NM_010939	Neuropilin 2
Itga8	NM_001001309	Integrin alpha 8
Synpo2	NM_080451	Synaptopodin 2
Dmd	NM_007868	Dystrophin, muscular dystrophy
Kcnmb1	NM_031169	Potassium large conductance calcium-activated channel, subfamily M, beta member 1
Lmod1	NM_053106	Leiomodin 1 (smooth muscle)
Phactr4	NM_175306	Phosphatase and actin regulator 4
Klf4	NM_010637	Kruppel-like factor 4 (gut)
Klf5	NM_009769	Kruppel-like factor 5
Smtn	NM_013870	Smoothelin
Spp1	NM_009263	Secreted phosphoprotein 1
Ace	NM_009598	Angiotensin I converting enzyme (peptidyl-dipeptidase A) 1
Rock1	NM_009071	Rho-associated coiled-coil containing protein kinase 1
Mef2c	NM_025282	Myocyte enhancer factor 2C
Ppp1r12a	NM_027892	Protein phosphatase 1, regulatory (inhibitor) subunit 12A
Myl9	NM_172118	Myosin, light polypeptide 9, regulatory
Rho	NM_145383	Rhodopsin
Camk2g	NM_178597	Calcium/calmodulin-dependent protein kinase II gamma
Camk2d	NM_023813	Calcium/calmodulin-dependent protein kinase II, delta
Ptk2b	NM_172498	PTK2 protein tyrosine kinase 2 beta
Tagln	NM_011526	Transgelin
Cav1	NM_007616	Caveolin 1, caveolae protein
Srgap1	NM_001081037	SLIT-ROBO Rho GTPase activating protein 1
Cfl2	NM_007688	Cofilin 2, muscle
Ssh2	NM_177710	Slingshot homolog 2 (Drosophila)
Tnc	NM_011607	Tenascin C
Sgcg	NM_011892	Sarcoglycan, gamma (dystrophin-associated glycoprotein)
Thbs4	NM_011582	Thrombospondin 4
Gapdh	NM_008084	Glyceraldehyde-3-phosphate dehydrogenase
Rn18s	NR_003278	18S ribosomal RNA
Hsp90ab1	NM_008302	Heat shock protein 90 alpha (cytosolic), class B member 1

Supplementary table 2. Fold change differences in gene expression between aortic VSMCs from NFATc2 KO and WT mice, or from NFATc3 KO and WT mice. Numbers represent ratios between KO and WT for each strain. Genes upregulated >2-fold are indicated in red; genes downregulated >2-fold are indicated in green.

Gene Symbol	Full Name	NFATc2 (KO/WT)	NFATc3 (KO/WT)
Srf	Serum response factor	**0.423**	0.548
Mkl1	MKL (megakaryoblastic leukemia)/myocardin-like 1	0.914	0.822
Gata6	GATA binding protein 6	1.288	0.755
Gata4	GATA binding protein 4	**0.122**	**16.482**
Cnn1	Calponin 1	0.660	**7.724**
Myh11	Myosin, heavy polypeptide 11, smooth muscle	1.833	**0.463**
Cacna1c	Calcium channel, voltage-dependent, L type, alpha 1C subunit	**0.143**	**0.362**
Clca1	Chloride channel calcium activated 1	1.477	0.530
Dcn	Decorin	1.346	**3.552**
Adamts7	A disintegrin-like and metallopeptidase (reprolysin type) with thrombospondin type 1 motif, 7	1.236	1.869
Trpc6	Transient receptor potential cation channel, subfamily C, member 6	1.572	**0.214**
Sync	Syncoilin	1.090	0.616
Nrp2	Neuropilin 2	0.519	1.904
Itga8	Integrin alpha 8	**0.255**	**2.489**
Synpo2	Synaptopodin 2	**0.473**	**0.459**
Dmd	Dystrophin, muscular dystrophy	0.612	1.588
Lmod1	Leiomodin 1 (smooth muscle)	**0.492**	**0.217**
Phactr4	Phosphatase and actin regulator 4	0.719	1.177
Klf4	Kruppel-like factor 4 (gut)	**2.242**	**0.110**
Klf5	Kruppel-like factor 5	0.547	**3.175**
Smtn	Smoothelin	0.737	0.821
Spp1	Secreted phosphoprotein 1	1.503	**6.205**
Ace	Angiotensin I converting enzyme (peptidyl-dipeptidase A) 1	1.398	**31.736**
Rock1	Rho-associated coiled-coil containing protein kinase 1	0.817	0.717
Ppp1r12a	Protein phosphatase 1, regulatory (inhibitor) subunit 12A	0.605	0.749
Myl9	Myosin, light polypeptide 9, regulatory	**0.358**	**0.473**
Rho	Rhodopsin	0.682	**2.180**
Camk2g	Calcium/calmodulin-dependent protein kinase II gamma	0.927	0.854
Camk2d	Calcium/calmodulin-dependent protein kinase II, delta	1.864	0.502
Ptk2b	PTK2 protein tyrosine kinase 2 beta	1.018	0.521
Tagln	Transgelin	0.536	**3.664**
Cav1	Caveolin 1, caveolae protein	0.768	**0.227**
Srgap1	SLIT-ROBO Rho GTPase activating protein 1	**2.352**	**0.278**
Cfl2	Cofilin 2, muscle	1.101	0.625
Ssh2	Slingshot homolog 2 (Drosophila)	**0.466**	1.448
Tnc	Tenascin C	1.027	**29.507**